

POLYMERIC NANOGELS AS GENE CARRIERS

Jin Lee

A dissertation submitted to the faculty of the University of North Carolina at Chapel Hill in partial fulfillment of the requirement for the degree of Doctor of Philosophy in the Division of Molecular Pharmaceutics at the School of Pharmacy

Chapel Hill

2007

Approved by:

Moo J. Cho, Ph.D., Advisor

Philip C. Smith, Ph.D., Chair

Jian Liu, Ph.D., Reader

Joseph M. DeSimone, Ph.D., Reader

Fan Yuan, Ph.D., Reader

ABSTRACT

JIN LEE: Polymeric Nanogels as Gene Carriers

(Under the direction of Moo J. Cho, PhD)

Developing efficient and safe vectors is one of the main challenges in gene therapy. Multiple fatal incidences in applying virus have brought safety issues to the attention and called for developing non-viral vectors, entailing lipoplex and polyplex. The present dissertation mainly focuses on a polyplex system. Inverse microemulsion-derived nanogel features a hydrophilic matrix, rendering the delivery of genes more compatible. Nanogel was modified with acid-buffering weak base, redox-sensitive cleavable crosslinker, and folate targeting ligand. Two types of plasmid DNA (pDNA)-nanogel formulations were assessed for transfection efficiency. First, luciferase pDNA was added to the microemulsion prior to the polymerization. It was hypothesized that pDNA will spontaneously reside in the aqueous phase and be well compacted. The energetics involved was not, however, sufficient enough to produce a stable system. Protamine-condensed pDNA increased the entrapment efficiency. Unfortunately, addition of methanol to dissolve the disulfide crosslinker disturbed microemulsion, reducing entrapment efficiency. Second, pDNA was mixed with pre-made cationic nanogels containing folate targeting ligands. Although pDNA-nanogel complex did not surpass the conventional transfecting reagents, it increased transfection efficiency in the folate receptor-expressing KB cells compared to the naked pDNA. Targeted formulations

represented superior transfection efficiency to the non-targeted counterparts. Disulfide-containing crosslinker was necessary for an enhanced transfection. Incorporation of weak base improved the transfection efficiency only in the formulation with low positive charges. Most importantly, the targeting capacity was able to overcome non-specific binding only when electrostatic interaction was minimal.

Comparing to the relatively well-established nanogels, PRINT particles are in the early stage of development as a potential drug/gene carrier, featuring an unprecedented monodispersity in various physicochemical properties. Better understanding of *in vivo* pharmacokinetics of PRINT particles would lead to optimizing pharmacodynamics as a gene carrier. [¹²⁵I]-PRINT particles following an IV injection into the healthy mice accumulated in liver and spleen. However, the relatively short blood circulation and the probable premature decomposition called for further investigation. Also a more sensitive and reproducible monitoring method is highly desirable. Due to its preliminary nature, the study results are placed in Appendix.

*To my parents, brothers, and my wife, Miyoung,
for their love, encouragement, and support.*

ACKNOWLEDGEMENTS

When I stepped into this country in the Summer 2001, I was overwhelmed by a new environment and unfamiliar circumstances. All of my previous knowledge in science and experience within the company just looked so trivial comparing to what I encountered at that time. Dr. M. J. Cho was the one who guided me toward a right track in science and the life in America. For that, I am deeply grateful to him. As a research advisor, he is stern but always generous with his time and knowledge. Through him, I have learned the rigor, the patience and the sincerity as a scientist. I would also like to thank Dr. Philip Smith for being a chair of my committee and for supporting my research. I am also deeply grateful to all of my committee members, Drs. Joseph DeSimone, Jian Liu, Fan Yuan for their guidance and encouragement. I am also indebted to Dr. Arlene Bridges for helping me with mass spectrometry, Dr. Karl Koshlap for his assistance with NMR, and Dr. Wallace Ambrose for his teaching of transmission electron microscopy. I would also like to express my deepest gratitude to Dr. Dhiren Thakker for encouraging me during my course work, Dr. Leaf Huang for his valuable suggestions on my project, Dr. Rihe Liu for the exciting discussion during the weekly journal club meeting. I would also like to thank Dr. Robert Shrewsbury for teaching me during my 3-year TA period and for his constant concerns on my progress. I wish to extend my sincere thanks to all of the divisional faculty and staff, especially Dr. Kathryn Fiscelli for her support in all aspects.

I would also like to thank the folks in the department of chemistry, Dr. Karen McAllister for initiating this project and teaching me of preparing nanogels, Dr. Andy Murphy, Dr. Patrick Pohlhaus, and Ms. Stephanie Gratton for providing me materials (PRINT particles and monomers) in doing cellular and animal experiments as well as their friendship. Also, I am grateful to the folks in Dr. Huang's lab for granting me their instrument and supplies, especially Dr. Feng Liu, Dr. Christine Conwell, and Star Li for their contribution to my project. The life with folks in 303 Beard and 1301 Kerr has been one of the most memorable parts in the years in the US. In particular, I would like to thank Mary Park, John An and Dr. Seongwon Hong for helping me to settle down in my very first year. I would also like to thank current and previous members of the Cho Lab (Dr. Sannie Chong, Jordan Roger Shuford, Dr. Aravind Asokan, Dr. Enzo Palma, Venita Gresham, Matthew Dufek, Leandra Miko, Roland Cheung, Michael Hackett, Dr. David Gaul) for their wonderful company.

No acknowledgement would be complete without mentioning family. I would especially like to thank my parents in Korea. It would have been very difficult for me to reach this moment of my life if it were not for their constant support and encouragement. I would also like to thank my brothers (Min, Sun/Joomi, Hojin/Eunyoung) for their love and encouragement. And most of all, I would like to thank my wife, Miyoung, for her help, support, and love in every moment during the past 11 years of my marriage, especially in the memorable 6 years in the US. No words can fully describe how thankful I am to have her as a partner in my life. This dissertation is a testament to their ever-present love, encouragement, and support. I dedicate this work to them with love and gratitude.

TABLE OF CONTENTS

	Page
LIST OF TABLES -----	xii
LIST OF FIGURES -----	xiii
LIST OF ABBREVIATIONS AND SYMBOLS -----	xvii
CHAPTER I. INTRODUCTION -----	1
1.1 Gene Vectors -----	1
1.2 Lipoplex -----	11
1.3 Polyplex -----	14
1.4 Cleavable Linkers -----	17
1.5 DNA Condensation -----	19
1.6 Statement of Purpose -----	22
1.7 References -----	28
CHAPTER II. SYNTHESIS AND CHARACTERIZATION OF MONOMERS AND CROSSLINKERS -----	42
2.1 Introduction -----	42
2.1.1 Overview -----	42
2.1.2 Endosome-to-Cytosol Translocation and Proton Sponge Hypothesis -----	42
2.1.3 Release of Plasmid DNA from Nanogels -----	45
2.2 Materials and Methods -----	48
2.2.1 Materials -----	48
2.2.2 Preparation of Imidazole-Containing Monomer (IPAA) -----	49

2.2.3 Measurement of pKa of Weak Base-Containing Monomer and Nanogel -----	49
2.2.4 Disulfide-Containing Crosslinker -----	50
2.3 Results and Discussion -----	53
2.3.1 Imidazole-Containing Monomer (IPAA) -----	53
2.3.2 pKa's of Weak Base-Containing Monomers and Nanogels -----	54
2.3.3 Disulfide-Containing Crosslinker -----	56
2.4 Conclusions -----	58
2.5 References -----	71
CHAPTER III. ENTRAPMENT OF PLASMID DNA IN NANOGEL -----	74
3.1 Introduction -----	74
3.2 Materials and Methods -----	76
3.2.1 Materials -----	76
3.2.2 Preparation of pDNA-Entrapped Nanogel from Inverse Microemulsion -----	78
3.2.3 Transmission Electron Microscopy (TEM) of pDNA-Entrapped Nanogel -----	79
3.2.4 Preparation of Macroemulsion-Derived, pDNA-Entrapped Nanogel -----	79
3.2.5 Radiolabeling of pDNA -----	80
3.2.5.1 Nick Translation -----	80
3.2.5.2 Methylation -----	81
3.2.6 Radiolabeling of Nanogel -----	82
3.2.7 Entrapment Efficiency -----	83
3.2.8 Size Measurement -----	83
3.2.9 Condensation of pDNA -----	84

3.2.9.1 Spermine: $\text{NH}_2(\text{CH}_2)_3\text{NH}(\text{CH}_2)_4\text{NH}(\text{CH}_2)_3\text{NH}_2 \cdot 4\text{HCl}$ -----	84
3.2.9.2 Poly(L-lysine) (PLL) -----	85
3.2.9.3 Alkyltrimethylammonium Bromide -----	85
3.2.9.4 Protamine -----	86
3.2.10 Recovery of Condensed pDNA in Aqueous Layer from Heptane/Water System -----	87
3.2.11 Transfection -----	87
3.3 Results and Discussion -----	89
3.3.1 Preparation of pDNA-Entrapped Nanogel and Characterization by TEM -----	89
3.3.2 Stability of pDNA under Free Radical-Initiated Polymerization -----	90
3.3.3 Radiolabeling of pDNA -----	93
3.3.4 Radiolabeling of Nanogel -----	95
3.3.5 Entrapment of Uncondensed pDNA -----	96
3.3.6 Entrapment of Condensed pDNA and Transfection Study -----	98
3.4 Conclusions -----	107
3.5 References -----	128
CHAPTER IV. COMPLEXATION OF PLASMID DNA WITH NANOGELE -----	131
4.1 Introduction -----	131
4.2 Materials and Methods -----	135
4.2.1 Materials -----	135
4.2.2 Preparation of Folate-Containing Monomers -----	136
4.2.2.1 Activation -----	136
4.2.2.2 Coupling -----	137
4.2.2.3 Acylation -----	137

4.2.3 Gel Electrophoresis -----	138
4.2.4 Size Measurement -----	139
4.2.5 Determination of Folate Concentration in Nanogels -----	139
4.2.6 Transfection -----	140
4.2.7 Luciferase Assay -----	142
4.3 Results and Discussion -----	143
4.3.1 Preparation of Folate-Containing Monomer -----	143
4.3.2 Determination of Folate Concentration in Nanogel -----	145
4.3.3 Transfection of KB Cells with Nanogel-Plasmid DNA Complex -----	146
4.4 Conclusions -----	154
4.5 References -----	166
CHAPTER V. CONCLUSIONS AND FUTURE PROSPECTS -----	172
5.1 Summary of Conclusions -----	172
5.2 Future Prospects -----	174
5.3 Concluding Remarks -----	178
5.4 References -----	179
APPENDIX I. PHARMACOKINETICS AND BIODISTRIBUTION OF PRINT PARTICLES IN MICE -----	181
A.1 Introduction -----	181
A.2 Materials and Methods -----	185
A.2.1 Materials -----	185
A.2.2 Preparation of PRINT Particles -----	186
A.2.2.1 Fluorescently-Labeled PRINT Particles -----	186
A.2.2.2 Radiolabeled PRINT Particles -----	188

A.2.3 Characterization of Fluorescently-Labeled PRINT Particles -----	189
A.2.3.1 Stability of Fluorescein-Conjugated Particles in Liver Homogenate ----	189
A.2.3.2 Kinetics of Fluorescence Intensity from Particles in NaOH -----	189
A.2.4 Pharmacokinetic and Biodistribution Studies of Fluorescently-Labeled PRINT Particles -----	190
A.2.5 Iodination of PRINT Particles -----	191
A.2.6 Pharmacokinetic and Biodistribution Studies of Radiolabeled PRINT Particles -----	192
A.3 Results and Discussion -----	194
A.3.1 Characterization of Fluorescently-Labeled PRINT Particles -----	194
A.3.2 Pharmacokinetic and Biodistribution Studies of Fluorescently-Labeled PRINT Particles -----	196
A.3.3 Pharmacokinetic and Biodistribution Studies of Radiolabeled PRINT Particles -----	199
A.4 Conclusions -----	204
A.5 References -----	220
APPENDIX II. MANUSCRIPT ACCEPTED FOR PUBLICATION -----	225

LIST OF TABLES

Table 1-1	Nuclear localization sequences -----	26
Table 2-1	Summary of pKa's of weak base-containing monomers and nanogels -----	63
Table 3-1	Size of pDNA-CTAB complex at various N/P ratios measured by dynamic light scattering -----	119
Table A-1	Particle sizes measured by scanning electron microscopy and dynamic light scattering -----	207
Table A-2	Blood PK parameters estimated from two-compartment model -----	219

LIST OF FIGURES

Figure 1-1	Various transport barriers involved in gene delivery -----	24
Figure 1-2	Various endocytosis pathways -----	25
Figure 1-3	Structures of some representative polymers used in polyplex systems -----	27
Figure 2-1	Illustration of proton sponge hypothesis -----	59
Figure 2-2	Synthetic scheme and ¹ H-NMR spectrum of imidazolylpropylacrylamide --	60
Figure 2-3	Titration of neutral and cationic nanogels containing morpholine moiety --	61
Figure 2-4	Potentiometric titration of monomers and nanogels containing weak bases -----	62
Figure 2-5	Titration of PEI and nanogels prepared with weak base-containing monomers; MEA, IPAA, or DMAEA -----	64
Figure 2-6	Fractionation of PEG monomethacrylate by a size exclusion chromatography -----	65
Figure 2-7	Reaction of CDI-activated PEGmA with isobutylamine -----	66
Figure 2-8	¹ H-NMR spectrum of PEG monomethacrylate and CDI-activated PEGmA -----	67
Figure 2-9	¹ H-NMR spectrum and mass spectrum of a disulfide containing, PEG-based diacrylate crosslinker -----	68
Figure 2-10	Schematic illustration of a typical polymerization reaction -----	69
Figure 2-11	Synthetic scheme of a disulfide-containing, PEG-based crosslinker -----	70
Figure 3-1	Preparation of pDNA-entrapped nanogel -----	109
Figure 3-2	Transmission electron micrographs of pDNA-entrapped inverse microemulsion and polymerized neutral nanogels -----	110
Figure 3-3	Stability of pDNA in emulsion-derived, free radical-initiated polymerization -----	111

Figure 3-4	Effect of HEA on the pDNA recovery in free radical-mediated emulsion polymerization -----	112
Figure 3-5	Radiolabeling of pDNA using nick translation -----	113
Figure 3-6	Radiolabeling of pDNA by methylation -----	114
Figure 3-7	Radiolabeling of acrylate derivatives by acetylation -----	115
Figure 3-8	Agarose gel (0.8%) electrophoresis of nanogel-entrapped pCMV-Luc of 6.2 kbp -----	116
Figure 3-9	Agarose gel (0.8%) electrophoresis of [^{14}C]-nanogel that had entrapped pCMV-Luc of 6.2 kbp -----	117
Figure 3-10	Condensation of pDNA by multivalent cationic molecules -----	118
Figure 3-11	Size of pDNA complex with dodecyltrimethylammonium bromide (DDTAB) and decyltrimethylammonium bromide (DTAB) -----	120
Figure 3-12	Condensation of pDNA with protamine as monitored by fluorescence ---	121
Figure 3-13	Size of pDNA-protamine complex -----	122
Figure 3-14	Recovery of pDNA condensed with protamine or cationic lipids -----	123
Figure 3-15	Agarose gel (0.8%) electrophoresis of pre-condensed, neutral nanogel-entrapped pCMV-Luc of 6.2 kbp -----	124
Figure 3-16	Illustration of protamine-condensed, neutral nanogel-entrapped pDNA after endocytosis -----	125
Figure 3-17	Agarose gel (0.8%) electrophoresis of protamine-condensed, neutral nanogel-entrapped pCMV-Luc of 6.2 kbp -----	126
Figure 3-18	Transfection of HeLa cells with pCMV-Luc protamine-condensed and entrapped in neutral nanogel -----	127
Figure 4-1	Synthetic scheme of PEG-based, acrylate-containing monomer -----	155
Figure 4-2	^1H -NMR (300 MHz) spectra of folate and <i>N</i> -hydroxysuccinimide-activated folate dissolved in DMSO- d_6 -----	156
Figure 4-3	^1H -NMR (300 MHz) spectra of PEG-conjugated folate and acrylate-containing PEG-folate conjugate dissolved in DMSO- d_6 -----	157

Figure 4-4	Spectrophotometric determination of the folate concentration in nanogels -----	158
Figure 4-5	Schematic illustration of pDNA complex with strategically-designed nanogel -----	159
Figure 4-6	Transfection of KB cells with pDNA-nanogel complex -----	160
Figure 4-7	Agarose gel electrophoresis run with nanogel-pDNA complex in the presence of dithiothreitol -----	161
Figure 4-8	Gel retardation study with nanogel-pDNA complex at various N/P ratios -----	162
Figure 4-9	Size of nanogels in various compositions and nanogel-pDNA complexes at different N/P ratios -----	163
Figure 4-10	Transfection of KB cells with nanogel-pDNA complex in Opti-MEM or in the presence of serum -----	164
Figure 4-11	Summary of transfection studies with various nanogel-pDNA complexes in KB cells -----	165
Figure A-1	Scanning electron micrographs of PRINT particles (data from S. Gratton and P. Pohlhaus in DeSimone Lab of UNC chemistry Department) -----	206
Figure A-2	Stability of PRINT particles in liver homogenates as studied in a dialysis set-up -----	208
Figure A-3	Hydroxide ion-catalyzed hydrolysis of fluorescein-labeled PRINT particles -----	209
Figure A-4	Kinetics of fluorescence intensity from PRINT particles that were incubated with NaOH -----	210
Figure A-5	Biodistribution of fluorescently-labeled PRINT particles of various sizes (200 nm, 500 nm, 1 μ m, 7 μ m, and 7 μ m with 50% porogen) following IV bolus tail vein injection of 0.32 mg particles per mouse (n=3 or 4) -----	211
Figure A-6	Biodistribution of fluorescently-labeled PRINT particles represented by organ or tissue (serum, liver, kidney, spleen, heart and lung) -----	212
Figure A-7	Total recovery of fluorescein-labeled PRINT particles -----	213
Figure A-8	Iodination of PRINT particle using Iodogen [®] pre-coated tube -----	214

Figure A-9	Biodistribution of [¹²⁵ I]-PRINT particles of 200 nm following IV bolus tail vein injection of 1.4 μCi (0.32 mg particles) per mouse -----	215
Figure A-10	Total recovery of 200 nm [¹²⁵ I]-PRINT particles -----	216
Figure A-11	Blood concentration as a function of time following IV bolus tail vein injection of 1.4 μCi (0.32 mg particles per mouse) [¹²⁵ I]-PRINT particles of 200 nm in mice (n=3 or 4) -----	217
Figure A-12	Two-compartment model used in the calculation of PK parameters in blood -----	218

LIST OF ABBREVIATIONS AND SYMBOLS

AETMAC	2-acryloxyethyltrimethylammonium chloride
AIBN	2,2'-azobis (2-methylpropionitril)
CDI	1,1'-carbonyldiimidazole
CDI-PEGmA	CDI-activated PEGmA
CMC	Critical micellar concentration
CTAB	Cetyltrimethylammonium bromide
DCC	Dicyclohexylcarbodiimide
DDTAB	Dodecyltrimethylammonium bromide
DLS	Dynamic light scattering
DMAEA	2-(dimethylamino)ethyl acrylate
DOPC	Dioleoylphosphatidylcholin
DOPE	Dioleoylphosphatidylethanolamine
DTAB	Decyltrimethylammonium bromide
EHP	Di(2-ethylhexyl) peroxydicarbonate
FBS	Fetal bovine serum
FR	Folate receptor
GPI	Glycosylphosphatidylinositol
GSH	Reduced form of glutathione
GSSG	Oxidized form of glutathione
HBSS	Hanks' balanced salt solution
HEA	2-hydroxyethyl acrylate

IPAA	Imidazoylethylpropylacrylamide
(k)bp	(kilo) base pair
LPD	Lipid-polymer (or protein)-DNA
MEA	2-N-morpholinoethyl acrylate
MEM	Minimum Essential Medium
N/P	Nitrogen-to-phosphate (i.e., positive-to-negative)
NLS	Nuclear localization sequence
PEG	Poly(ethylene glycol)
PEG-A	PEG monoacrylate
PEGdiA	Poly(ethylene glycol) diacrylate
PEGmA	PEG monomethacrylate
PEI	Poly(ethylenimine)
PEO	Poly(ethylene oxide)
PHS	<i>p</i> -hydroxystyrene
PLL	Poly(L-lysine)
PRINT	Particle Replication In Non-wetting Templates
RES	Reticuloendothelial system
SAM	S-adenosyl-L-methionine
SSXL	Disulfide-containing, PEG-based crosslinker
T(A)E	Tris-(acetate-)EDTA
TEA	<i>N,N,N</i> -triethylamine
W/O	Water-in-oil

CHAPTER I

INTRODUCTION

1.1 Gene Vectors

Along with the increased attention to human gene therapy, much research effort has been geared to the development of gene delivery vectors aiming for enhanced uptake of genetic materials by target cells and the facile transport of the nucleic acids to the cytosol and subsequently to the nucleus. As viruses can perform these tasks, early on viral vectors had been developed in the gene therapy field (Culver *et al.* 1992; Kasahara *et al.* 1994; Gunzburg and Salmons 1996). Although this strategy delivers genes in an efficient manner, it has been limited due to general toxicity, carcinogenesis, immunogenicity, and low target tissue penetration problems. For instance, the sudden death of an 18-year-old patient from activated innate immunity in a gene therapy trial brought the safety issues into focus in using viruses as gene carriers (Marshall 1999). The interest of investigators accordingly has been moved to non-virus-derived vectors. Although non-viral vectors developed to date are inferior to their viral counterparts with regard to efficiency, they are relatively safe and amenable to large-scale production. Improving the efficiency and specificity will make non-viral vectors more attractive tools in gene therapy. Non-viral vectors mostly consist of lipid- or polymer-based formulations, commonly referred to as lipoplex and polyplex, respectively. They are in

essence utilizing the electrostatic interaction between polyanionic charges of genes and cationic carriers. However, in vivo application of these approaches is greatly compromised by the unwanted interaction of positively charged vectors with the anionic serum components. Ideally, for clinical applications gene vectors should be nontoxic, nonimmunogenic, and serum compatible.

As depicted in **Figure 1-1**, non-viral gene vectors must overcome multiple transport barriers to cellular gene delivery. Cellular binding and uptake represent the first obstacle (steps **2** and **3**). Endocytosis is the generally accepted mechanism by which gene vectors enter the cell (Wattiaux *et al.* 2000). Polyanionic cell surface proteoglycans are believed to play a role in the non-specific interaction with cationic vectors with excess positive charges. Proteoglycan consists of a core protein and covalently linked highly anionic glycosaminoglycan chains such as heparin and heparan sulfate (Hardingham and Fosang 1992). Many pieces of evidence can be found in early investigations with polylysine (Mislick and Baldeschwieler 1996) and cationic lipid (Mounkes *et al.* 1998). In the presence of glycosaminoglycan sulfation inhibitors such as sodium chlorate (NaClO_3) or glycosaminoglycan lyases such as heparinase II, gene expression was significantly reduced, providing further evidence (Baeuerle and Huttner 1986).

At the tissue/organ level, it is often desirable to deliver a therapeutic gene to a specific cell type. In theory, introducing a targeting ligand to the gene vector can enhance transfection efficiency at lower and safer doses via more specific binding to the target cell population and subsequent receptor-mediated endocytosis. Subsequent to use of asialoorosomucoid (Wu and Wu 1987) and transferrin (Wagner *et al.* 1990) as targeting

moieties, many other ligands have been exploited in this field, including growth factors (Sosnowski *et al.* 1996), insulin (Huckett *et al.* 1990), integrin-binding motifs (Harvie *et al.* 2003), heregulin (Medina-Kauwe *et al.* 2001), antibodies (Chen *et al.* 1994; Merwin *et al.* 1995; Kircheis *et al.* 1997), and small molecules such as folate (Lee and Huang 1996). See **Chapter IV** for further discussions. The entry pathway upon cellular binding will be dictated by the targeting ligand of choice and the cell type. As shown in **Figure 1-2**, endocytosis can be divided into two broad categories depending on the involvement of receptors.

The classical clathrin-mediated endocytosis account for the majority of cellular entry pathways of receptor-ligand complexes (Mukherjee *et al.* 1997). Upon receptor binding, clathrin structures accumulate on the intracellular surface of the plasma membrane and invaginate to form clathrin-coated pits. The coated pits are then pinched off into vesicles that are later uncoated. After the vesicles containing cargos merge with early (or sorting) endosomes, the destinations of these endosomes are two fold. They traffic either to lysosomes through late endosomes upon further pH decrease or to recycling endosomes as exemplified in transferrin and its receptor (Phillips 1995). Many studies demonstrated that growth factors, hormones, lipoproteins and immune complexes use this pathway to enter the cell (Ukkonen *et al.* 1986).

Many pathogens including SV40 and cholera toxin are believed to use the caveolar pathway to avoid lysosomal degradation (Cohen *et al.* 2004). Caveolae are flask-shaped invaginations of the plasma membrane with a diameter of 50-80 nm (Pelkmans and Helenius 2002). They are rich in cholesterol and sphingolipids and characterized by the integral membrane protein, caveolin. Constitutive endocytic uptake mechanism mediated by caveolae is, however, somewhat controversial (Hommelgaard *et al.* 2005) with endocytosis being

down-regulated by caveolin itself (Le *et al.* 2002). Clathrin and caveolae independent yet lipid raft mediated endocytosis is found to internalize cytokine receptors (e.g., IL-2 receptor) (Lamaze *et al.* 2001) and glycosylphosphatidylinositol (GPI)-anchored proteins (Sabharanjak *et al.* 2002). The clathrin independent, caveolae-mediated endocytic pathway appears to play a role in the cellular uptake of folate and its conjugate via folate receptor-mediated endocytosis. This process was used as a strategic modification of the nanogel in **Chapter IV**.

Large particulate vectors are internalized to the cell via macropinocytosis or phagocytosis. Macropinosomes are large irregular vesicles of 0.5 – 5 μm in diameter that are formed by actin-driven protrusion (ruffling) of the plasma membrane (Grimmer *et al.* 2002). Membrane ruffling is nonclathrin-mediated. Rejman and colleagues (2004) suggested that 500-nm microspheres enter cells by macropinocytosis. Macropinosomes may provide an alternative cell entry route by avoiding intersection with lysosomes and subsequent lysosomal degradation (Conner and Schmid 2003). However, some negative role of macropinocytosis was reported in transfecting HepG2 cells with histidinylated polyplex in that the low transfection efficiency was attributed to a delayed translocation of the polyplex from the macropinosome to the cytosol (Goncalves *et al.* 2004). Phagocytosis is initiated by the interaction of cell surface receptor with foreign particles (Niedergang and Chavrier 2004). Only professional antigen presenting cells such as macrophages and dendritic cells express the large number of surface receptors that can initiate efficient phagocytosis (Aderem and Underhill 1999; Allavena *et al.* 2004). The entrapment of foreign particles leads into phagosomes that mature upon acidification and fuse with lysosomes (Swanson and Baer 1995). Strong enhancement of phagocytosis by cationic particles has been demonstrated in macrophages and dendritic cells (e.g., Thiele *et al.* 2001). Cell type dependency of cellular

entry pathway is also found in macropinosomes in that only immature dendritic cells carry out this process constitutively (West *et al.* 2000). Specific cell types such as HepG2 cells have been used to distinguish clathrin-mediated pathway from caveolae-associated route of cationic vectors since this cell line is known to lack caveolae (Fujimoto *et al.* 2000).

The size of vectors is also a factor in determining a pathway of cellular entry. In general virus sized particles (20-200 nm) are believed to take clathrin-dependent or caveolae associated pathways considering the vesicle size of these routes. Along with Rejman's findings (2004) mentioned above, particles larger than 500 nm in diameter appear to enter the cell via phagocytosis or receptor independent pathways such as pinocytosis (Simoes *et al.* 1999). Thus, particulate vectors can take any of these pathways depending on the size and composition (e.g., incorporation of targeting ligands). It is also possible that multiple routes concurrently contribute to the uptake of particulate vectors. As observed with the conjugates of peptide derived from HIV transactivator of transcription, more complexity emerges with the possibility for targeting ligand directed vectors to behave differently from the native ligand in choosing the cellular uptake pathway (Eguchi *et al.* 2001; Wadia *et al.* 2004). More importantly, avoiding lysosomes by taking alternative cell entry pathways do not necessarily guarantee high levels of final gene expression as speculated in Goncalves *et al.* (2004).

The second barrier in cellular transfection is the endosome-to-cytosol translocation of gene vectors or pDNA itself (step 4 in **Figure 1-1**). Endocytosed vectors containing pDNA eventually traffic to lysosomes where they are degraded by lysosomal proteases. As the luminal pH decreases from ~6 to ~5, early endosomes mature to late endosomes that fuse with lysosomes (Luzio *et al.* 2001). Endocytosis via alternative pathways discussed earlier

can avoid lysosomes but likely ends up with entrapping in endosomes. The clever way of virus in utilizing pH decrease in escaping endosomal compartment has been adopted in gene vectors. The conformational change in virus proteins yields an amphipathic helical structure that is capable of inducing membrane fusion (Klasse *et al.* 1998). Thus, the main idea was that vectors possessing endosomolytic components should ensure early escape from endo-lysosomal compartment, resulting in enhanced transfection efficiency. This hypothesis was supported by the observation that neutral phospholipid dioleoylphosphatidylethanolamine (DOPE) incorporated into lipoplex enhanced transfection efficiency (Farhood *et al.* 1995). Transition from bilayer to inverted hexagonal structures and membrane destabilizing activity are thought to be the main characteristics of DOPE that render this phospholipid more fusogenic than other neutral phospholipids such as dioleoylphosphatidylcholine (DOPC) (Koltover *et al.* 1998). Lipoplex containing DOPE showed indeed better transfection efficiency than DOPC-derived counterpart (Mok and Cullis 1997). The hypothesized mechanism of lipoplex fusion and the subsequent DNA release was proposed by Xu and Szoka (1996). This report suggested that flip-flop movements of anionic phospholipid from the cytoplasmic facing monolayer of the endosomal membrane into the inner endosomal lumen induced the formation of a neutral ion pair with cationic lipid of lipoplex. However, the number of anionic lipids theoretically calculated in a given endosomal membrane surface was not high enough to facilitate the membrane fusion, compromising the aforementioned hypothesis (Barron and Szoka Jr 1999).

Unlike cationic lipid, cationic polymers lack hydrophobic domains and therefore are incapable of fusing with or destabilizing endosomal membrane. One strategy has been conjugation of pore-forming peptide domains with polyplexes. The examples are diphtheria

toxin translocation domain chemically coupled to polylysine (Fisher and Wilson 1997), melittin incorporated in poly(ethylenimine) (PEI) (Ogris *et al.* 2001a) and GALA (a Glu-Ala-Leu-Ala repeat) conjugated to dendrimers (Haensler and Szoka 1993). These studies also demonstrated that endosomolytic activities of the pore-forming peptides are still intact when linked covalently to the polymers.

An alternative approach was PEI. Its efficiency was attributed to the so-called ‘proton sponge effect’ (Boussif *et al.* 1995). Tertiary amine moieties with pKa of 5.5-7.0 in PEI and dendrimers are believed to responsible for this effect by absorbing protons in the endosomes, subsequently delaying the trafficking to lysosomes and eventually disrupt endosomal membrane. Although this hypothesis was once challenged (Godbey *et al.* 2000), more recent findings reaffirmed the theory (Merdan *et al.* 2002; Thomas and Klibanov 2002) and a mechanistic explanation was well documented by Sonawane *et al.* (2003). More delineated speculation as well as a methodological application of this hypothesis is also presented in **Chapter II**.

Following endosomal escape, gene vectors may encounter another obstacle before reaching perinuclear area. Since the cytosolic space is a full of viscous fluids, the passive diffusion of the particulate systems within this milieu may be extremely slow (Luby-Phelps *et al.* 1987). It was reported that the mobility of DNA in the cytoplasm is indeed dependent on DNA size with 6 kbp DNA remaining cytoplasm while 21 bp DNA diffusing into the nucleus in 5 min after microinjection into the cytoplasm (Lukacs *et al.* 2000). Gene vectors therefore will need some type of assistance from active cytosolic transport systems to approach the vicinity of the nucleus. Molecular motors associated with the microtubule network or actin filaments are known to transport vesicles, organelles and other colloidal

structures in the cytoplasm (Hamm-Alvarez 1998). One of these systems may well contribute to the transport of the gene vectors. Dynein system is one of the motor proteins and normally associated with the endocytic pathway (Walker and Sheetz 1993). In this context, if the gene vectors exit the endosome too early, the probability for them to reach the nucleus, the deeper site of the cell, could be lower.

DNA has must dissociate from the vector to allow the access of the transcription apparatus of the cell. Although the exact site is still not clear, vector unpacking or dissociation is certainly another hurdle for the gene vector to overcome (step **5** in **Figure 1-1**). As far as lipoplex is concerned, the uncoupling between cationic lipids and pDNA seems to be required prior to the transport into the nucleus. For example, the direct injection of lipoplex into the nucleus or even into the cytoplasm resulted in very low levels of gene expression (Zabner *et al.* 1995). This study also implies that vector unpacking occurs during normal endocytic pathway. Early investigations suggested that lipoplex dissociates through the interaction (including fusion process) with the cytosolic membrane network such as endoplasmic reticulum, Golgi, mitochondria, and nuclear membrane (El Ouahabi *et al.* 1999; Cornelis *et al.* 2002).

In the case of polyplex, the site of dissociation appears to be more complicated. Pollard and colleagues (1998) suggested that the dissociation could occur in the nucleus. This is based on their findings that polyplex directly injected into the nucleus showed a significant gene expression. However, later study demonstrated that the population of polyplexes detected inside the nucleus did not contribute to the gene expression measured (Bieber *et al.* 2002). Nevertheless, this group and other investigators (Schaffer *et al.* 2000) still observed

high concentration of polyplexes in the perinuclear region. Although the site of dissociation has yet to be determined, the molecular weight of polymers in the polyplex system seems to affect the kinetics of vector unpacking. High molecular weight poly(L-lysine) was found to remain bound to pDNA in the perinuclear region while majority of shorter version of this polymer was found as free form around the nucleus (Schaffer *et al.* 2000). This observation implies that low-molecular-weight-polymer-based polyplex has faster dissociation compared to its larger counterpart-based polyplex. The dissociation kinetics appears to reflect the transfection efficiency. Shorter poly(L-lysine)-based polyplex showed a higher transfection while longer ones exhibited more sustained gene expression (Ziady *et al.* 1999). The dissociation of PEI-based polyplex seems relatively slow. A few studies suggested that it might occur between 4 hrs and 18 hrs after incubation with the cells (Ogris *et al.* 2001b; Bieber *et al.* 2002). Poly(ethylenimine) also showed a similar correlation between the size and the transfection efficiency (Turunen *et al.* 1999; Bieber and Elsasser 2001), probably due to the faster dissociation in the smaller polymer-based polyplex systems. Once again, the site of dissociation of gene vectors is still poorly understood.

Another key limiting factor in transfection is an inefficient nuclear entry of pDNA (step 6 in **Figure 1-1**). The size of the nucleus pore complex is approximately 25 nm and 9 nm in outer and inner diameters, respectively (Pante and Aebi 1996). This narrow opening permits transport of relatively small molecules (less than 40 kDa) (Stoffler *et al.* 1999) and is also expected to limit the translocation of pDNA across the nuclear membrane. Nuclear entry of pDNA can be speculated in two ways in the light of the mechanism. A passive pDNA entry into the nucleus is possible during cell division when the nuclear membrane is

temporarily decomposed. Brunner and colleagues (2000) found that cells transfected with lipoplex and polyplex near the M phase (mitosis) (i.e., G2 or late S phase) showed much higher transfection efficiency than when transfected at quiescent cell cycle phases such as G1 or early S phase. These authors also demonstrated that different types of gene vectors showed nonidentical sensitivity toward cell cycle status with regard to transfection efficiency (Brunner *et al.* 2002). Several other investigations suggested that the dependence of nuclear entry on cell division cycle is also cell type specific (Dowty *et al.* 1995; Ludtke *et al.* 2002).

A second type of pDNA nuclear entry can be achieved by coupling of nuclear localization sequence (NLS) containing peptides to pDNA. Short clusters of basic amino acids such as lysine or arginine comprise NLS as shown in **Table 1-1**. These sequences are recognized by cytoplasmic proteins known as karyopherins or importins and form a pore targeting complex (Imamoto 2000). This complex binds to nuclear pore complex to translocate through the pore (Gorlich and Mattaj 1996). As discussed in **Chapter IV**, M9- and SV40-derived NLSs have been applied in the gene delivery field. Pollard and colleagues (1998) suggested the existence of a different nuclear entry mechanisms involved in lipoplex and polyplex systems as evidenced by the findings that polyplex was superior to lipoplex when microinjected to the cytoplasm. Interestingly, other investigators speculate a possibly additional role of endocytosis in the nuclear entry of lipoplex system by transporting pDNA from near the plasma membrane to the perinuclear region (Dowty *et al.* 1995; Cornelis *et al.* 2002).

1.2 Lipoplex

Direct intra-tissue injection of naked pDNA demonstrated gene expression *in vivo* (Wolff *et al.* 1990), however, a reasonable efficiency has been achieved only when this approach was applied through the limited sites of the body such as intramuscular therapy (Rolland and Mumper 1998). Thus, gene therapy still requires vectors when other routes of administration are needed such as intratracheal and intravenous injection. As of January 2007, 8 % of ongoing gene therapy clinical trials were based on lipoplex (<http://www.wiley.co.uk/genetherapy/clinical/>).

Cationic lipids are amphiphilic molecules consisting of a polar headgroup, a linker and a hydrophobic domain. The head groups utilized are quaternary ammonium salt, amine, amidine, guanidium, pyridinium, and more recently developed sugar-based gemini moiety (Johnsson *et al.* 2003). Linker chemistries involve ethers, esters, amides, carbamates, and disulfides. Hydrophobic tail groups usually consist of saturated or unsaturated alkyl chains (12-18 carbons in length) or cholesteryl groups. The effect of these variations on the physicochemical and transfection properties of lipoplexes has been previously reviewed (Zuhorn and Hoekstra 2002). The first successful *in vitro* transfection using cationic lipid was reported by Felgner *et al.* (1987). The replacement of the ether linker of this earlier cationic lipid by ester bonds demonstrated low cytotoxicity. The introduction of protonatable amine groups to the lipoplex was also intended to reduce the side effects of the lipid-based systems and led this formulation to the clinical trial (Caplen *et al.* 1995).

The amine incorporation to the cationic lipid for the lipoplex system was first proposed by Behr and his colleagues (Behr *et al.* 1989). Amine-containing cationic lipids, lipoamines, are known to have pH-buffering functions (Zuidam and Barenholz 1998) and this property may well contribute to the effective transfection efficiency shown by the Lipofectamine[®], one of the most effective transfecting reagent in the market. Lipofectamine[®] is composed of multiamine containing lipid, *N,N*-dimethyl-*N*-[2-(sperminecarboxamido)ethyl]-2,3-bis(dioleyloxy)-1-propaniminium pentahydrochloride, and a neutral helper lipid, 1,2-dioleoyl phosphatidylethanolamine (DOPE). While amines in the head group in Lipofectamine provide strong interaction with DNA along with pH-buffering effect mentioned earlier, it is speculated that DOPE is more responsible for the enhanced transfection efficiency by this lipoplex (Wheeler *et al.* 1996). 1,2-dioleoyl phosphatidylethanolamine was found to favor the formation of inverted hexagonal phases, which provides the fusogenic activity to the endocytosed lipoplex (Koltover *et al.* 1998). A slight excess of positive charges is known to confer a higher transfection efficiency probably due to more efficient interaction with negatively charged cell surface (Sakurai *et al.* 2000). Many studies demonstrated that the cationic lipid-to-DNA charge ratio determines the size of the ensuing structures (e.g., Eastman *et al.* 1997). In terms of transfection efficiency, lipoplexes in a certain range of sizes (0.4-1.4 μm in diameter) have been superior to the smaller or larger ones (Kawaura *et al.* 1998; Ross and Hui 1999).

In vivo application of lipoplexes via intravenous injection, for example, showed high protein expression in the lung (Ishiwata *et al.* 2000) probably due to endothelial accumulation of the systems. Diverting biodistribution of lipoplexes has been attempted in

several ways and include incorporation of synthetic cholic acid analog into the lipoplex (Niedzinski *et al.* 2000), polymerization of cationic acrylamide lipid (Wu *et al.* 2001) and coating with poly(ethylene glycol) (PEG) (Zhang *et al.* 1999; Harvie *et al.* 2000). These approaches demonstrated improved stabilization of lipoplexes in plasma and the PEG coating also allowed improved gene expression in the distal tumors (Anwer *et al.* 2000).

Complexation between cationic lipids and nucleic acids appears a simple mixing. However, the preparation of the lipoplex formulations using aforementioned cationic lipids requires carefully optimized conditions such as concentrations of components, temperature, reaction environment and kinetics of mixing. Any changes or differences in these factors can determine the outcome of gene therapies utilizing lipoplexes. In this context, Gao and Huang (1996) developed an alternative formulation by incorporating small amount of a multivalent cationic polymer such as polylysine or protamine into a lipoplex, so-called LPD, to generate pDNA particles. This system presented superior gene expression efficiency to a conventional lipoplex *in vitro* as well as *in vivo*. Although being less sensitive to the preparational protocols, polyplexes will also need similar formulating optimizations. This subject on polyplexes will be discussed in the following section and is also intensively speculated in the **Chapters III and IV**.

1.3 Polyplex

Compared to cationic lipids, cationic polymers condense DNA more efficiently (Ruponen *et al.* 1999). Cationic polymers are also superior in the macroscopic stabilities such as size and shape over time especially in the dispersed state since polyplex assembly does not entail interactions among the polycations as seen in the case of lipid-based formulation (Simberg *et al.* 2001). Polyplexes rarely need adjuvants and easily manipulated by chemical modification to achieve higher transfection efficiency compared to lipid-containing counterparts (Gebhart and Kabanov 2001). One of the first applications of synthetic cationic polymer in gene delivery can found in 1960's with diethylaminoethyl-modified dextran (Vaehri and Pagano 1965). The polymer-based DNA complex now termed 'polyplex' involves polycations in the formulation.

Polycations include naturally occurring proteins such as histones (Esser *et al.* 2000), cationized human albumin (Fischer *et al.* 2001) as well as polysaccharides such as chitosan and its derivatives. Chitosan consists of glucosamine units having an apparent pKa of 6.5 and has been known to enhance the transport of peptide drugs across the cell membrane (Thanou *et al.* 2001). Chitosan as a gene vector was firstly proposed by Mumper *et al.* (1995) and further characterized by Jane (2001) and Borchard (2001) regarding the effect of molecular weight, DNA or salt concentration, pH of media, and charge ratio on the final size of chitosan-DNA complex. The derivatives of chitosan as gene vectors were also reviewed by Liu and Yao (2002) and include self-aggregating deoxycholic acid conjugates, dodecylated chitosan for improved stability, quaternized derivatives for enhanced solubility, and targeting

ligand conjugates such as galactose- or transferrin-modified chitosans. Chitosan was also the first orally active gene delivery system (Roy *et al.* 1999).

Among synthetic cationic polymers are poly(L-lysine), PEI, polyamidoamine dendrimers, and other polymers such as poly(L-ornithine) (Pouton *et al.* 1998), poly(4-hydroxy-L-proline ester) (Lim *et al.* 1999), polylactide co-glycolide (Cohen *et al.* 2000), and poly(β -aminoester) (Lynn *et al.* 2001). Chemical structures of some representative cationic polymers are shown in **Figure 1-3**.

One of the polycations used for gene delivery in early stage was polylysine. The gene transfer efficiency of polylysine-containing polyplex is relatively poor and most of the polylysine-derived formulations involve cell or tissue specific ligands such as asialoorosomucoid for hepatocellular gene targeting (Wu and Wu 1987) or the addition of endosomolytic agents such as chloroquine (Wadhwa *et al.* 1997). Many of polylysine derivatives entail the conjugation of histidine moiety for endosomal buffering capacity (e.g. Midoux and Monsigny 1999), or incorporation of cysteines for facile DNA release (McKenzie *et al.* 2000a). Polylysine polyplex showed protection of DNA from serum nucleases (Chiou *et al.* 1994) but found to be cleared from the blood rapidly by serum protein opsonization upon the intravenous injection (Dash *et al.* 1999).

One of the most promising polycations up to date is PEI. Since Bousiff and colleagues (1995) introduced its potential versatile efficiency in vitro as well as in vivo, both branched and linear PEI have been utilized as effective tools in delivering of various genes (Boussif *et al.* 1996; Chemin *et al.* 1998). Branched PEI consists of approximately 25, 50 and 25 % of primary, secondary, and tertiary amines, respectively. Primary amines seem to

participate in the complexation with DNA by an electrostatic interaction while secondary and tertiary amines contribute to the endosomal disruption after endocytosis due to their buffering effect. High-molecular-weight (generally higher than 25 kDa) PEI showed enhanced transfection efficiency but increased cytotoxicity (Fischer *et al.* 1999; Godbey *et al.* 1999) while smaller counterparts (less than 1.8 kDa) displayed minimal transfection efficiency with negligible toxicity. In the light of these observations, small version of PEI flanked with PEG linker was developed and used in cellular pDNA delivery (Ahn *et al.* 2002). This strategy demonstrated marginally improved transfection with significantly reduced cytotoxicity. Modification of PEI with PEG has also been used for manipulating in vivo biodistribution of PEI-containing polyplexes (Nguyen *et al.* 2000). Polyethylene oxide conjugate of 25-kDa PEI rendered significantly improved gene expression in mouse liver while lung was the primary organ of gene expression when injected with unmodified PEI-derived polyplex. Poly(ethylene glycol) coating, however, reduced in vitro cellular uptake and transfer of polyplex (Harvie *et al.* 2000). Targeting ligand incorporation to this polymer has shown enhanced transfection in some cell lines (Zanta *et al.* 1997; Ogris *et al.* 2001b).

Various generations (G4-G9) of polyamidoamine dendrimers have been studied as gene delivery systems (Bielinska *et al.* 1997; Du *et al.* 1998). The generation of dendrimer is determined by the number of tertiary amine centers. Surface primary amines of dendrimers contribute to DNA binding and the increase in this terminal amines appears to enhance gene delivery (Toth *et al.* 1999). Similarly to PEI, the internal tertiary amines seem to neutralize acidic pH environment of the endosome after internalization via endocytosis and induce the eventual DNA release into the cytosol (Tang *et al.* 1996). These authors and others (Hudde *et al.* 1999) speculated that the hydrolytic degradation of amide bond in polyamidoamine

dendrimers in aqueous milieu could increase the flexibility of the polymer in the endosome and improved transfection.

1.4 Cleavable Linkers

In the application of cleavable linkers in the gene vectors, it is important that the environment-stimulated response must be sensitive enough to be triggered at the appropriate time and place during the cellular trafficking process to avoid premature or too delayed response. To trigger the linker breakage, cleavable vectors used various stimuli such as decrease in pH, change in redox potential, enzymes, and more recently photosensitivity.

Biological rationale for redox-sensitive lipoplex is that the lipoplex located within the cell is presented with relatively high concentration of reductive substances such as reduced glutathione (Meister and Anderson 1983). The practical application of the redox-sensitive linkers in lipoplexes can found in Tang and Hughes (1998) and Balakirev *et al.* (2000). Dauty and colleagues (2001) used thiol-disulfide reaction to create gemini surfactants from cationic cysteine detergents. Disulfide linkages have been also applied in polyplex systems containing polylysine or PEI (McKenzie *et al.* 2000b; Gosselin *et al.* 2001; Oupicky *et al.* 2001) and more deliberate contemplation on this redox-sensitive linker is conducted in **Chapter II.**

The incorporation of cleavable linkers has been a very promising strategy to improve the therapeutic index of drug-macromolecule conjugates, especially in the field of cancer therapy. For instance, doxorubicin was conjugated to *N*-(2-hydroxypropyl)methacrylamide copolymer through a tetrapeptide linker, Gly-Phe-Leu-Gly. This peptide is known to be susceptible to lysosomal enzymes such as cathepsin B (Putnam and Kopecek 1995; Pechar *et al.* 2000). Preclinical study demonstrated that the level of lysosomal enzyme expression in solid tumors correlated with the activity of this formulation (Loadman *et al.* 1999). Another example of cleavable linker used in drug-macromolecular conjugates is acid-sensitive carboxylic hydrazone bond. Hydrazone derivative of doxorubicin showed improved efficacy with reduced toxicity profile by selectively binding to circulating albumins upon intravenous administration (Mansour *et al.* 2003).

Gene vectors have also adopted cleavable linkers to facilitate the release of their cargos, usually pDNA, under specific environment. The pH in the endosomal compartment is lowered gradually upon endosomal maturation to 5-6 by ATP-dependent proton pumps of endosomal membrane (Mukherjee *et al.* 1997). Thus, the incorporation of pH-sensitive bonds in the lipoplex will destabilize lipoplex structure and release entrapped or bound pDNA. Acid sensitive functionalities applied in lipoplexes include vinyl ethers (Boomer *et al.* 2002), ketal/acetal (Zhu *et al.* 2002), ortho esters (Zhu *et al.* 2000), and hydrazone groups (Aissaoui *et al.* 2004). There are also multiple applications of ester bonds in lipoplexes. The utilization of these hydrolysis-prone bonds was initiated in an attempt to face the cytotoxicity problem encountered in the non-cleavable vector systems. Since Leventis and Silvius (1990) firstly developed hydrolysable ester containing cationic lipid, many studies have applied this

strategy to improve the lipoplex systems (van der Woude *et al.* 1997; Aberle *et al.* 1998). Nagasaki and colleagues (2003) developed photoresponsive cationic lipid. In this study, COS-1 cells transfected with the photosensitive lipoplex was shortly irradiated using UV (365 nm) and these cells showed enhanced transfection efficiency.

In the polyplex systems, biodegradable ester bonds have been utilized in crosslinking low molecular weight polymers as seen in polylysine derivatives by Lim *et al.* (2000). These strategies achieved reduced cytotoxicity but suffer from inferior transfection efficiency. Poor transfection was attributed to too fast a hydrolysis and lack of endosomal escape. In the later study, these authors obtained improved transfection efficiency by using a branched network of amino esters (Lim *et al.* 2002).

1.5 DNA Condensation

One of the tasks gene vectors are expected to perform is compacting DNA into small particles of virus-like dimensions. This compaction will help to protect DNA from its premature degradation before reaching the intracellular target sites such as nucleus. The term ‘condensation’ is sometimes indistinguishably used from aggregation or precipitation. Generally, condensation is limited for the states in which the aggregate forms in more orderly morphology with a finite size (Bloomfield 1996). DNA packaging by virus and chromatin implies the importance of DNA compaction into condensed structures in the field of non-viral gene vector for its success. The condensation of DNA involves the neutralization of

phosphate groups to reduce the repulsion among DNA substructures. Efficient DNA condensation has been represented by a variety of substances including divalent ions (e.g., Mn^{2+} , Ca^{2+} and Mg^{2+}), naturally occurring basic proteins (e.g., histones), neutral polymers such as PEG, alcohols, cationic surfactants, and multivalent cations such as spermine and protamine. Polymeric cations such as polylysine and cationic liposomes also showed DNA condensing capacities (Gustafsson *et al.* 1995; Tang and Szoka 1997).

Melnikov *et al.* (1995) investigated DNA structure change induced by cationic surfactant. This study demonstrated that DNA chains transited from random coil to compact globular state in a discrete manner as the concentration of the surfactant (cetyltrimethylammonium bromide) increased. The self-assembly of DNA has been under intense investigation by several different groups. Blessing and colleagues (1998) developed a cysteine-containing detergent of 10 carbons in a length and demonstrated this cationic surfactant condensed DNA into an individual particle, which were converted to a lipoplex upon air-induced dimerization of the surfactants. Szoka and his colleagues (2000) synthesized a novel cationic surfactant containing an isothiuronium moiety in the headgroup. This moiety was cleaved under basic conditions, which rendered sulfhydryl group exposed to the subsequent oxidation to form a stable DNA complex. This surfactant was also found to possess relatively high critical micelle concentration (> 10 mM), allowing larger amount of DNA complexed in this formulation. Based on this observation, pursuit and application of various cationic surfactants to form fine DNA condensates will be discussed in **Chapter III**. Another noticeable observation in the both aforementioned studies is that the final DNA assemblies had net negative charges. The authors implied that this feature might favor the in

vivo situations due to the probable reduction in the interaction between blood proteins and the formulation, which usually causes the rapid clearance of gene vectors from the systemic circulation.

The effect of the structure of spermine derivatives on the DNA condensation has been elucidated by several groups (e.g., Wilson and Bloomfield 1979; Schellman and Parthasarathy 1984; Vijayanathan *et al.* 2001). These studies report that there is an optimal carbon number in the structure of spermine derivatives (i.e., 4-8 carbons) and DNA compaction is achieved when approximately 90% of the negative charges of DNA are neutralized by multivalent cations.

Protamine has been used as an excellent DNA condenser and proposed to possess nuclear localization sequence-like region (Sorgi *et al.* 1997; Li *et al.* 1998). Recently, the role of protamine in condensing DNA as well as in nuclear transport was intensively investigated by Masuda *et al.* (2005). This study demonstrated that the presence of protamine in the polyplex system indeed increased the access to intra-nuclear transcription.

Representative substances among those discussed above were tested for their capacity in condensing pDNA and the possible application of the pre-condensed pDNA in preparing pDNA-entrapped nanogel formulation was speculated, which is the main context of **Chapter III**.

1.6 Statement of Purpose

Most of the pre-existing gene vectors introduced in the sections **1.2** and **1.3** only partially satisfy the requirements in overcoming multiple transport barriers to the intracellular, nuclear-targeted, gene delivery discussed in the section **1.1**. The present dissertation work was undertaken as an effort to develop a multifunctional polymer-based gene vector that is responding to the different intracellular environment. Chemical modifications of the polymeric nanogel entail incorporating acid-buffering weak bases, redox-sensitive disulfide crosslinkers, and folate targeting ligands to the nanogel. Weak base is expected to promote endosome-to-cytosol translocation of polyplexes by proton sponge effect (see section **1.3**). Disulfide-containing crosslinker should facilitate pDNA release from the nanogel through facilitated breakage of nanogel structure in the intracellular reducing environment as exemplified by the previous gene vector formulations (see section **1.4**). The synthesis and the characterization of the two aforementioned components in the nanogel modification are discussed in **Chapter II**. Incorporation of folic acid ligand renders the nanogel containing pDNA binding to the cell in a specific manner. The synthetic strategy to graft nanogel with a folate ligand is shown in **Chapter IV**.

Chapter III and **IV** are concerned with two different pDNA-nanogel formulations. Conventional polyplex systems usually utilize an electrostatic interaction between pre-made cationic polymers and polyanionic pDNA. An alternative formulation suggested in the present dissertation is to literally entrap pDNA inside the nanogel matrix. It could provide additional advantages such as an enhanced protection of pDNA from premature degradation

by nucleases *in vivo*, a reduced cytotoxicity that is usually caused by the extra positive charges of polyplex systems, and improved physical stability as a pharmaceutical formulation. Thus, the entrapment formulation is intensively explored in **Chapter III**. In this chapter, several condensation reagents among those introduced in the section **1.5** are utilized to reduce the hydrodynamic diameter of pDNA prior to the entrapment and consequently to increase entrapment efficiency. In this context, **Chapter IV** deals with a second pDNA-nanogel formulation, i.e., a complexation of pDNA with the pre-made targeted cationic nanogel. Here, folate-grafted nanogels complexed with luciferase-expressing pDNA at certain N/P (amine-to-phosphate or positive-to-negative) ratios are treated to the folate receptor-overexpressing cell. Luciferase protein expression is then monitored as a measure of the gene delivery efficiency of a given test formulations, in comparison with commercial transfection reagents such as Lipofectamine[®] 2000 and poly(ethylenimine).

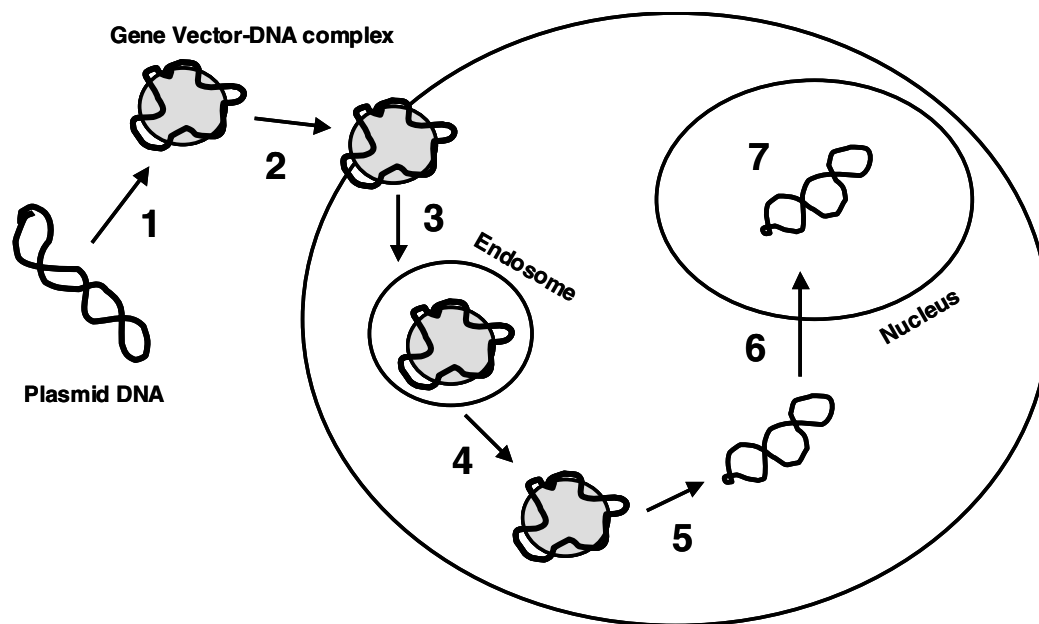


Figure 1-1: Various transport barriers involved in gene delivery: **1**, formation of plasmid DNA (pDNA)-vector complex; **2**, cellular binding of pDNA-vector complex; **3**, cellular uptake via endocytosis; **4**, endosome-to-cytosol translocation (endosomal escape); **5**, dissociation of pDNA-vector complex (release of pDNA from the vector); **6**, trafficking of pDNA through the cytosol and nuclear entry; and **7**, transcription in the nucleus.

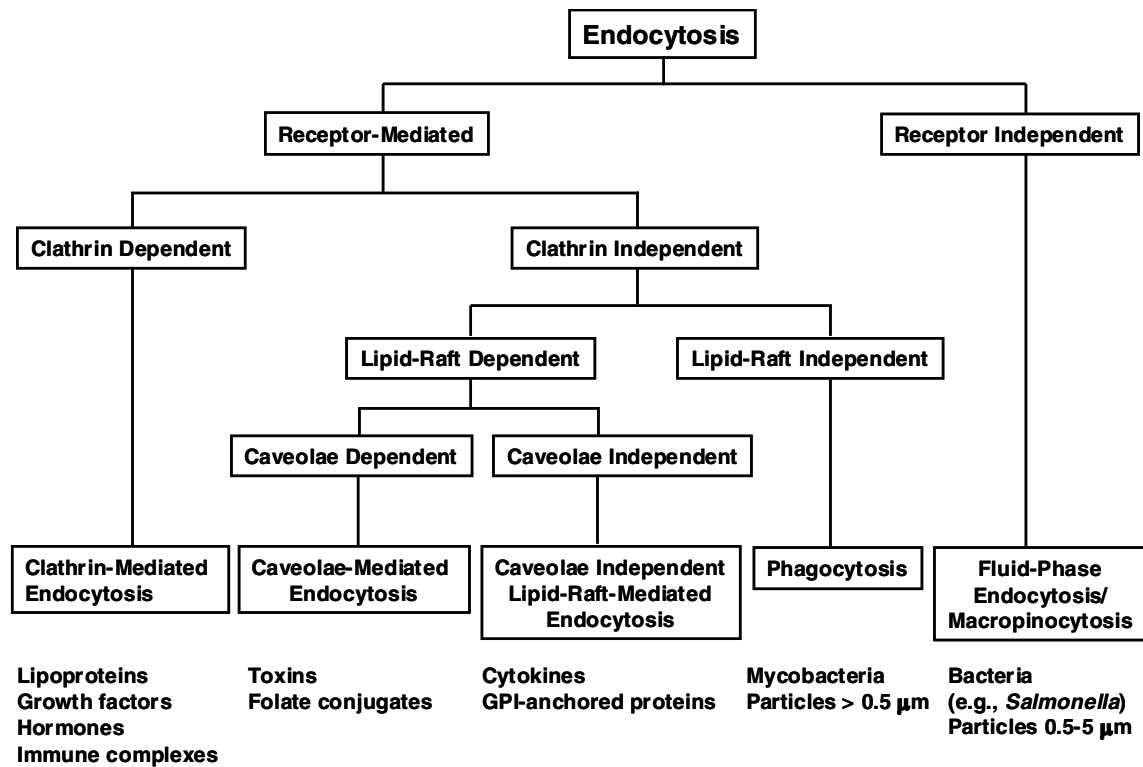


Figure 1-2: Various endocytosis pathways as proposed from Xiang *et al.* (2006). Some examples of each pathway are presented.

Table 1-1: Nuclear Localization Sequences (NLS)^a

Type	Source	Sequence
Monopartite NLS	SV40 T Antigen	PKKKRKV
	SV40 Vp3	KKKRRK
	Adenovirus E1a	KRPRP
	Human <i>c-myc</i>	PAAKRVKLD, RQRRNELKRSP
Bipartite NLS	Nucleoplasmin	KRPAATKKAGQAKKKK
	<i>Xenopus</i> N1	VRKKRKTEESPLKDKDAKKSKQE
	Mouse FGF3	RLRRDAGGRGGVYEHLLGGAPRRRK
	PARP	KRKGDEVLDGVDECAKKSCK
Nonclassical NLS	M9 of hnRNP A1	NQSSNFGPMKGGNFGGRSSGPYGGGGQYFAKPRNQGGY

^a; reproduced from Martin and Rice (2007). Monopartite and bipartite contain one and two clusters of basic amino acids, respectively. The abbreviations used represent the followings: SV, simian virus; FGF3, fibroblast growth factor 3; PARP, poly (ADP-ribose) polymerase; and hnRNP, heterogeneous nuclear ribonucleoprotein.

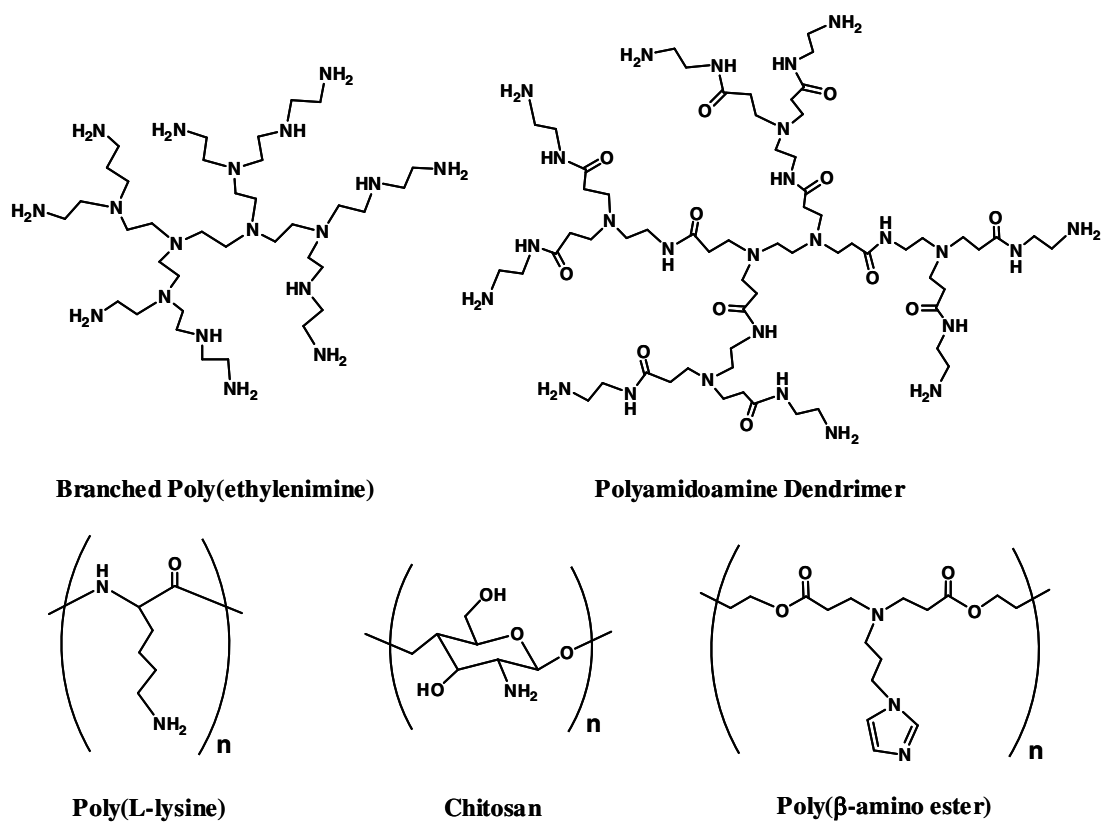


Figure 1-3: Structures of some representative polymers used in polyplex systems.

1.7 References

- Aberle A.M., Tablin F., Zhu J., Walker N.J., Gruenert D.C. and Nantz M.H. (1998). "A novel tetraester construct that reduces cationic lipid-associated cytotoxicity. Implications for the onset of cytotoxicity." *Biochemistry* 37 (18): 6533-40.
- Aderem A. and Underhill D.M. (1999). "Mechanisms of phagocytosis in macrophages." *Annu Rev Immunol* 17: 593-623.
- Ahn C.H., Chae S.Y., Bae Y.H. and Kim S.W. (2002). "Biodegradable poly(ethylenimine) for plasmid DNA delivery." *J Control Release* 80 (1-3): 273-82.
- Aissaoui A., Martin B., Kan E., Oudrhiri N., Hauchecorne M., Vigneron J.P., Lehn J.M. and Lehn P. (2004). "Novel cationic lipids incorporating an acid-sensitive acylhydrazone linker: synthesis and transfection properties." *J Med Chem* 47 (21): 5210-23.
- Allavena P., Chieppa M., Monti P. and Piemonti L. (2004). "From pattern recognition receptor to regulator of homeostasis: the double-faced macrophage mannose receptor." *Crit Rev Immunol* 24 (3): 179-92.
- Anwer K., Kao G., Proctor B., Rolland A. and Sullivan S. (2000). "Optimization of cationic lipid/DNA complexes for systemic gene transfer to tumor lesions." *J Drug Target* 8 (2): 125-35.
- Baeuerle P.A. and Huttner W.B. (1986). "Chlorate--a potent inhibitor of protein sulfation in intact cells." *Biochem Biophys Res Commun* 141 (2): 870-7.
- Balakirev M., Schoehn G. and Chroboczek J. (2000). "Lipoic acid-derived amphiphiles for redox-controlled DNA delivery." *Chem Biol* 7 (10): 813-9.
- Barron L.G. and Szoka Jr F.C. (1999). The perplexing delivery mechanism of lipoplexes. In: Nonviral Vectors for Gene Therapy. Huang L., Hung M. C. and Wagner E., Academic Press: San Diego.: pp 229-266.
- Behr J.P., Demeneix B., Loeffler J.P. and Perez-Mutul J. (1989). "Efficient gene transfer into mammalian primary endocrine cells with lipopolyamine-coated DNA." *Proc Natl Acad Sci U S A* 86 (18): 6982-6.
- Bieber T. and Elsasser H.P. (2001). "Preparation of a low molecular weight polyethylenimine for efficient cell transfection." *Biotechniques* 30 (1): 74-7, 80-1.
- Bieber T., Meissner W., Kostin S., Niemann A. and Elsasser H.P. (2002). "Intracellular route and transcriptional competence of polyethylenimine-DNA complexes." *J Control Release* 82 (2-3): 441-54.

- Bielinska A.U., Kukowska-Latallo J.F. and Baker J.R., Jr. (1997). "The interaction of plasmid DNA with polyamidoamine dendrimers: mechanism of complex formation and analysis of alterations induced in nuclease sensitivity and transcriptional activity of the complexed DNA." *Biochim Biophys Acta* 1353 (2): 180-90.
- Blessing T., Remy J.S. and Behr J.P. (1998). "Monomolecular collapse of plasmid DNA into stable virus-like particles." *Proc Natl Acad Sci U S A* 95 (4): 1427-31.
- Bloomfield V.A. (1996). "DNA condensation." *Curr Opin Struct Biol* 6 (3): 334-41.
- Boomer J.A., Thompson D.H. and Sullivan S.M. (2002). "Formation of plasmid-based transfection complexes with an acid-labile cationic lipid: characterization of in vitro and in vivo gene transfer." *Pharm Res* 19 (9): 1292-301.
- Borchard G. (2001). "Chitosans for gene delivery." *Adv Drug Deliv Rev* 52 (2): 145-50.
- Boussif O., Lezoualc'h F., Zanta M.A., Mergny M.D., Scherman D., Demeneix B. and Behr J.P. (1995). "A versatile vector for gene and oligonucleotide transfer into cells in culture and in vivo: polyethylenimine." *Proc Natl Acad Sci U S A* 92 (16): 7297-301.
- Boussif O., Zanta M.A. and Behr J.P. (1996). "Optimized galenics improve in vitro gene transfer with cationic molecules up to 1000-fold." *Gene Ther* 3 (12): 1074-80.
- Brunner S., Furtbauer E., Sauer T., Kursa M. and Wagner E. (2002). "Overcoming the nuclear barrier: cell cycle independent nonviral gene transfer with linear polyethylenimine or electroporation." *Mol Ther* 5 (1): 80-6.
- Brunner S., Sauer T., Carotta S., Cotten M., Saltik M. and Wagner E. (2000). "Cell cycle dependence of gene transfer by lipoplex, polyplex and recombinant adenovirus." *Gene Ther* 7 (5): 401-7.
- Caplen N.J., Alton E.W., Middleton P.G., Dorin J.R., Stevenson B.J., Gao X., Durham S.R., Jeffery P.K., Hodson M.E., Coutelle C. and et al. (1995). "Liposome-mediated CFTR gene transfer to the nasal epithelium of patients with cystic fibrosis." *Nat Med* 1 (1): 39-46.
- Chemin I., Moradpour D., Wieland S., Offensperger W.B., Walter E., Behr J.P. and Blum H.E. (1998). "Liver-directed gene transfer: a linear polyethylenimine derivative mediates highly efficient DNA delivery to primary hepatocytes in vitro and in vivo." *J Viral Hepat* 5 (6): 369-75.
- Chen J., Stickles R.J. and Daichendt K.A. (1994). "Galactosylated histone-mediated gene transfer and expression." *Hum Gene Ther* 5 (4): 429-35.
- Chiou H.C., Tangco M.V., Levine S.M., Robertson D., Kormis K., Wu C.H. and Wu G.Y. (1994). "Enhanced Resistance to Nuclease Degradation of Nucleic-Acids Complexed to Asialoglycoprotein-Polylysine Carriers." *Nucleic Acids Research* 22 (24): 5439-5446.

- Cohen A.W., Hnasko R., Schubert W. and Lisanti M.P. (2004). "Role of caveolae and caveolins in health and disease." *Physiol Rev* 84 (4): 1341-79.
- Cohen H., Levy R.J., Gao J., Fishbein I., Kousaev V., Sosnowski S., Slomkowski S. and Golomb G. (2000). "Sustained delivery and expression of DNA encapsulated in polymeric nanoparticles." *Gene Ther* 7 (22): 1896-905.
- Conner S.D. and Schmid S.L. (2003). "Regulated portals of entry into the cell." *Nature* 422 (6927): 37-44.
- Cornelis S., Vandenbranden M., Ruyschaert J.M. and Elouahabi A. (2002). "Role of intracellular cationic liposome-DNA complex dissociation in transfection mediated by cationic lipids." *DNA Cell Biol* 21 (2): 91-7.
- Culver K.W., Ram Z., Wallbridge S., Ishii H., Oldfield E.H. and Blaese R.M. (1992). "In vivo gene transfer with retroviral vector-producer cells for treatment of experimental brain tumors." *Science* 256 (5063): 1550-2.
- Dash P.R., Read M.L., Barrett L.B., Wolfert M.A. and Seymour L.W. (1999). "Factors affecting blood clearance and in vivo distribution of polyelectrolyte complexes for gene delivery." *Gene Ther* 6 (4): 643-50.
- Dauty E., Remy J.S., Blessing T. and Behr J.P. (2001). "Dimerizable cationic detergents with a low cmc condense plasmid DNA into nanometric particles and transfect cells in culture." *J Am Chem Soc* 123 (38): 9227-34.
- Dowty M.E., Williams P., Zhang G., Hagstrom J.E. and Wolff J.A. (1995). "Plasmid DNA entry into postmitotic nuclei of primary rat myotubes." *Proc Natl Acad Sci U S A* 92 (10): 4572-6.
- Du B., Zhou R.J. and Zhuo R.X. (1998). "Synthesis of cyclic core dendritic polymer and its usage as a vector for transferring foreign DNA into human cells." *Chinese Chemical Letters* 9 (7): 635-638.
- Eastman S.J., Siegel C., Tousignant J., Smith A.E., Cheng S.H. and Scheule R.K. (1997). "Biophysical characterization of cationic lipid: DNA complexes." *Biochim Biophys Acta* 1325 (1): 41-62.
- Eguchi A., Akuta T., Okuyama H., Senda T., Yokoi H., Inokuchi H., Fujita S., Hayakawa T., Takeda K., Hasegawa M. and Nakanishi M. (2001). "Protein transduction domain of HIV-1 Tat protein promotes efficient delivery of DNA into mammalian cells." *J Biol Chem* 276 (28): 26204-10.
- El Ouahabi A., Thiry M., Schiffmann S., Fuks R., Nguyen-Tran H., Ruyschaert J.M. and Vandenbranden M. (1999). "Intracellular visualization of BrdU-labeled plasmid DNA/cationic liposome complexes." *J Histochem Cytochem* 47 (9): 1159-66.

- Esser D., Amanuma H., Yoshiki A., Kusakabe M., Rudolph R. and Bohm G. (2000). "A hyperthermostable bacterial histone-like protein as an efficient mediator for transfection of eukaryotic cells." *Nat Biotechnol* 18 (11): 1211-3.
- Farhood H., Serbina N. and Huang L. (1995). "The role of dioleoyl phosphatidylethanolamine in cationic liposome mediated gene transfer." *Biochim Biophys Acta* 1235 (2): 289-95.
- Felgner P.L., Gadek T.R., Holm M., Roman R., Chan H.W., Wenz M., Northrop J.P., Ringold G.M. and Danielsen M. (1987). "Lipofection: a highly efficient, lipid-mediated DNA-transfection procedure." *Proc Natl Acad Sci U S A* 84 (21): 7413-7.
- Fischer D., Bieber T., Brusselbach S., Elsasser H. and Kissel T. (2001). "Cationized human serum albumin as a non-viral vector system for gene delivery? Characterization of complex formation with plasmid DNA and transfection efficiency." *Int J Pharm* 225 (1-2): 97-111.
- Fischer D., Bieber T., Li Y., Elsasser H.P. and Kissel T. (1999). "A novel non-viral vector for DNA delivery based on low molecular weight, branched polyethylenimine: effect of molecular weight on transfection efficiency and cytotoxicity." *Pharm Res* 16 (8): 1273-9.
- Fisher K.J. and Wilson J.M. (1997). "The transmembrane domain of diphtheria toxin improves molecular conjugate gene transfer." *Biochem J* 321 (Pt 1): 49-58.
- Fujimoto T., Kogo H., Nomura R. and Une T. (2000). "Isoforms of caveolin-1 and caveolar structure." *J Cell Sci* 113 Pt 19: 3509-17.
- Gao X. and Huang L. (1996). "Potentiation of cationic liposome-mediated gene delivery by polycations." *Biochemistry* 35 (3): 1027-36.
- Gebhart C.L. and Kabanov A.V. (2001). "Evaluation of polyplexes as gene transfer agents." *J Control Release* 73 (2-3): 401-16.
- Godbey W.T., Barry M.A., Saggau P., Wu K.K. and Mikos A.G. (2000). "Poly(ethylenimine)-mediated transfection: a new paradigm for gene delivery." *J Biomed Mater Res* 51 (3): 321-8.
- Godbey W.T., Wu K.K. and Mikos A.G. (1999). "Size matters: molecular weight affects the efficiency of poly(ethylenimine) as a gene delivery vehicle." *J Biomed Mater Res* 45 (3): 268-75.
- Goncalves C., Mennesson E., Fuchs R., Gorvel J.P., Midoux P. and Pichon C. (2004). "Macropinocytosis of polyplexes and recycling of plasmid via the clathrin-dependent pathway impair the transfection efficiency of human hepatocarcinoma cells." *Mol Ther* 10 (2): 373-85.

- Gorlich D. and Mattaj I.W. (1996). "Nucleocytoplasmic transport." *Science* 271 (5255): 1513-8.
- Gosselin M.A., Guo W. and Lee R.J. (2001). "Efficient gene transfer using reversibly cross-linked low molecular weight polyethylenimine." *Bioconjug Chem* 12 (6): 989-94.
- Grimmer S., van Deurs B. and Sandvig K. (2002). "Membrane ruffling and macropinocytosis in A431 cells require cholesterol." *J Cell Sci* 115 (Pt 14): 2953-62.
- Guang Liu W. and De Yao K. (2002). "Chitosan and its derivatives--a promising non-viral vector for gene transfection." *J Control Release* 83 (1): 1-11.
- Gunzburg W.H. and Salmons B. (1996). "Development of retroviral vectors as safe, targeted gene delivery systems." *J Mol Med* 74 (4): 171-82.
- Gustafsson J., Arvidson G., Karlsson G. and Almgren M. (1995). "Complexes between cationic liposomes and DNA visualized by cryo-TEM." *Biochim Biophys Acta* 1235 (2): 305-12.
- Haensler J. and Szoka F.C., Jr. (1993). "Polyamidoamine cascade polymers mediate efficient transfection of cells in culture." *Bioconjug Chem* 4 (5): 372-9.
- Hamm-Alvarez S.F. (1998). "Molecular motors and their role in membrane traffic." *Adv Drug Deliv Rev* 29 (3): 229-242.
- Hardingham T.E. and Fosang A.J. (1992). "Proteoglycans: many forms and many functions." *FASEB J* 6 (3): 861-70.
- Harvie P., Dutzar B., Galbraith T., Cudmore S., O'Mahony D., Anklesaria P. and Paul R. (2003). "Targeting of lipid-protamine-DNA (LPD) lipopolyplexes using RGD motifs." *J Liposome Res* 13 (3-4): 231-47.
- Harvie P., Wong F.M. and Bally M.B. (2000). "Use of poly(ethylene glycol)-lipid conjugates to regulate the surface attributes and transfection activity of lipid-DNA particles." *J Pharm Sci* 89 (5): 652-63.
- Hommelgaard A.M., Roepstorff K., Vilhardt F., Torgersen M.L., Sandvig K. and van Deurs B. (2005). "Caveolae: stable membrane domains with a potential for internalization." *Traffic* 6 (9): 720-4.
- Huckett B., Ariatti M. and Hawtrey A.O. (1990). "Evidence for targeted gene transfer by receptor-mediated endocytosis. Stable expression following insulin-directed entry of NEO into HepG2 cells." *Biochem Pharmacol* 40 (2): 253-63.
- Hudde T., Rayner S.A., Comer R.M., Weber M., Isaacs J.D., Waldmann H., Larkin D.F. and George A.J. (1999). "Activated polyamidoamine dendrimers, a non-viral vector for gene transfer to the corneal endothelium." *Gene Ther* 6 (5): 939-43.

- Imamoto N. (2000). "Diversity in nucleocytoplasmic transport pathways." *Cell Struct Funct* 25 (4): 207-16.
- Ishiwata H., Suzuki N., Ando S., Kikuchi H. and Kitagawa T. (2000). "Characteristics and biodistribution of cationic liposomes and their DNA complexes." *J Control Release* 69 (1): 139-48.
- Janes K.A., Calvo P. and Alonso M.J. (2001). "Polysaccharide colloidal particles as delivery systems for macromolecules." *Adv Drug Deliv Rev* 47 (1): 83-97.
- Johnsson M., Wagenaar A. and Engberts J.B. (2003). "Sugar-based gemini surfactant with a vesicle-to-micelle transition at acidic pH and a reversible vesicle flocculation near neutral pH." *J Am Chem Soc* 125 (3): 757-60.
- Kasahara N., Dozy A.M. and Kan Y.W. (1994). "Tissue-specific targeting of retroviral vectors through ligand-receptor interactions." *Science* 266 (5189): 1373-6.
- Kawaura C., Noguchi A., Furuno T. and Nakanishi M. (1998). "Atomic force microscopy for studying gene transfection mediated by cationic liposomes with a cationic cholesterol derivative." *FEBS Lett* 421 (1): 69-72.
- Kircheis R., Kichler A., Wallner G., Kursa M., Ogris M., Felzmann T., Buchberger M. and Wagner E. (1997). "Coupling of cell-binding ligands to polyethylenimine for targeted gene delivery." *Gene Ther* 4 (5): 409-18.
- Klasse P.J., Bron R. and Marsh M. (1998). "Mechanisms of enveloped virus entry into animal cells." *Adv Drug Deliv Rev* 34 (1): 65-91.
- Koltover I., Salditt T., Radler J.O. and Safinya C.R. (1998). "An inverted hexagonal phase of cationic liposome-DNA complexes related to DNA release and delivery." *Science* 281 (5373): 78-81.
- Lamaze C., Dujancourt A., Baba T., Lo C.G., Benmerah A. and Dautry-Varsat A. (2001). "Interleukin 2 receptors and detergent-resistant membrane domains define a clathrin-independent endocytic pathway." *Mol Cell* 7 (3): 661-71.
- Le P.U., Guay G., Altschuler Y. and Nabi I.R. (2002). "Caveolin-1 is a negative regulator of caveolae-mediated endocytosis to the endoplasmic reticulum." *J Biol Chem* 277 (5): 3371-9.
- Lee R.J. and Huang L. (1996). "Folate-targeted, anionic liposome-entrapped polylysine-condensed DNA for tumor cell-specific gene transfer." *J Biol Chem* 271 (14): 8481-7.
- Leventis R. and Silvius J.R. (1990). "Interactions of mammalian cells with lipid dispersions containing novel metabolizable cationic amphiphiles." *Biochim Biophys Acta* 1023 (1): 124-32.

- Li S., Rizzo M.A., Bhattacharya S. and Huang L. (1998). "Characterization of cationic lipid-protamine-DNA (LPD) complexes for intravenous gene delivery." *Gene Ther* 5 (7): 930-7.
- Lim Y.B., Choi Y.H. and Park J.S. (1999). "A self-destroying polycationic polymer: Biodegradable poly(4-hydroxy-L-proline ester)." *J Am Chem Soc* 121 (24): 5633-5639.
- Lim Y.B., Han S.O., Kong H.U., Lee Y., Park J.S., Jeong B. and Kim S.W. (2000). "Biodegradable polyester, poly[alpha-(4-aminobutyl)-L-glycolic acid], as a non-toxic gene carrier." *Pharm Res* 17 (7): 811-6.
- Lim Y.B., Kim S.M., Suh H. and Park J.S. (2002). "Biodegradable, endosome disruptive, and cationic network-type polymer as a highly efficient and nontoxic gene delivery carrier." *Bioconjug Chem* 13 (5): 952-7.
- Loadman P.M., Bibby M.C., Double J.A., Al-Shakhaa W.M. and Duncan R. (1999). "Pharmacokinetics of PK1 and doxorubicin in experimental colon tumor models with differing responses to PK1." *Clin Cancer Res* 5 (11): 3682-8.
- Luby-Phelps K., Castle P.E., Taylor D.L. and Lanni F. (1987). "Hindered diffusion of inert tracer particles in the cytoplasm of mouse 3T3 cells." *Proc Natl Acad Sci U S A* 84 (14): 4910-3.
- Ludtke J.J., Sebestyen M.G. and Wolff J.A. (2002). "The effect of cell division on the cellular dynamics of microinjected DNA and dextran." *Mol Ther* 5 (5 Pt 1): 579-88.
- Lukacs G.L., Haggie P., Seksek O., Lechardeur D., Freedman N. and Verkman A.S. (2000). "Size-dependent DNA mobility in cytoplasm and nucleus." *J Biol Chem* 275 (3): 1625-9.
- Luzio J.P., Mullock B.M., Pryor P.R., Lindsay M.R., James D.E. and Piper R.C. (2001). "Relationship between endosomes and lysosomes." *Biochem Soc Trans* 29 (Pt 4): 476-80.
- Lynn D.M., Anderson D.G., Putnam D. and Langer R. (2001). "Accelerated discovery of synthetic transfection vectors: parallel synthesis and screening of a degradable polymer library." *J Am Chem Soc* 123 (33): 8155-6.
- Mansour A.M., Dreves J., Esser N., Hamada F.M., Badary O.A., Unger C., Fichtner I. and Kratz F. (2003). "A new approach for the treatment of malignant melanoma: enhanced antitumor efficacy of an albumin-binding doxorubicin prodrug that is cleaved by matrix metalloproteinase 2." *Cancer Res* 63 (14): 4062-6.
- Marshall E. (1999). "Gene therapy death prompts review of adenovirus vector." *Science* 286 (5448): 2244-5.
- Martin M.E. and Rice K.G. (2007). "Peptide-guided gene delivery." *AAPS J* 9 (1): E18-29.

- Masuda T., Akita H. and Harashima H. (2005). "Evaluation of nuclear transfer and transcription of plasmid DNA condensed with protamine by microinjection: the use of a nuclear transfer score." *FEBS Lett* 579 (10): 2143-8.
- McKenzie D.L., Kwok K.Y. and Rice K.G. (2000a). "A potent new class of reductively activated peptide gene delivery agents." *J Biol Chem* 275 (14): 9970-7.
- McKenzie D.L., Smiley E., Kwok K.Y. and Rice K.G. (2000b). "Low molecular weight disulfide cross-linking peptides as nonviral gene delivery carriers." *Bioconjug Chem* 11 (6): 901-9.
- Medina-Kauwe L.K., Maguire M., Kasahara N. and Kedes L. (2001). "Nonviral gene delivery to human breast cancer cells by targeted Ad5 penton proteins." *Gene Ther* 8 (23): 1753-61.
- Meister A. and Anderson M.E. (1983). "Glutathione." *Annu Rev Biochem* 52: 711-60.
- Melnikov S.M., Sergeyev V.G. and Yoshikawa K. (1995). "Transition of Double-Stranded DNA Chains between Random Coil and Compact Globule States Induced by Cooperative Binding of Cationic Surfactant." *J Am Chem Soc* 117 (40): 9951-9956.
- Merdan T., Kunath K., Fischer D., Kopecek J. and Kissel T. (2002). "Intracellular processing of poly(ethylene imine)/ribozyme complexes can be observed in living cells by using confocal laser scanning microscopy and inhibitor experiments." *Pharm Res* 19 (2): 140-6.
- Merwin J.R., Carmichael E.P., Noell G.S., DeRome M.E., Thomas W.L., Robert N., Spitalny G. and Chiou H.C. (1995). "CD5-mediated specific delivery of DNA to T lymphocytes: compartmentalization augmented by adenovirus." *J Immunol Methods* 186 (2): 257-66.
- Midoux P. and Monsigny M. (1999). "Efficient gene transfer by histidylated polylysine/pDNA complexes." *Bioconjug Chem* 10 (3): 406-11.
- Mislick K.A. and Baldeschwieler J.D. (1996). "Evidence for the role of proteoglycans in cation-mediated gene transfer." *Proc Natl Acad Sci U S A* 93 (22): 12349-54.
- Mok K.W. and Cullis P.R. (1997). "Structural and fusogenic properties of cationic liposomes in the presence of plasmid DNA." *Biophys J* 73 (5): 2534-45.
- Mounkes L.C., Zhong W., Cipres-Palacin G., Heath T.D. and Debs R.J. (1998). "Proteoglycans mediate cationic liposome-DNA complex-based gene delivery in vitro and in vivo." *J Biol Chem* 273 (40): 26164-70.
- Mukherjee S., Ghosh R.N. and Maxfield F.R. (1997). "Endocytosis." *Physiol Rev* 77 (3): 759-803.

- Mumper R.J., Wang J.J., Claspell J.M. and Rolland A.P. (1995). "Novel polymeric condensing carriers for gene delivery." *Proc. Intl. Symp. Controlled Rel. Bioact. Mater.* 22: 178-179.
- Nagasaki T., Taniguchi A. and Tamagaki S. (2003). "Photoenhancement of transfection efficiency using novel cationic lipids having a photocleavable spacer." *Bioconjug Chem* 14 (3): 513-6.
- Nguyen H.K., Lemieux P., Vinogradov S.V., Gebhart C.L., Guerin N., Paradis G., Bronich T.K., Alakhov V.Y. and Kabanov A.V. (2000). "Evaluation of polyether-polyethyleneimine graft copolymers as gene transfer agents." *Gene Ther* 7 (2): 126-38.
- Niedergang F. and Chavrier P. (2004). "Signaling and membrane dynamics during phagocytosis: many roads lead to the phagos(R)ome." *Curr Opin Cell Biol* 16 (4): 422-8.
- Niedzinski E.J., Bennett M.J., Olson D.C. and Nantz M.H. (2000). "Gastroprotection of DNA with a synthetic cholic acid analog." *Lipids* 35 (7): 721-7.
- Ogris M., Carlisle R.C., Bettinger T. and Seymour L.W. (2001a). "Melittin enables efficient vesicular escape and enhanced nuclear access of nonviral gene delivery vectors." *J Biol Chem* 276 (50): 47550-5.
- Ogris M., Steinlein P., Carotta S., Brunner S. and Wagner E. (2001b). "DNA/polyethylenimine transfection particles: influence of ligands, polymer size, and PEGylation on internalization and gene expression." *AAPS PharmSci* 3 (3): E21.
- Oupicky D., Carlisle R.C. and Seymour L.W. (2001). "Triggered intracellular activation of disulfide crosslinked polyelectrolyte gene delivery complexes with extended systemic circulation in vivo." *Gene Ther* 8 (9): 713-24.
- Ouyang M., Remy J.S. and Szoka F.C., Jr. (2000). "Controlled template-assisted assembly of plasmid DNA into nanometric particles with high DNA concentration." *Bioconjug Chem* 11 (1): 104-12.
- Pante N. and Aeby U. (1996). "Molecular dissection of the nuclear pore complex." *Crit Rev Biochem Mol Biol* 31 (2): 153-99.
- Pechar M., Ulbrich K., Subr V., Seymour L.W. and Schacht E.H. (2000). "Poly(ethylene glycol) multiblock copolymer as a carrier of anti-cancer drug doxorubicin." *Bioconjug Chem* 11 (2): 131-9.
- Pelkmans L. and Helenius A. (2002). "Endocytosis via caveolae." *Traffic* 3 (5): 311-20.
- Phillips S.C. (1995). "Receptor-mediated DNA delivery approaches to human gene therapy." *Biologicals* 23 (1): 13-6.

- Pollard H., Remy J.S., Loussouarn G., Demolombe S., Behr J.P. and Escande D. (1998). "Polyethylenimine but not cationic lipids promotes transgene delivery to the nucleus in mammalian cells." *J Biol Chem* 273 (13): 7507-11.
- Pouton C.W., Lucas P., Thomas B.J., Uduchi A.N., Milroy D.A. and Moss S.H. (1998). "Polycation-DNA complexes for gene delivery: a comparison of the biopharmaceutical properties of cationic polypeptides and cationic lipids." *J Control Release* 53 (1-3): 289-99.
- Putnam D. and Kopecek J. (1995). "Enantioselective release of 5-fluorouracil from N-(2-hydroxypropyl)methacrylamide-based copolymers via lysosomal enzymes." *Bioconjug Chem* 6 (4): 483-92.
- Rejman J., Oberle V., Zuhorn I.S. and Hoekstra D. (2004). "Size-dependent internalization of particles via the pathways of clathrin- and caveolae-mediated endocytosis." *Biochem J* 377 (Pt 1): 159-69.
- Rolland A.P. and Mumper R.J. (1998). "Plasmid delivery to muscle: Recent advances in polymer delivery systems." *Adv Drug Deliv Rev* 30 (1-3): 151-172.
- Ross P.C. and Hui S.W. (1999). "Lipoplex size is a major determinant of in vitro lipofection efficiency." *Gene Ther* 6 (4): 651-9.
- Roy K., Mao H.Q., Huang S.K. and Leong K.W. (1999). "Oral gene delivery with chitosan--DNA nanoparticles generates immunologic protection in a murine model of peanut allergy." *Nat Med* 5 (4): 387-91.
- Ruponen M., Yla-Herttuala S. and Urtti A. (1999). "Interactions of polymeric and liposomal gene delivery systems with extracellular glycosaminoglycans: physicochemical and transfection studies." *Biochim Biophys Acta* 1415 (2): 331-41.
- Sabharanjak S., Sharma P., Parton R.G. and Mayor S. (2002). "GPI-anchored proteins are delivered to recycling endosomes via a distinct cdc42-regulated, clathrin-independent pinocytic pathway." *Dev Cell* 2 (4): 411-23.
- Sakurai F., Inoue R., Nishino Y., Okuda A., Matsumoto O., Taga T., Yamashita F., Takakura Y. and Hashida M. (2000). "Effect of DNA/liposome mixing ratio on the physicochemical characteristics, cellular uptake and intracellular trafficking of plasmid DNA/cationic liposome complexes and subsequent gene expression." *J Control Release* 66 (2-3): 255-69.
- Schaffer D.V., Fidelman N.A., Dan N. and Lauffenburger D.A. (2000). "Vector unpacking as a potential barrier for receptor-mediated polyplex gene delivery." *Biotechnol Bioeng* 67 (5): 598-606.
- Schellman J.A. and Parthasarathy N. (1984). "X-Ray-Diffraction Studies on Cation-Collapsed DNA." *Journal of Molecular Biology* 175 (3): 313-329.

- Simberg D., Danino D., Talmon Y., Minsky A., Ferrari M.E., Wheeler C.J. and Barenholz Y. (2001). "Phase behavior, DNA ordering, and size instability of cationic lipoplexes. Relevance to optimal transfection activity." *J Biol Chem* 276 (50): 47453-9.
- Simoes S., Slepishkin V., Pires P., Gaspar R., de Lima M.P. and Duzgunes N. (1999). "Mechanisms of gene transfer mediated by lipoplexes associated with targeting ligands or pH-sensitive peptides." *Gene Ther* 6 (11): 1798-807.
- Sonawane N.D., Szoka F.C., Jr. and Verkman A.S. (2003). "Chloride accumulation and swelling in endosomes enhances DNA transfer by polyamine-DNA polyplexes." *J Biol Chem* 278 (45): 44826-31.
- Sorgi F.L., Bhattacharya S. and Huang L. (1997). "Protamine sulfate enhances lipid-mediated gene transfer." *Gene Ther* 4 (9): 961-8.
- Sosnowski B.A., Gonzalez A.M., Chandler L.A., Buechler Y.J., Pierce G.F. and Baird A. (1996). "Targeting DNA to cells with basic fibroblast growth factor (FGF2)." *J Biol Chem* 271 (52): 33647-53.
- Stoffler D., Fahrenkrog B. and Aepli U. (1999). "The nuclear pore complex: from molecular architecture to functional dynamics." *Curr Opin Cell Biol* 11 (3): 391-401.
- Swanson J.A. and Baer S.C. (1995). "Phagocytosis by zippers and triggers." *Trends Cell Biol* 5 (3): 89-93.
- Tang F. and Hughes J.A. (1998). "Introduction of a disulfide bond into a cationic lipid enhances transgene expression of plasmid DNA." *Biochem Biophys Res Commun* 242 (1): 141-5.
- Tang M.X., Redemann C.T. and Szoka F.C., Jr. (1996). "In vitro gene delivery by degraded polyamidoamine dendrimers." *Bioconjug Chem* 7 (6): 703-14.
- Tang M.X. and Szoka F.C. (1997). "The influence of polymer structure on the interactions of cationic polymers with DNA and morphology of the resulting complexes." *Gene Therapy* 4 (8): 823-832.
- Thanou M., Verhoef J.C. and Junginger H.E. (2001). "Chitosan and its derivatives as intestinal absorption enhancers." *Adv Drug Deliv Rev* 50 Suppl 1: S91-101.
- Thiele L., Rothen-Rutishauser B., Jilek S., Wunderli-Allenspach H., Merkle H.P. and Walter E. (2001). "Evaluation of particle uptake in human blood monocyte-derived cells in vitro. Does phagocytosis activity of dendritic cells measure up with macrophages?" *J Control Release* 76 (1-2): 59-71.
- Thomas M. and Klivanov A.M. (2002). "Enhancing polyethylenimine's delivery of plasmid DNA into mammalian cells." *Proc Natl Acad Sci U S A* 99 (23): 14640-5.

- Toth I., Sakthivel T., Wilderspin A.F., Bayele H., O'Donnell M., Perry D.J., Pasi K.J., Lee C.A. and Florence A.T. (1999). "Novel cationic lipidic peptide dendrimer vectors - In vitro gene delivery." *Stp Pharma Sciences* 9 (1): 93-99.
- Turunen M.P., Hiltunen M.O., Ruponen M., Virkamaki L., Szoka F.C., Jr., Urtti A. and Yla-Herttuala S. (1999). "Efficient adventitial gene delivery to rabbit carotid artery with cationic polymer-plasmid complexes." *Gene Ther* 6 (1): 6-11.
- Ukkonen P., Lewis V., Marsh M., Helenius A. and Mellman I. (1986). "Transport of macrophage Fc receptors and Fc receptor-bound ligands to lysosomes." *J Exp Med* 163 (4): 952-71.
- Vaheri A. and Pagano J.S. (1965). "Infectious Poliovirus Rna - a Sensitive Method of Assay." *Virology* 27 (3): 434-436.
- van der Woude I., Wagenaar A., Meekel A.A., ter Beest M.B., Ruiters M.H., Engberts J.B. and Hoekstra D. (1997). "Novel pyridinium surfactants for efficient, nontoxic in vitro gene delivery." *Proc Natl Acad Sci U S A* 94 (4): 1160-5.
- Vijayanathan V., Thomas T., Shirahata A. and Thomas T.J. (2001). "DNA condensation by polyamines: a laser light scattering study of structural effects." *Biochemistry* 40 (45): 13644-51.
- Wadhwa M.S., Collard W.T., Adami R.C., McKenzie D.L. and Rice K.G. (1997). "Peptide-mediated gene delivery: influence of peptide structure on gene expression." *Bioconjug Chem* 8 (1): 81-8.
- Wadia J.S., Stan R.V. and Dowdy S.F. (2004). "Transducible TAT-HA fusogenic peptide enhances escape of TAT-fusion proteins after lipid raft macropinocytosis." *Nat Med* 10 (3): 310-5.
- Wagner E., Zenke M., Cotten M., Beug H. and Birnstiel M.L. (1990). "Transferrin-polycation conjugates as carriers for DNA uptake into cells." *Proc Natl Acad Sci U S A* 87 (9): 3410-4.
- Walker R.A. and Sheetz M.P. (1993). "Cytoplasmic microtubule-associated motors." *Annu Rev Biochem* 62: 429-51.
- Wattiaux R., Laurent N., Wattiaux-De Coninck S. and Jadot M. (2000). "Endosomes, lysosomes: their implication in gene transfer." *Adv Drug Deliv Rev* 41 (2): 201-8.
- West M.A., Prescott A.R., Eskelinen E.L., Ridley A.J. and Watts C. (2000). "Rac is required for constitutive macropinocytosis by dendritic cells but does not control its downregulation." *Curr Biol* 10 (14): 839-48.

- Wheeler C.J., Felgner P.L., Tsai Y.J., Marshall J., Sukhu L., Doh S.G., Hartikka J., Nietupski J., Manthorpe M., Nichols M., Plewe M., Liang X., Norman J., Smith A. and Cheng S.H. (1996). "A novel cationic lipid greatly enhances plasmid DNA delivery and expression in mouse lung." *Proc Natl Acad Sci U S A* 93 (21): 11454-9.
- Wilson R.W. and Bloomfield V.A. (1979). "Counterion-induced condensation of deoxyribonucleic acid. a light-scattering study." *Biochemistry* 18 (11): 2192-6.
- Wolff J.A., Malone R.W., Williams P., Chong W., Acsadi G., Jani A. and Felgner P.L. (1990). "Direct gene transfer into mouse muscle in vivo." *Science* 247 (4949 Pt 1): 1465-8.
- Wu G.Y. and Wu C.H. (1987). "Receptor-mediated in vitro gene transformation by a soluble DNA carrier system." *J Biol Chem* 262 (10): 4429-32.
- Wu J., Lizarzaburu M.E., Kurth M.J., Liu L., Wege H., Zern M.A. and Nantz M.H. (2001). "Cationic lipid polymerization as a novel approach for constructing new DNA delivery agents." *Bioconjug Chem* 12 (2): 251-7.
- Xiang S.D., Scholzen A., Minigo G., David C., Apostolopoulos V., Mottram P.L. and Plebanski M. (2006). "Pathogen recognition and development of particulate vaccines: does size matter?" *Methods* 40 (1): 1-9.
- Xu Y. and Szoka F.C., Jr. (1996). "Mechanism of DNA release from cationic liposome/DNA complexes used in cell transfection." *Biochemistry* 35 (18): 5616-23.
- Zabner J., Fasbender A.J., Moninger T., Poellinger K.A. and Welsh M.J. (1995). "Cellular and molecular barriers to gene transfer by a cationic lipid." *J Biol Chem* 270 (32): 18997-9007.
- Zanta M.A., Boussif O., Adib A. and Behr J.P. (1997). "In vitro gene delivery to hepatocytes with galactosylated polyethylenimine." *Bioconjug Chem* 8 (6): 839-44.
- Zhang Y.P., Sekirov L., Saravolac E.G., Wheeler J.J., Tardi P., Clow K., Leng E., Sun R., Cullis P.R. and Scherrer P. (1999). "Stabilized plasmid-lipid particles for regional gene therapy: formulation and transfection properties." *Gene Ther* 6 (8): 1438-47.
- Zhu J., Munn R.J. and Nantz M.H. (2000). "Self-cleaving ortho ester lipids: A new class of pH-vulnerable amphiphiles." *J Am Chem Soc* 122 (11): 2645-2646.
- Zhu M.Z., Wu Q.H., Zhang G.S., Ren T., Liu D.X. and Guo Q.X. (2002). "Synthesis and evaluation of cationic lipids bearing cholesteryl groups for gene delivery in vitro." *Bulletin of the Chemical Society of Japan* 75 (10): 2207-2213.
- Ziady A.G., Ferkol T., Dawson D.V., Perlmutter D.H. and Davis P.B. (1999). "Chain length of the polylysine in receptor-targeted gene transfer complexes affects duration of reporter gene expression both in vitro and in vivo." *J Biol Chem* 274 (8): 4908-16.

- Zuhorn I.S. and Hoekstra D. (2002). "On the mechanism of cationic amphiphile-mediated transfection. To fuse or not to fuse: is that the question?" *J Membr Biol* 189 (3): 167-79.
- Zuidam N.J. and Barenholz Y. (1998). "Electrostatic and structural properties of complexes involving plasmid DNA and cationic lipids commonly used for gene delivery." *Biochim Biophys Acta* 1368 (1): 115-28.

CHAPTER II

SYNTHESIS AND CHARACTERIZATION OF MONOMERS AND CROSSLINKERS

2.1 Introduction

2.1.1 Overview

Previous studies (McAllister *et al.* 2002) indicated that nanogels enter the cell via an endocytic process. As such pDNA-carrying nanogels require: (1) a strategy for transferring the nanogel formulation from the port of entry to the cell (i.e., endosomes) to its main body (i.e., cytosol) for subsequent entry to the nucleus; and (2) the release of entrapped pDNA from the nanogels at some appropriate site during endocytosis. In essence, these subjects comprise the independent variables in preparing nanogel formulations while gene expression in various cell lines is the dependent variable in the experimental design.

2.1.2 Endosome-to-Cytosol Translocation and Proton Sponge Hypothesis

Similar to macromolecules, submicron particulates are unable to penetrate cell membranes. They enter cells via endocytosis involving invagination of plasma membrane. Upon endosomal maturation, various enzymes become activated with concurrent decrease in

pH to as low as 4.5 in the lysosomal compartment. Unless timely escape of the luminal content to cytosol is guaranteed, endocytosed particulates are eventually directed to lysosome in which biochemical degradation occurs. Permeabilization of endosomal membrane has thus become a subject of intense investigations in the field (Asokan and Cho 2003; Chen *et al.* 2003). Polyplex systems entail electrostatic association between cationic polymer and polyanionic pDNA and they are effective in transfecting various cells *in vitro*, when an excess positive charge is maintained in the complex (Behr 1993). While positive charges are necessary to condense the DNA (Bloomfield 1996), the excess charges are believed to promote binding of the complex to cells via negatively charged proteoglycans on the cell surface such as heparan sulfates (Garnett 1999). For efficient gene transfection, excess positive charges would be a necessary but not a sufficient condition since there is a large discrepancy in transfection efficiency among various cationic polymers. Poly(ethylenimine) (PEI) (Kichler *et al.* 2001) or dendrimers (Haensler and Szoka 1993) showed significantly superior transfection efficiency to poly(lysine), implying presence of some other key element(s) yet to be clearly elucidated. Poly(ethylenimine), linear or branched, is a cationic polymer optimally suited for condensing pDNA. Its high buffering capacity at the acidic environment of the endosome enables the PEI-pDNA complex to escape endosomes into cytosol and gain an access to the nucleus (Zanta *et al.* 1997; Li *et al.* 1998) via so-called proton sponge effect described below.

Widely accepted proton sponge hypothesis involves the sequential events depicted in **Fig 2-1**. The polyplex binds the cell plasma membrane to initiate adsorptive endocytosis. As the luminal pH decreases due to membrane-bound H^+ -ATPase, the H_3O^+ introduced is

continuously used up in protonating the weak base moieties on the polymer. Since the protonated polymer cannot diffuse out of the endosome due to its size and polarity, influx and accumulation of anions, mainly Cl^- , take place in accordance of charge balance. This process continues with osmotic swelling and eventual rupture of endosomes. The net result is discharge of the endosome luminal content to cytosol prior to being delivered to lysosome for degradation. The above mechanism has been unambiguously supported by a series of mechanistic studies by Sonawane and his colleagues (2003). In essence, weak bases that are present in the cationic polymer play a major role in promoting the endosome-to-cytosol translocation of polyplexes. Endosomes show pH values between 4.3 and 6.9, mostly frequently pH ~ 5.0 , due to an endosomal acidification process (Lee *et al.* 1996). Thus, in order to make this scenario work, the weak base should remain neutral at pH 7.4 but protonated at the pH of early endosomes, ideally $\text{pK}_a \sim 6.5$ (Asokan and Cho 2002). There is an expectation that electrostatic repulsion between the pre-existing positive charges (i.e., in case of cationic monomer-incorporated nanogel) and incoming protons will reduce the basicity of the weak base, resulting in a decrease of its apparent pK_a (Onufriev *et al.* 2001). The selection of weak base in a positively charged polymer system will thus favor the one with a higher pK_a in bulk phase. Imidazole or *N,N*-dimethylethanolamine derivatives would be an ideal candidate for this purpose since they have bulk phase pK_a of 6.8 and 8.4, respectively. The latter monomer would be preferred at a high concentration of permanent positive charges in the polymer network since the more cationic monomer exists the more decrease in apparent pK_a is expected to occur. Along the line with this anticipation, imidazole derived monomer will be more suitable at low content of cation in terms of protonation in the endosome.

2.1.3 Release of Plasmid DNA from Nanogels

Polyplex systems, or the polyelectrolyte complexes of pDNA with polycations, have been widely used to develop polymer-based gene vectors. Colocalization studies that employed confocal fluorescence microscopy and numerous probe molecules clearly demonstrated that the nucleic acids delivered by nanogels should be dissociated from the carrier at some point during endocytosis to exert biological function (McAllister *et al.* 2002). Incorporation of ability of responding to environmental changes or stimuli into polyplex would promise a significant improvement of the delivery efficacy. Not only external stimuli such as ultrasound, heat, magnetic field, light but also endogenous changes such as pH decrease can facilitate spatial and temporal control of the release of gene cargos. Another example of the latter is the redox potential gradient existing between extracellular space and various subcellular organelles. Incorporation of a disulfide bond(s) into the backbone of the delivery devices provides them with a capability to disintegrate themselves in the reducing subcellular space. Most likely, glutathione (GSH, γ -glutamyl-L-cysteinylglycine) and thioredoxin, either alone or in combination with redox enzymes, play a major role in the intracellular reduction of disulfide bonds. GSH is the most abundant intracellular sulfhydryl and the concentration of GSH is an additive function of both the oxidized (GSSG) and the reduced forms (GSH). Cytosol is the principal site of GSH synthesis and the concentration of GSH here is 1-11 mM (Kosower and Kosower 1978; Gilbert 1990; Hwang *et al.* 1995). This is significantly higher than extracellular (i.e., blood plasma) GSH concentration ($\sim 1.5 \mu\text{M}$) (Jones *et al.* 1998). The overall cellular GSH/GSSH ratio (30/1 to $> 100/1$) is also higher than that of extracellular space ($\sim 7/1$) (Jones *et al.* 1998). The level of GSH varies in

different subcellular organelles. The highest reducing capacity is usually found in the nucleus and the nucleus GSH levels can reach up to 20 mM (Smith *et al.* 1996) . Mitochondria is another major pool of GSH (~ 5 mM) in the cell (Wahllander *et al.* 1979) while endoplasmic reticulum is more oxidizing than the cytosol (Hwang *et al.* 1992).

While the possibility of endosomal-lysosomal reduction of disulfide bonds has been reported (Collins *et al.* 1991; Fivaz *et al.* 2002; Saito *et al.* 2003), recent report (Austin *et al.* 2005) suggests that both the endosomal and lysosomal environments are rather oxidizing environment and disulfide bond reduction occurs rather inefficiently. A most recent study on the subject was again supportive of reductive endosome (Yang *et al.* 2006), creating more controversies. Much earlier, Feener and colleagues (1990) suggested that the reduction process might involve Golgi apparatus instead of being associated with lysosomes or endosomes. This and other studies (Sahaf *et al.* 2005) also implied that cellular plasma membrane is a possible site of reduction by surface proteins such as protein disulfide isomerase. Even though one cannot rule out the possibility that the enzymatic reduction in the endosome could play a role in disulfide bond cleavage by acid-activated enzymes such as Gamma-interferon-inducible lysosomal thiol reductase (Arunachalam *et al.* 2000), current understanding of subcellular trafficking of polyplexes suggests that intracellular reduction of disulfide bonds will proceed preferentially in the cytosol and nucleus.

The main purpose of incorporating disulfide bonds in the polyplexes is to increase a transient stability by enhancing the affinity of a polycation to the nucleic acid. Disulfide bonds can be introduced into the structure of polyplexes by using: (1) cationic molecules

containing more than two sulfhydryl functionalities and their *in situ* oxidation (McKenzie *et al.* 2000; Soundara Manickam *et al.* 2005); (2) commercially available disulfide containing crosslinking agents (e.g., dimethyl-3,3'-dithiobispropionimidate) (Gosselin *et al.* 2001; Oupicky *et al.* 2001); or (3) construction of disulfide containing polymers prior to polyplex formation (Oishi *et al.* 2005). The cleavage of disulfide bond incorporated in the backbone of the polyplex systems can induce a facile release of the cargo (e.g., pDNA) by physical breakdown of the carrier matrix and/or by reducing the affinity of nucleic acids (i.e., polyanions) to the polycationic polymers (Pichon *et al.* 2002; Carlisle *et al.* 2004). The former approach using neutral nanogels in delivering pDNA was investigated in **Chapter III** (entrapment of pDNA inside neutral nanogel matrix) and the latter was described in **Chapter IV** (polyplex formation of pDNA with cationic nanogel) in this dissertation.

In this chapter, the preparation and characterization of weak base monomers and nanogels are described. The characterization is mainly in terms of pKa of starting monomers as well as after polymers are formed. Also discussed are the synthetic strategies for a disulfide-containing crosslinker.

2.2 Materials and Methods

2.2.1 Materials

Acryloyl chloride, isobutylamine, 1,1'-carbonyldiimidazole (CDI), PEG monomethacrylate (PEGMA, M_n of PEO = 375 g/mol), 2-hydroxyethyl acrylate (HEA), *N,N,N*-triethylamine (TEA), $CDCl_3$ (deuteriochloroform), sodium sulfate, cystamine·2HCl, 1-(3-aminopropyl) imidazole, 2-(dimethylamino)ethyl acrylate (DMAEA), PEI (25 kDa, branched), anhydrous acetonitrile and anhydrous dioxane were purchased from Sigma-Aldrich. All ACS grade organic solvents such as methanol, chloroform, n-butanol and heptane were purchased from Fisher Scientific and used without any further purification. Standard solutions (1 N NaOH and 12 N HCl) were purchased from Fisher Scientific. Poly(ethylene glycol) diacrylate (PEGdiA, M_n of PEO = 375 g/mol), PEG monoacrylate (PEG-A, M_n of PEO = 200 g/mol or 375 g/mol) and 2-acryloxyethyltrimethylammonium chloride (AETMAC) at 80% in water, and 2-*N*-mopholinoethyl acrylate (MEA) were purchased from Polysciences, Inc. (Warrington, PA) and used as received. Di(2-ethylhexyl) peroxydicarbonate (Trigonox EHP) was purchased from Akzo Nobel (Chicago, IL) and stored at - 20°C until used. Laureth-3 was purchased from Heterene, Inc. (Paterson, NJ) and filtered through 0.22 μ m PTFE syringe filter (Fisher Scientific) before used.

2.2.2 Preparation of Imidazole-Containing Monomer (IPAA)

Into a 25-mL round-bottom flask, 1 mmol of 1-(3-aminopropyl) imidazole (122 μ L), 1 mmol of TEA (140 μ L) and 1.5 mL of anhydrous acetonitrile were added. Acryloyl chloride (85 μ L, 1 mmol) in 0.5 mL of acetonitrile was then added to the flask. The reaction took place in the ice bath for the first 30 min and continued at room temperature thereafter. Additional 0.2 mmol of acryloyl chloride (17 μ L) was added to the reaction at 4 hrs and the reaction was stirred overnight under an atmosphere of nitrogen. The resulting product was filtered through a filter paper (Whatman, Florham Park, NJ) and the filtrate was further purified by a column chromatography on silica gel using NH_4OH :methanol:chloroform (1%:15%:84% v/v) as a mobile phase.

2.2.3 Measurement of pKa of Weak Base-Containing Monomer and Nanogel

Weak base monomers (0.25 mmol) were dissolved in 5 mL of distilled water. Two mol-equivalent of HCl in 5 mL water was added into the weak base solution. After brief vortex-mixing, acidified weak base solutions were titrated by gradual addition of 0.1 N NaOH solutions. Blank titration was performed by titrating 0.05 N HCl with 0.1 N NaOH solution. The blank titration was subtracted from the monomer or nanogel titration, resulting in the net titration. Nanogels were prepared by the method described in elsewhere (McAllister *et al.* 2002) with a modification to incorporate weak base monomers (also see **Figure 2-10**). An optically transparent inverse microemulsion was prepared by combining heptane, surfactant (laureth-3) and aqueous monomer solution in the typical weight ratio of

86:4:10. The aqueous solution contains all polar acrylates such as HEA, PEGdiA (crosslinker), AETMAC (cationic monomer), and one of the three weak base monomers mentioned above. The composition of nanogels for the measurement of pKa was fixed at 25% (w/w) weak base, 12% crosslinker, 25% cationic monomer if required, and the rest was HEA. A small amount of free radical initiator (Trigonax EHP) in heptane (~ 5 mM as a final concentration) was added to the microemulsion. The reaction mixture was then stirred at room temperature overnight, under argon atmosphere and protected from light. After the polymerized emulsion was diluted with a biphasic water/heptane mixture, the aqueous phase was collected and washed with n-butanol several times to extract the surfactant. The residual surfactant was removed using dialysis with a dialysis bag of 100 kDa MWCO (Spectrum Laboratories, Inc., Rancho Dominguez, CA). The final preparation was sterile filtered using a 0.22 μ m PVDF syringe filter (Fisher Scientific) and stored at 4°C until further analysis. Regular nanogels containing PEGdiA (12%) and HEA (88%) were prepared as a control for pKa determination. Nanogels containing approximately 0.25 mmol of weak bases in 5 mL of water were mixed with 0.1 N HCl solution (5 mL) and titrated by adding 0.1 N NaOH solution gradually. PEI of 25 kDa, one of the standard polymeric transfecting reagents in the field, was also titrated similarly to nanogels.

2.2.4 Disulfide-Containing Crosslinker

As shown in the **Figure 2-11**, pre-fractionated PEG-based materials were activated with CDI followed by a coupling with free base form of disulfide-containing amine compound (cystamine). The details are described as follows.

Fractionation of PEGmA one milliliter (1.101 g) of PEGmA (M_n of PEO \sim 375 g/mol) was loaded on Sephadex G-50 medium column (Sigma). Flow rate and fraction size were 7 mL/ 4 min/ tube. Water served as the eluent. Fraction number 20 through 26 were collected and dried thoroughly in a rotary evaporator prior to further processing. PEGmA fractionated (\sim 10 mg) was dissolved in 0.75 mL of $CDCl_3$ and identified in 1H -NMR. The average molecular weight was estimated based on the mass spectrometry via an electrospray ionization coupled with a subsequent quadrupole ion-trap and was approximately 450 g/mol. Total yield of fractionation was approximately 73%.

Optimization of CDI activation CDI (1.2 mmol) and PEGmA (0.3 mmol, M_n of PEO \sim 200 g/mol) were added into a 25-mL round bottom flask containing 4 mL of anhydrous dioxane under magnetic stirring. The reaction mixture was stirred at room temperature for the specified time (0, 15, 30 min, 1, 2, 4, 8, 12, 18, and 24 hrs). Equivalent volume of water and chloroform were then added and the mixture was stirred vigorously. The reaction mixture was additionally washed with water and chloroform layer was collected. Two equivalent of isobutylamine was added to the chloroform layer and the mixture was gently stirred at room temperature. After 14 hrs, 1.5 mL of water was added to extract imidazole generated from the reaction (**Figure 2-7**). Aqueous layer containing imidazole was collected, washed with equivalent volume of chloroform, and subject to UV spectrometry at 206 nm to determine the amount of imidazole.

CDI activation Into 1.6 mmole of previously fractionated PEGmA in 5 mL of anhydrous dioxane, 4.8 mmole of CDI as powder was added and the reaction was stirred at

room temperature. After 3 hrs, 40 mL of brine (saturated NaCl solution in water) was added to the reaction to degrade unreacted CDI followed by multiple inversions and the addition of 10 mL of chloroform. The reaction mixture was then shaken vigorously to extract imidazole generated from the reaction into aqueous layer. Chloroform layer was collected and another 40 mL of brine was added for the second extraction. Chloroform layers were combined together, dried with sodium sulfate, evaporated under vacuum to dryness and redissolved in a mobile phase (methanol:chloroform = 10:90). Reaction mixture was then loaded on a silica gel column and the chromatography was performed at 4°C.

Free base formation of cystamine Into 11.1 mL of water, 1.1 g (8.88 mmol as HCl) of cystamine·2HCl was dissolved and the solution was put into a 500-mL separation funnel. Chloroform (80 mL) and 1 N NaOH (8.9 mL) were added to the cystamine solution followed by vigorous shaking. Chloroform layer was then collected to a clean 1000-mL beaker and the extraction was repeated 4 times by adding fresh 80 mL of chloroform to the remained upper aqueous layer. Combined chloroform layers were dried with sodium sulfate, transferred to a tare-weighed 500-mL round bottom flask, and evaporated to dryness. Free base form of cystamine extracted was stored at 4°C under nitrogen atmosphere until further usage.

Coupling Into 25-mL round bottom flask placed on an ice bath, 0.3 mmol of CDI-activated PEGmA (CDI-PEGmA) and 2 mL of anhydrous acetonitrile were added. Free base form of cystamine (0.3 mmol) dissolved in 1 mL anhydrous acetonitrile was added to the flask dropwise (i.e., initial net stoichiometry of CDI-PEGmA:cystamine = 1:2). Reaction mixture was stirred at 4°C for 18 hrs and additional CDI-PEGmA (0.27 mmole) was then

added to the reaction in that the final net stoichiometry of CDI-PEGmA to cystamine was 1.9 to 2.0. The reaction was kept stirred for additional 24 hrs at 4°C. The reaction mixture was then evaporated thoroughly and redissolved in 8 mL of chloroform. To extract imidazole from the reaction into aqueous layer, 24 mL of brine was added followed by vigorous inversion. Chloroform layer was collected, dried using sodium sulfate, evaporated and redissolved in a mobile phase (methanol:chloroform = 10:90). The reaction mixture was further purified in a column chromatography on silica gel using above-mentioned mobile phase. The final product was a clear viscous liquid and stored at 4°C until used.

2.3 Results and Discussion

2.3.1 Imidazole-Containing Monomer (IPAA)

The imidazole-containing monomer was prepared as shown in **Figure 2-2A**. The reaction yield was approximately 80%. Upon adding acryloyl chloride to the reaction, yellowish precipitation was formed as a byproduct in 5 min. Alternative solvent such as methylene chloride could be used instead of acetonitrile to avoid the precipitation. It may also improve the reaction yield. The final product was a yellow viscous liquid and the chemical structure was identified with ¹H-NMR spectrometry as shown in **Figure 2-2**. NMR showed all of the anticipated peaks including the protons from imidazole (peaks **b**, **c**, and **d**) and acrylate moieties (peaks **e**, **f**, and **g**). It was stored at 4°C and protected from light until used.

2.3.2 pKa's of Weak Base-Containing Monomers and Nanogels

As the pH decreases in the endosome, protonation of one base moiety can reduce the basicity of the adjacent one, in effect resulting in a series of weak bases with continuously changing apparent pKa along with protonation (Fischer *et al.* 2002). Such an effect was first investigated with the morpholine-containing monomer, MEA (see **Table 2-1** for structure) with pKa 6.2. The issues addressed here were: 1) how protonation of a given site affects the pKa of adjacent base when a neutral polymer was processed; and 2) how the presence of quaternary ammonium cations affects the overall pKa of the weak base. As shown in **Figure 2-4C**, MEA at 20 mM titrated with NaOH in the presence of HCl represented a single half-neutralization point, or pKa at 6.20. In contrast, when MEA was incorporated by 25% (w/w) into neutral and cationic nanogels (**Figure 2-3**), the net titration curves demonstrated two apparent pKa values, 3.8 and 6.2 for the former and 3.8 and 6.0 for the latter. A similar phenomenon of approximating two populations of weak bases was also reported when *N,N*-dimethylaminoethyl methacrylate was introduced to PEI (Funhoff *et al.* 2004). The extra pKa observed in nanogels (**Table 2-1**) may indicate the presence of weaker base population and can be explained by the effect of pre-protonated weak base moieties in the polymers as discussed earlier. That is, the protons initially bound to weak bases will repulse the upcoming protons, inhibit their binding into the adjacent weak bases and show decreased apparent pKa, whereas the change in the first pKa from 6.2 in **Figure 2-3A** to 6.0 in **Figure 2-3B** is due to the effect of pre-existing quaternary ammonium ions. Titration of DMAEA as monomer and when incorporated in the nanogel (**Figure 2-4G and H**) showed a similar pattern of change in apparent pKa (i.e., 8.41 in monomer and 4.06/8.35 in nanogel). Imidazole-containing

monomer (IPAA) showed 6.83 of pKa as expected from the intrinsic pKa of imidazole moiety (**Figure 2-4E**). Interestingly, the apparent pKa (6.30) of IPAA-containing nanogel (**Figure 2-4F**) decreased significantly compared to that of monomer. It might be due to a stronger electrostatic repulsion by previously-protonated sites than in the case of other weak base-containing nanogels. When neutral nanogels dispersed at a concentration of ~ 5 mg/ml in 10 ml of 0.05 N HCl were titrated with 0.1 N NaOH (**Figure 2-4B**) the profile of titration curve was similar to the blank titration of the same HCl solution with the same titrant (**Figure 2-4A**). As shown in the panels **D**, **F**, and **H** on **Figure 2-4**, nanogels containing weak bases showed buffer capacity around their respective pKa, which is not observed in regular nanogels (**Figure 2-4B**) composed of only PEGdiA and HEA. Taken together, the data indicates that pKa values of monomers in bulk phase can be used in predicting those in polymers.

According to Van Slyke's equation, the buffer capacity is highest at the pKa of the buffer component. The titration curves obtained from weak base containing neutral nanogels were superimposed with one another in **Figure 2-5**. The highest buffer capacity at pH 6.5 (i.e. pH of early endosome), the reciprocal of the slope of the tangent line on the titration curve at pH 6.5, was observed in the nanogels prepared with morpholine-derivatives with pKa 6.2 or imidazole-derivative with pKa 6.3. When compared to that of PEI, these two nanogels possessed almost two-fold higher buffer capacity. Another nanogel prepared using dimethylethanolamine-derivative with pKa 8.3 showed an almost identical buffer capacity as the other two but the maximal capacity appeared at a higher pH, reflecting its higher pKa. It might be less optimal to serve as a proton sponge inside endosome. Altogether, these data

support that the nanogels prepared using weak base monomers selected here can be superior to PEI in terms of transfection efficiency, one of the best polyplex systems available in the field.

2.3.3 Disulfide-Containing Crosslinker

In a typical procedure to prepare nanogels, the average MW of PEO moiety in PEGdiA used as a crosslinker was approximately 200 g/mol. In order to increase the solubility of the final product, longer chain of PEG-containing monoacrylate, PEG-A (M_n of PEO ~ 375 g/mol), was used as the starting material. However, CDI activated PEG-A turned out to degrade during coupling reaction due to a nucleophilic attack by the primary amine of the cystamine toward acrylate moiety (i.e., multiple bands showed up on thin layer chromatography). Thus, PEGmA that contains sterically-hindered acrylate moiety by the addition of methyl group was used for the reaction to prevent this problem. Since PEG-based compound is a mixture of different length of species, PEGmA was first fractionated using Sephadex G-50 (**Figure 2-6**). The population of higher molecular weight was collected and used as the starting material for the activation with CDI.

The reaction condition of CDI activation was optimized by measuring the amount of imidazole produced from the reaction of CDI-PEGmA with a primary amine-containing model compound, isobutylamine. As shown in **Figure 2-7**, the amount of imidazole represented by an optical density at 206 nm reached a maximum level when the CDI activation continued approximately for 2 hrs and remained almost identical thereafter up to

24 hrs. Accordingly, the activation of PEGmA with CDI was carried out for 3 hrs at room temperature for the reaction. Since the water solubility of CDI-PEGmA was found to be very poor, purification and separation were performed by extracting with brine followed by a silica gel column chromatography. The purified CDI-activated PEGmA was identified with thin layer chromatography (TLC) and ^1H -NMR. One single spot was detected on the TLC (data not shown) and the ^1H -NMR spectrum of CDI-PEGmA is shown in **Figure 2-8**. As indicated in the **Figure 2-8**, both moieties of the polyethylene (c) and acrylate (b) remained intact but hydroxyl group (a) of PEGmA has disappeared in CDI-activated intermediate with gaining of imidazole moiety (d). Yield of CDI activation was approximately 46%.

Initially, a two-phase solvent system such as aqueous buffer-acetonitrile mixture was attempted for the coupling reaction to dissolve both CDI-PEGmA (intermediate product) and cystamine-2HCl. In order to facilitate the reaction, free base form of cystamine was first prepared by repeated chloroform extractions of free base form from pH-adjusted (i.e., pH 8.5) cystamine dihydrochloride aqueous solution. Extraction yield of free base form of cystamine using total 20-volume of chloroform was close to 100%. After extraction, cystamine was verified in ^1H -NMR (data not shown) and no structural change was observed. The yield of coupling reaction was approximately 73%. The structural verification of the final product was performed using ^1H -NMR and mass spectrometry (**Figure 2-9**), confirming a disulfide-containing, PEG-based diacrylate compound.

2.4 Conclusions

When weak bases are incorporated in the nanogel (i.e., polymer system), the weak bases possess widely spread pKa values and become weaker in the presence of permanent positive charges. Nanogels prepared using morpholine- and imidazole-derivative showed almost 2-fold higher buffer capacity at pH 6.5 (i.e., pH of early endosome) than PEI. Disulfide containing, PEG-based crosslinker was successfully synthesized and served as a cleavable crosslinker when incorporated in the nanogel. The monomers synthesized in this chapter were used to test proton sponge hypothesis using the nanogel system and to assess how the presence of degradable crosslinker affects gene transfection, which are discussed in the following chapters.

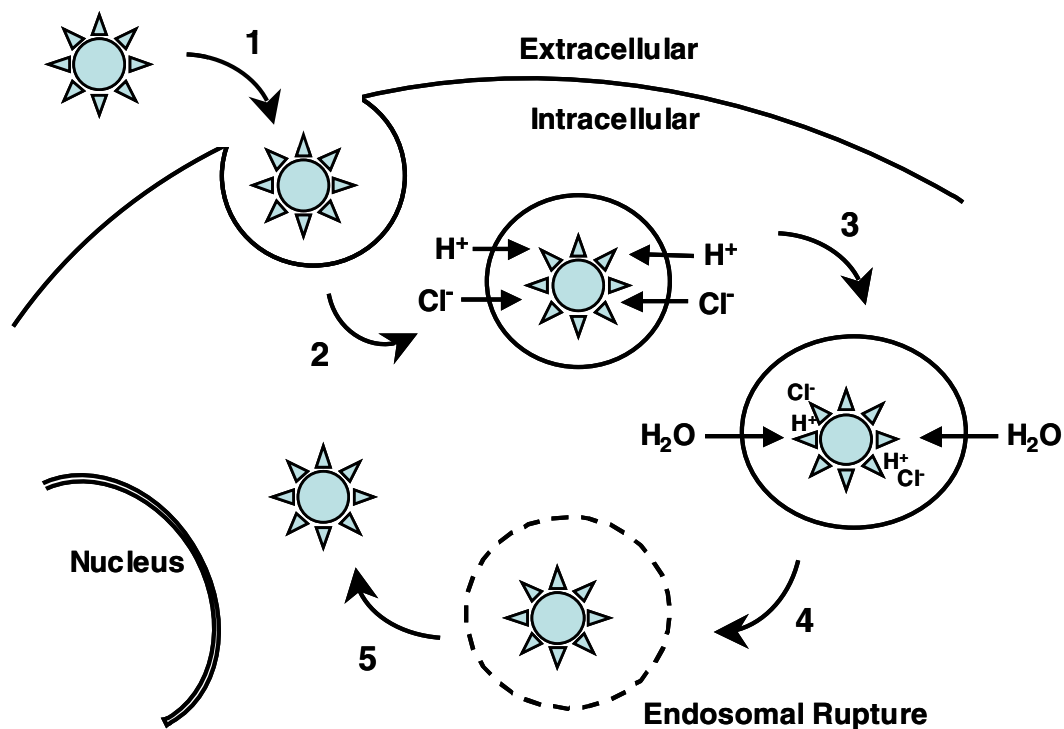
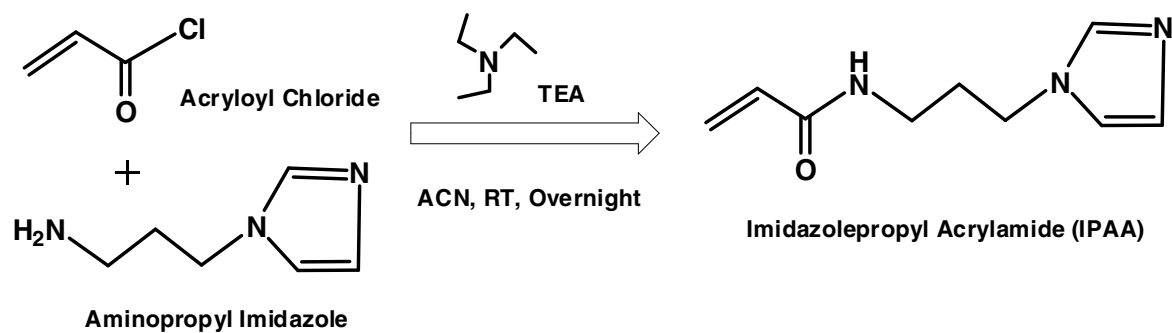


Figure 2-1: Illustration of proton sponge hypothesis. [1] Polyplex is internalized by invagination of the cell membrane. [2] As the endosomal compartment is acidified by the proton pumps located in the endosomal membrane, chloride counter ion comes in for a charge valence, and [3] increased osmolarity inside the endosome results in the influx of water. [4] Consequently, endosomal vesicle swells with the increasing volume of water, leading to an eventual rupture and [5] the release of the content into the cytosol.

A



B

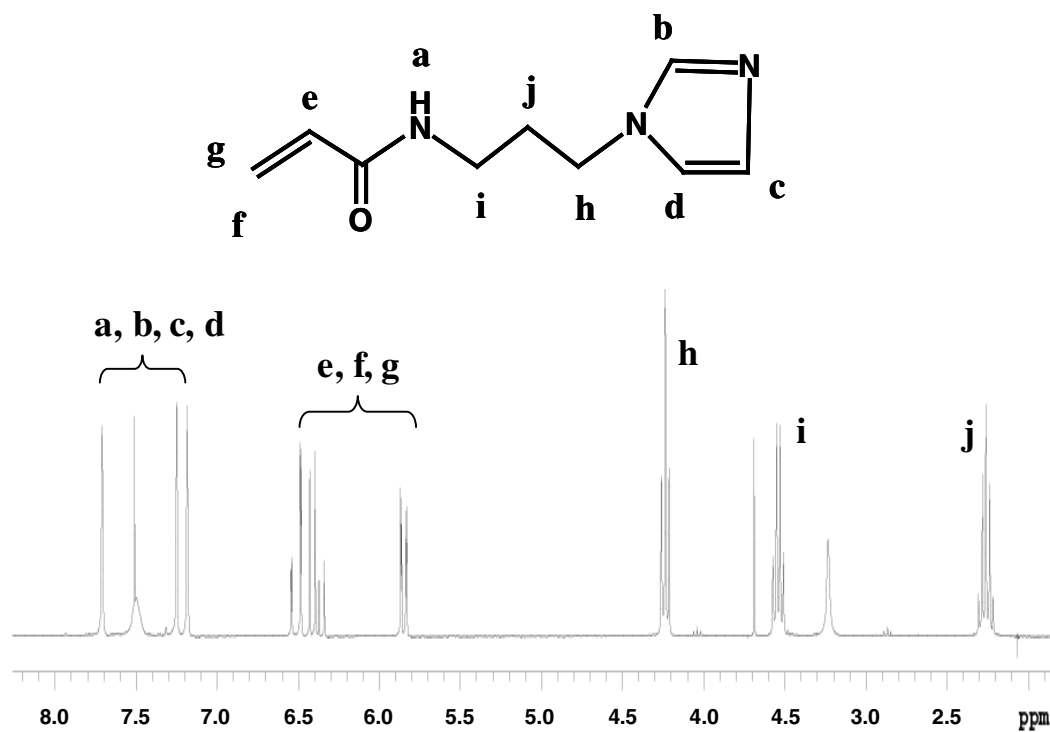


Figure 2-2: Synthetic scheme (A) and ¹H-NMR spectrum (B) of imidazolypropyl-acrylamide (IPAA).

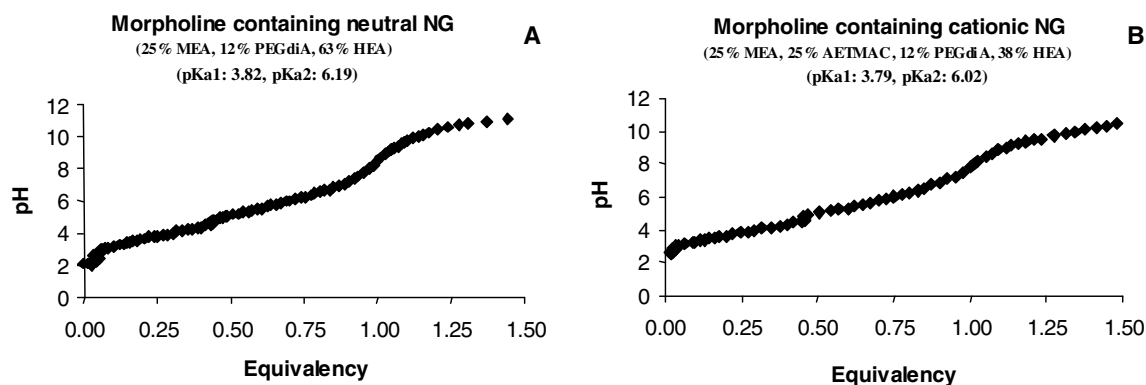


Figure 2-3: Titration of neutral (**A**) and cationic (**B**) nanogels containing morpholine moiety. Both nanogels were prepared with 25% (w/w) 2-*N*-morpholinoethyl acrylate (MEA), 12% PEG diacrylate (PEGdiA, crosslinker), 25% 2-acryloxyethyltrimethylammonium chloride (AETMAC, only for **B**) and 2-hydroxyethyl acrylate (HEA) for the rest. Nanogels (0.25 mmol as MEA) were mixed with HCl and titrated with 0.1 N NaOH. Blank titration (i.e., HCl titrated with NaOH) was subtracted from the nanogel titration, resulting in net titration curves shown above. The second end point of the titration curve was set at one unit equivalency.

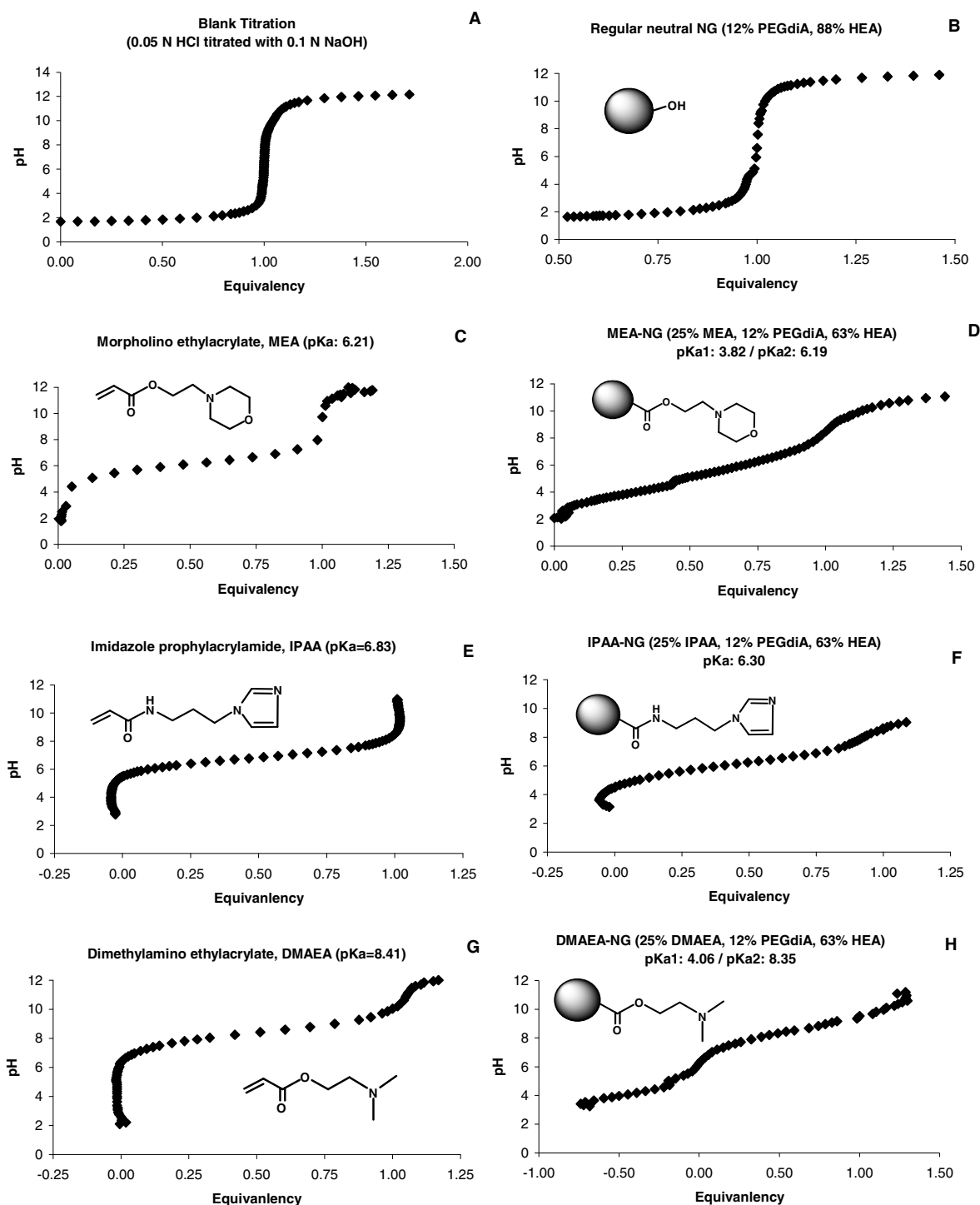
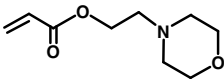
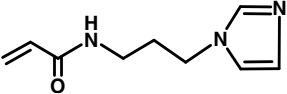
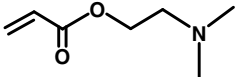


Figure 2-4: Potentiometric titration of monomers and nanogels containing weak bases. Blank titration (A) was subtracted from monomer (C, E, and G) or nanogel titration (B, D, F, and H). One unit equivalency on the X-axis was set at the end point of each titration curve.

Table 2-1: Summary of pKa's of Weak Base-Containing Monomers and Nanogels.

Weak Base		pKa of Monomer	pKa of Nanogel
2- <i>N</i> -morpholinoethylacrylate (MEA)		6.21	3.82 / 6.19
Imidazolylpropylacrylamide (IPAA)		6.83	6.30
2-(dimethylamino)ethylacrylate (DMAEA)		8.41	4.06 / 8.35

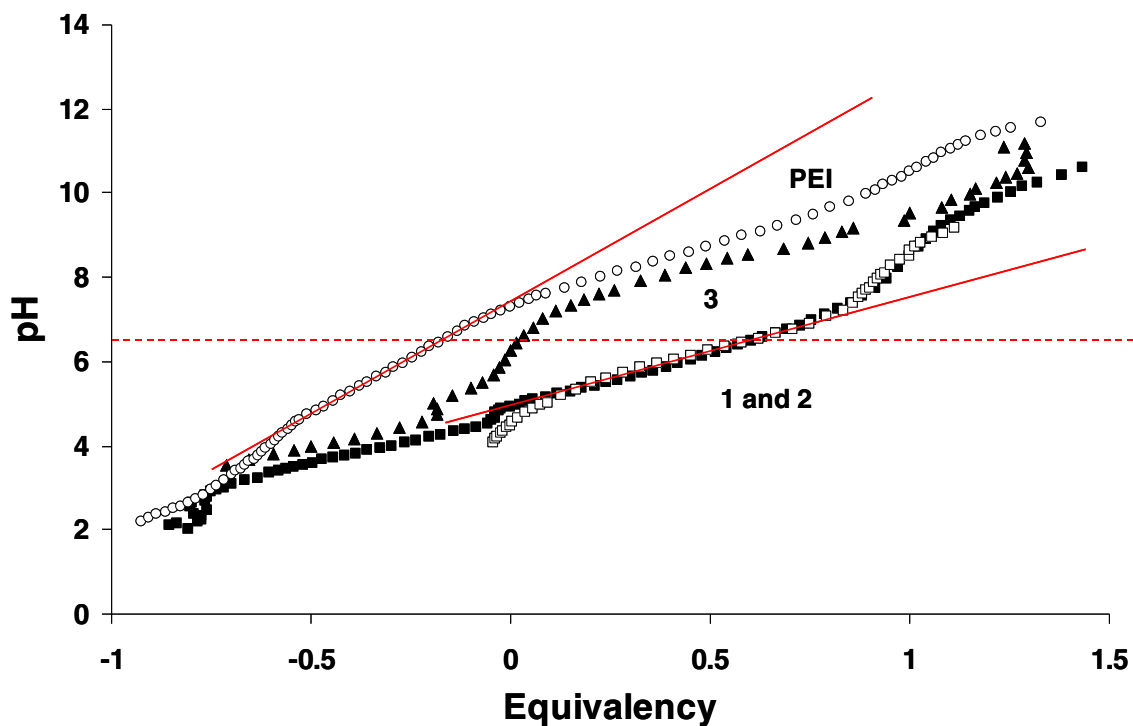


Figure 2-5: Titration of PEI (25 kDa, branched) and nanogels prepared with weak base-containing monomers **1** (2-*N*-morpholinoethyl acrylate), **2** (imidazolypropyl acrylamide), or **3** [2-(dimethylamino)ethyl acrylate]. Nanogels were prepared using 25% (w/w) of a weak base-containing monomer, 12% PEG diacrylate (crosslinker), and 63% 2-hydroxyethyl acrylate. All samples contained an identical amount of HCl and titrated with NaOH. The buffer capacity at pH 6.5 is the reciprocal of the slope of the tangent lines shown in the curve.

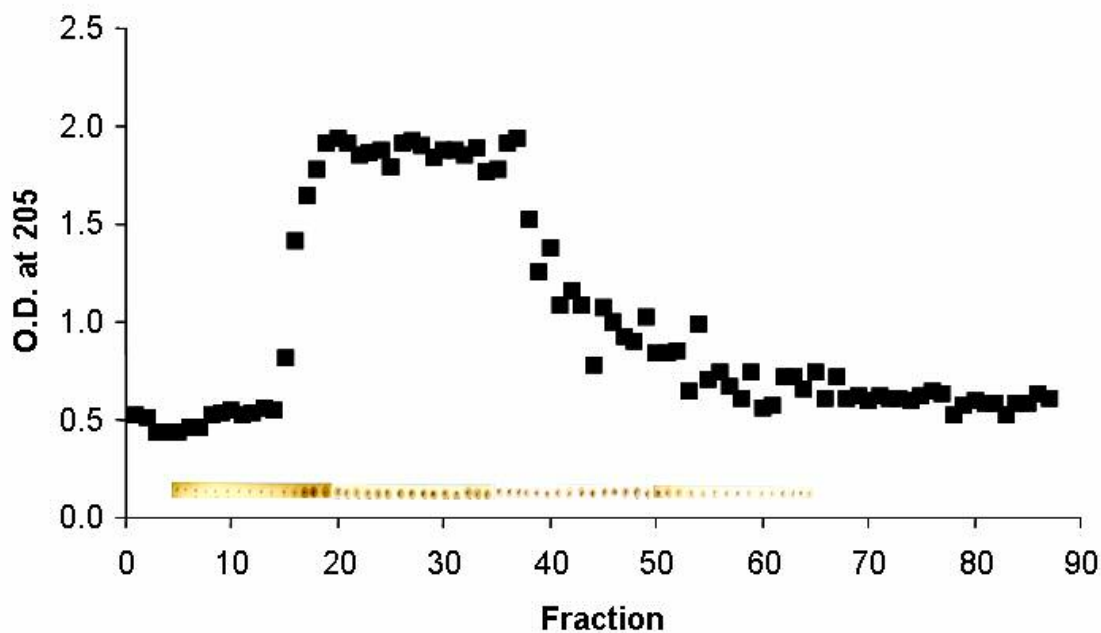


Figure 2-6: Fractionation of PEG monomethacrylate (PEGmA) by a size exclusion chromatography. PEGmA (average M_n of PEO ~ 375 g/mol) was loaded on Sephadex G-50 column using water as an eluant. PEGmA was monitored using UV spectrometry at 205 nm (**upper square dots**) as well as thin layer chromatography (TLC, **lower band containing small dots**) in a silica-coated aluminum plate. Fractions 16 through 26 were collected, dried under vacuum and used as a starting material for the subsequent carbonyldiimidazole activation.

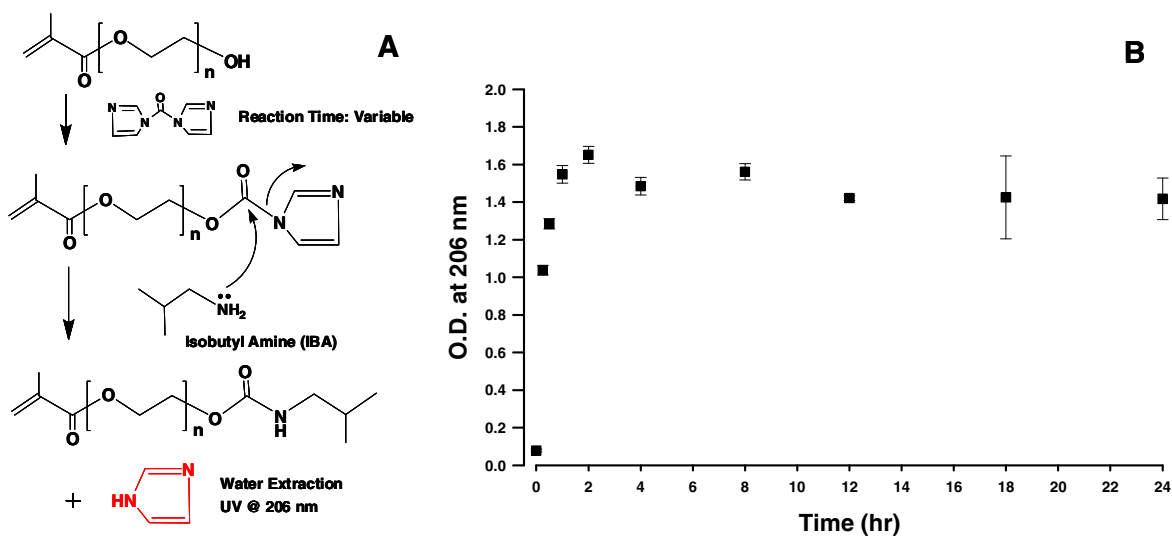


Figure 2-7: Reaction of carbonyldiimidazole (CDI)-activated PEG monomethacrylate with isobutylamine (**A**). The reaction time of the first step (activation) varied from 0 min up to 24 hrs as shown in **B**. Imidazole was produced as a byproduct from the second step of the reaction, extracted in water, and measured at 206 nm using UV spectrometer (**B**). The amount of imidazole generated from second step (substitution reaction) was considered to reflect the extent of CDI activation (i.e., first step).

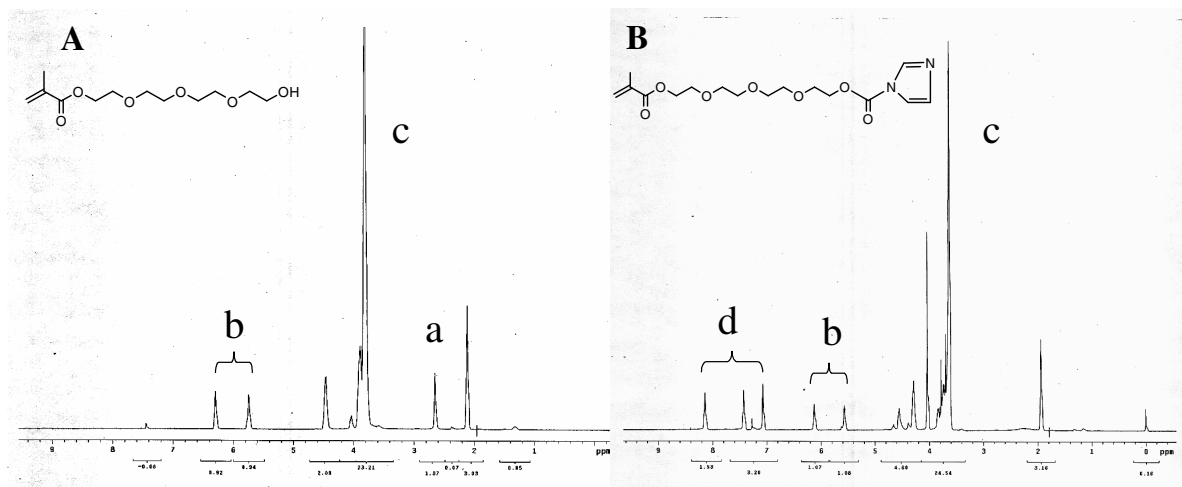


Figure 2-8: ^1H -NMR spectrum of PEG monomethacrylate, PEGMA (A) and CDI-activated PEGMA, CDI-PEGMA (B). Disappearance of peak **a** in A (hydroxyl group of PEGMA) and advent of peaks **d** in B (imidazole moiety of CDI-PEGMA) was mainly monitored.

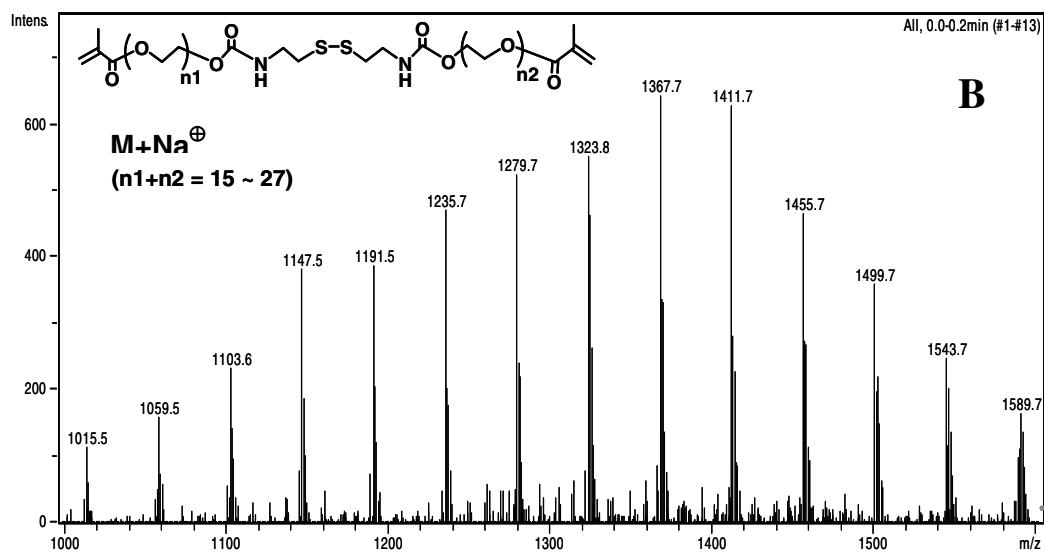
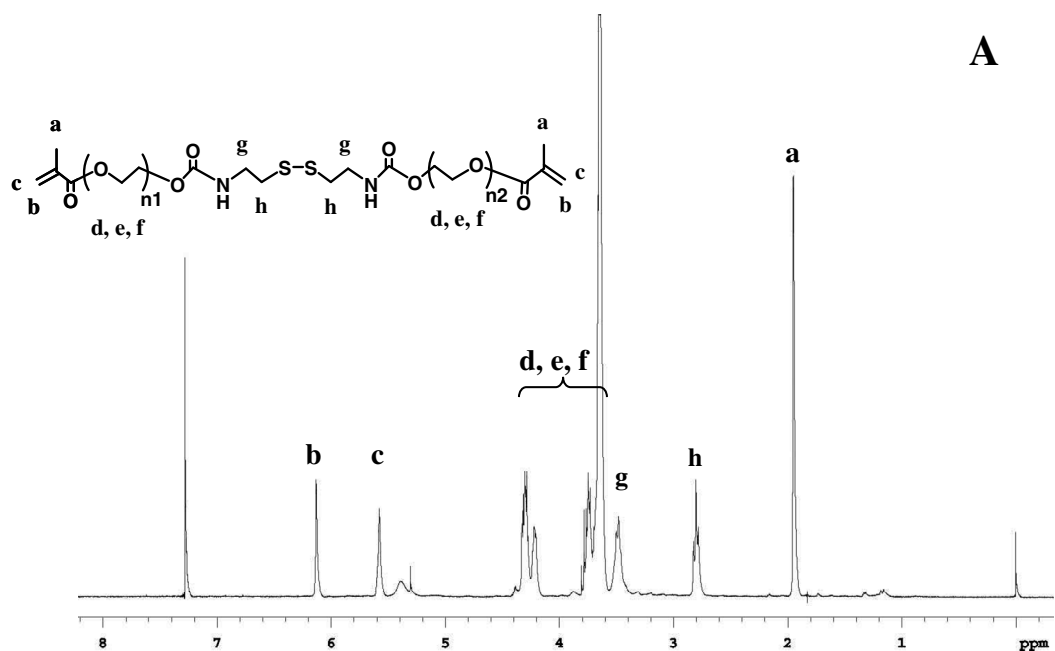


Figure 2-9: ¹H-NMR spectrum (**A**) and mass spectrum (**B**) of a disulfide containing, PEG-based diacrylate crosslinker. The compound was dissolved in CDCl₃ and methanol for NMR analysis and mass spectrometry, respectively. Mass spectrometry was performed via an electrospray ionization coupled with a subsequent quadrupole ion-trap.

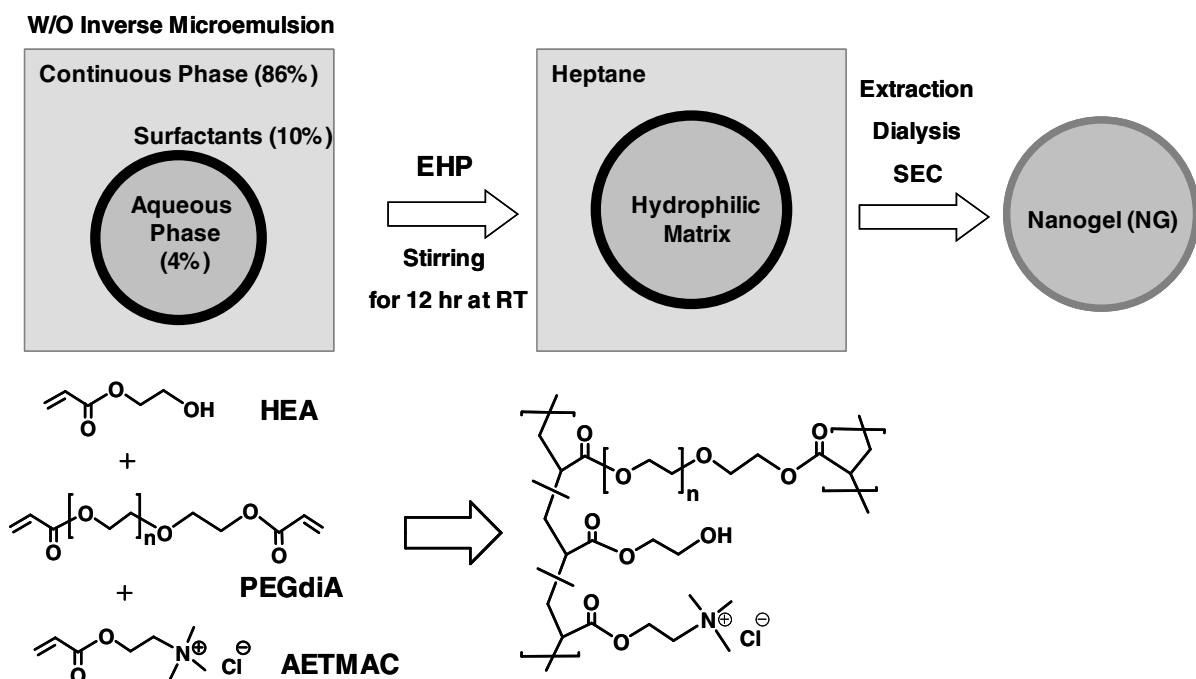


Figure 2-10: Schematic illustration of a typical polymerization reaction. W/O inverse microemulsion is formed by adding aqueous layer (~ 4% w/w) containing all of the water-miscible acrylate monomers into the mixture of heptane (i.e., continuous phase) and 10% (w/w) surfactant (laureth-3). Polymerization is initiated by the subsequent addition of a free radical initiator (Trigonax EHP, 2-ethylhexyl peroxydicarbonate). The reaction runs overnight and the final nanogels are purified using heptane extraction, n-butanol washing, and dialysis or size exclusion chromatography. Exemplary monomers and part of the polymerized nanogels are shown in the lower panel.

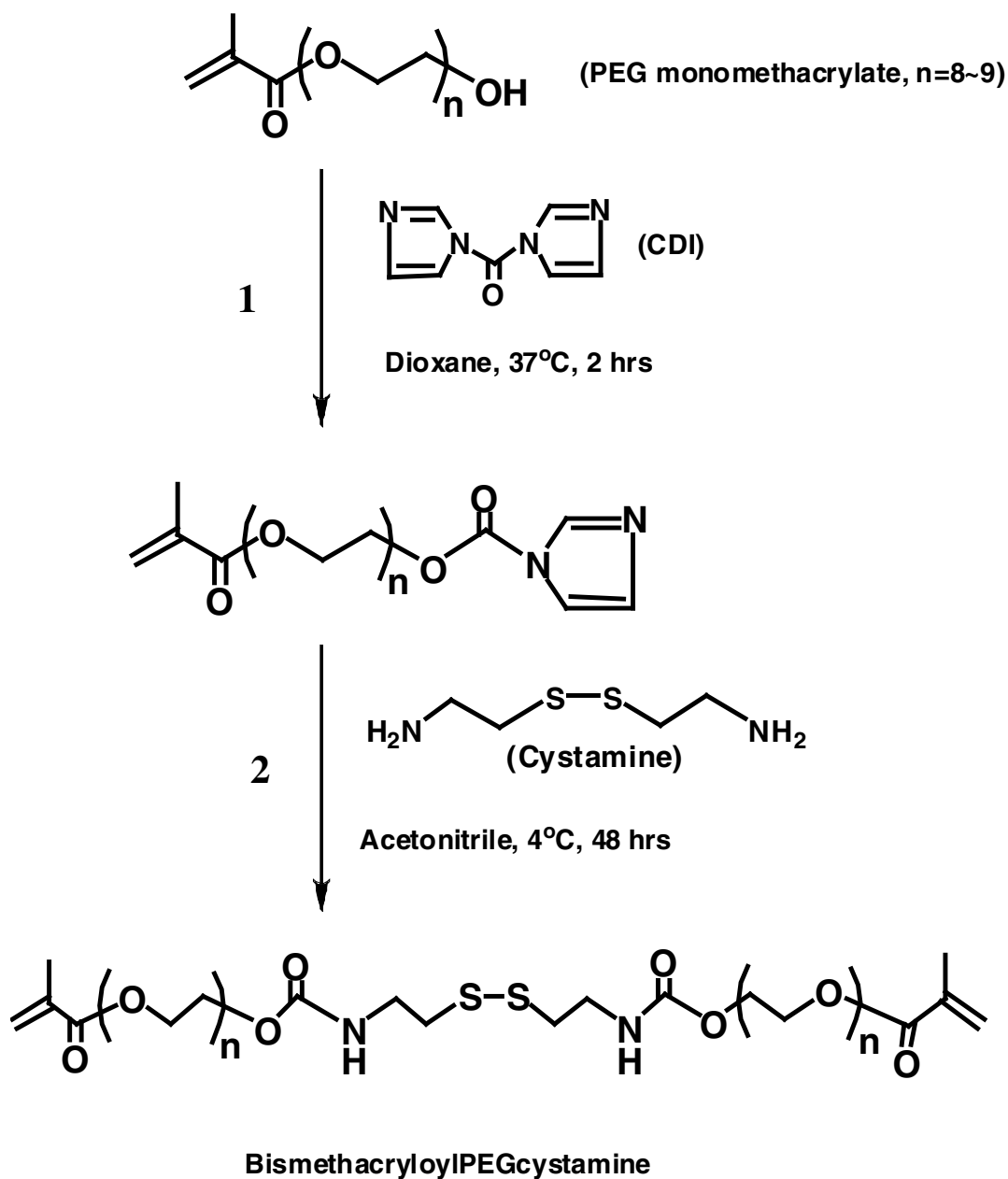


Figure 2-11: Synthetic scheme of a disulfide-containing, PEG-based crosslinker. PEGmA (average M_n of PEO ~ 375 g/mol) was activated with CDI (step 1) and the intermediate was coupled with the free base form of cystamine (step 2). The final product was purified using a column chromatography on silica gel.

2.5 References

- Arunachalam B., Phan U.T., Geuze H.J. and Cresswell P. (2000). "Enzymatic reduction of disulfide bonds in lysosomes: characterization of a gamma-interferon-inducible lysosomal thiol reductase (GILT)." *Proc Natl Acad Sci U S A* 97 (2): 745-50.
- Asokan A. and Cho M.J. (2002). "Exploitation of intracellular pH gradients in the cellular delivery of macromolecules." *J Pharm Sci* 91 (4): 903-13.
- Asokan A. and Cho M.J. (2003). "Cytosolic delivery of macromolecules. II. Mechanistic studies with pH-sensitive morpholine lipids." *Biochim Biophys Acta* 1611 (1-2): 151-60.
- Austin C.D., Wen X., Gazzard L., Nelson C., Scheller R.H. and Scales S.J. (2005). "Oxidizing potential of endosomes and lysosomes limits intracellular cleavage of disulfide-based antibody-drug conjugates." *Proc Natl Acad Sci U S A* 102 (50): 17987-92.
- Behr J.P. (1993). Synthetic gene-transfer vectors, *Acc. Chem. Res.* **26**: 274-278.
- Bloomfield V.A. (1996). "DNA condensation." *Curr Opin Struct Biol* 6 (3): 334-41.
- Carlisle R.C., Etrych T., Briggs S.S., Preece J.A., Ulbrich K. and Seymour L.W. (2004). "Polymer-coated polyethylenimine/DNA complexes designed for triggered activation by intracellular reduction." *J Gene Med* 6 (3): 337-44.
- Chen F.J., Asokan A. and Cho M.J. (2003). "Cytosolic delivery of macromolecules: I. Synthesis and characterization of pH-sensitive acyloxyalkylimidazoles." *Biochim Biophys Acta* 1611 (1-2): 140-50.
- Collins D.S., Unanue E.R. and Harding C.V. (1991). "Reduction of disulfide bonds within lysosomes is a key step in antigen processing." *J Immunol* 147 (12): 4054-9.
- Feener E.P., Shen W.C. and Ryser H.J. (1990). "Cleavage of disulfide bonds in endocytosed macromolecules. A processing not associated with lysosomes or endosomes." *J Biol Chem* 265 (31): 18780-5.
- Fischer D., von Harpe A., Kunath K., Petersen H., Li Y. and Kissel T. (2002). "Copolymers of ethylene imine and N-(2-hydroxyethyl)-ethylene imine as tools to study effects of polymer structure on physicochemical and biological properties of DNA complexes." *Bioconjug Chem* 13 (5): 1124-33.
- Fivaz M., Vilbois F., Thurnheer S., Pasquali C., Abrami L., Bickel P.E., Parton R.G. and van der Goot F.G. (2002). "Differential sorting and fate of endocytosed GPI-anchored proteins." *Embo J* 21 (15): 3989-4000.

- Funhoff A.M., van Nostrum C.F., Koning G.A., Schuurmans-Nieuwenbroek N.M., Crommelin D.J. and Hennink W.E. (2004). "Endosomal escape of polymeric gene delivery complexes is not always enhanced by polymers buffering at low pH." *Biomacromolecules* 5 (1): 32-9.
- Garnett M.C. (1999). "Gene-delivery systems using cationic polymers." *Crit Rev Ther Drug Carrier Syst* 16 (2): 147-207.
- Gilbert H.F. (1990). "Molecular and cellular aspects of thiol-disulfide exchange." *Adv Enzymol Relat Areas Mol Biol* 63: 69-172.
- Gosselin M.A., Guo W. and Lee R.J. (2001). "Efficient gene transfer using reversibly cross-linked low molecular weight polyethylenimine." *Bioconjug Chem* 12 (6): 989-94.
- Haensler J. and Szoka F.C., Jr. (1993). "Polyamidoamine cascade polymers mediate efficient transfection of cells in culture." *Bioconjug Chem* 4 (5): 372-9.
- Hwang C., Lodish H.F. and Sinskey A.J. (1995). "Measurement of glutathione redox state in cytosol and secretory pathway of cultured cells." *Methods Enzymol* 251: 212-21.
- Hwang C., Sinskey A.J. and Lodish H.F. (1992). "Oxidized redox state of glutathione in the endoplasmic reticulum." *Science* 257 (5076): 1496-502.
- Jones D.P., Carlson J.L., Samiec P.S., Sternberg P., Jr., Mody V.C., Jr., Reed R.L. and Brown L.A. (1998). "Glutathione measurement in human plasma. Evaluation of sample collection, storage and derivatization conditions for analysis of dansyl derivatives by HPLC." *Clin Chim Acta* 275 (2): 175-84.
- Kichler A., Leborgne C., Coeytaux E. and Danos O. (2001). "Polyethylenimine-mediated gene delivery: a mechanistic study." *J Gene Med* 3 (2): 135-44.
- Kosower N.S. and Kosower E.M. (1978). "The glutathione status of cells." *Int Rev Cytol* 54: 109-60.
- Lee R.J., Wang S. and Low P.S. (1996). "Measurement of endosome pH following folate receptor-mediated endocytosis." *Biochim Biophys Acta* 1312 (3): 237-42.
- Li S., Deshmukh H.M. and Huang L. (1998). "Folate-mediated targeting of antisense oligodeoxynucleotides to ovarian cancer cells." *Pharm Res* 15 (10): 1540-5.
- McAllister K., Sazani P., Adam M., Cho M.J., Rubinstein M., Samulski R.J. and DeSimone J.M. (2002). "Polymeric nanogels produced via inverse microemulsion polymerization as potential gene and antisense delivery agents." *J Am Chem Soc* 124 (51): 15198-207.
- McKenzie D.L., Kwok K.Y. and Rice K.G. (2000). "A potent new class of reductively activated peptide gene delivery agents." *J Biol Chem* 275 (14): 9970-7.

- Oishi M., Hayama T., Akiyama Y., Takae S., Harada A., Yamasaki Y., Nagatsugi F., Sasaki S., Nagasaki Y. and Kataoka K. (2005). "Supramolecular assemblies for the cytoplasmic delivery of antisense oligodeoxynucleotide: polyion complex (PIC) micelles based on poly(ethylene glycol)-SS-oligodeoxynucleotide conjugate." *Biomacromolecules* 6 (5): 2449-54.
- Onufriev A., Case D.A. and Ullmann G.M. (2001). "A novel view of pH titration in biomolecules." *Biochemistry* 40 (12): 3413-9.
- Oupicky D., Carlisle R.C. and Seymour L.W. (2001). "Triggered intracellular activation of disulfide crosslinked polyelectrolyte gene delivery complexes with extended systemic circulation in vivo." *Gene Ther* 8 (9): 713-24.
- Pichon C., LeCam E., Guerin B., Coulaud D., Delain E. and Midoux P. (2002). "Poly[Lys-(AEDTP)]: a cationic polymer that allows dissociation of pDNA/cationic polymer complexes in a reductive medium and enhances polyfection." *Bioconj Chem* 13 (1): 76-82.
- Sahaf B., Heydari K., Herzenberg L.A. and Herzenberg L.A. (2005). "The extracellular microenvironment plays a key role in regulating the redox status of cell surface proteins in HIV-infected subjects." *Arch Biochem Biophys* 434 (1): 26-32.
- Saito G., Amidon G.L. and Lee K.D. (2003). "Enhanced cytosolic delivery of plasmid DNA by a sulfhydryl-activatable listeriolysin O/protamine conjugate utilizing cellular reducing potential." *Gene Ther* 10 (1): 72-83.
- Smith C.V., Jones D.P., Guenther T.M., Lash L.H. and Lauterburg B.H. (1996). "Compartmentation of glutathione: implications for the study of toxicity and disease." *Toxicol Appl Pharmacol* 140 (1): 1-12.
- Sonawane N.D., Szoka F.C., Jr. and Verkman A.S. (2003). "Chloride accumulation and swelling in endosomes enhances DNA transfer by polyamine-DNA polyplexes." *J Biol Chem* 278 (45): 44826-31.
- Soundara Manickam D., Bisht H.S., Wan L., Mao G. and Oupicky D. (2005). "Influence of TAT-peptide polymerization on properties and transfection activity of TAT/DNA polyplexes." *J Control Release* 102 (1): 293-306.
- Wahllander A., Soboll S., Sies H., Linke I. and Muller M. (1979). "Hepatic mitochondrial and cytosolic glutathione content and the subcellular distribution of GSH-S-transferases." *FEBS Lett* 97 (1): 138-40.
- Yang J., Chen H., Vlahov I.R., Cheng J.X. and Low P.S. (2006). "Evaluation of disulfide reduction during receptor-mediated endocytosis by using FRET imaging." *Proc Natl Acad Sci U S A* 103 (37): 13872-7.
- Zanta M.A., Boussif O., Adib A. and Behr J.P. (1997). "In vitro gene delivery to hepatocytes with galactosylated polyethylenimine." *Bioconj Chem* 8 (6): 839-44.

CHAPTER III

ENTRAPMENT OF PLASMID DNA IN NANOGEL

3.1 Introduction

Since cationic polymers were introduced in the 1980s by Wu and colleagues (1987) as a non-viral vector, numerous polycations have been used for formulating DNA and other nucleic acids into complexes now termed polyplexes (Felgner *et al.* 1997). These formulations are based on electrostatic association between polyanionic DNA and positively charged polymers (e.g., Brown *et al.* 2001). However, the heterogeneous morphology of the polyplex system can make this type of formulation less favorable for practical applications. For instance, the molecular complexes as a pharmaceutical formulation suffer greatly from instability and the lack of reproducibility in their function as well as production. In theory and concept these problems associated with the polyplex system can be resolved by entrapping DNA inside the polymer matrix.

Polymeric nanoparticles are commonly prepared by polymerizing monomers present in the dispersed phase of a microemulsion system. A microemulsion is an optically isotropic and a thermodynamically stable micellar system comprised of water, oil and amphiphile (Danielsson and Lindman 1981). Unlike regular emulsions, they form

spontaneously without addition of mechanical energy. When polymerized, resulting nanoparticles show some of the properties of gels as well as colloids. As such they are often referred to as 'nanogels'. In terms of size, the nanoparticles derived from the microemulsions adopted in this dissertation work are similar to virus, which is significantly smaller than liposomes or O/W macroemulsions of 200 to 300 nm. Entrapment of nucleic acids in the nanogel would be feasible if one uses an inverse water-in-oil (W/O) microemulsion. Since pDNA with thousands of negative charges will not partition into the organic phase in the inverse microemulsion system, pDNA is to likely condense itself to reside in the aqueous phase along with monomers and crosslinkers. The model nucleic acid to be entrapped in nanogels in present study is plasmid DNA (pDNA) of 5-6 kbp. It was thought that the hydrophilic matrix of nanogels may render pDNA to coil itself into the aqueous droplets.

There are some potential hurdles in preparing pDNA-entrapped nanogel formulation. First, drug loading could be limited due to the small size of nanogel and the diluted nature of the system. However, pDNA as a cargo may have an advantage over other therapeutic molecules in that only a few copies are to be delivered. Secondly, the pDNA should remain intact during polymerization. This is important issue because the present polymerization involves free radical reaction (see results section **3.3.2** for detailed discussion on this subject). In addition, the polymer network enclosing pDNA should break down at some point during endocytic pathway or cytosolic trafficking so that the cargo can be released. As demonstrated by Budker *et al.* (2002), when pDNA of 5.9 kbp is entrapped in the aqueous phase of inverse microemulsions, pDNA is condensed as a ring or toroid structure. This finding is consistent

with the fact that the limited bendability of double stranded DNA tends to keep them in solution as a stiff rod up to about 150 bp, or 50 nm (Blackburn and Gait 1996). When forced to bend, the radius of curvature depends on the energetics involved. Since this diameter is close to that of individual nanogel particles, pDNA will likely dissociate from the nanogel only when the latter breaks down resulting in a complete loss of structural integrity. The synthetic strategy for cleavable linker was addressed in **Chapter II**.

In this chapter, the main topics of discussion are preparation of pDNA-entrapped nanogels and a series of efforts aimed for improving the entrapment efficiency. The latter includes the application of DNA condensing reagents as well as various radiolabeling methods in monitoring pDNA as a cargo and nanogel as a carrier.

3.2 Materials and Methods

3.2.1 Materials

Luciferase-encoding plasmid DNAs such as pGL3 Control Vector (5.2 kbp) and pCMV-Luc (6.2 kbp) were purchased from Promega (Madison, WI) and Elim Biopharmaceutical, Inc. (Hayward, CA), respectively. Laureth-3 was purchased from Heterene, Inc. (Paterson, NJ). Span 80 and Tween 80 were purchased from Aldrich. These surfactants were filtered through 0.22 μ m syringe filter (Fisher Scientific) before used. Mineral oil and all the organic solvents in ACS reagent grade were purchased from Fisher

Scientific. Poly(L-lysine)·HCl of 30-70 kDa or 4-15 kDa, poly(L-lysine)·HBr of 25 kDa, 2,2'-azobis (2-methylpropionitril) (AIBN), acetic anhydride, Tris-EDTA (TE) buffer of pH 7.4, ethidium bromide (EB) at 10 mg/mL, spermine·4HCl, antibiotics, protamine sulfate salt from salmon (Grade X), and all alkyltrimethylammonium bromides were purchased from Sigma. Poly(ethylene glycol) diacrylate (PEGdiA, M_n of PEO = 375 g/mol), PEG monoacrylate (PEG-A, M_n of PEO = 375 g/mol) and 2-acryloxyethyltrimethylammonium chloride (AETMAC) at 80 % in water were purchased from Polysciences (Warrington, PA). All monomers were used without any further purification. Poly(ethylene glycol) monomethacrylate (PEGmA, M_n of PEG = 375 g/mol), 2-hydroxyethyl acrylate (HEA), *N,N,N*-triethylamine (TEA), and 4-dimethylaminopyridine were purchased from Aldrich. Di(2-ethylhexyl) peroxydicarbonate (Trigonox EHP) was purchased from Akzo Nobel (Chicago, IL) and stored in - 20°C until used. [5,5'-³H]-deoxycytidine 5'-triphosphate, tetrasodium salt, (dCTP, specific activity; 60 Ci/mmol) and S-[methyl-³H]-adenosyl-L-methionine (SAM, specific activity; 85 Ci/mmol) at 0.55 mCi/mL in 10 mM sulfuric acid solution:ethanol (9:1) were purchased from Perkin Elmer Life and Analytical Sciences, Inc.(Waltham, MA). [1-¹⁴C]-Acetic anhydride (specific activity; 5 mCi/mmol) at 3 mCi/mL in dimethylformamide was purchased from American Radiolabeled Chemicals, Inc. (St. Louis, MO). Linear polyacrylamide at 5 mg/mL in water was purchased from Ambion (Austin, TX) and stored in - 20°C until used. NE buffer (10 X), CpG methylase (M. Sss I) at 20,000 U/mL and BstU I at 10,000 U/mL were purchased from New England Biolabs, Inc. (Ipswich, MA). Microspin G-25 column was purchased from Amersham Biosciences (Piscataway, NJ). SYBR Gold (10 X) was purchased from Molecular Probe (Eugene, OR).

Opti-MEM, Hanks' balanced salt solution (HBSS), Minimum Essential Medium (MEM) and fetal bovine serum (FBS) were purchased from Gibco BRL (Gaithersburg MD).

3.2.2 Preparation of pDNA-Entrapped Nanogel from Inverse Microemulsion

Microemulsion-derived polymeric nanogel was developed earlier (McAllister *et al.* 2002) and for this part of study, a mixture of [^3H]-pDNA and cold pDNA was added to aqueous phase along with other monomers to form microemulsion. Detailed procedures are as follows and depicted in **Figure 3-1**. An optically transparent inverse microemulsion is prepared by combining heptane as a continuous phase, surfactant [laureth-3, $\text{CH}_3(\text{CH}_2)_{12}\text{O}(\text{CH}_2\text{CH}_2\text{O})_3\text{H}$] and aqueous monomer solution in the typical weight ratio of 86:10:4. The aqueous solution contained all polar acrylates such as HEA, PEGdiA as a crosslinker, and AETMAC as positively charged monomer if needed. At this point, one of the weak base-containing monomers and pDNA were also added to the aqueous solution. For the test formulations, a disulfide crosslinker substituted the regular PEG crosslinker, PEGdiA. A small volume of the initiator, Trigonax EHP, in heptane with a final concentration of approximately 5mM was added to the microemulsion. The reaction mixture was then stirred at room temperature overnight, under argon atmosphere and protected from light. After the polymerized microemulsion was diluted with a biphasic water/heptane mixture, the aqueous phase was collected by centrifugation for 15 min at $2,500 \times g$ (GS-6R, Beckman, Fullerton, CA) and washed with n-butanol several times to extract the surfactant. The residual surfactant and unreacted monomers were further removed using dialysis with a dialysis bag

of MWCO 100 kDa (Pierce Biotechnology, Rockford, IL). The final preparation was stored at 4°C until used.

3.2.3 Transmission Electron Microscopy (TEM) of pDNA-Entrapped Nanogel

Procedure for electron microscopy was based on the method described earlier (Budker *et al.* 2002) but modified partly to obtain an improved resolution. A drop of poly-L-lysine (30-70 kDa) solution in water (10 mg/mL) was put onto Formvar-coated 200-mesh grid for 1 min. After the solution was removed by blotting on the filter paper and the grid was dried for a few min, a drop of sample was placed on the grid. After 4-5 min, the solution was removed and the grid was washed three times with n-butanol and one time with isopropanol followed by a single water washing. The staining was performed with 2% uranyl acetate for 30 sec. The samples were examined using a Philips CM12 electron microscope (Eindhoven, Netherlands) with 100 kv accelerating voltage. Digital images were made with a Gatan 780 DuoScan camera system attached to the microscope.

3.2.4 Preparation of Macroemulsion-Derived, pDNA-Entrapped Nanogel

In order to explore a possibility to prepare nanogels that entrap pDNA, polymerization was also attempted using a regular inverse emulsion. The procedure was based on Kriwet *et al.*(1998). Aqueous phase accounted for 30% (w/w) of whole formulation and consisted of monomers such as HEA or PEGmA and pDNA (pGL3 or pCMV-Luc) in diluted TE buffer. Continuous phase was mineral oil by 70 weight percent including 2% of

surfactants, Span 80:Tween 80 (3:1). Aqueous phase was added gradually into oil phase while magnetic stirring. Emulsion was heated to 50°C in water bath and purged with argon for 20 min. 2,2'-azobis (2-methylpropionitril) in benzene was added to the reaction by 0.125% and the reaction was kept stirred at 50°C for 4 hrs. After cooling down at room temperature, reaction mixture was diluted with equivalent volume of distilled water followed by centrifugation at 14,000 x g for 10 min on Eppendorf Model 5415D Microcentrifuge (Eppendorf, Westbury, NY). Aqueous layer (bottom layer) was collected and washed with hexane four times. Plasmid DNA was extracted using ethanol precipitation, reconstituted in TE buffer and subject to electrophoresis on 0.75% agarose gel.

3.2.5 Radiolabeling of pDNA

3.2.5.1 Nick Translation

Plasmid DNA labeling was performed using commercially available kit from Amersham Biosciences (N5000) as described below. Into a clean 2-mL microcentrifuge tube containing 1 µg of pDNA (pGL3) diluted in distilled water at 100 ng/µL, 20 µL of nucleotide-containing buffer (dNTP), 15 µL of [³H]-dCTP, 10 µL of enzyme solution (0.5 units/µl DNA polymerase I and 10 pg/µl DNase I), and 45 µL of sterile distilled water were added. Following gentle mixing and brief spinning, the mixture was incubated at 15°C for 2 hrs. The reaction was stopped by adding 10 µL of 0.2 M EDTA (pH 8.0). Unincorporated nucleotides were removed using Sephadex G-25 spin column (Amersham Biosciences, Piscataway, NJ) at 800 x g for 2 min.

Further purification was performed by phenol/chloroform extraction and ethanol precipitation. In general, oligonucleotides larger than 20-mer (i.e., 20 nucleotides) precipitates out, leaving unincorporated nucleotides in solution. A pre-mixture of phenol/chloroform (Sigma) was added to an equal volume of aqueous pDNA solution. The mixture was vortexed and placed on dry ice for 1 min followed by centrifugation at 12,000 x g for 5 min at 4°C. Equivalent volume of fresh chloroform was added to the aqueous layer. Mixture was then vortexed briefly, placed on dry ice for 1 min, centrifuged at 12,000 x g for 5 min at 4°C and the top layer was subject to ethanol precipitation. Into the aqueous layer collected previously, 1 µL of linear polyacrylamide (5mg/mL), one volume of 4 M ammonium acetate (pH 4.5), and four volumes of 95% ethanol were added while gentle mixing by inversion. The mixture was chilled for 15 min on dry ice before centrifuged at 14,000 x g for 30 min at 4°C. The pellet obtained was washed with 500 µL of 80% ethanol, air-dried and re-dissolved in 100 µL of TE buffer. The specific activity was measured using Nanodrop Model 1000 (NanoDrop Technologies, Wilmington, DE) and a Packard Model Tri-Carb 2900TR liquid scintillation counter (Packard Bioscience Company, Meriden, CT). The yield was 65-90% and specific activity was $0.5-2 \times 10^7$ dpm/µg of pDNA.

3.2.5.2 Methylation

Enzymatic methylation was utilized to radiolabel pDNA (Bureau *et al.* 2004). Into a 2-mL microcentrifuge tube containing 100 µCi of [³H]-SAM (a substrate of CpG methylase and the source of methyl group) and 10 X NE buffer, 4 µg of template pDNA (pCMV Luc, 6.2 kbp), CpG methylase (10 U/µg pDNA), and 16 µL of 1 M Tris free base in water were

added. Total final volume was made to 40 μL using distilled water. [^3H]-SAM (180 μL) originally dissolved in the mixture of 10mM H_2SO_4 and ethanol (9:1) was added to the reaction tube and concentrated (final volume was 1-3 μL) using a Speed Vac Model Savant SC 110 (Global Medical Instrumentation, Inc, Ramsey, MN). To adjust pH of the reaction to 7-8, Tris solution was added to the reaction in such a way 8.5 μL of Tris solution was added to 100 μL of SAM. The reaction was incubated at 37°C water bath for 2 hrs. Unincorporated [^3H]-SAM was removed using Sephadex G-25 microspin column. Tritium labeled pDNA was further purified by phenol/chloroform extraction and ethanol precipitation. Specific activity and yield were calculated in the same manner as described in section 3.2.4.1. The specific activity thus achieved was $\sim 2 \times 10^6$ dpm/ μg of pDNA.

3.2.6 Radiolabeling of Nanogel

Nanogel was radiolabeled by incorporating [^{14}C]-labeled, PEG-based monomer that was synthesized as follows. Mixture of [^{14}C]-acetic anhydride and cold acetic anhydride was added to 25-mL round bottom flask containing 1.5-mole equivalent of PEG-A (average M_n of PEO =375) in 5 mL of anhydrous methylene chloride. One mole equivalent of TEA as a proton scavenger and one-tenth mole equivalent of 4-dimethylaminopyridine as a catalyst were added and the reaction was kept under magnetic stirring for 2 hrs at room temperature. In the anhydride mixture used, the mole ratio of hot to cold acetic anhydride was approximately 0.006 to 1 and the initial amount of hot acetic anhydride was 1.3×10^7 dpm (6 μCi). After 2 hrs, the product was purified in a column chromatography on silica gel using

the mixture of methanol and chloroform (15:85% v/v) as a mobile phase. The reaction yield was approximately 90% and the specific activity thus obtained was 1.7×10^5 dpm/mg.

3.2.7 Entrapment Efficiency

Subsequent to concentration in Speed Vac, nanogels entrapping pDNA were electrophoresed on agarose gel (0.8% w/v) (Denville Scientific, Metuchen, NJ) for 45 min at 90 volts in Tris-acetate-EDTA (TAE) buffer. Ethidium bromide was included in the gel at a final concentration of 0.5 $\mu\text{g/mL}$ to monitor the location of pDNA using a Bio-Rad Versa Doc Model 1000 Imaging System (Bio-Rad Laboratories, Inc., Hercules, CA). To assess the entrapment efficiency of pDNA in nanogel, each lane of an agarose gel was cut into 3-5 segments from the top to the bottom. Gel segments were put into 20-mL glass vials containing 9 mL of scintillation cocktail solution (UltimaTM Gold XR, Sigma) and incubated overnight on the rocker at room temperature before reading radioactivity in a Packard Model Tri-Carb 2900TR liquid scintillation counter (Packard Bioscience Company, Meriden, CT).

3.2.8 Size Measurement

Hydrodynamic diameter was measured at 23°C using viscosity of 0.933 centipoise and refraction index of 1.333 on a NICOMP Model 370 dynamic light scattering instrument (Particle Sizing Systems, Santa Barbara, CA), equipped with a 30-mW laser (632.8-nm wavelength) and an Avalanche photodiode detector. The scattered light intensity detected at a 90° angle was treated using the Gaussian or multimodal Nicomp analysis, depending on the

polydispersity of the samples. Data presented here corresponds to the volume-weighted distribution. The mean diameters shown were averages of duplicate measurements performed on different samples for periods of time long enough (from 10 to 40 min) to collect statistically reliable data.

3.2.9 Condensation of pDNA

For this portion of the present study, pCMV-Luc purchased from Elim Biopharmaceutical (Hayward, CA) was used as received.

3.2.9.1 Spermine: $\text{NH}_2(\text{CH}_2)_3\text{NH}(\text{CH}_2)_4\text{NH}(\text{CH}_2)_3\text{NH}_2 \cdot 4\text{HCl}$

Spermine·4HCl was considered to have 4 positive charges per molecule at physiological pH. At various charge ratios (i.e., 0.01 – 1,000), spermine was mixed with 1 µg of pDNA in 0.5 X TE buffer and incubated for 30 min at room temperature. SYBR Gold (1 X) was added to the mixture and the mixture was briefly vortexed and put on a rocker for 20 min before fluorescence measurement at 495nm/537nm (Ex/Em) using a Perkin Elmer Model LS50B spectrofluorometer (Perkin Elmer Life and Analytical Sciences, Inc., Waltham, MA). For the size measurement of spermine-pDNA complex, 20 µg of pDNA was added into a glass cuvette containing varying amount of spermine dropwise under vortex-mixing and the mixture was subject to size analysis on NICOMP for 10 min.

3.2.9.2 Poly(L-lysine) (PLL)

The average molecular weight of PLL (4-15 kDa) used was 9,500 g/mol. Into 10 µg of pDNA in 600 µL of 0.5 X TE buffer, a constant amount of PLL was consecutively added until the charge ratio (positive to negative) reached 0.8 with 5-min vortexing and 10-min size measurement after each addition.

3.2.9.3 Alkyltrimethylammonium Bromide

Constant amount (9 µg) of cetyltrimethylammonium bromide [$\text{CH}_3(\text{CH}_2)_{15}\text{N}(\text{CH}_3)_3\text{Br}$, **CTAB**] was consecutively added to 80 µg of pDNA in 500 µL of 0.5 X TE until the N/P ratio reached 1.1. After each addition, the mixture was vortex-mixed briefly and the size measurement was performed for 10 min. Into a separate tube, 40 µg of pDNA was added dropwise into a glass cuvette (Fisher Scientific) containing different amount of dodecyltrimethylammonium bromide [$\text{CH}_3(\text{CH}_2)_{11}\text{N}(\text{CH}_3)_3\text{Br}$, **DDTAB**] and the size of complex was measured in NICOMP for 10 min. The complex formation was performed in 500 µL of a mixture of TE buffer and water. The portion of TE buffer (10mM Tris/1mM EDTA, pH 8) in the mixture varied from 0 to 100 %. Into a glass cuvette containing varying amount of decyltrimethylammonium bromide [$\text{CH}_3(\text{CH}_2)_9\text{N}(\text{CH}_3)_3\text{Br}$, **DTAB**], 20 µg of pDNA in distilled water or 0.5 X TE was added dropwise under vortex-mixing and the mixture was subject to NICOMP.

3.2.9.4 Protamine

Protamine used for this study is a basic protein of 5.1 kDa derived from salmon. It consists of 31 amino acids (H-PRRRSSSRPVRRRRRPRVSRRRRRRGGRRRR-OH) and most of them are arginine (i.e., 21 R per molecule). Condensation of pDNA by protamine was monitored using dye exclusion assay and displacement assay. In the former, protamine was complexed with pDNA at various N/P ratios (i.e., 0 to 5), followed by 20-min incubation at room temperature before 1 X SYBR Gold was added. Fluorescence was measured after a thorough mixing for 10 min using a Perkin Elmer Model LS50B spectrofluorometer. In the latter assay, ethidium bromide was mixed with pDNA first such that the mole ratio between ethidium bromide and base pair of pDNA was 1 to 1. The mixture was then incubated for 3 min at room temperature before and after the consecutive addition of constant amount of protamine followed by fluorescence measurement. The data was represented by relative fluorescence (F_R), which was calculated from the following equation.

$$F_R (\%) = \frac{(F_M - F_E)}{(F_{ED} - F_E)} \times 100$$

Where F_M , Fluorescence of pDNA-EtBr in the presence of protamine; F_E , Fluorescence of EtBr alone; and F_{ED} , Fluorescence of pDNA-EtBr in the absence of protamine.

For the size measurement of protamine-condensed pDNA, 10 μ g of pDNA was added dropwise into a series of glass cuvettes containing different amount of protamine under vortex mixing and the size of complex was measured in NICOMP for 10 min. The complex

formation was performed in 500 μ L of a mixture of TE buffer and water. The portion of TE buffer (10mM Tris/1mM EDTA, pH 8) in the mixture varied from 0 to 100%.

3.2.10 Recovery of Condensed pDNA in Aqueous Layer from Biphasic Heptane/Water System

The mixture of [3 H]-pCMV Luc and cold pDNA was added slowly into the water solution of protamine or other cationic lipids (CTAB, DDTAB, and DTAB) and 40-volume of heptane was added to the complex solution followed by brief vortex and centrifugation. The aqueous layer was collected and subject to DPM reading using a liquid scintillation counter. Various N/P ratios (i.e., 0.2 to 100) and different adding orders (i.e., pDNA to protamine or vice versa) were tested in forming protamine-pDNA complex to compare recovery efficiency under the specified reaction conditions. Pre-coating of vessels was performed by multiple rinsing of 2-mL tubes and tips with 1 mL of PLL-HBr (25 kDa) at 5 mg/mL and drying at a 50°C-oven for 2 hrs. Into a pre-coated tube, DDTAB was added first followed by the consecutive addition of pDNA and heptane. The layer collection and DPM reading were performed in the same manner as described above.

3.2.11 Transfection

Human colon carcinoma HeLa cells from ATCC (Manassas, VA) were seeded at 5×10^4 cells per well in 0.5 mL of MEM in 24-well flask (Corning, Inc., Corning, New York) 18 hrs prior to transfection. Immediately before transfection, cells were rinsed with HBSS and

supplemented with 0.5 mL of Opti-MEM. The nanogel formulations containing plasmid DNA were diluted in 100 μ L of Opti-MEM, vortexed and added to the cells. After 4-hr incubation, the medium was removed, rinsed with HBSS and supplemented with normal growth medium (MEM) containing 10% fetal bovine serum and 1% antibiotics (penicillin/streptomycin). Luciferase gene expression was monitored 48 hrs later by using a commercial kit (Promega Corporation, Madison, WI). Briefly, the culture medium was discarded and cell lysate was harvested after incubation of cells for 5 min at room temperature in 100 μ L of 1 X lysis reagent (Promega). The cell lysate was vortexed gently and centrifuged for 2 min at 12,000 x g at 4°C. Twenty microliters of supernatant was diluted into 100 μ L of luciferase reaction buffer (Promega) and the luminescence was integrated over 10 sec in a Monolight Model 3010 luminometer (Analytical Luminescence Laboratory, Sparks, MD). Each transfection experiment was run in quadruplicate and was expressed as relative light unit per microgram of cell protein. The total protein content was measured using bicinchoninic acid (BCA) assay (Pierce Biotechnology, Rockford, IL).

3.3 Results and Discussion

3.3.1 Preparation of pDNA-Entrapped Nanogel and Characterization by TEM

Figure 3-1 illustrates how pDNA was entrapped in nanogel formulation. As indicated in **Chapter II**, one of the key features of nanogels derived from W/O inverse microemulsion is its hydrophilic matrix, which enables the entrapment of polar substances such as nucleic acids. As expected, pDNA was compatible with other monomer components in the aqueous phase and did not form any precipitates when mixed with heptane, the continuous phase. Polymerization and purification were performed similarly to what discussed in the **Chapter II**. Further investigation such as entrapment efficiency, interaction with monomers, and stability of pDNA under free radical reaction will be discussed in the latter sections in the present chapter.

In an early stage of the development of this formulation, pDNA-entrapped nanogel was examined under microscope. **Figure 3-2** shows microemulsion (arrows in **A-C**) and polymerized nanogels (**D-F**) entrapping pGL3 of 5.2 kbp negatively stained using 2% uranyl acetate. As shown in **A, B** and **C** in **Figure 3-2**, multiple ring-like structures (arrows) were observed, demonstrating that pDNA was indeed entrapped in the formulation. Similar observation was reported in earlier works by other investigators (e.g., Budker *et al.* 2002). Since no purification step was attempted for the present microemulsion formulation, significant amount of other substances, mostly surfactants, co-existed. The bottom panels (**D, E** and **F**) in **Figure 3-2** represented TEM of purified nanogels containing pDNA. Sephadex

G-15 (Sigma) column was used for the additional purification of nanogels in the present study. The diameters of the purified nanogel formulations in the figures ranged from 100 to 300 nm. However, the size represented here must have represented the flattened structures of the nanogel on the grids even though they contained 12% of crosslinker (i.e., PEGdiA). The monolithic appearance of pDNA-containing nanogel (**D**, **E**, and **F**) may well represent one of the following possibilities: (1) even though negative staining was attempted using uranyl acetate, the actual staining performed could be a positive staining under the condition carried out in this study; (2) the probable collapse of the top part of the specimen into the center might decrease the resolution in the center. This is particularly feasible considering that the specimen was dried rather intensively. Trace amount of unwanted substances observed in purified nanogel formulations (arrow heads in **Figure 3-2D**) could be an artifact derived from the specimen preparation or staining processes. Taken together, TEM pictures presented here demonstrated that pDNA was indeed entrapped in the formulation.

3.3.2 Stability of pDNA under Free Radical-Initiated Polymerization

DNA can be degraded by both oxygen- and carbon-centered free radicals that can attack both sugar and base moieties (Breen and Murphy 1995). The initiator used in polymerizing water-soluble acrylates was lipid-soluble Trigonax EHP. Thermal hemolytic degradation at room temperature generates CO₂ and oxygen-centered radicals, which abstract hydrogen from the terminal ethylene carbon of acrylate. The resulting carbon-centered radicals then propagate to form polymer chains. As a result, both types of radicals will bombard nucleic acids residing in the aqueous phase of microemulsion along with monomers.

Naked pDNA also could be susceptible to radical attack but, there is a substantial protection of DNA from radicals by components in a formulation such as ascorbic acid (Quick and Anseth 2003). Since radical scavengers works against polymerization, unrelated small yeast RNA was used as a radical “decoy” that may interact with radicals at reactivity similar to that of pDNA but based on the law of mass action may protect pDNA. In this part of the study, regular emulsion containing one of the acrylate monomers along with pDNA was used in testing the effect of free radicals on the stability of pDNA. The reason why regular emulsion system, instead of microemulsion, was utilized here was because polymerization derived from microemulsion is taking significant amount of time and involves so many purification steps. By adopting the procedures of Kriwet *et al.*(1998), series of tests could be performed in more efficient fashion. The concentration of pDNA in aqueous phase of emulsion was set to 40 µg/mL, which is the lowest end of the concentration range (i.e., 40-200 µg/mL) that will be used in the eventual preparation of pDNA-entrapped nanogel for transfection study.

As shown in **Figure 3-3**, pDNA under AIBN-initiated radical reaction (lane **4** through **11**) appeared to remain intact and no decomposed DNA fragment at lower part of gel was observed. The pDNAs recovered from the radical-mediated polymerization showed very similar mobility on the gel to that of pDNA extracted from the mixture with pre-made polymers (lane **12**). Interestingly, the formulation with larger amounts of monomers (lane **4**) showed improved recovery of pDNA than in the formulations containing less amounts of monomers (lane **6** and **8**). The addition of yeast RNA did not make much difference (lane **10** vs. **4**) under the present condition. All pDNA extracted from the reaction were identified using a corresponding restriction enzyme, Hind III (odd numbered lanes). The effect of

monomer in different concentrations on the recovery of pDNA from polymerization was further investigated using pCMV-Luc of 6.2 kbp and another monomer, HEA.

As shown in **Figure 3-4A**, the recovery of pDNA in aqueous layer after emulsion polymerization increased in HEA concentration-dependent manner (see lane **3** through **6**). This is in agreement with the previous findings with PEGmA (M_n of PEO=375 g/mol). Another noticeable observation was that pDNA transformed toward open relaxed circular form after being through polymerization while control pDNA (lane **2**) and pDNA extracted from a simple mixture with pre-made polymer (lane **7**) showed a typical ratio between open relaxed circular (upper band) and supercoiled form (lower band). Since there was no apparent degraded fragments on the gel when pDNA extracted after polymerization loaded, it is difficult to attribute the low recovery of pDNA with less amount of monomers to degradation of pDNA under this condition. Thus, in the following investigation, interface was also included for examination of pDNA recovery. **Figure 3-4B** demonstrated that the presence of HEA rendered more pDNA to stay in the aqueous layer (lane **5**) while most of pDNA resided in the interface (lane **7**) rather than aqueous phase. Taken together, pDNA was stable under radical polymerization when formulated at 40 $\mu\text{g/mL}$ in aqueous phase. The recovery of pDNA in aqueous phase improved in the presence of monomers such as HEA and PEGmA.

3.3.3 Radiolabeling of pDNA

To facilitate the detection of pDNA in the next series of experiments, pDNA was labeled with radioisotopes. Two different methodologies in radiolabeling were applied and described in the present section.

The first method attempted was nick translation reaction. Nick translation employs two enzymes as described earlier by other investigators (Kelly *et al.* 1970; Rigby *et al.* 1977). As illustrated in **Figure 3-5A**, pancreatic deoxyribonuclease (DNase I) creates random nicks on the strands. *E. coli* DNA polymerase I has three distinct activities; 5'-3' template-dependent DNA polymerase activity, 5'-3' exonuclease activity, and 3'-5' exonuclease activity. The nick translation uses the first two of these activities. DNA polymerase I adds sequentially new nucleotides on 3'-end of a nick within a DNA duplex while removing nucleotides from the adjacent 5'-terminus of the nick. During this procedure, radiolabeled nucleotides, [³H]-dCTPs, are incorporated into the pDNA to produce a uniformly-labelled population of pDNA. The specific activity achieved was 1.8×10^7 dpm/ μ g, which agrees with that reported by the kit supplier (Amersham Biosciences, Piscataway, NJ). However, when the integrity of tritium labeled pDNA was tested on the agarose gel, the labeled pDNA was found to be fragmented during the labeling and showed up as 200-500 base pair fragments on the gel (lane **C** and **D** in **Figure 3-5B**). This is approximately one tenth of the original pDNA in size. Although nick translation has been applied in labeling PCR products as *in situ* hybridization probes for immunocytochemistry (e.g., Baldini *et al.* 1992; Parrilla *et al.* 2003), this method is patently not suitable for the present investigation, where an intact,

non-degraded radiolabeled pDNA is needed in assessing the behavior in nanogel formulations.

The second attempt to radiolabel pDNA was methylation. A typical procedure for preparing [^3H]-pDNA using this method can be found in Bureau *et al.* (2004). The enzyme CpG methylase (M. Sss I) methylates specifically C-5 positions of cytosine residues within the double-stranded dinucleotide (C-G) recognition sequences (**Figure 3-6A**) using SAM (**Figure 3-6B**) as a methyl donor. This enzymatic methylation only occurred at pH 7-8 and Tris base needed to be added to neutralize sulfuric acid coming from [^3H]-SAM stock solution. Tritium labeled pDNA appeared very similar to the unmodified pDNA when run on 0.8% agarose gel in terms of the movement of two different biological structures, open relaxed and supercoiled form, on the gel (upper and lower band in the lane **B** of **Figure 3-6D**, respectively). The gel segment corresponding to [^3H]-pDNA (**B2** in **Figure 3-6E**) showed almost 100% DPM level of total input.

The specific activity achieved was 1.81×10^6 DPM / μg of pDNA. Unmethylated CpG motifs are prevalent in bacterial but not vertebrate DNAs (Nur *et al.* 1985). Methylation on CpG sites protects pDNA from digestion by restriction enzymes whose recognition sites either contain the sequence CG or overlap the dinucleotide. As shown in **Figure 3-6C**, unmethylated pDNA was susceptible to BstU I derived from *Bacillus stearothermophilus* and produced 5 to 6 smaller fragments (lane **3**). The complete blocking of cleavage was achieved when the substrate, SAM, was used in 5-fold molar excess of the CpG acceptor sites to methylate constant amount of pDNA (lane **9**). Considering pCMV-Luc derived from firefly

was labeled in the presence of excess amount of substrate (SAM) and the CpG acceptor sites counted in one molecule of pDNA was 309, the maximum achievable specific activity would be 1×10^7 dpm/ μ g. It thus appears to indicate that only part of CpG sites, approximately 15-20%, is originally unmethylated and generates the present specific activity. Taken together, the present data demonstrated the integrity of [3 H]-pDNA labeled by methylation would be suitable with the subsequent studies.

3.3.4 Radiolabeling of Nanogel

Radiolabeling of nanogel with different isotopes makes it possible to monitor nanogel and pDNA independently during in situ entrapment. It was achieved by radiolabeling one of the monomers and incorporating it into the polymerization. Unfortunately, however, the acetylated HEA (**Figure 3-7A**), which initially attempted to be labeled, was too hydrophobic to partition into aqueous phase during microemulsion formation even when 50% methanol was added to the aqueous phase. A PEG-based monomer, more polar compound, was thus selected and acetylated with [14 C]-acetic anhydride. As shown in **Figure 3-7B**, PEGmA with MW of ~ 400 g/mol was acetylated with [14 C]-acetic anhydride to prepare the radiolabeled monomer, acryloylPEGacetate. It indeed remained in the aqueous phase, implying that this monomer is compatible with microemulsion polymerization. The specific activity was 1.7×10^5 DPM/mg of monomer. This was hot enough for analysis when incorporated to nanogel.

3.3.5 Entrapment of Uncondensed pDNA

First attempt to entrap pDNA in nanogels is summarized in **Figure 3-8**. Mixture of [^3H]-pDNA and cold pDNA was introduced to microemulsion system. The composition of microemulsion was either 10% crosslinker (PEGdiA)/90% HEA or 10% PEGdiA/65% HEA/25% cationic monomer, AETMAC. The former formulation produced neutral nanogel entrapping pDNA while the latter generated pDNA-entrapped cationic nanogel. In the neutral nanogel (**Figure 3-8**, lane **B**), pDNA traveled the same distance as the control pDNA (lane **E**). About 44 % of radioactivity was recovered at the top of the gel (right panel, **B1**), indicating that close to a half of pDNA was entrapped in the nanogel and retained at the loading well. The present level of entrapment, 44%, is in agreement with what Goh and colleagues reported with pDNA-entrapped microparticle system (2004). In case of the cationic nanogels, no significant pDNA was detected in the middle part of the gel for both entrapment (lane **C**) and mixture formulations (lane **D**). In a closer examination, pDNA in these two formulations appeared to move upward, implying that the net charge of these formulations was positive. In these two groups, above 80% of radioactivity was found at the top of the gel (right panel, **C1** and **D1**), while only 10% of radioactivity was detected in the middle of the gel. In the entrapment formulation using cationic nanogel (lane **C**), part of pDNA could be entrapped inside of nanogel and another part of them bound on the surface by electrostatic interaction. In the mixture of pDNA with cationic nanogel (lane **D**), which served as a control group for this study, majority of pDNA remained bound to the nanogel, similar to the case of entrapment formulation.

In the next series of experiments (**Figure 3-9**), nanogels were prepared by incorporating [^{14}C]-PEG acrylate (4% w/w) and the amount of pDNA was reduced compared to the previous experiment (i.e., pDNA:monomers = 1:10,000 vs. 1:3,000 in **Figure 3-8**). The main objective of this study was to see if there would be any improvement in entrapment efficiency under this set of conditions. Here, the charge ratio between cationic monomers and phosphate groups of pDNA was adjusted in such a way that the formulations contained 0-, 1-, or 10-fold excess amount of positive charges. In the previous experiment (**Figure 3-8**), the charge ratio (N/P ratio) was found to be approximately 1,000 (i.e., large excess of positive charge). Three out of the five test groups were entrapment formulations (**Figure 3-9**, lane **B-D**) and designed to have different charge ratios. The other two test groups were mixtures of pDNA with pre-made neutral (lane **E**) or cationic nanogel (lane **F**). As shown in the right panel of **Figure 3-9**, the radioactivity for ^{14}C (open bars) was measurable only in the loading well of the gel. The total recovery of ^{14}C radioactivity was as low as 10-13%. Although the net reaction yield of polymerization is known to be around 45 %, the low level of ^{14}C recovery found here may represent that the incorporation of [^{14}C]-PEG acrylate into nanogel was not as good as the other monomers probably due to its limited water solubility.

As to pDNA in the entrapment formulations (lane **B-D**), a trace amount of pDNA was barely observed on the middle part of the gel. Radioactivity reading of ^3H was also very low (8-12% of initial amount) at the top of the gel (right panel, **B1**, **C1**, and **D1**), indicating a limited amount of pDNA entrapped in the nanogel in all test groups. Unexpectedly, significant amount of radioactivity from ^3H (25-60% of initial amount) was detected at the lower part of the gel in all test groups (right panel, **B3**, **C3**, and **D3**) while only 3-4% of

initial input of radioactivity was measured in the mixtures (**E3** and **F3**). This could well be due to degradation of pDNA during polymerization. The concentrations of pDNA in TE buffer of aqueous phase were 333 and 100 µg/mL in the previous (**Figure 3-8**) and present experiments, respectively. Since pDNA was found to be stable even at a concentration as low as 40 µg/mL in an emulsion system (**Figures 3-3** and **3-4**), the condition that the pDNA encountered during EHP-initiated microemulsion polymerization might have been much harsher than with the emulsion system. Even though there was some success in entrapping pDNA in the nanogel (44% in the first experiment), the result was not reproducible when reduced amount of pDNA used. The incidence of probable degradation of pDNA during the processing was also observed, indicating that some additional efforts for tuning the reaction condition will be needed. Overall, pDNA entrapment was less favorable in this system than once expected.

3.3.6 Entrapment of Condensed pDNA and Transfection Study

In order to increase the pDNA entrapment efficiency, condensation of pDNA was attempted prior to polymerization. Condensing reagents tried in the present study included multivalent cationic molecules such as spermine, PLL, and protamine as well as cationic surfactants such as alkyltrimethylammonium bromide. Polyamines such as spermine (tetravalent) and spermidine (trivalent) have been utilized in precipitating or condensing DNA for the past several decades (Hoopes and McClure 1981; Porschke 1984; Raspaud *et al.* 1999; de Frutos *et al.* 2001; Vijayanathan *et al.* 2001; Kral *et al.* 2002). Dye exclusion by pDNA-spermine complex was utilized to monitor pDNA condensation (**Figure 3-10A**). Even

at N/P ratio=1,000, however, the level of fluorescence stayed high and never reduced to baseline level (i.e., approximately 20 by SYBR Gold alone), implying that the condensation was not completed with spermine. Size measurement of spermine-pDNA complex at various N/P ratios also supported the observation. The size of complex was smallest at N/P=1 with approximately 500 nm, however, increased significantly with higher N/P ratios (**Figure 3-10B**). The present data clearly indicate that spermine is not suitable since the size of complex was still too large and complete condensation was not obtained.

Many examples of utilizing PLL as a condensing reagent can be seen in previous studies (Hansma *et al.* 1998; Kogure *et al.* 2004; Masuda *et al.* 2005). In most of these investigations used PLL of ~ 25 kDa to condense pDNA of 5-6 kbp. As shown in **Figure 3-10C**, the size of PLL (25 kDa)-pDNA (6.2 kbp) complex ranged from 180 nm to over 2 microns depending on N/P ratio applied. However, the N/P ratio that produced relatively small complex (i.e., less than 200 nm) was too narrow a range, 0.4 to 0.6 in N/P. In addition, the size of complex abruptly increased outside of this range even up to over micron size, implying that aggregation of the complex at high N/P ratio.

Interaction of pDNA with cationic surfactants such as cetyltrimethylammonium bromide (CTAB) have been extensively investigated as exemplified by Melnikov *et al.* (1995). This study demonstrated that the DNA-CTAB complex changes from coil-like to globular state depending on the concentration of CTAB and that aggregation occurs when the surfactant concentration further increased and became close to its critical micellar concentration (CMC). **Table 3-1** represents the change in size of pDNA-CTAB complex

with varying N/P ratios. The concentration of CTAB was 5×10^{-5} M at N/P=1, which is approximately 18-fold lower than its CMC, 9×10^{-4} M. Most of the complexes showed multiple size populations and none of the major populations were smaller than 200 nm. Since a surfactant forms micelle at a concentration above its CMC, the actual amount of unassociated surfactant available for the complexation with pDNA will be limited by its CMC. In addition, the interaction of pDNA with micelles leads to aggregations. Thus, the higher CMC a surfactant has, the more pDNA can be added in the complex formation, leading to a higher yield of entrapment of DNA. Ouyang *et al.* (2000) also suggested that CMC must be higher than 10^{-2} M for cationic surfactant to become a practically useful DNA condensing reagent. Dodecyltrimethylammonium bromide (DDTAB) and decyltrimethylammonium bromide (DTAB) are with CMC of 1.6×10^{-2} M and 6.8×10^{-2} M, respectively (Rosen 1978). With this high CMC values, these agents were tried in condensing pDNA in the follow-up studies.

As shown in **Figure 3-11A**, not only N/P charge ratio but also the concentration of pDNA was a factor in determining the final size of condensed pDNA with lower concentration generating smaller size. The concentration of TE buffer was also a critical function in that the size increased almost linearly with TE buffer concentration (panel **C**). The most reproducible result by DDTAB was yielded when pDNA condensed in water at N/P=4 as represented in panel **B**. The final concentration of pDNA was as high as 80 $\mu\text{g/mL}$. In the case of DTAB (C_{10}), a much higher N/P ratio (i.e., 80) was needed to achieve small size of condensed pDNA (~ 50 nm) in both TE and water solution (panel **D**).

Protamines, which package DNA in vertebrate sperm cells, have been showing promising results in condensing pDNA as demonstrated in previous investigations (e.g., Allen *et al.* 1995; Vilfan *et al.* 2004; Masuda *et al.* 2005) and have been used for gene delivery (Li and Huang 1997; Faneca *et al.* 2004; Maruyama *et al.* 2004). The condensation of pDNA with protamine was monitored using both dye exclusion assay (**Figure 3-12A**) and displacement assay (**Figure 3-12B**). The methodology applied here to monitor DNA condensation was exemplified in Budker *et al.* (2002) and Geall and Blagbrough (2000). Ethidium bromide is known to intercalate into base pairs of DNA intensifying fluorescence at least 20-fold probably due to the blockage of transferring a proton to the polar solvent in the more hydrophobic intercalated environment (Olmsted and Kearns 1977). SYBR Gold is presumed to act in the same way when bound to DNA. At N/P=2, protamine-condensed pDNA excluded the access of dye and showed almost same value of fluorescence as that of dye alone (panel **A**). Ethidium bromide that was previously bound to pDNA is displaced by protamine, resulting in a decreased fluorescence intensity. As shown in panel **B**, the relative fluorescence intensity of pDNA bound-ethidium bromide reached almost baseline (i.e., that of unbound ethidium bromide) when N/P ratio approached 2.0. Taken together, the present set of data indicates that protamine is very efficient in condensing pDNA even at a relatively low N/P ratio.

As shown in **Figure 3-13**, the resulting protamine-pDNA complex formed in water was 110 nm even at N/P ratio 0.2 (panel **A**). At this N/P ratio, the net charge of the complex remains negative rendering its partition to the aqueous phase favorable. The concentration of pDNA in panel **A** was 20 µg/mL in water. At the same concentration but in TE buffer, the

size of complex increased by TE-concentration dependent manner (panel C). The extent of complex size growing in TE buffer was more profound than the case with DDTAB shown earlier in **Figure 3-11C**. If the upper size limit of the complex favorable in microemulsion is assumed to be around 200 nm, the maximum concentration of pDNA complexed with protamine in aqueous phase would be close to 200 $\mu\text{g/mL}$ as represented in panel B of **Figure 3-13**. Another interesting finding was that the order of mixing between protamine and pDNA also determined the final size of the complex. The size of complex formed by slowly adding pDNA to protamine (open bars in panel B) was significantly larger than the case of reverse-ordered addition (i.e., adding protamine to pDNA, gray or closed bars in panel B), especially at high pDNA concentration. The complex size remained close to 200 nm even at N/P ratio 1.0 and at 200 μg pDNA/mL in water. The present observation suggests that 1 mL of aqueous phase can accommodate up to 200 μg of pDNA when complexed with protamine by N/P ratio 0.2 -1.0.

DNA condensation is a dynamic decrease in the volume occupied by a DNA molecule and is difficult to clearly distinguish from aggregation or precipitation. Condensation is a general term for the situations in which the aggregate is of finite size and orderly morphology such as toroids, rods, or spheroids (Bloomfield 1996). Thus condensation of pDNA by multivalent cationic molecules or surfactants is basically aggregation phenomenon in some sense. However, if aggregation occurs too aggressively in the formulation, it will affect not only the size of complex but also the recovery of the condensed pDNA in aqueous phase since the original polar property of pDNA will change when complexed with condensing reagents.

Figure 3-14A shows the percent recovery of pDNA condensed with various compounds, assessed by monitoring radioactivity in the aqueous phase. The latter was collected from the biphasic system consisting of 950 μ L of heptane and 50 μ L of water as described in Methods section. The N/P ratio used in each different condensing reagent was the ratio at which the smallest complex was observed (e.g., protamine condensed pDNA of 60 nm at N/P=100 as shown in **Figure 3-13A**). In the case of CTAB, the N/P ratio 20 was selected based on the investigation of Melnikov *et al.* (1995). In general, the recovery of condensed pDNA in aqueous layer was very low and ranged from 5% in CTAB to 36% in protamine. Since no measurable radioactivity was detected in heptane layer, the rest of condensed pDNA probably stayed in the interface or remained stuck on the wall of vessels or tips used to transfer sample solution. As proven in the subsequent experiment, the assumption was correct and as much as 60% of initial amount of radioactivity was measured in the tubes (data not shown). To resolve this problem, tubes was pre-coated using PLL (25 kDa) solution before pDNA condensation was performed. The recovery of pDNA condensed with DDTAB indeed improved and 75% of initial radioactivity was measured in aqueous layer in the pre-coated tube while only 17% recovered in the uncoated tube (**Figure 3-14B**). Although the recovery of condensed pDNA in the precoated tube was still lower than that of uncondensed pDNA (92%), this investigation demonstrated that condensed pDNA loses its hydrophilicity and results in adsorption onto the vessel and that pre-coating with another polycations can prevent the loss due to adsorption.

Based on this discovery, inverse microemulsion with the pre-condensed pDNA in aqueous phase was then polymerized with 20% crosslinker (PEGdiA) and 80% HEA. Percent

pDNA entrapped in this ‘neutral’ nanogel was assessed with the agarose gel electrophoresis by reading [^3H] radioactivity. As shown in **Figure 3-15**, as much as 56% of the initial loaded pDNA was detected at loading well (**D1** in the right panel, also see lane **D** in the left panel). When uncondensed pDNA used, only approximately 27% of pDNA was entrapped in the nanogel (**B1** and lane **B**). As expected, in a simple mixture of pDNA and pre-made neutral nanogel (lane **E**), unassociated pDNA moved similarly to the control pDNA on the gel (lane **F**). With DDTAB (C12), the total recovery was minimal (lane **C**). Although pDNA was condensed with DDTAB in pre-coated tubes as in previous investigation, the adsorption of DDTAB-condensed pDNA toward vessels still remained relatively high during polymerization resulting in a low recovery. Alternatively this low recovery could be attributed to the higher affinity of DDTAB in the heptane-water interface than toward pDNA during polymerization, which must have produced unsatisfactory condensation of pDNA. But, no further investigation was performed to address this issue.

The study involving protamine was carried out at an N/P ratio 0.2 in which the complex itself carries a net negative charge. As illustrated by **Figure 3-16**, under this situation the proton sponge effect may not be fully realized. In the endosome protons introduced by proton pump (**square symbol** in the figure) will protonate weak base moiety (**triangle symbol** in the figure) and the accompanying chloride ions will have two different destinations. They can bind to protonated weak base moiety on the nanogel and remain inside of endosome. This will facilitate endosomal rupture by increased osmotic pressure, a desirable pathway (**Pathway 1** in the figure). Alternatively, chloride ions could bind to the counter cations of the complex (**Pathway 2**), which may leave the endosome via some

transporter or carrier system (**Pathway 3**). This pathway cannot provide osmotic pressure. In short, condensation of pDNA at N/P ratio 0.2 would be countereffective in the overall vector design. Since it is difficult to estimate how much weak base is enough for overcoming the above dilemma and what the upper limit of base incorporation is, it would be more desirable if a higher N/P ratio such as 1.0, instead of 0.2, can be used to keep the net charge of condensed pDNA neutral. For this reason, the recovery of condensed pDNA in aqueous layer was further investigated using protamine at various N/P ratios. As shown in **Figure 3-14C**, the recovery of pDNA decreased as N/P ratio increased. For instance, only 30% was recovered when the ratio reached 1.0. Note, however, that in a reduced concentration of pDNA (i.e., 200 $\mu\text{g/mL}$ in water), the recovery remained as high as 96% before and after adding heptane. The addition of alcohols decreased the recovery especially after adding heptane (60%) and significant amount of radioactivity (12-18%) was detected in tubes, implying alcohols affect the physical property of protamine-condensed pDNA. This is important to know because methanol will need to be added to aqueous layer to improve the solubility of disulfide crosslinker (see **Chapter II**). Finally, the effect of pDNA concentration on the recovery was further investigated represented in **Figure 3-14D**. Up to 200 $\mu\text{g/mL}$, the recovery of pDNA remained high (~ 95%) and was close to that of uncondensed pDNA at the concentration of 100 $\mu\text{g/mL}$.

The integrated efforts have thus yielded several nanogel formulations that entrap protamine-condensed pDNA for transfection study in the cell. **Figure 3-17** shows the agarose gel electrophoresis of various nanogel formulations containing [^3H]-pDNA. Nanogels were crosslinked using either disulfide crosslinker (SSXL; lane **B-E**) or PEGdiA (lane **F**) and

contained 25% (w/w) weak base, morpholinoethylacrylate (MEA). In the pre-condensation, pDNA was complexed with protamine at various N/P ratios (i.e., 0 to 4). Bright bands were detected in all nanogels that contained SSXL at near the loading wells, which was not the case in PEGdiA-derived nanogel. Radioactivity was, however, minimal in all the formulations (**right panel**), implying not much pDNA was entrapped in the nanogel. Indeed fact, no significant radioactivity was detected throughout the gel (i.e., less than 1%). It is possible that most of pDNA was not able to stay in aqueous phase in the microemulsion and/or during polymerization. This fairly low pDNA recovery can be attributed to the interference of pDNA condensation and the possible instability of microemulsion due to the presence of a significant amount of methanol. Methanol was necessary in improving the solubility of the disulfide-containing crosslinker, SSXL. Alternatively, the presence of MEA might not be compatible with the pre-condensed pDNA under this reaction condition. In the left panel of **Figure 3-17**, the bright bands observed on the top of the gel probably came from the disulfide moiety incorporated in the nanogel. Disulfide derivatives indeed show up under UV lamp when loaded on thin layer chromatography.

As shown in **Figure 3-18**, when HeLa cells were treated with these formulations, no significant transfection was observed in all test groups (**B-F**). This was most likely due to small amount of pDNA delivered to the cell. When calculated from the entrapment efficiency in the gel data, it was as low as 0.01 μg per well. Each well in 24-well plate contained 5×10^4 HeLa cells. PEI of 25 kDa was used as positive control for this study and showed a high gene expression. In PEI-transfected cells, two different amounts of pDNA (0.2 in **I** and **J**; 1 μg in **G** and **H**) were complexed with PEI at two different N/P ratios (4 in **G** and **I**; 10 in **H** and **J**).

Although the difference in pDNA amount treated to constant number of cells was only 5 fold, the improvement in gene expression was more profound (i.e., 200 fold at N/P=4 and 10,000 fold at N/P=10). The N/P ratio dependency in gene expression was also reported by other investigators (e.g., Boussif *et al.* 1995).

3.4 Conclusions

Entrapment of pDNA in a neutral nanogel would have some potential advantage over conventional polyplex system, in which pDNA is simply mixed with pre-made polymeric particles. Because of the net charge of the formulation is neutral, it would reduce cytotoxicity to the cell. Since the pDNA is theoretically present inside the polymer matrix, the protection of pDNA from biochemical degradation by nucleases in the serum *in vivo* would have been better realized. However, the preparation becomes a challenging task. The first issue was to do with the stability of pDNA under free radical-initiated polymerization. It was shown that pDNA can be intact so long as its concentration is greater than approximately 100 µg/mL and pDNA stays in aqueous layer in the emulsion system. For the purpose of monitoring, pDNA and nanogel were successfully radiolabeled using methylation and acetylating, providing relatively high specific activities, 2×10^6 DPM/µg and 2×10^5 DPM/mg, respectively.

Various reagents were employed to condense pDNA prior to entrapment. Here, protamine-condensed pDNA showed improved entrapment efficiency in the nanogel; 56% of initial loaded pDNA. However, the final formulation of nanogel entrapping pre-condensed

pDNA was difficult to achieve mainly because of possible instability of the microemulsion in the presence of added methanol. No positive data were obtained in the transfection study when the present formulation was fed to the cell. This is in turn due to the low entrapment of pDNA in the nanogel. Instead of further investigation on the entrapment formulation, an approach with a mixture formulation of pre-made nanogel with pDNA was pursued in **Chapter IV**.

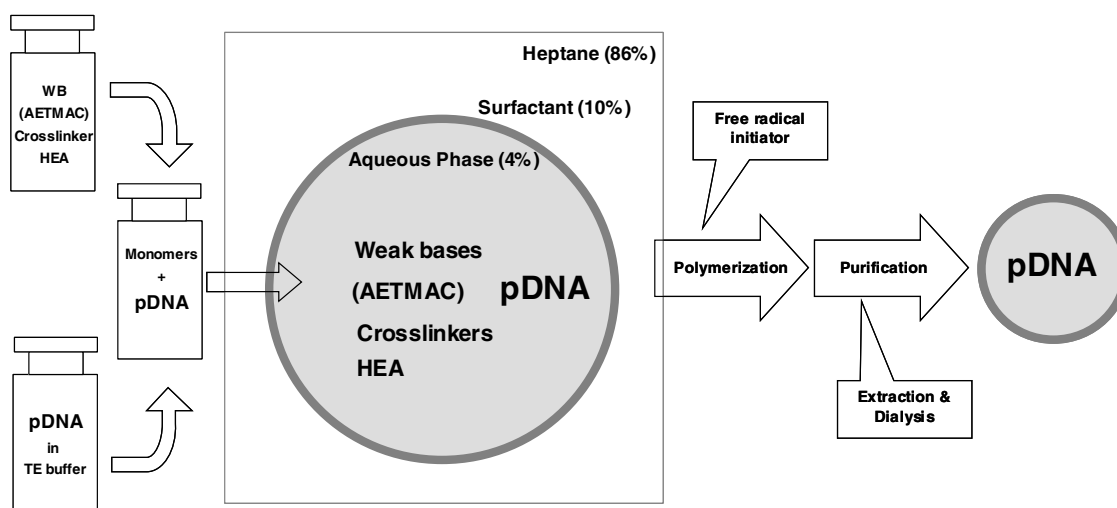


Figure 3-1: Preparation of pDNA-entrapped nanogel. Monomer stock and pDNA solution are mixed into aqueous phase, which is then added to heptane phase containing 10%, w/w surfactant (laureth-3). Microemulsion is formed by brief vortexing and polymerized by adding free radical initiator, EHP. Nanogel is water-extracted from heptane layer and further purified using dialysis with 100 kDa MW cut off dialysis bag. Abbreviations used are: WB, weak base; AETMAC, 2-acryloxyethyltrimethylammonium chloride; HEA, 2-hydroxyethyl acrylate; and TE, Tris-EDTA.

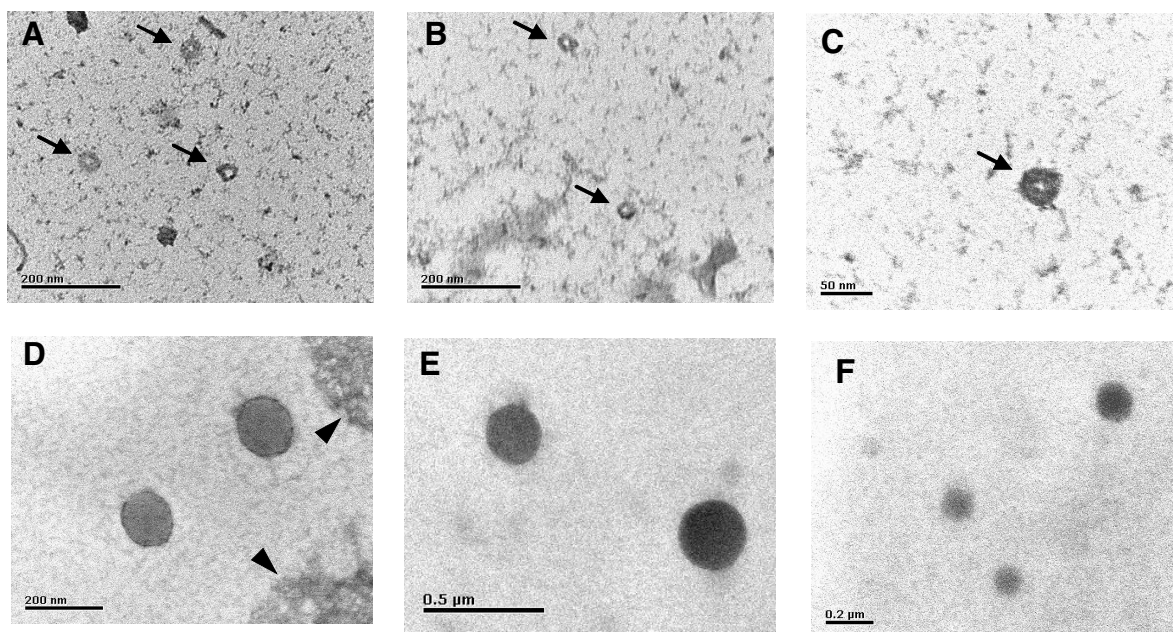


Figure 3-2: Transmission electron micrographs of pDNA-entrapped inverse microemulsion (**A**, **B**, and **C**) and polymerized neutral nanogels (**D**, **E**, and **F**). Plasmid DNA (pGL3 Control Vector, 5.2 kbp) was added into aqueous layer along with monomers (12% PEGdiA and 88% HEA) to form microemulsion (arrows in **A**, **B** and **C**). Free radical-initiated polymerization was conducted overnight at room temperature and nanogel was purified using water extraction, n-butanol washing, and size exclusion chromatography on Sephadex G-15 (**D**, **E**, and **F**). The concentration of pDNA was 5 μg in 1 mL of heptane/surfactant and the microemulsion was used as it is for microscopic examination without further purification. In both cases, negative staining was adopted using 2% uranyl acetate. Trace amount of unidentifiable substances were observed in purified nanogel formulations (arrow heads in **D**) and could be an artifact derived from the specimen preparation or staining processes.

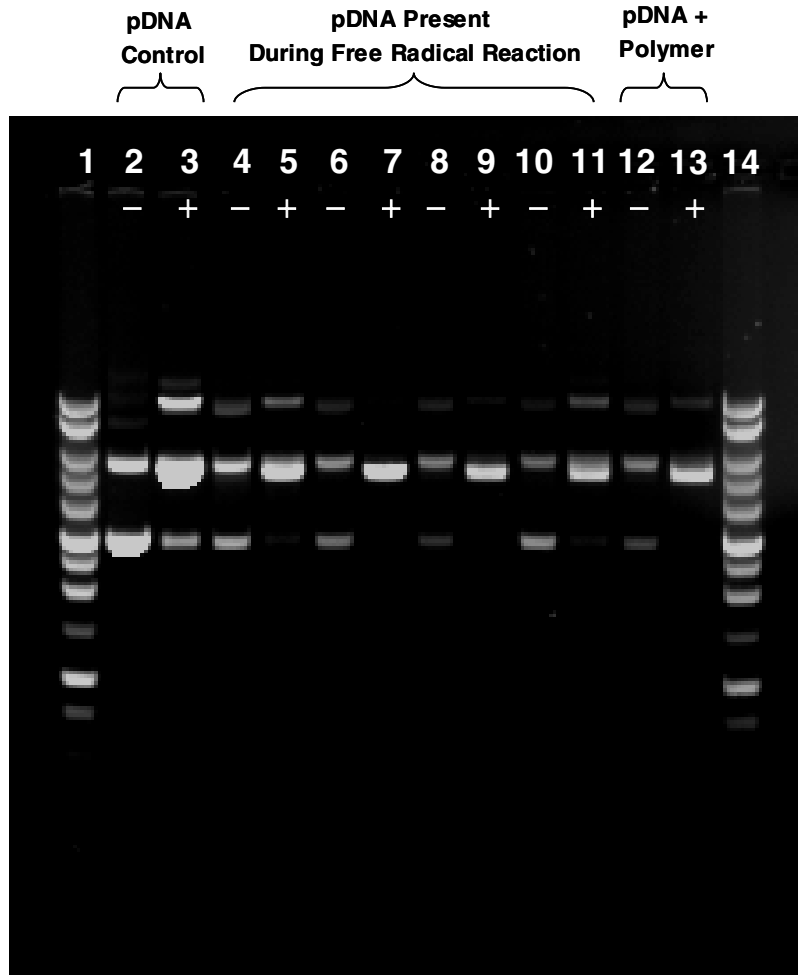


Figure 3-3: Stability of pDNA in emulsion-derived, free radical-initiated polymerization. pGL3 Control Vector (Promega) was added to aqueous phase containing monomers such that concentration of pDNA was 40 $\mu\text{g/mL}$ in TE buffer. The aqueous phase (30%, w/w) was mixed with mineral oil (68%, w/w) containing 2% surfactants (Span 80:Tween 80=3:1). Polymerization was initiated by adding 0.125% AIBN and kept stirred for 4 hrs at 50 $^{\circ}\text{C}$. Plasmid DNA was water-extracted from the reaction mixture, washed with hexane, and precipitated with 95% ethanol before gel electrophoresis on 0.75% agarose gel. Emulsion contained various amount of PEG monomethacrylate (Lanes 4, 5, 10, and 11; 20% of aqueous phase: Lanes 6 and 7; 5% of aqueous phase: Lanes 8 and 9; 1.25% of aqueous phase). Excess amount of yeast RNA was added in lane 10 and 11. As a mixture formation, pDNA was added to pre-made polymer solution (Lane 12 and 13) and extracted as described above. Incubation with Hind III (37 $^{\circ}\text{C}$, 1 hr) generated linear form of pDNA (**odd numbered lanes**).

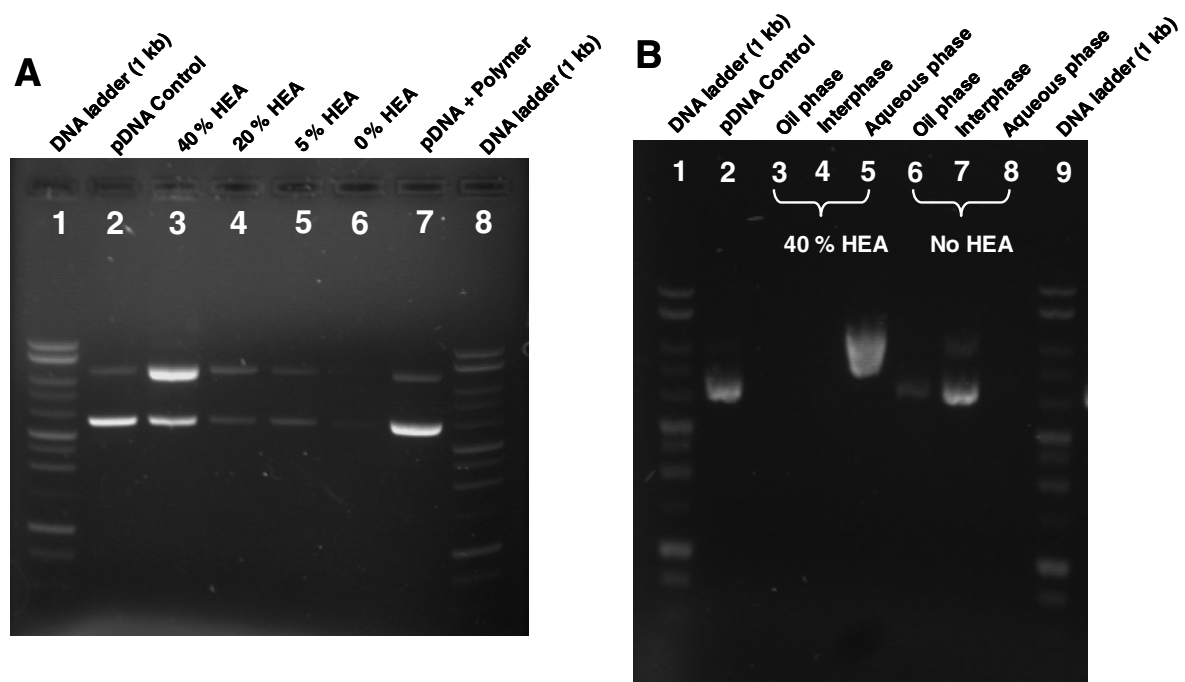


Figure 3-4: Effect of HEA on the pDNA recovery in free radical-mediated emulsion polymerization. Plasmid DNA (pCMV-Luc) was added to aqueous phase containing monomers such that concentration of pDNA was 40 $\mu\text{g/mL}$ in TE buffer. The composition of emulsion, the procedure in polymerization, and purification were the same as described in **Figure 3-3**. **[A]** The extracted pDNA was electrophoresed on 0.75% agarose gel. Emulsion contained various amount of HEA (lanes 3-6). Lane 7 represents a mixture of pDNA and pre-made polymer derived from 40% HEA-containing aqueous phase. Control pDNA showed two bands, supercoiled and open relaxed circular form (Lane 2). **[B]** Emulsion contained 40% of HEA (lanes 3-5) or no HEA (lanes 6-8) in aqueous phase. In the absence of HEA, pDNA was recovered in the interface mostly as supercoiled form (lane 7) while majority of pDNA showed up in aqueous phase apparently as open relaxed circular form in the presence of HEA (lane 5).

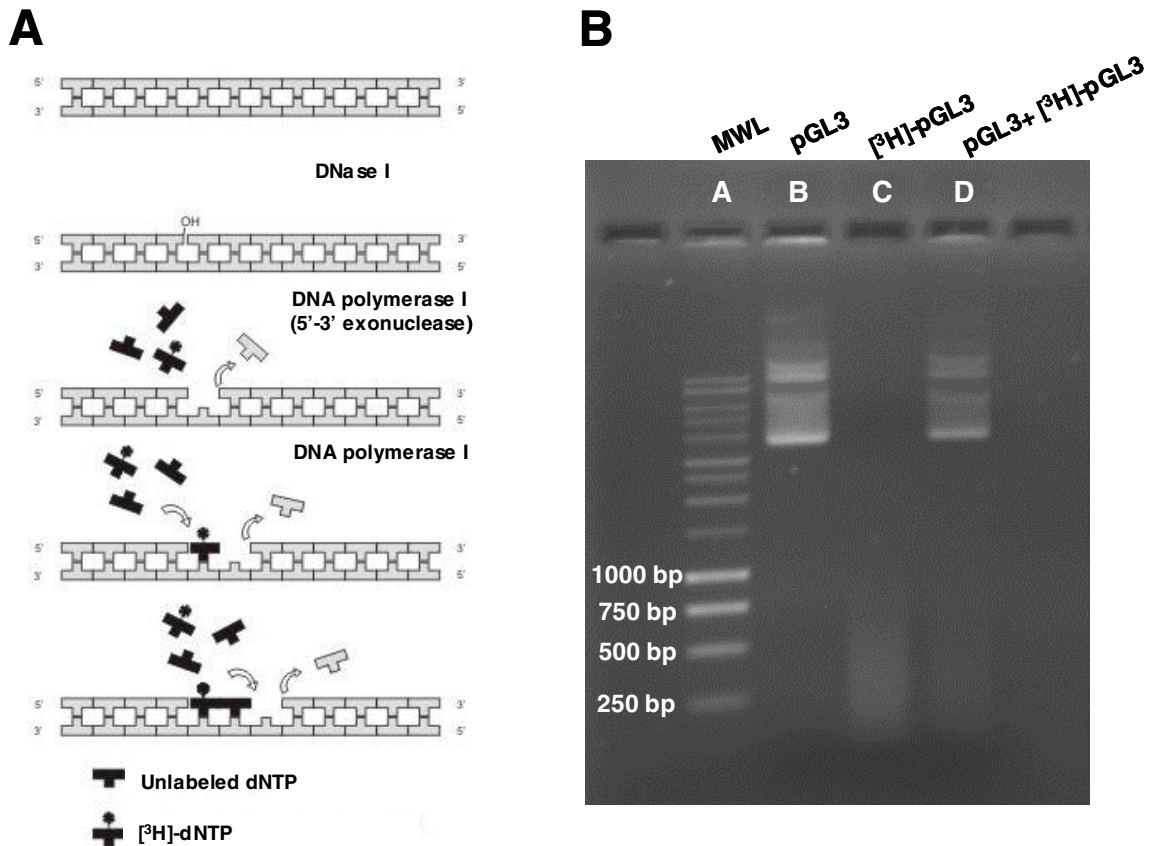


Figure 3-5: Radiolabeling of pDNA using nick translation. **[A]** DNase I creates random nicks on the strands. *E.coli* DNA polymerase I adds sequentially new nucleotides to the 3'-end of a nick within a DNA duplex while removing nucleotides from the adjacent 5'-terminus. During this procedure, radiolabeled nucleotides, $[^3\text{H}]\text{-dCTPs}$, are incorporated into the pDNA to produce radiolabeled pDNA. The specific activity obtained with this procedure was 1.8×10^7 dpm/ μg . **[B]** The integrity of tritium labeled pDNA was confirmed on the agarose gel. The labeled pDNA showed small fragments of 200-500 base pairs on the gel (lanes **C** and **D**), which is approximately one-tenth of the original pDNA in size.

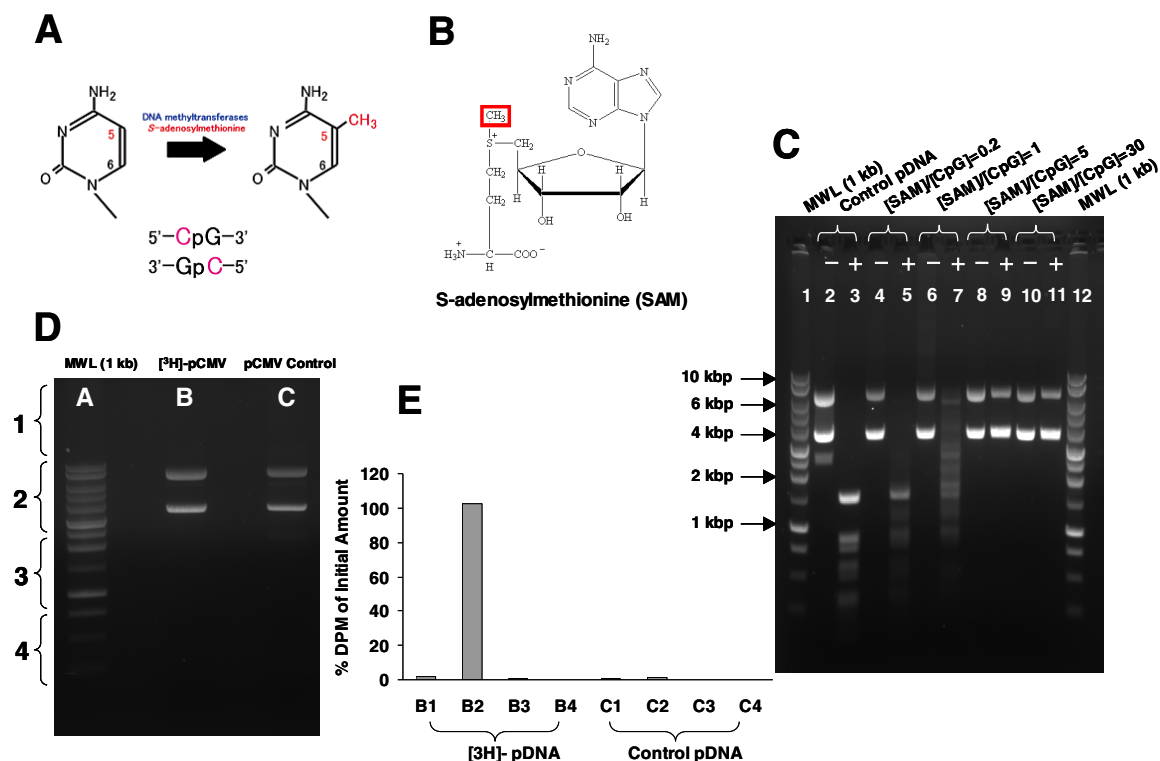


Figure 3-6: Radiolabeling of pDNA by methylation. Enzyme CpG methylase methylates specifically C-5 positions of cytosine residues within the double-stranded dinucleotide (C-G) recognition sequences using S-adenosylmethionine (SAM, **B**) as a methyl donor (**A**). This enzymatic methylation needs pH 7-8 and 5-fold molar excess of SAM was used for complete methylation as demonstrated by the rejection of BstU I restriction of methylated pDNA (**C**). Tritium labeled pDNA appeared very similar to the unmodified pDNA when run on 0.8% agarose gel in terms of the movement of two different biological structures, open relaxed (upper band) and supercoiled form (lower band), on the gel (**D**). The gel segment corresponding to [³H]-pDNA showed almost 100% DPM level of total input (**E**). The specific activity achieved was 1.81×10^6 DPM / μ g of pDNA.

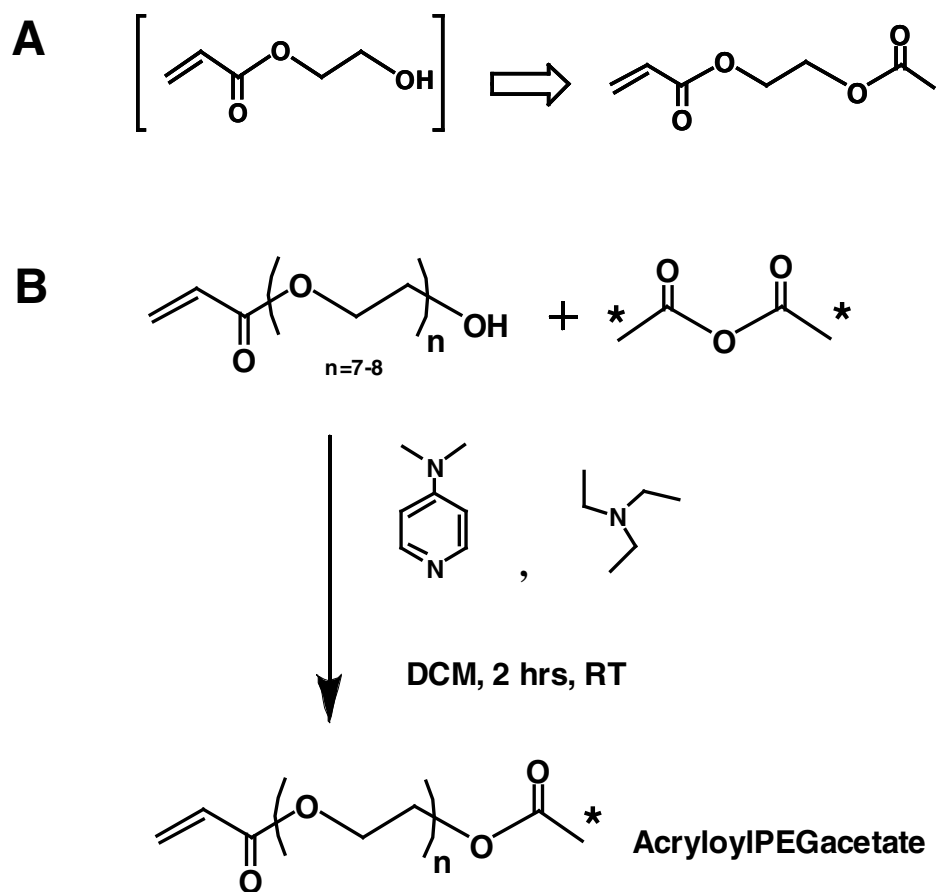


Figure 3-7: Radiolabeling of acrylate derivatives by acetylation. Mixture of [^{14}C]-acetic anhydride (1.3×10^7 dpm, 6 μCi) and cold acetic anhydride (0.006:1) was reacted with 1.5-mole equivalent of PEG monoacrylate (average M_n of PEO =375), 1 mole equivalent of TEA and 0.1 mole equivalent of 4-dimethylaminopyridine. The reaction was kept under magnetic stirring for 2 hrs at room temperature and the product was purified in column chromatography on silica gel using the mixture of methanol and chloroform (15:85% v/v) as mobile phase. The specific activity obtained was 1.7×10^5 dpm/mg.

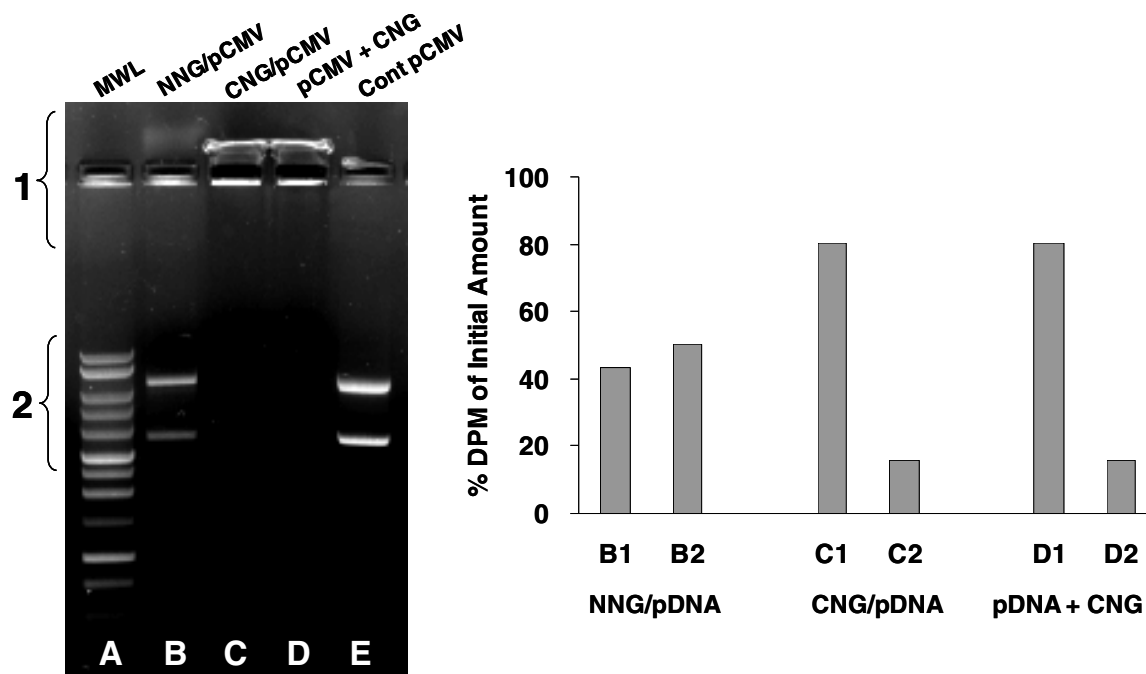


Figure 3-8: Agarose gel (0.8%) electrophoresis of nanogel-entrapped pCMV-Luc of 6.2 kbp. Molecular weight ladder (A) and pDNA alone (0.2 μ g, E) were loaded as references. Mixture of [3 H]-pDNA and cold pDNA was added to aqueous phase before polymerization (B and C, the final concentration of pDNA was 333 μ g/mL TE buffer) or mixed with polymerized cationic nanogel (D). The weight ratio between pDNA and monomers was 1:3,000 and N/P ratio in the cationic nanogel-pDNA formulations was approximately 1,000 (i.e., excess of positive charge). The composition of nanogels were 10% PEGdiA and 90% HEA (B), or 10% PEGdiA, 25% AETMAC (cationic monomer) and 65% HEA (C and D). Whole gel was cut into segments for DPM reading after overnight incubation in 20-mL vials containing scintillation cocktail (right panel).

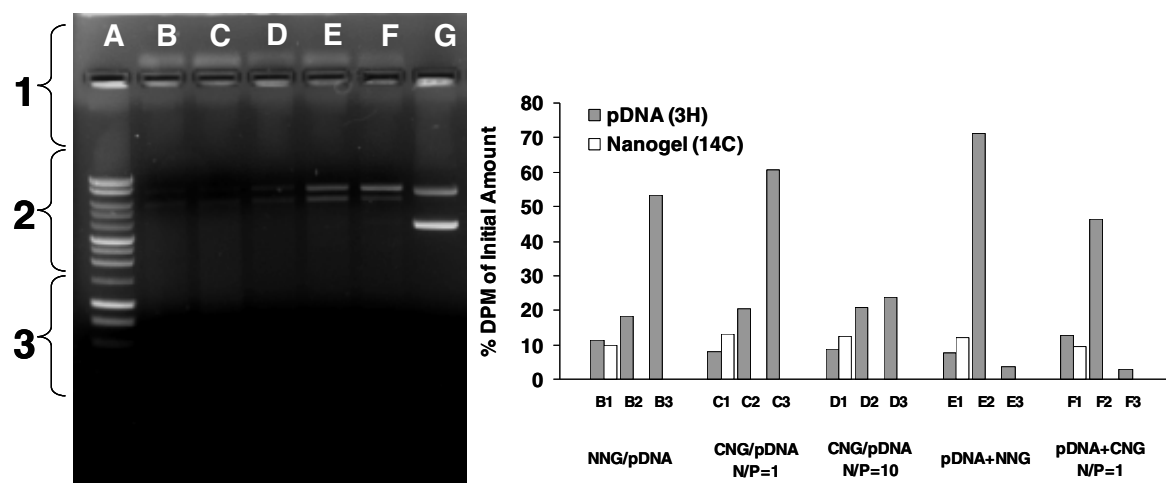


Figure 3-9: Agarose gel (0.8%) electrophoresis of [^{14}C]-nanogel that had entrapped pCMV-Luc of 6.2 kbp. Molecular weight ladder (A) and pDNA alone (0.15 μg , G) were loaded as references. Mixture of [^3H]-pDNA and cold pDNA was added to aqueous phase before polymerization (B, C and D, the final concentration of pDNA was 100 $\mu\text{g}/\text{mL}$ TE buffer) or mixed with pre-made neutral (E) or cationic nanogel (F). The weight ratio between pDNA and monomers were 1:10,000 and N/P ratios in the cationic nanogel-pDNA formulations were 1 (C and F) and 10 (D). The composition of nanogels were 10% PEGdiA, 4% [^{14}C]-PEG acrylate and 86% HEA in all formulations. Small amount of AETMAC (0.006% in C and F; 0.06% in D) was additionally added to prepare cationic nanogels. The gel was cut into segments for DPM reading after overnight incubation in 20-mL vials containing scintillation cocktail (**right panel**).

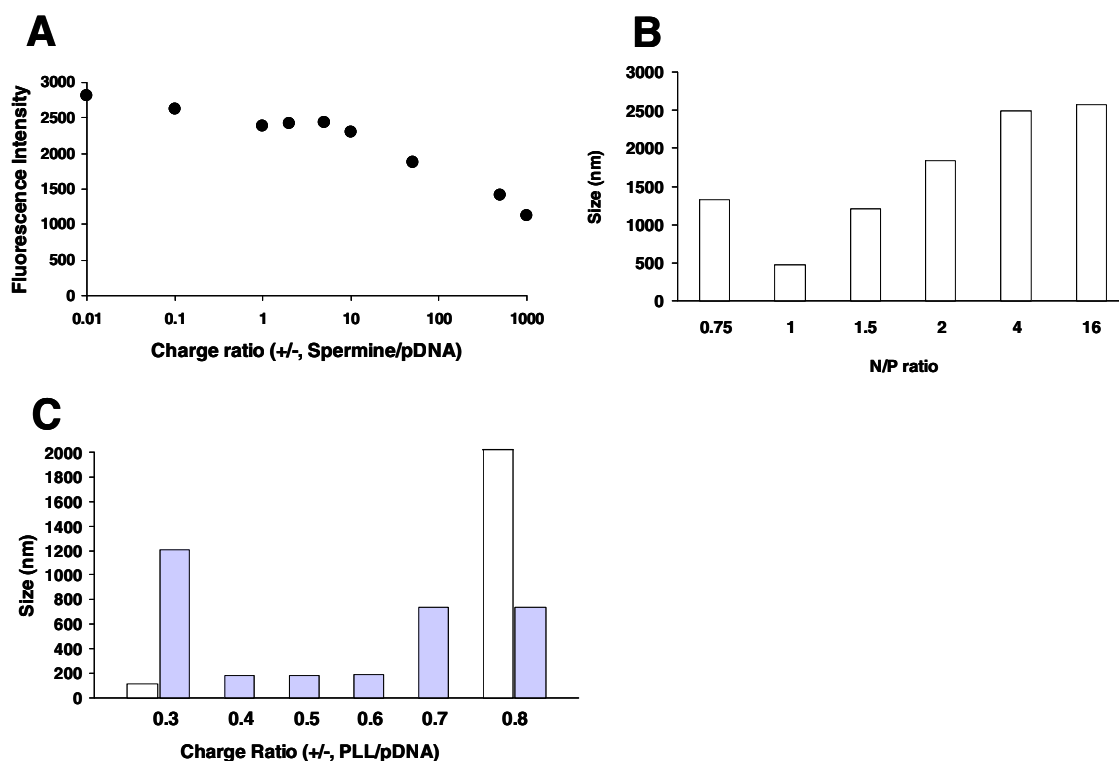


Figure 3-10: Condensation of pDNA by multivalent cationic molecules. [A] Spermine was mixed with 1 μg of pDNA in 0.5 X TE buffer at varying charge ratios and incubated for 30 min at room temperature. SYBR Gold (1 X) was added to the mixture followed by 20-min rocking before fluorescence measurement at 495/537 nm as excitation/emission. [B] Into a glass cuvette containing varying amount of spermine, 20 μg of pDNA was added dropwise under vortex-mixing and the mixture was subject to size analysis on NICOMP. [C] Into 10 μg of pDNA in 600 μL of 0.5 X TE buffer, constant amount of PLL was consecutively added until the charge ratio (positive to negative) reached 0.8 with 5-min mixing and 10-min size measurement after each addition. At ratios 0.3 and 0.8, multiple size populations were observed and the frequencies of these two size components were approximately 70 % (open bar) and 30% (gray bar) in both cases.

Table 3-1: Size of pDNA-CTAB (Cetyltrimethylammonium Bromide) Complex at Various N/P Ratios Measured by Dynamic Light Scattering Using Multimodal Nicomp Analysis.

N/P ^a	0.1	0.2	0.4	0.6	0.8	1.1
Size	1000 (84%) ^b	340 (84%)	459 (87%)	1434 (62%)	1004 (78%)	1825 (88%)
(nm)	120 (16%)	51 (16%)	54 (13%)	222 (28%) 54 (10%)	116 (19%) 22 (3%)	40 (12%)

^a: N/P indicates the ratio of positive charge of CTAB to negative charge of phosphate groups in pDNA.

^b: Percentage in parentheses represent the frequency of each size population.

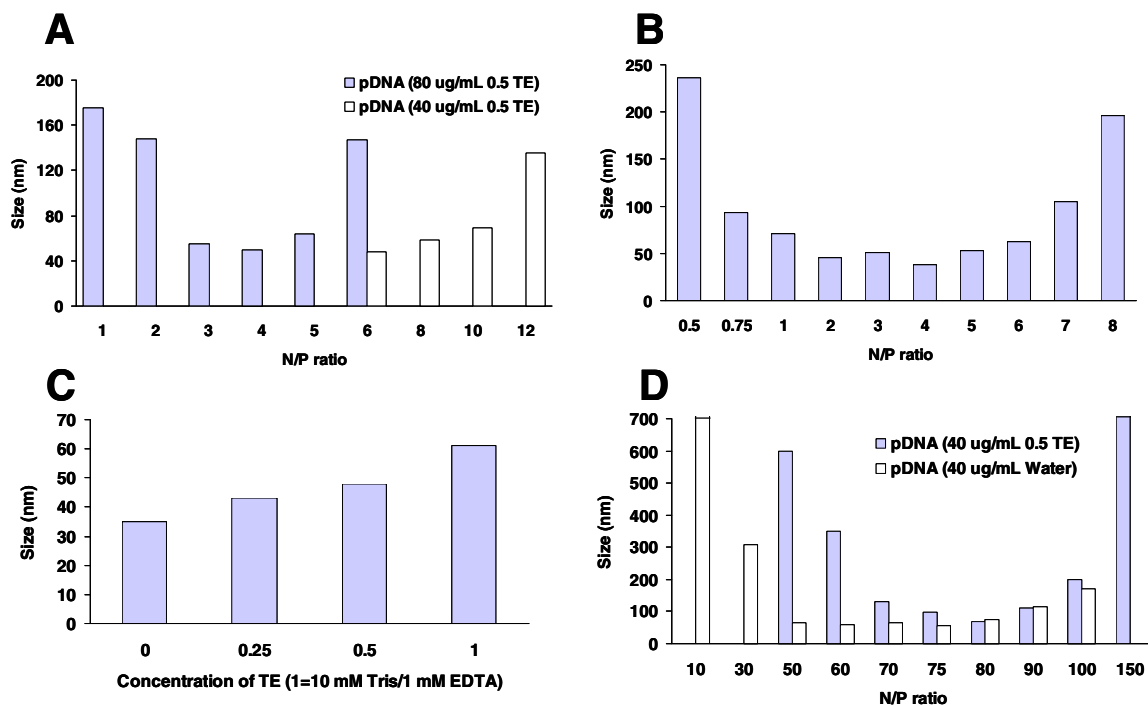


Figure 3-11: Size of pDNA complex with dodecyltrimethylammonium bromide (DDTAB) (**A**, **B**, and **C**) and decyltrimethylammonium bromide (DTAB) (**D**). DDTAB was mixed with pDNA at different concentrations in 0.5 X TE (**A**) or with pDNA of 80 $\mu\text{g/mL}$ in water (**B**). Size of DDTAB-pDNA (80 μg pDNA /mL) complex increased linearly with increased concentration of TE buffer (**C**). DTAB was mixed with pDNA of 40 $\mu\text{g/mL}$ in 0.5 X TE or in water (**D**). Size was measured by dynamic light scattering on NICOMP.

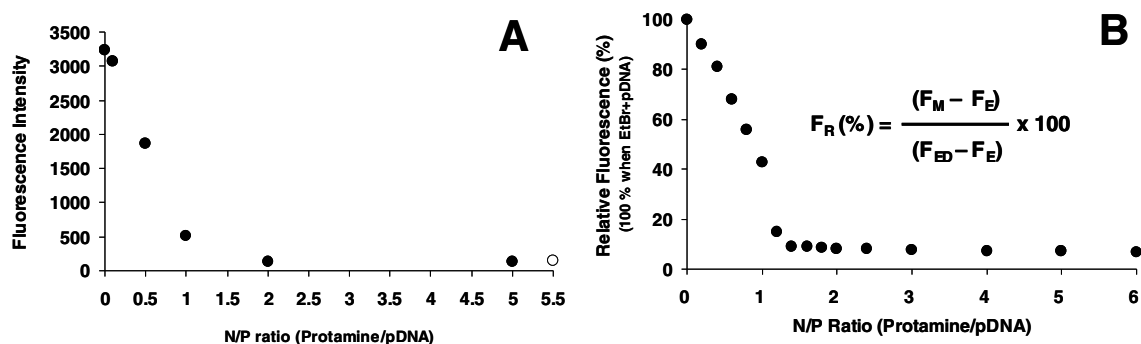


Figure 3-12: Condensation of pDNA with protamine as monitored by fluorescence. **[A]** Dye exclusion assay was performed by adding SYBR Gold to protamine-pDNA complex. Open circle represents baseline fluorescence of dye alone. **[B]** Displacement assay was conducted by adding protamine to the mixture of pDNA with ethidium bromide. Relative fluorescence (F_R) was calculated using the equation shown in the figure, where F_M , Fluorescence of pDNA-EtBr in the presence of protamine; F_E , Fluorescence of EtBr alone; and F_{ED} , Fluorescence of pDNA-EtBr in the absence of protamine.

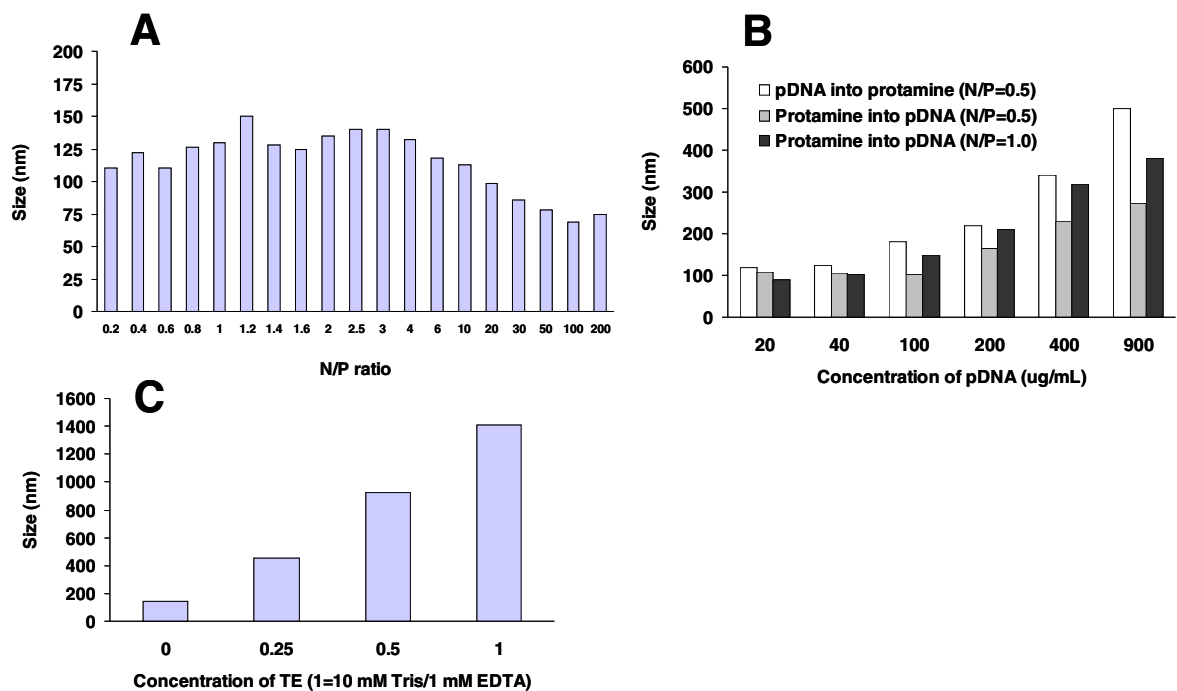


Figure 3-13: Size of pDNA-protamine complex. [A] Into a protamine solution, pDNA was slowly and continuously added such that the final concentration of pDNA was 20 μg pDNA/mL in water. [B] Different order of mixing was studied in condensing pDNA with protamine at N/P 0.5 and 1.0 such that the final concentration of pDNA was 20-900 μg /mL in water. [C] Increased concentration of TE buffer resulted in larger size of protamine-pDNA complex at 20 μg pDNA/mL.

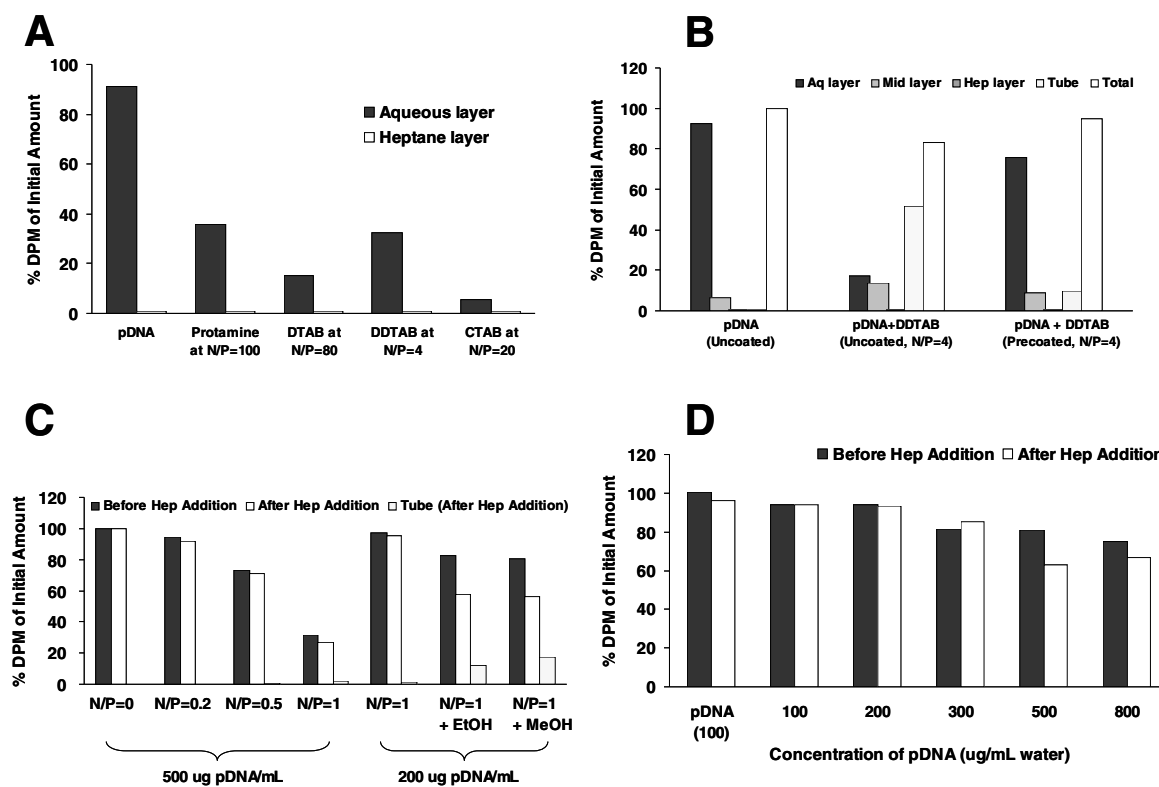


Figure 3-14: Recovery of pDNA condensed with protamine or cationic lipids. [A] pDNA was condensed with various condensing reagents at different N/P ratios and radioactivity recovered in the aqueous layer was reported here. At the N/P ratios studied, smallest complexes were observed in previous studies. [B] Dodecyltrimethylammonium bromide (DDTAB) was complexed with pDNA at N/P=4 in PLL(25 kDa)-precoated tubes containing water and radioactivity was measured in various sites including middle layer and tubes. [C] pDNA recovery was assessed after adding protamine to pDNA at the concentration of 200-500 ug pDNA/mL in water with various N/P ratios. [D] The recovery of condensed pDNA by protamine in water at N/P=1 was affected by increasing concentration of pDNA.

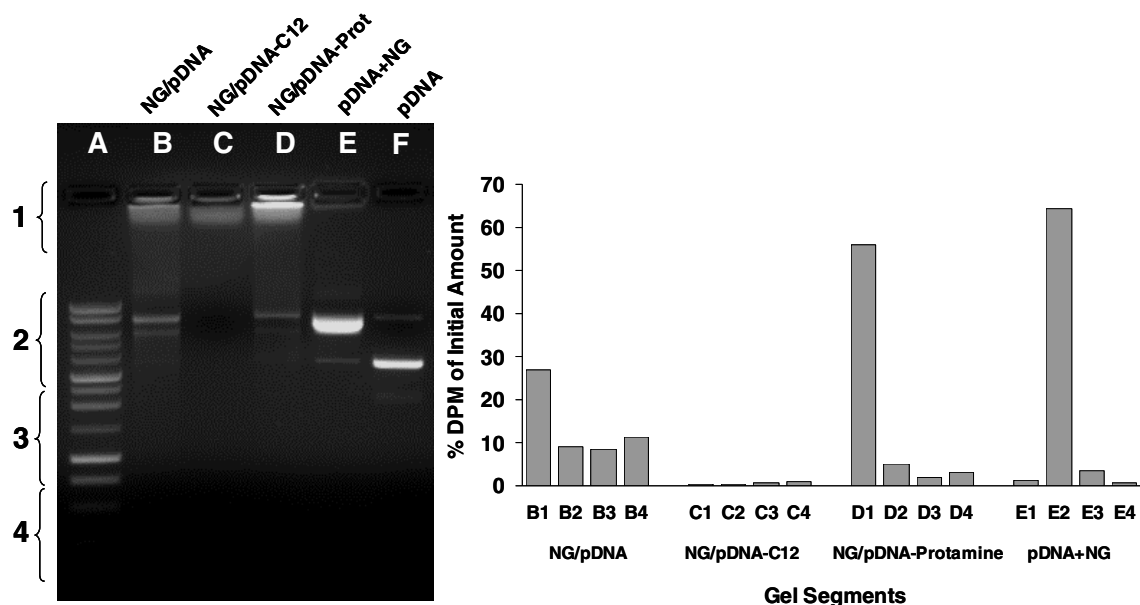


Figure 3-15: Agarose gel (0.8%) electrophoresis of pre-condensed, neutral nanogel-entrapped pCMV-Luc of 6.2 kbp. Molecular weight ladder (A) and pDNA alone (0.15 μ g, F) were loaded as references. Mixture of [3 H]-pDNA and cold pDNA was condensed with DDTAB (C12) in PLL-precoated tube at N/P=4 (C) or with protamine at N/P=0.2 (D) before adding to the aqueous phase for polymerization. Uncondensed pDNA was added during polymerization (B) or mixed with pre-made neutral nanogel (E). The weight ratio between pDNA and monomers were 1:4,000 the concentration of pDNA was 250 μ g/mL in aqueous phase, which consisted of 50% monomer/50% water (w/w). The composition of nanogel was 20% PEGdiA and 80% HEA in all formulations. The gel was cut into segments for DPM reading after overnight incubation in 20-mL vials containing scintillation cocktail (**right panel**).

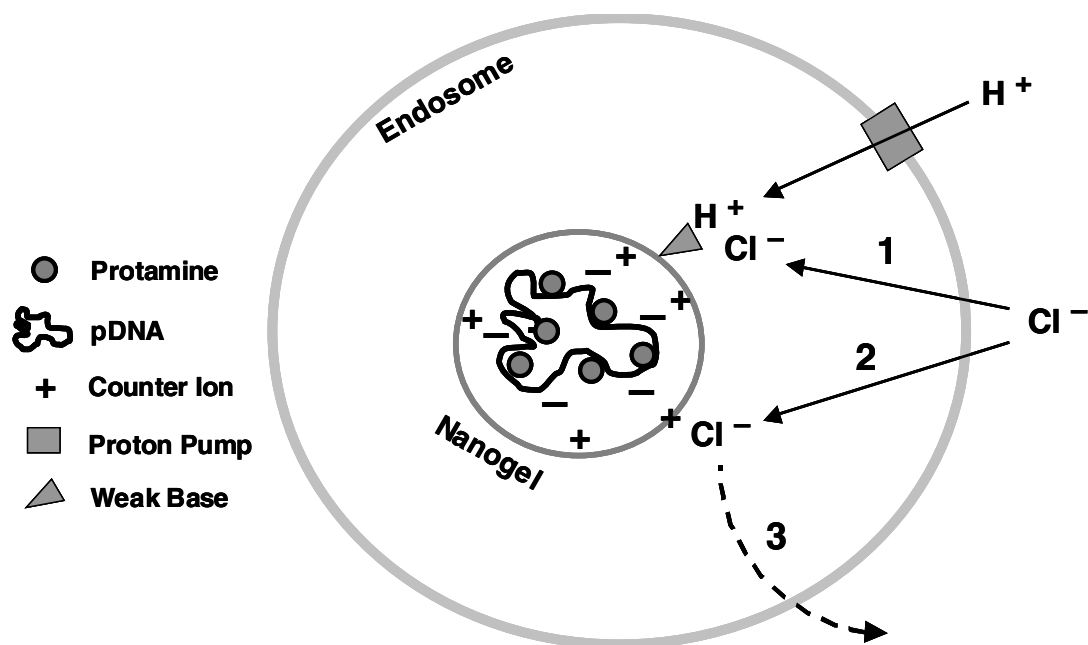


Figure 3-16: Illustration of protamine-condensed, neutral nanogel-entrapped pDNA after endocytosis. Plasmid DNA condensed with protamine at N/P=0.2 is entrapped in the nanogel and internalizes the cell via endocytosis. The net charge of the complex is negative and thus positive counter ions (+ symbol) co-exist accordingly. Protons introduced through proton pump (square symbol) protonate weak base moiety (triangle symbol) but chloride ions that follow in for charge balance will have two different destinations. They bind to protonated weak base moiety on the nanogel, remain inside of endosome, and facilitate endosomal rupture by increased osmotic pressure (**Pathway 1**). Alternatively, chloride ions bind to the counter ions (**Pathway 2**), have the ability to leave the endosome (**Pathway 3**) and provide no help in terms of endosomal escape of the formulation.

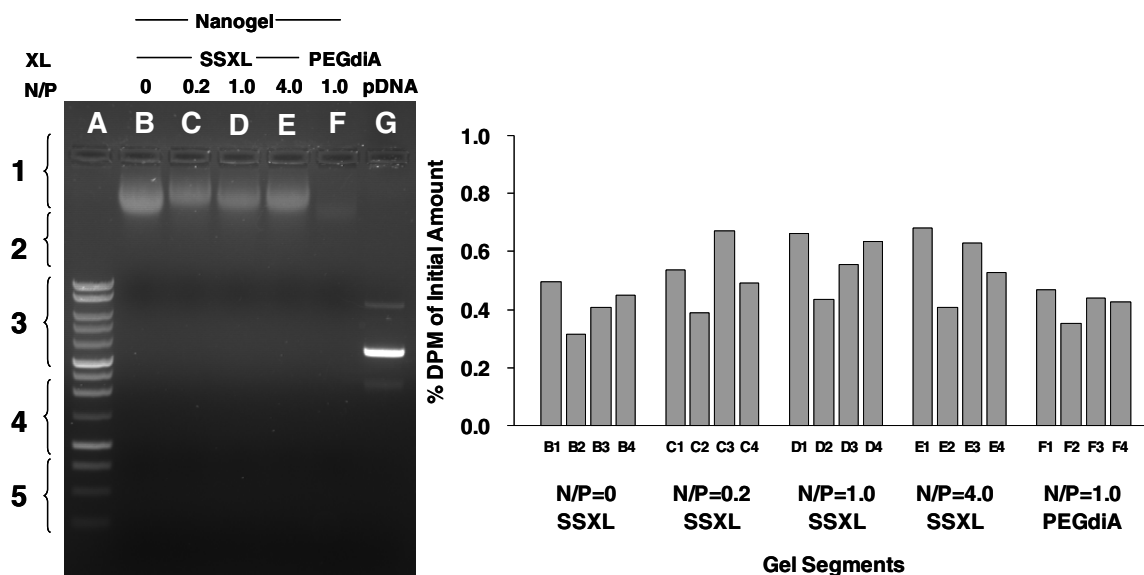


Figure 3-17: Agarose gel (0.8%) electrophoresis of protamine-condensed, neutral nanogel-entrapped pCMV-Luc of 6.2 kbp. Molecular weight ladder (A) and pDNA alone (0.15 μ g, G) were loaded as references. Mixture of [3 H]-pDNA and cold pDNA was condensed with protamine at various N/P ratios (B-F) before adding to the aqueous phase for polymerization. The weight ratio between pDNA and monomers were 1:6,000 and the concentration of pDNA was 200 μ g/mL in the aqueous phase, which consisted of 40% monomer/30% methanol/30% water (w/w). The composition of nanogel was 10% PEGdiA (F) or disulfide containing crosslinker (SSXL; B-E), 25% morpholinoethylacrylate (MEA), and 65% HEA in all formulations. Aqueous phase of microemulsion in all formulations contained 50% methanol. The gel was cut into segments for DPM reading after overnight incubation in 20-mL vials containing scintillation cocktail (right panel).

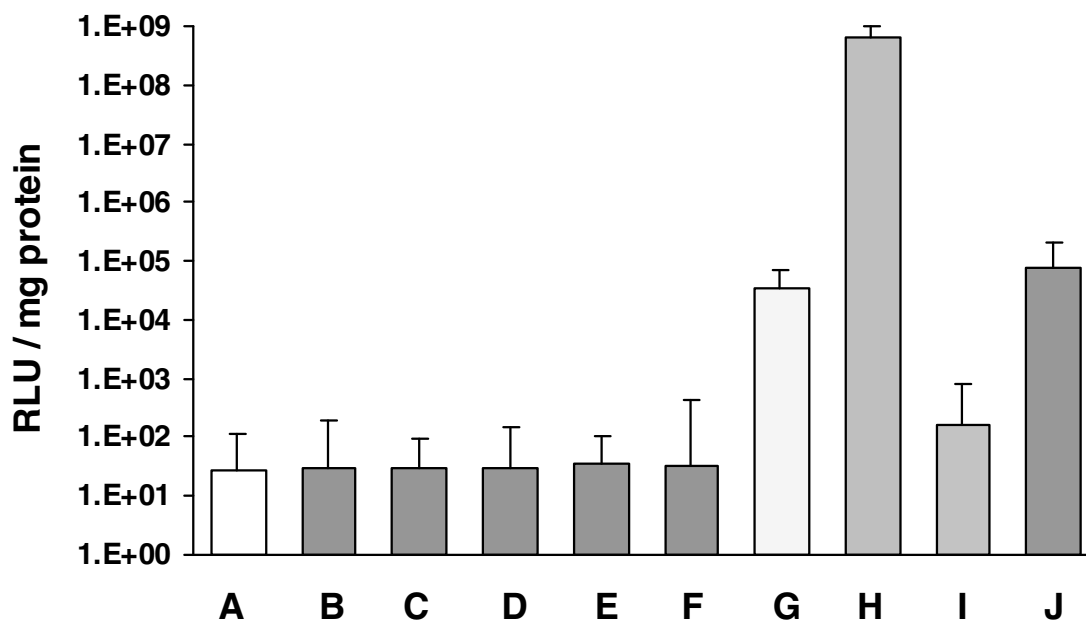


Figure 3-18: Transfection of HeLa cells with pCMV-Luc of 6.2 kbp protamine-condensed and entrapped in neutral nanogel. Mixture of [^3H]-pDNA and cold pDNA was condensed with protamine at various N/P ratios (**B-F**) before adding to the aqueous phase for polymerization. The composition of nanogels were 10% PEGdiA (**F**) or disulfide containing crosslinker, SSXL (**B-E**) and 25% morpholinoethylacrylate (MEA) and 65% HEA in all formulations. pDNA (1 μg) alone (**A**) or nanogel formulations containing pDNA (**B-F**) were added to 5×10^4 cells seeded in 24-well plate. The amount of pDNA in nanogel formulations per well was approximately 0.01 μg based on the calculation from entrapment study (i.e., entrapped from initial loaded pDNA was only 0.5%). Poly(ethylenimine) was complexed with pDNA (1 μg in **G** and **H**; 0.2 μg in **I** and **J**) at N/P=4 (**G** and **I**) or 10 (**H** and **J**). All formulations were incubated with cells for 4 hrs and cells were rinsed with HBSS briefly and provided with fresh growth medium. At 48-hr post transfection, cell was lysed and the cell lysate was subject to luciferase assay and BCA protein assay. The transfection represented by relative light unit (RLU) normalized by protein amount.

3.5 References

- Allen M.J., Bradbury E.M. and Balhorn R. (1995). "The natural subcellular surface structure of the bovine sperm cell." *J Struct Biol* 114 (3): 197-208.
- Baldini A., Ross M., Nizetic D., Vatcheva R., Lindsay E.A., Lehrach H. and Siniscalco M. (1992). "Chromosomal assignment of human YAC clones by fluorescence in situ hybridization: use of single-yeast-colony PCR and multiple labeling." *Genomics* 14 (1): 181-4.
- Blackburn G.M. and Gait M.J. (1996). *Nucleic Acids in Chemistry and Biology*, 2nd Ed., Oxford University Press, New York, NY: pp. 46-50.
- Bloomfield V.A. (1996). "DNA condensation." *Curr Opin Struct Biol* 6 (3): 334-41.
- Boussif O., Lezoualc'h F., Zanta M.A., Mergny M.D., Scherman D., Demeneix B. and Behr J.P. (1995). "A versatile vector for gene and oligonucleotide transfer into cells in culture and in vivo: polyethylenimine." *Proc Natl Acad Sci U S A* 92 (16): 7297-301.
- Breen A.P. and Murphy J.A. (1995). "Reactions of oxyl radicals with DNA." *Free Radic Biol Med* 18 (6): 1033-77.
- Brown M.D., Schatzlein A.G. and Uchegbu I.F. (2001). "Gene delivery with synthetic (non viral) carriers." *Int J Pharm* 229 (1-2): 1-21.
- Budker V.G., Slattum P.M., Monahan S.D. and Wolff J.A. (2002). "Entrapment and condensation of DNA in neutral reverse micelles." *Biophys J* 82 (3): 1570-9.
- Bureau M.F., Naimi S., Torero Ibad R., Seguin J., Georger C., Arnould E., Maton L., Blanche F., Delaere P. and Scherman D. (2004). "Intramuscular plasmid DNA electrotransfer: biodistribution and degradation." *Biochim Biophys Acta* 1676 (2): 138-48.
- Danielsson I. and Lindman B. (1981). "The Definition of Micro-Emulsion." *Colloids and Surfaces* 3 (4): 391-392.
- de Frutos M., Raspaud E., Leforestier A. and Livolant F. (2001). "Aggregation of nucleosomes by divalent cations." *Biophys J* 81 (2): 1127-32.
- Faneca H., Simoes S. and Pedroso de Lima M.C. (2004). "Association of albumin or protamine to lipoplexes: enhancement of transfection and resistance to serum." *J Gene Med* 6 (6): 681-92.
- Felgner P.L., Barenholz Y., Behr J.P., Cheng S.H., Cullis P., Huang L., Jessee J.A., Seymour L., Szoka F., Thierry A.R., Wagner E. and Wu G. (1997). "Nomenclature for synthetic gene delivery systems." *Hum Gene Ther* 8 (5): 511-2.

- Geall A.J. and Blagbrough I.S. (2000). "Rapid and sensitive ethidium bromide fluorescence quenching assay of polyamine conjugate-DNA interactions for the analysis of lipoplex formation in gene therapy." *J Pharm Biomed Anal* 22 (5): 849-59.
- Goh S.L., Murthy N., Xu M. and Frechet J.M. (2004). "Cross-linked microparticles as carriers for the delivery of plasmid DNA for vaccine development." *Bioconjug Chem* 15 (3): 467-74.
- Hansma H.G., Golan R., Hsieh W., Lollo C.P., Mullen-Ley P. and Kwoh D. (1998). "DNA condensation for gene therapy as monitored by atomic force microscopy." *Nucleic Acids Res* 26 (10): 2481-7.
- Hoopes B.C. and McClure W.R. (1981). "Studies on the selectivity of DNA precipitation by spermine." *Nucleic Acids Res* 9 (20): 5493-504.
- Kelly R.B., Cozzarelli N.R., Deutscher M.P., Lehman I.R. and Kornberg A. (1970). "Enzymatic synthesis of deoxyribonucleic acid. XXXII. Replication of duplex deoxyribonucleic acid by polymerase at a single strand break." *J Biol Chem* 245 (1): 39-45.
- Kogure K., Moriguchi R., Sasaki K., Ueno M., Futaki S. and Harashima H. (2004). "Development of a non-viral multifunctional envelope-type nano device by a novel lipid film hydration method." *J Control Release* 98 (2): 317-23.
- Kral T., Hof M. and Langner M. (2002). "The effect of spermine on plasmid condensation and dye release observed by fluorescence correlation spectroscopy." *Biol Chem* 383 (2): 331-5.
- Kriwet B., Walter E. and Kissel T. (1998). "Synthesis of bioadhesive poly(acrylic acid) nano- and microparticles using an inverse emulsion polymerization method for the entrapment of hydrophilic drug candidates." *J Control Release* 56 (1-3): 149-58.
- Li S. and Huang L. (1997). "In vivo gene transfer via intravenous administration of cationic lipid-protamine-DNA (LPD) complexes." *Gene Ther* 4 (9): 891-900.
- Maruyama K., Iwasaki F., Takizawa T., Yanagie H., Niidome T., Yamada E., Ito T. and Koyama Y. (2004). "Novel receptor-mediated gene delivery system comprising plasmid/protamine/sugar-containing polyanion ternary complex." *Biomaterials* 25 (16): 3267-73.
- Masuda T., Akita H. and Harashima H. (2005). "Evaluation of nuclear transfer and transcription of plasmid DNA condensed with protamine by microinjection: the use of a nuclear transfer score." *FEBS Lett* 579 (10): 2143-8.
- McAllister K., Sazani P., Adam M., Cho M.J., Rubinstein M., Samulski R.J. and DeSimone J.M. (2002). "Polymeric nanogels produced via inverse microemulsion polymerization as potential gene and antisense delivery agents." *J Am Chem Soc* 124 (51): 15198-207.

- Melnikov S.M., Sergeyev V.G. and Yoshikawa K. (1995). "Transition of Double-Stranded DNA Chains between Random Coil and Compact Globule States Induced by Cooperative Binding of Cationic Surfactant." *J Am Chem Soc* 117 (40): 9951-9956.
- Nur I., Szyf M., Razin A., Glaser G., Rottem S. and Razin S. (1985). "Procaryotic and eucaryotic traits of DNA methylation in spiroplasmas (mycoplasmas)." *J Bacteriol* 164 (1): 19-24.
- Olmsted J., 3rd and Kearns D.R. (1977). "Mechanism of ethidium bromide fluorescence enhancement on binding to nucleic acids." *Biochemistry* 16 (16): 3647-54.
- Ouyang M., Remy J.S. and Szoka F.C., Jr. (2000). "Controlled template-assisted assembly of plasmid DNA into nanometric particles with high DNA concentration." *Bioconjug Chem* 11 (1): 104-12.
- Parrilla I., Vazquez J.M., Oliver-Bonet M., Navarro J., Yelamos J., Roca J. and Martinez E.A. (2003). "Fluorescence in situ hybridization in diluted and flow cytometrically sorted boar spermatozoa using specific DNA direct probes labelled by nick translation." *Reproduction* 126 (3): 317-25.
- Porschke D. (1984). "Dynamics of DNA condensation." *Biochemistry* 23 (21): 4821-8.
- Quick D.J. and Anseth K.S. (2003). "Gene delivery in tissue engineering: a photopolymer platform to coencapsulate cells and plasmid DNA." *Pharm Res* 20 (11): 1730-7.
- Raspaud E., Chaperon I., Leforestier A. and Livolant F. (1999). "Spermine-induced aggregation of DNA, nucleosome, and chromatin." *Biophys J* 77 (3): 1547-55.
- Rigby P.W., Dieckmann M., Rhodes C. and Berg P. (1977). "Labeling deoxyribonucleic acid to high specific activity in vitro by nick translation with DNA polymerase I." *J Mol Biol* 113 (1): 237-51.
- Rosen M.J. (1978). *Surfactants and Interfacial Phenomena* Wiley, New York, NY.
- Vijayanathan V., Thomas T., Shirahata A. and Thomas T.J. (2001). "DNA condensation by polyamines: a laser light scattering study of structural effects." *Biochemistry* 40 (45): 13644-51.
- Vilfan I.D., Conwell C.C. and Hud N.V. (2004). "Formation of native-like mammalian sperm cell chromatin with folded bull protamine." *J Biol Chem* 279 (19): 20088-95.
- Wu G.Y. and Wu C.H. (1987). "Receptor-mediated in vitro gene transformation by a soluble DNA carrier system." *J Biol Chem* 262 (10): 4429-32.

CHAPTER IV

COMPLEXATION OF PLASMID DNA WITH NANOGEL

4.1 Introduction

The poor performance of pDNA-entrapped neutral nanogels in transfecting cells that was described in the previous chapter led to another approach in utilizing nanogels as gene carriers. Adopting the very conventional polyplex system, pre-made cationic nanogels may deliver genetic materials to intended sites of the cell (e.g., cytosol and nucleus) in efficient way.

Non-specific binding of cationic particulate drug carriers to the cell is mediated by the electrostatic interaction between excess positive charges on the carrier and the negative charges on the cell surface. In contrast, active or targeted drug delivery systems can have higher selectivity and low collateral side-effects by recognizing molecular markers, which are often overexpressed in the cells under disease state such as tumor (Arap *et al.* 1998; Hood *et al.* 2002; Lu *et al.* 2002; Kukowska-Latallo *et al.* 2005). The molecular recognition processes entail ligand-receptor interactions: examples may include antibodies (Gao *et al.* 2004), endogenous targeting peptides or proteins (Raden and Gilmore 1998; Bellocq *et al.*

2003; Faraasen *et al.* 2003), nucleic acid-based aptamers (Nimjee *et al.* 2005), and low molecular weight compounds (Benns and Kim 2000).

Ligands bound to the corresponding receptors generally enter the cells via receptor-mediated endocytosis. Since the concept of receptor-mediated endocytosis was formulated in the investigation on the regulation of cellular cholesterol metabolism by low density lipoproteins in 1974 (Goldstein and Brown), the process was recognized during the subsequent decade as a major mechanism by which vertebrate cells internalize many macromolecules (Pastan and Willingham 1981; Bretscher and Pearse 1984). The phenomena were observed in various transport proteins such as cholesterol-carrying lipoprotein (Anderson *et al.* 1982) and the iron transport protein transferrin (Hopkins 1985) as well as many other non-transport plasma proteins such as asialoglycoproteins (Berg *et al.* 1983) and immune complexes (Schachtschabel *et al.* 1996; Shimizu *et al.* 1996). Some growth factors such as epidermal growth factor (Carpenter and Cohen 1979) and classical polypeptide hormones such as insulin (Ullrich *et al.* 1985) also enter the cell by receptor-mediated endocytosis.

Due to size, small MW ligand such as folic acid of MW 441 have distinct advantages over the macromolecular ligands mentioned above in that they are usually non-immunogenic and allow well-defined conjugation chemistry. Folate, a generic term for folic acid-related compounds, also retains its affinity for the corresponding receptor upon conjugation via its gamma carboxyl to a drug or drug carriers (Reddy and Low 1998; Wang and Low 1998; Sudimack and Lee 2000). Cellular uptake of folate, an essential vitamin, is mediated by a low

affinity but widely expressed reduced-folate carrier (K_d ; $\sim 1 \mu\text{M}$) as well as a high affinity/low capacity folate receptors (K_d ; 0.1 - 1 nM) (Juillerat-Jeanneret and Schmitt 2006). Reduced folate carrier transports primarily reduced folates such as 5-methyltetrahydrofolate. Folate receptor (FR), also known as folate-binding protein, transports oxidized folates such as folic acid. Human FR has three isoforms with about 70% genetic homology to one another (Prasad *et al.* 1994). Two membrane-bound FR isoforms (i.e., α and β) have been reported. They are 38-kDa glycosylphosphatidylinositol (GPI)-anchored glycoproteins that are often highly expressed in a number of epithelial carcinomas (Antony 1996; Wu *et al.* 1999) but present in only a limited number on normal cells (Sapra and Allen 2003). These FR isoforms show distinctive tissue distribution patterns. FR- α is frequently expressed in many malignant tissues of epithelial origin including ovary, uterus, brain and kidney (Ross *et al.* 1994; Weitman *et al.* 1994; Toffoli *et al.* 1997). The expression of FR- β is amplified in hematopoietic, nonepithelial cells such as in spleen and thymus (Ross *et al.* 1994), myelogenous leukemias (Garin-Chesa *et al.* 1993) and activated macrophages (Nakashima-Matsushita *et al.* 1999). In contrast to GPI-anchored isoforms, FR- γ and its truncated form γ' lack the anchor and exist as soluble forms of the folate receptors at very low levels (Shen *et al.* 1994). FR- α is one of the most widely utilized strategies for site-specific drug delivery based on a receptor-mediated endocytosis (Kamen and Capdevila 1986; Leamon and Low 1991; Sabharanjak and Mayor 2004; Kelemen 2006; Salazar and Ratnam 2007).

There have been conflicting reports on the mechanism involved in the internalization and trafficking of FR and folate conjugates (Rothberg *et al.* 1990; Anderson *et al.* 1992; Mayor *et al.* 1994). The fate of the cargo when they are released from the endocytosed

conjugate is also not clearly understood. Monovalent folate conjugate appears to undergo a rapid receptor recycling to plasma membrane via moderately acidic compartment, presumably following caveolae-dependent lipid-raft pathway (Sabharanjak and Mayor 2004; Yang *et al.* 2007). The caveolae is 50-80 nm in size and a flask-shaped cell membrane invagination that often serves as a transcytotic shuttle for entrapped substances. Caveolae can discharge the luminal content directly to cytosol in agreement with an earlier model of so-called potocytosis (Mineo and Anderson 2001; Anderson and Jacobson 2002). In contrast, when multiple copies of folate are chemically attached to a particulate drug carrier such as liposome, FR clustering may occurs in caveolae (Sabharanjak and Mayor 2004), resulting in a delivery of the assembly to lysosome-like compartment where luminal pH can be as low as 4.3 (Lee *et al.* 1996). Although the mechanism has yet to be further clarified, folates obviously move across the plasma membrane into the cytosol (Kamen and Capdevila 1986).

Folate receptor-mediated drug delivery has expanded to in gene delivery in the past decade. Folate-expressing liposomes (Lee and Huang 1996; Li *et al.* 1998) as well as biodegradable nanospheres (Leong *et al.* 1998) have been formulated for the receptor-specific cellular delivery of genes. The incorporation of flexible linker such as PEG between the carrier and folate enhanced cell surface recognition; a spacer of approximately 25 nm from PEG of MW 3.3 kDa appeared to allow the folate to find an unoccupied, cell surface folate receptor most efficiently (Lee and Low 1994). The folate-PEG conjugates has been applied to delivery of a wide range of therapeutic materials to tumor cells, including chemotherapeutic compounds (Saul *et al.* 2003; Hilgenbrink and Low 2005) and oligonucleotides (Wang *et al.* 1995; Leamon *et al.* 2003).

In the present chapter, pDNA was complexed with pre-made cationic nanogels that were strategically designed to target folate receptor-overexpressing tumor cells. Nanogels were modified with folates by incorporating folate-containing monomers during polymerization. Gene expression, represented by luciferase enzyme activity in the cell treated with this formulation, was assessed as the dependent variable of the study.

4.2 Materials and Methods

4.2.1 Materials

Folic acid was purchased from Spectrum Chemical Manufacturing Corporation (Gardena, CA) and used as received. All ACS grade organic solvents including dimethyl sulfoxide, diethyl ether, heptane and dichloromethane and 1 N NaOH standard solution were purchased from Fisher Scientific. *N*-hydroxysuccinimide, *N,N,N*-triethylamine, PEI of 25 kDa, and acryloyl chloride were purchased from Aldrich. The sources of monomers used in the preparation of nanogel were represented in the previous chapter. Poly(ethylene glycol) bisamine (average MW of 3350 g/mol) and dicyclohexylcarbodiimide (DCC) were purchased from Sigma. Ethidium bromide at 10 mg/mL in Tris-acetate-EDTA (TAE) buffer was purchased from Fluka and stored at - 4°C. Plasmid DNA (pCMV-Luc) at 1 mg/mL in water was purchased from Elim Biopharmaceutical (Hayward, CA). Agarose gel was purchased from Denville Scientific (Metuchen, NJ). Folate-free RPMI 1640, antibiotics, fetal bovine serum, Opti-MEM, Hank's balanced salt solution (HBSS) and DL-dithiothreitol were

purchased from Gibco BRL (Gaithersburg MD). Lipofectamine[®] 2000 were purchased from Invitrogen (Carlsbad, CA) and used following the instruction from the manufacturer. Charcoal-stripped fetal bovine serum was purchased from Gemini Bio-Products (West Sacramento, CA).

4.2.2 Preparation of Folate-Containing Monomers

4.2.2.1 Activation

The synthetic scheme of folate containing, acrylate monomer is represented in **Figure 4-1**. Activated ester and PEG conjugate of folate were synthesized based on Guo and Lee (1999) with appropriate alteration in stoichiometry. One gram of folate (2.27 mmol) was dissolved in 12 mL of anhydrous DMSO at room temperature. Dicyclohexylcarbodiimide (0.94 g, 4.56 mmol) was dissolved in 8 mL of DMSO and added to the reaction while magnetic stirring followed by the addition of two equivalents of *N*-hydroxysuccinimide (0.52 g, 4.52 mmol). *N,N,N*-triethylamine (0.5 mL, 3.59 mmol) was added as a proton scavenger. Reaction was protected from light by wrapping the vessel with aluminum foil and stirred at room temperature. After 14 hrs, reaction was filtered through glass wool to remove insoluble byproduct (i.e., dicyclohexylurea), evaporated to dryness (5 hrs at 55°C with 4 torr) and reconstituted in 10 mL of anhydrous diethyl ether to precipitate out the product. After ether wash 3X, the precipitates were filtered using a sintered glass filter and dried in an oven at 60°C for 30 min. The yield based on both carboxyl groups (i.e., in alpha and gamma positions) on folate activated was approximately 93%.

4.2.2.2 Coupling

Activated folate (229 mg, 0.36 mmol, compound **5** in **Figure 4-1**) was dissolved in 15 mL of DMSO and added dropwise to 1 g (0.3 mmol) of PEG bisamine in 6 mL of DMSO. The reaction was stirred at room temperature protected from the light. After 3 hrs, three volumes of distilled water was added to the reaction to deactivate remained succinimide moieties on the folic acid. After stirring 10 min, the reaction mixture was filtered using a sintered glass filter and concentrated at 55-60°C for 3 hrs under vacuum. The concentrated reaction mixture (~ 1.5 mL) in DMSO was mixed with 3.5 mL of water before loading on a Sephadex G-25 (Sigma) column using water as an eluant. The elution rate/sample size was 8 mL/4 min/tube and the void volume was approximately 30 mL. After the chromatography, 10 fractions were collected, concentrated at 37°C for 4 hrs under vacuum, filtered using a sintered glass filter (70-100 micron), and lyophilized for 20 hrs. On a silica gel TLC plate (Aldrich), the reaction mixture contained multiple spots that were UV-detectable (folate) and charred (PEG) with ammonium sulfate spray as well (methanol:chloroform:acetic acid = 30:65:5 as a developing solvent). Yield calculated using average MW of 3770 g/mol was approximately 52%.

4.2.2.3 Acylation

Two equivalent of triethylamine (20 μ L, ~ 0.14 mmol) was added to compound **8** (258 mg, ~ 0.07 mmol) dissolved in 13 mL of cold anhydrous dichloromethane while magnetic stirring. Into the reaction mixture, 1.5 equivalent of acryloyl chloride (9 μ L) in 2

mL of dichloromethane was added dropwise. The reaction was kept on the ice for 2 hr followed by additional 2-hr incubation at room temperature with magnetic stirring. After 4 hrs, reaction mixture was evaporated to dryness under vacuum (room temperature for 15 min), reconstituted in 4 mL of distilled water, and loaded on a Sephadex G-25 column using water as eluant. The elution rate/sample size was 8 mL/4 min/tube and the void volume was approximately 29 mL. Four fractions were collected, concentrated under vacuum (room temperature for 30 min), dialyzed against water using dialysis cassettes (MWCO 2 kDa, Pierce Biotechnology, Rockford, IL) for 20 hrs while changing water every 6-8 hrs, and lyophilized for 20 hrs. The reaction yield calculated based on the average MW of 3830 g/mol was approximately 76%.

4.2.3 Gel Electrophoresis

In the present study a plasmid containing a luciferase reporter gene (pCMV-Luc, 6.2 kbp) was used as a model pDNA. Retardation of the pDNA bound to cationic nanogels was observed on 0.8% agarose gel. Agarose gel was prepared in TAE buffer and contained 0.5% (v/v) ethidium bromide. Cationic nanogels composed of PEGdiA:AETMAC:HEA (10%:6%:84%, w/w) was mixed with 0.2 μ g of pDNA to achieve various N/P ratios (0, 1, 2, 4, 10, 20, and 40), stirred briefly, and incubated at room temperature for 10 min before gel loading. Electrophoresis was run for 45 min at 90 volts in 1 X TAE buffer and ethidium bromide-intercalated pDNA was detected under UV using a Bio-Rad Versa Doc Model 1000 Imaging System (Bio-Rad Laboratories, Inc., Hercules, CA). For assessing the release of pDNA from nanogel with N/P ratio 4 or 10, nanogel was mixed with pDNA (0.2 μ g) in water,

stirred briefly, and incubated 10 min at room temperature before the addition of various concentration (0, 0.01, 0.05, 0.2, 1, 2, and 10 mM as final concentration) of dithiothreitol. The complex was further incubated at 37°C for 3 hrs and was loaded on 0.8% agarose gel containing 0.5% (v/v) ethidium bromide. Electrophoresis was performed under the same condition as described in the retardation study.

4.2.4 Size Measurement

Hydrodynamic diameters of nanogel or nanogel-pDNA complex were measured at 23°C using viscosity of 0.933 centipoise and refraction index of 1.333 on a NICOMP Model 370 dynamic light scattering instrument (Particle Sizing Systems, Santa Barbara, CA), equipped with a 30-mW laser (632.8-nm wavelength) and an Avalanche photodiode detector. The concentration of nanogel in size measurement was 2-4 mg/mL in water. The scattered light intensity detected at a 90° angle was treated using the Gaussian or multimodal Nicomp analysis, depending on the polydispersity of the samples, and the data presented corresponds to the volume-weighted distribution. The mean diameters shown were averages of duplicated measurements performed on different samples for periods of time long enough (from 10 to 40 min) to collect statistically reliable data.

4.2.5 Determination of Folate Concentration in Nanogels

Nanogels were prepared following the procedure described in **Chapter II**. The folate-containing monomer (**12** in **Figure 4-1**) was added to the aqueous phase before forming

microemulsion. In order to measure a concentration of folate in nanogel formulations, standard curve was prepared by mixing regular control nanogel (10% PEGdiA, crosslinker and 90% HEA) in water with known concentration of folate. The concentration of nanogels in all the mixtures was fixed at around 3.4 mg/mL. Regular and folate-containing nanogels were lyophilized and reconstituted in 0.5 N NaOH followed by 20-min sonication in a high-power bath-type sonicator (Model G112SP1T, Laboratory Supplies Co. Inc., Hicksville, NY). The final concentration of nanogels in both formulations was adjusted to 10 mg/mL. Absorbance of nanogel solutions was measured at 259 nm using nanodrop Model 1000 (NanoDrop Technologies, Wilmington, DE). Absorbance at 259 nm from regular nanogels was used as a background value and subtracted from that of folate-containing nanogels.

4.2.6 Transfection

The human squamous cell carcinoma of the oral cavity, KB cells, were purchased from UNC tissue culture facility and maintained in folate free RPMI 1640 supplemented with 100 U/mL penicillin, 100 µg/mL streptomycin, and 10% FBS for the initial 3 weeks. The cells transfected with the first set of nanogel-pDNA complexes (N/P ratio 2 and 10) were cultured in the folate-free RPMI with charcoal-stripped FBS (i.e., folate-free FBS) for another 3 days and seeded in 24-well plates (5×10^4 cells/well) under this media condition one day prior to transfection. Regular tissue culture media were not used because they contain micromolar levels of folate (i.e., order of magnitudes higher than that of the physiological level) and may block receptor binding of folate conjugates. The KB cells treated with a second set of nanogel-pDNA complexes (N/P ratio 4) were cultured in folate-

free RPMI with charcoal-stripped FBS for 2 weeks. These KB cells were then maintained and seeded in folate free RPMI with 5% regular FBS. Sixteen hours later, medium was removed and nanogel-pDNA complex was added to the cells. The cells were incubated in 1 mL of Opti-MEM or folate free RPMI with 5% FBS for 4 hrs.

One microgram (or 3 μg in NG-pDNA complex with N/P ratio 4) of pDNA and 0.1 mg of NG were mixed, stirred briefly, and stored at room temperature for 10 min before the treatment. For the competition experiments, 50- to 1,000-fold molar excess of free folate was added to the cells along with the test groups. Dimethyl sulfoxide or 1 N NaOH was used to dissolve folate and the final concentration of dimethyl sulfoxide or NaOH during transfection was 0.03% (v/v) and 1 mM, respectively. Lipofectamine[®] 2000 was mixed with pDNA by 1.5:1.0 ($\mu\text{L}:\mu\text{g}$) ratio and incubated 10 min before treatment. Poly(ethylenimine) of 25 kDa was complexed with pDNA at N/P ratio 4 and 10. The N/P ratio was calculated assuming the $-\text{NH}-\text{CH}_2-\text{CH}_2-$ moiety as a unit positive charge. Based on this calculation, one microgram of pDNA was mixed with 0.52 μg and 1.3 μg of PEI for N/P ratio 4 and 10, respectively, and the complex was introduced to the cells after 10-min incubation. After 4-hr transfection, Opti-MEM or RPMI was removed from the cells and the cells were rinsed with 0.5 mL of HBSS and supplemented with 1 mL of folate-free RPMI containing charcoal-stripped FBS followed by additional 44-hr incubation at 37°C in a 5% CO₂ humidified atmosphere. For the second set of experiment with N/P ratio 4, cells were maintained in folate free RPMI containing 5% regular FBS for the additional 44-hr incubation period.

4.2.7 Luciferase Assay

At 48 hrs post-transfection, media was removed, rinsed with 0.2 mL of 1 X PBS, and added 100 μ L of cell lysis buffer (Promega Corporation, Madison, WI). Cell lysates were collected in 1.5-mL polypropylene tubes, vortexed for 10 sec, and centrifuged for 2 min at 12,000 x g. An aliquot of supernatant was used in quantifying luciferase gene expression using a commercial kit (Promega Corporation, Madison, WI) and a luminometer (Monolight 3010, Analytical Luminescence Laboratory, San Diego, CA). The results were expressed as relative light units (RLU) integrated over 10 sec per mg cell protein lysate (i.e., RLU/mg of protein) using the bicinchoninic acid (BCA) assay (Pierce Biotechnology, Rockford, IL). The errors bars represent standard deviation derived from quadruplicate transfection experiments (\pm S.D., n=4).

4.3 Results and Discussion

4.3.1 Preparation of Folate-Containing Monomer

Structural identification of all intermediates involved (compounds **5** and **8** in the **Figure 4-1**) and the final product (compound **12** in **Figure 4-1**) was carried out using ^1H -NMR in DMSO-d_6 . **Figure 4-2B** shows ^1H -NMR (Gemini 300) spectrum of *N*-hydroxysuccinimide-activated folate (compound **5** in **Figure 4-1**). Since two molar equivalents of *N*-hydroxysuccinimide (compound **3**) was used in the first step, in some products both α - and γ -carboxyl groups could have been activated. It was difficult to distinguish mono-activated (i.e., alpha or gamma only) species from doubly activated product through NMR. According to an early investigation (Atkinson *et al.* 2001), γ -carboxyl group is approximately 2x more reactive than the one at α -position. The identification of the product (compound **5**) was not further investigated because it would not affect the eventual outcome of the synthesis. The next step involves coupling with a primary amine **7** in almost 1:1 stoichiometry. Under this reaction condition, even if the product has two activated moieties, only one of them will react with **7** while the other one become deactivated when water is introduced.

The superiority of modified folate in one carboxyl group over the other in terms of recognition by folate receptor still remains unresolved (Wang *et al.* 1996; Leamon *et al.* 2003). **Figure 4-2B** shows that activated folate **5** has an unresolved signal at 2.9 ppm from succinimide moieties (**I'** in the spectrum) that is absent in the original folate (**Figure 4-2A**),

while the unique signals from folate (**g** and **f** in the both spectra) remains intact. Extra signals shown in **Figure 4-2B** probably represent impurities coming from the reaction byproduct, dicyclohexylurea **6**. Dicyclohexylurea is a typical byproduct from a carboxyl-alcohol conjugation reaction mediated by dicyclohexylcarbodiimide **2** and is very difficult to remove completely.

In the next coupling step, a slight excess of (1.2 equiv.) of *N*-hydroxysuccinimide activated folate **5** was used in reacting with PEG-based bisamine **7**. This stoichiometry would produce the mixture of the intended product **8** and trace amount of byproduct with both amine groups coupled with compound **5**. However, this byproduct, if any, is not expected to react with acryloyl chloride **11** in the next acylation step, and eventually will be removed during nanogel preparation that involves dialysis using 100-kDa MWCO dialysis bag. It is a better situation than having an unreacted PEG bisamine after coupling reaction, which could react with acryloyl chloride **11** to result in incorporating unwanted primary amines in the final the nanogel formulation. **Figure 4-3A** shows that the long chain of PEG moiety (**m** in the spectrum) is clearly indicated by the NMR spectrum of the coupling product **8**. The primary amine (**n** in the spectrum) in the compound **8** was very difficult to detect clearly because it was buried under the signal of methylene protons (**k** in the spectrum).

The next and final step entails the introduction of acrylate moiety to the folate-PEG conjugate for providing a free radical receiving site in polymerization. As represented in **Figure 4-3B**, proton signals from acrylate moiety (**o**, **p** and **q**) clearly appeared in the spectrum, verifying that compound **8** with primary amine was successfully synthesized in the

previous step. The final product **12** was lyophilized under high vacuum at - 45°C for storage. The product was finally purified using a dialysis cassette with MWCO of 2 kDa, removing low molecular weight species of product. Note that product was derived from a PEG mixture of various MW with an average value of 3350 g/mol. The molecular weight of compound **12**, approximately 3.8 kDa, which was not that far from the exclusion cut off size of dialysis bag. Nevertheless, the reaction yield of acylation was relatively high (76%).

4.3.2 Determination of Folate Concentration in Nanogel

The concentration of folate moiety in the nanogel was measured spectrophotometrically. Folate in alkalic solution (i.e., pH 13) has two UV-Vis λ at 259 and 368 nm with extinction coefficient of 3.23×10^4 and 7.41×10^3 , respectively. As shown in the **Figure 4-4**, the concentration of folate in the nanogel prepared with folate monomer (compound **12** in **Figure 4-1**) was found to be 21 μ M. This value is very close to the anticipated concentration, 26 μ M that is calculated from the initial amount of folate-containing monomer incorporated in the polymerization (i.e., 1.0% w/w of total monomers). Taken together, the present observation demonstrated that folate was indeed incorporated in the nanogel with intended weight percent. No attempt was made to determine how much of these were indeed expressed on the surface of nanogels. It is tempting to speculate that the hydrophobic folate moiety of compound **12** may prefer to reside in the heptane phase while PEG may prefer the aqueous phase such that the conjugate is concentrated at the interface of microemulsion. If this is the case, folate group will stay primarily on the surface of the polymerized nanogel, facilitating recognition by cell surface folate receptor.

4.3.3 Transfection of KB Cells with Nanogel-Plasmid DNA Complex

The overall scheme of nanogel formulation is illustrated in **Figure 4-5**. The formulation contains disulfide bond aiming for the facile release of pDNA upon reaching a reducing environment in the cell. Weak bases for the proton sponge effect and targeting ligand, folate, were also included in the formulation. Introducing pDNA into the rationale-based nanogel was followed by cellular transfection in folate receptor expressing KB cells.

As shown in the upper panel of **Figure 4-6**, all the nanogel formulations turned out to be less efficient, as much as by 4 orders of magnitude, in gene expression than PEI and Lipofectamine[®] 2000. Poly(ethylenimine) at N/P ratio 10, represented as **P** in the figure, showed a higher transfection efficiency than at N/P ratio 4 (**O**) by 2 orders of magnitude, which is in agreement previous reports (Boussif *et al.* 1995). Nanogel formulations, however, increased gene expression by up to 15-fold compared to pCMV-Luc alone (**A**) that serves as a negative control. Performance of nanogel formulations without controls is summarized in the lower panel of **Figure 4-6** on a linear scale. There was a trend that nanogels targeted with folate increased gene expression by up to 8-fold except for nanogels that do not contain weak base with N/P =10 (**L** and **M**). In these test groups, the binding of nanogels to the cell could have been mediated mainly by charge interaction between negative charges on the cell surface and excess amount of positive charges on the nanogels. Such a non-specific binding could have overwhelmed the chance for targeting ligands on the nanogels to bind to the folate receptor on the cell. Upon co-incubation with 50-fold excess free folate, transfection efficiency decreased in most of the test groups (gray bars on the figure). The present

observation agrees well with a previous study, which reported that targeting effect was more evident at low N/P ratios with slightly positively charged DNA complexes (Guo and Lee 1999).

The incorporation of weak base such as histidine in the polymer has been reported to enhance gene transfer in mammalian cells due to its endosomal buffering capacity (Midoux and Monsigny 1999; Benns *et al.* 2000; Pack *et al.* 2000). The presence of weak base in the nanogel improved transfection efficiency only in the targeted, disulfide crosslinker-containing nanogels with N/P ratio 2 (closed bars in **B** and **D** compared to closed bar in **F**). Interestingly, these test groups showed most obvious targeting effect, which was clearly abolished in the presence of free folates as represented in the gray bars of **B** and **D**. Dimethylamine-derived nanogels (**D**) showed slightly better transfection than imidazole-containing formulations (**B**) with the same composition. In all test groups, incorporation of the cleavable linker improved gene expression by up to 4-fold and the improvement appeared to be more profound in the targeted formulations at lower N/P ratio (see **B** vs. **C** and **D** vs. **E**).

Agarose gel electrophoresis run with pDNA-nanogel complex (**Figure 4-7**) shows that pDNA was not released at N/P ratio 10 from either disulfide crosslinked or non-cleavable linker-containing nanogels even in the presence of 10 mM dithiothreitol a reducing reagent, when incubated at 37°C for 3 hrs (left panel in **Figure 4-7**). In contrast, pDNA was released from the nanogels with N/P ratio 4 when incubated with dithiothreitol of 1 mM or higher. At 10 mM, a physiologically relevant (i.e., cytosolic) concentration (Kosower and Kosower 1978), a significant amount of pDNA was released from nanogels within 3 hrs

(right panel in **Figure 4-7**). The facile release of pDNA from the nanogels with N/P ratio 2 could contribute to the increase in transfection. At N/P ratio 10, the electrostatic association of pDNA to cationic nanogels might have overridden rendering free pDNA less accessible for eventual nuclear entry.

Figure 4-8 represents the retarded movement of pDNA on the agarose gel when bound to cationic nanogels at various N/P ratios. Nanogel-bound pDNA even moved upward on the gel (i.e., toward cathode) at N/P ratio 10 or higher. Most of pDNA were bound to nanogel at N/P ratio around 4 while a significant portion of pDNA remained as free form (i.e., unbound to nanogel) at N/P ratio 2. The loose binding could cause a decrease in the actual amount of pDNA that had an access to nucleus because of the premature degradation during the cellular transfection steps. As shown in **Figure 3-18**, which dealt with PEI formulations with 0.2 or 1.0 μg of pDNA, transfection efficiency is not simply proportional to the amount of pDNA present in the formulation. Thus a formulation containing more pDNA with optimal N/P ratio could induce much more profound gene expression.

As shown in **Figure 4-9A**, the size of nanogel before mixed with pDNA was different depending on the composition. Compared to the size of regular control nanogels (~ 80 nm, dotted line in the figure), imidazole-containing nanogels were bigger (~ 120 nm) but dimethylamine-containing formulations tended to be smaller (~ 60 nm). In the preparation of disulfide-containing nanogels, 50% (w/w) methanol had to be added in the aqueous phase due to the solubility of disulfide crosslinker. The addition of methanol appeared to influence the formation of microemulsion and increased the eventual size of the particles. There was no

significant difference in the size between targeted nanogels and non-targeted counterparts or between the formulations prepared with two different N/P ratios. As shown in **Figure 4-9B**, after mixed with pDNA, the size of the complex increased within a few minutes, approximately 2- to 3-fold with N/P ratio 2 and 10, respectively. The size of nanogel-pDNA complex at N/P ratio 2 continuously increased with time while the complex at N/P ratio 10 remained the same after the immediate size increase. The size increase of the complex may well be due to the aggregation, which is usually more severe in the case of neutral particles. The present observation demonstrated very a similar phenomenon.

For the subsequent study, dimethylamine-containing, cleavable (i.e., disulfide crosslinked) nanogel at N/P ratio 4 that was grafted with targeting ligand was selected in performing KB cell transfection. The KB cells used were confirmed for their expression of folate receptor using anti-FR- α monoclonal antibody and FITC-PEG-folate conjugate in a flow cytometer (data not shown). According to the electrophoresis result (**Figure 4-8**), most of the pDNA remained bound to nanogel at an N/P ratio 4 and thus this value was chosen for the study. N/P ratio 2 and 10 may have some disadvantage over 4 because at these ratios pDNA is either incompletely or too tightly bound to nanogels.

In this series of experiments, the substitution level (i.e., incorporation percentage) of folate-containing monomer in nanogel formulation was fixed at 0.1 mol % (3 weight %). Various incorporation levels of folate targeting ligand in the lipid- or polymer-based formulation have been attempted from 0.03 mol % up to 5% on in vitro as well as in vivo settings (Hofland *et al.* 2002; Reddy *et al.* 2002; Bruckheimer *et al.* 2004; Hattori and

Maitani 2005). Reddy et al. (2000) showed that the incorporation level of targeting ligand had some optimal range for more efficient targeting effect. They used 0.1 mol % of targeting ligand in the formulation. In the competition group for the present study, the concentration of free folic acid was 1 mM, which was close to 1,000-fold molar excess over that of folate ligand on the nanogel. The amount of pDNA per well also increased from 1 to 3 μ g to obtain higher resolution in terms of gene expression among test groups. As shown in the upper panel of **Figure 4-10**, nanogel test groups again showed inferior gene expression compared to all other commercially available transfection reagents by 2 to 4 orders of magnitude. Dimethylamine-containing nanogels showed a marginal improvement in gene expression (1.5 to 3.5 fold) compared to pDNA alone. Interestingly, cleavable nanogels without any weak base but grafted with targeting ligand (closed bar in **D** in the upper panel of **Figure 4-10**) represented a significant increase, \sim 400-fold vs. pDNA alone. Formulations without weak base showed a clear trend of improvement in gene expression by the presence of cleavable linkers (**D** vs. **E**). The trend was also seen in the previous formulation with N/P ratio 10 (see **L** vs. **M** in the lower panel of **Figure 4-6**). In the present study, however, the incorporation of targeting ligand to the nanogels without weak base also contributed to the enhancement of transfection efficiency, which agrees with the case of N/P ratio 2 previously shown in the lower panel of **Figure 4-6**.

In a separate set of experiment, transfection was carried out in the presence of 5% serum to see its effect on the transfection of KB cells with formulations. As shown in the lower panel of **Figure 4-10**, the difference in transfection efficiency between nanogel formulations and commercial reagents did not diminish significantly. There was

approximately 3-fold increase in gene expression by the presence of weak base in non-cleavable nanogels regardless of targeting ligand incorporation (**C** vs. **E**). However, in the cleavable nanogels (i.e., disulfide-containing nanogels) nanogels without weak base worked better (**D** vs. **B**). Throughout the test groups, targeted nanogels showed improved gene expression by approximately 5-fold compared to non-targeted formulations and most improvement was observed without weak base, cleavable linker possessing nanogels by 50-fold increase vs. pDNA alone (closed bar in **D**). Again, the presence of disulfide crosslinker improved transfection efficiency only in nanogels without weak base.

Figure 4-11 summarizes the overall gene expression normalized to free pDNA alone when 5×10^4 cells were treated with 1 μg of pDNA. At a lower N/P ratio such as 2, the net charge of nanogel-pDNA complex was close to neutral and the presence of weak base increased transfection efficiency especially in the targeted and cleavable linker containing formulations (**A**). This is attributed to their buffering capacity inside of endosomes. Unexpectedly, however, this was the only group that showed a significant benefit from the incorporation of weak base. As the excess amount of positive charges in nanogels increased (i.e. with N/P ratios 4 and 10), there was no improvement from the presence of weak base in the formulations (**E** - **P**). Decrease in apparent pKa of weak base containing nanogel by pre-existing positive charges may explain the present observation. Weak base-containing formulations with higher N/P ratios showed a far inferior transfection efficiency to formulations without weak base. It is not known the cause of the present findings.

Although it is difficult to determine how much weak base will be needed in order to expect the ‘proton sponge’ effect, more weak bases may well induce an improved acid buffering ability in the endosome. For example, as high as 75% (w/w) of imidazole was conjugated to PLL and the formulation showed a significant improvement in transfection efficiency (Putnam *et al.* 2001). Unfortunately, the maximum amount of weak bases that can be incorporated in the present nanogel was 25% (w/w) because the higher concentration of weak base caused phase separation of microemulsion. The amount of weak base in the present nanogel formulations might be thus suboptimal. Alternatively, the buffering ability of weak base incorporated in the nanogel might not have contributed to the improvement of the gene expression, as indicated by a minimal correlation between buffering capacity of imidazole-containing polymer and gene expression (Kulkarni *et al.* 2005). The present study also raised a question about the role of pH buffering in the endocytosis and gene delivery.

With a larger excess of positive charges in the nanogel-pDNA complexes, non-specific bindings (i.e., electrostatic interaction between cationic nanogel and anionic cell surface) appeared to override a specific receptor-ligand binding. Nanogel formulations in this category showed reduced or almost no targeting effects as represented in the formulation with N/P ratio 10 (**K** and **L** in **Figure 4-11**). According to the present study, the optimal formulation would be a cleavable (i.e., disulfide-containing), targeted nanogel with the net charge of close to the neutral. Even though some improved transfection was observed in lower N/P ratio formulation, weak base may not be a necessary element under present condition. With certain type of targeting ligand such as folate in the formulation, it may

trigger cytosolic translocation of genes or gene-carrier complexes following the endocytic cellular entry by ambiguous mechanism(s) (Turek *et al.* 1993).

The overall inferior ability of nanogel formulation could be also caused by poor pDNA stability in the formulations. Although gel retardation data (**Figure 4-8**) demonstrated that majority of pDNA remained bound to the nanogel at certain N/P ratios and pDNA was expected to be intact in this condition, the stability of pDNA in the cellular system was not verified in this study. Compared to the status in the commercial transfecting reagents, pDNA in the nanogel system could be more vulnerable to the given cellular environment. A further uncertainty is associated with nuclear entry. Once released into the cytosol, the transfecting pDNA must enter the nucleus to be transcribed. The double membrane structure surrounding nucleus contains an octagonal opening, known as nuclear pore complex, that allow the transport of water-soluble molecules across the nuclear envelope. The functional diameter of this complex is known to be approximately 25 nm (Fahrenkrog and Aebersold 2003). This narrow opening is expected to limit nuclear transport of pDNA. There is some indication that PEI has an ability to facilitate pDNA translocation into the nucleus in addition to its proposed buffering capacity (Pollard *et al.* 1998). Although the present study started with an assumption that endosome-to-cytosol translocation of polyplex would be a critical obstacle in transfection, the observation made with nanogels here may highlight the necessity of additional strategic modification to attain nuclear entry. The efforts to increase nuclear import include a coupling of peptides containing nuclear localization sequences to pDNA. Electrostatic interactions or peptide nucleic acid-mediated hybridization has been involved in the coupling strategies (Branden *et al.* 1999; Subramanian *et al.* 1999). Taken together, the

different ability in transporting pDNA into the nucleus might have resulted in a significant difference in transfection efficiency between nanogel formulations and the commercially available transfecting reagents such as PEI.

4.4 Conclusions

The present study was an extension of promising results shown in the previous literature that demonstrated surface modification using PEG-folate conjugates to gene vectors led to selective gene expression in folate-expressing cells in vitro (Lee and Low 1994; Guo and Lee 1999; Leamon *et al.* 1999; Reddy *et al.* 1999). Although the overall transfection efficiency of the test formulations did not surpass commercial transfecting reagents, the present investigation highlights several factors for the optimal gene carrier formulations to possess. First, the incorporation of cleavable linker to the carrier matrix can facilitate gene release from the carrier. The present findings with disulfide crosslinker-containing nanogels thus support the early investigation by McKenzie *et al.* (2000). They reported that substitution of some lysine residues by cysteine increased the gene transfer efficiency of the PLL polyplex. These observations strongly indicate that pDNA release is triggered by the intracellular reduction of disulfide bonds. Secondly, the conjugation of targeting ligand improves gene expression via selective and specific binding to the cell. Lastly but not in the least, the net charge of the overall polyplex should be close to neutral to achieve a specific ligand-receptor binding in transfection. That is, targeting capacity of the ligand-coated carrier can overcome non-specific binding only when the electrostatic attraction is minimal.

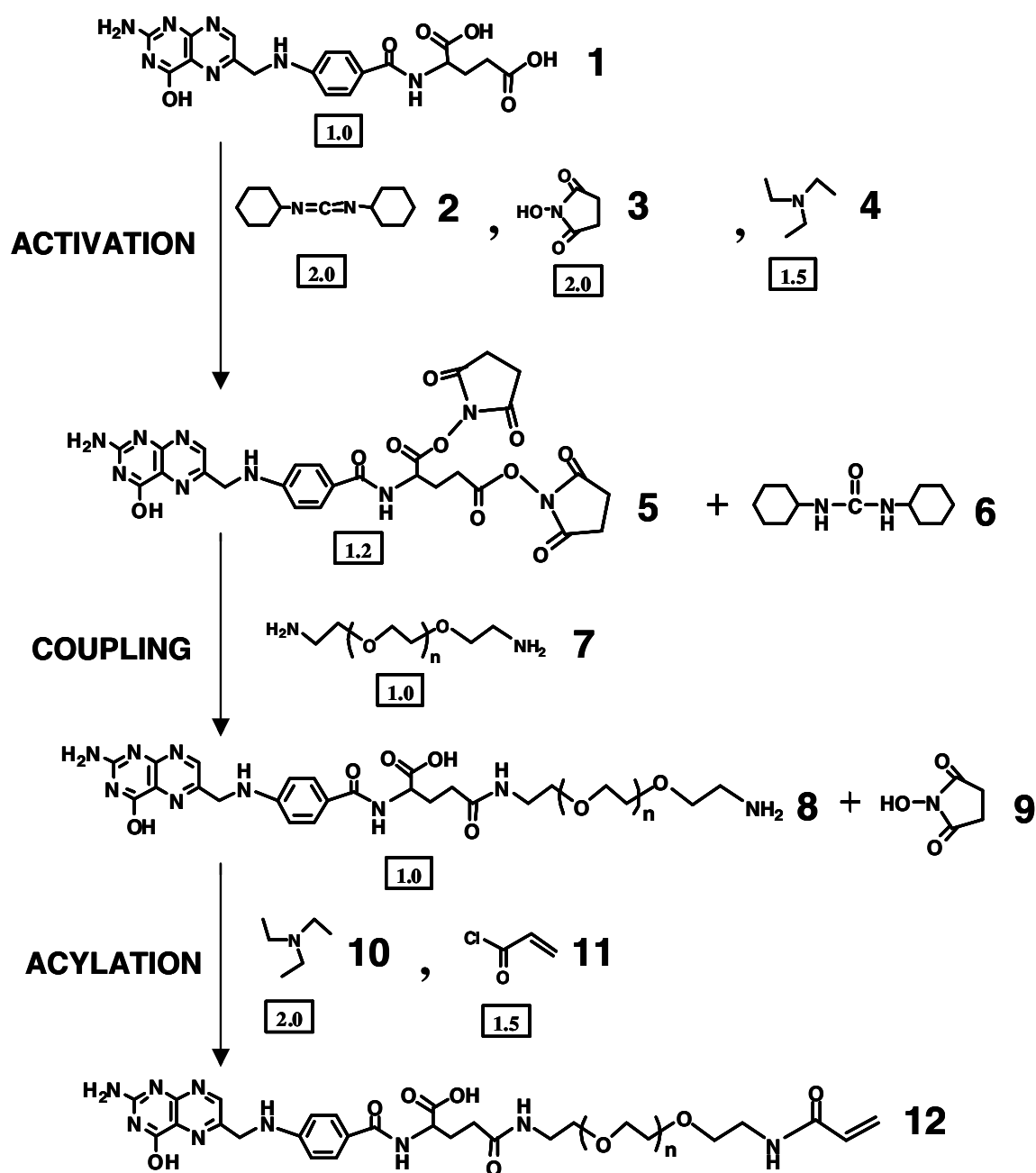


Figure 4-1: Synthetic scheme of PEG-based, acrylate-containing monomer. The overall scheme consists of three parts, activation of folate with *N*-hydroxysuccinimide, coupling with PEG bisamine, and acylation with acryloyl chloride. Numbers in the squares represent stoichiometry of the respective reaction. Byproducts, dicyclohexylurea, **6** from activation and *N*-hydroxysuccinimide, **9** from coupling reaction were also shown in the figure. Detailed reaction conditions are described in Materials and Methods.

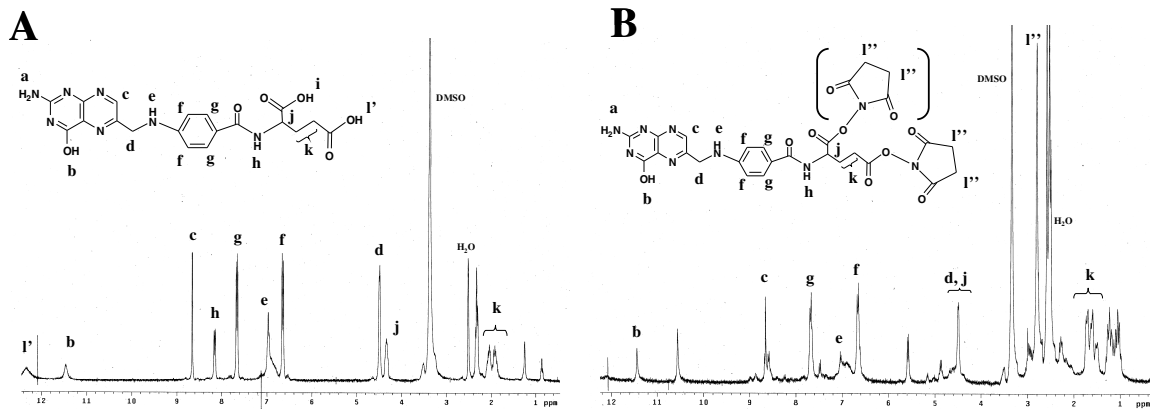


Figure 4-2: ¹H-NMR (300 MHz) spectra of folate (**A**) and *N*-hydroxysuccinimide-activated folate (**B**) dissolved in DMSO-d₆. Characteristic peaks in folate (**g** and **f**) were monitored to identify folate moiety in the present and the subsequent synthesis. The number of succinimide moiety in the activated folate (**B**) was not well established in the present study but assumed to be two per one molecule of the product (compound **5** in **Figure 4-1**) according to the integration.

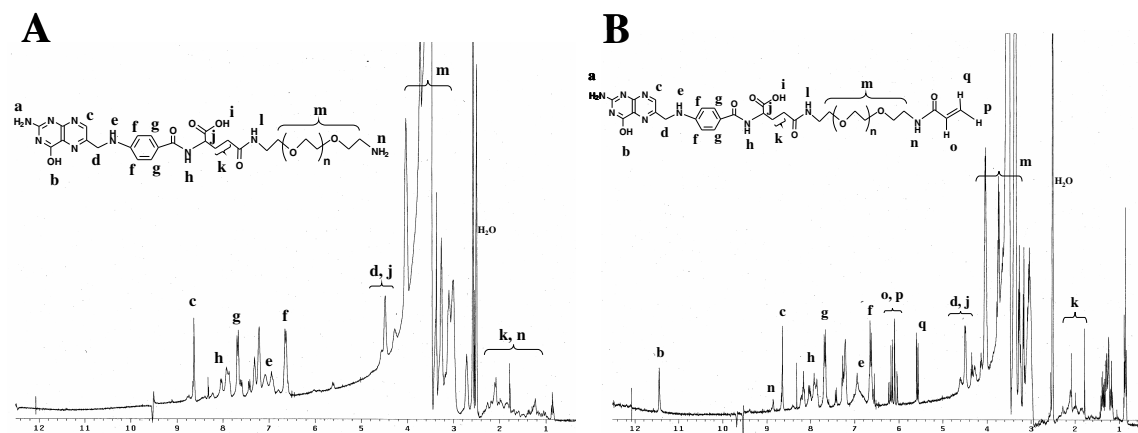


Figure 4-3: ^1H -NMR (300 MHz) spectra of PEG-conjugated folate (**A**) and acrylate-containing PEG-folate conjugate (**B**) dissolved in DMSO-d_6 . Appearance of new peak(s) was monitored in the respective product: long carbon chain, **m** in **A**; and acrylate protons, **o**, **p** and **q** in **B**.

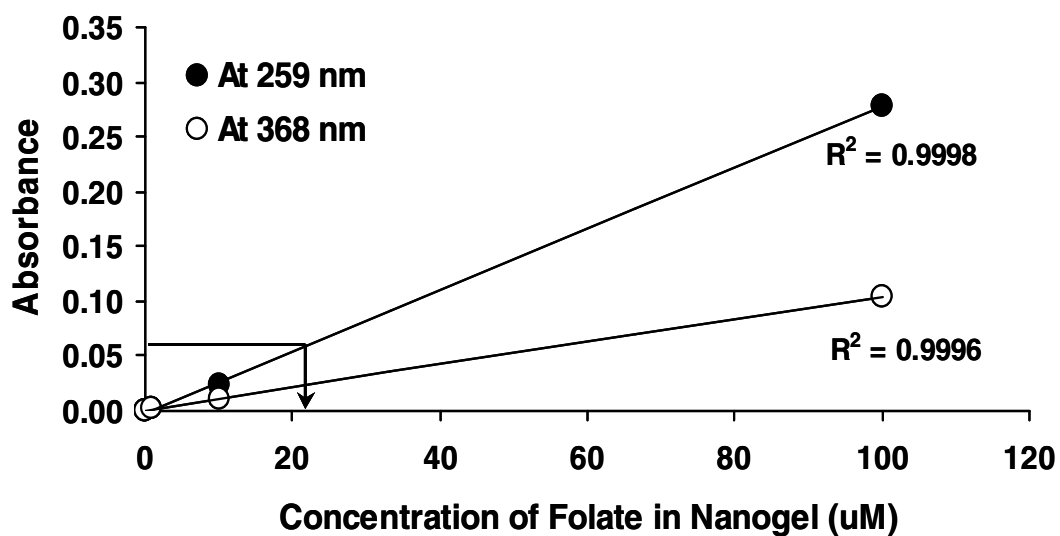


Figure 4-4: Spectrophotometric determination of the folate concentration in nanogels. Nanogels were lyophilized overnight and reconstituted in 0.5 N-NaOH followed by 20-min sonication prior to spectrophotometric measurement at 259 nm. The measured concentration of folate in the nanogel, 21 μM , was found to agree well with the anticipated concentration, 26 μM .

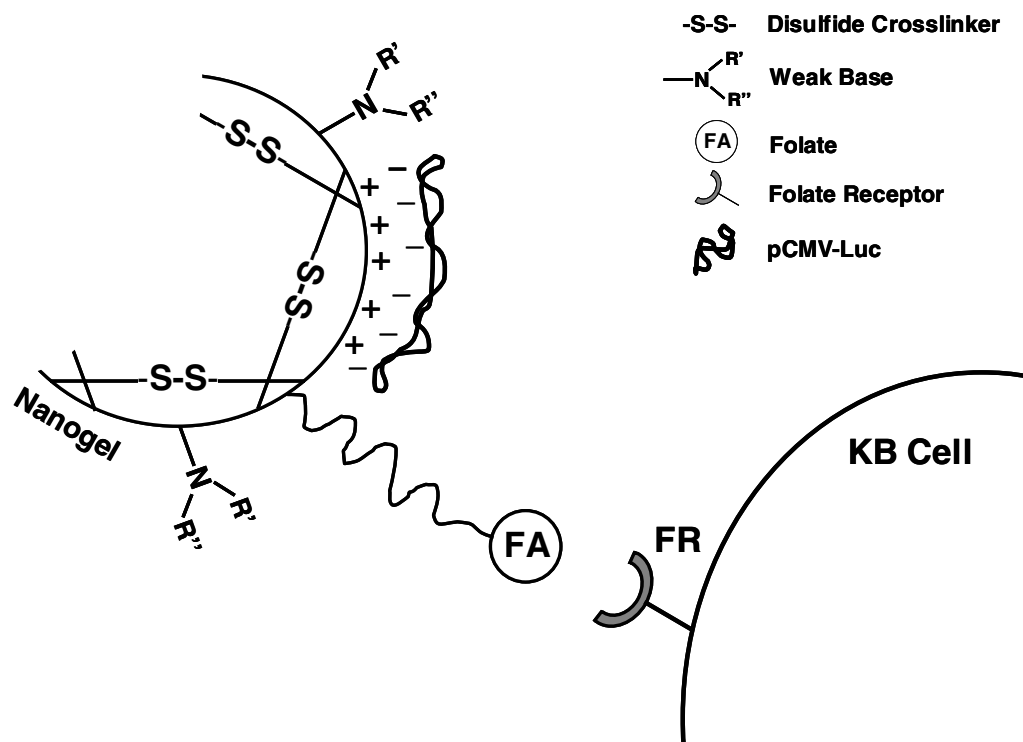


Figure 4-5: Schematic illustration of pDNA complex with strategically-designed nanogel. The typical weight percent of each component in the nanogel was 10%, 25%, and 3 % for disulfide crosslinker, weak base, and folate ligand, respectively. Nanogel was complexed with pCMV-Luc with positive-to-negative charge ratio (N/P ratio) 2, 4, or 10.

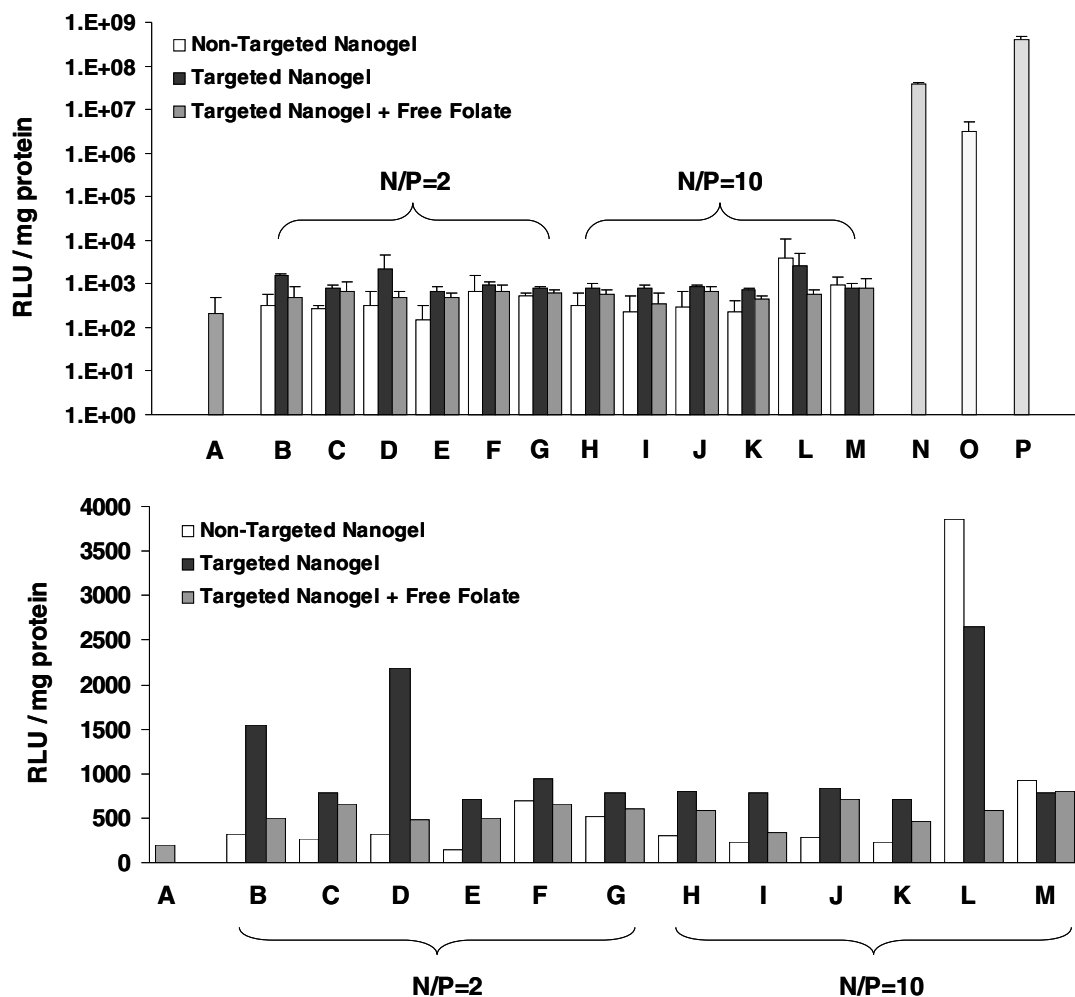


Figure 4-6: Transfection of KB cells with pDNA-nanogel complex. Cationic nanogel (0.1 mg) was complexed with 1 μ g of pDNA at two different N/P ratios and the complex was treated to 5×10^4 KB cells per well in 24-well plate. Transfection was continued for 4 hrs. Subsequently the formulation-containing medium was replaced with fresh media and cells were further incubated for additional 44 hrs before luciferase assay. Data was represented as log (**upper panel**) or normal (**lower panel**) scale of gene expression in Y-axis versus test formulations in X-axis. Test groups in graphs A and B are represented as follows: A, pDNA alone; B, D, F, H, J, and L, disulfide crosslinked nanogel; C, E, G, I, K, and M, non-cleavable crosslinker containing nanogel; B, C, H, and I, imidazole-containing nanogel; D, E, J, and K, dimethylamine-containing nanogel; F, G, L, and M, nanogels without weak base; N, Lipofectamine[®] 2000; and O and P, PEI of 25 kDa at N/P ratio 4 and 10, respectively.

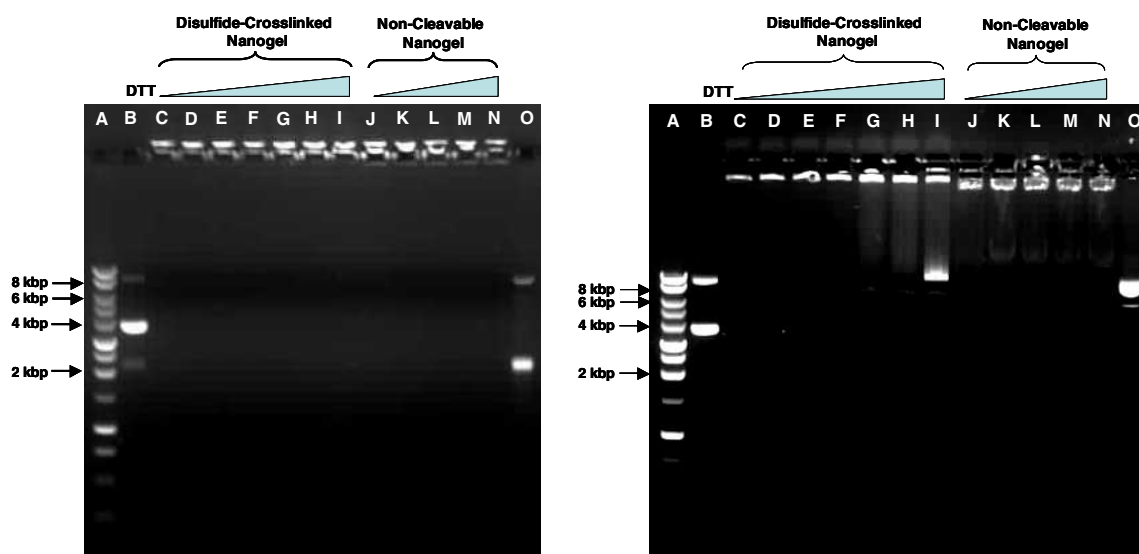


Figure 4-7: Agarose gel electrophoresis run with nanogel-pDNA complex in the presence of dithiothreitol. Cationic nanogel containing cleavable crosslinker (lane **C-I**) or non-cleavable crosslinker (lane **J-N**) was complexed with pDNA at N/P ratio 10 (**right panel**) or 4 (**left panel**) and incubated for 3 hrs at 37°C in the presence of varying concentration of dithiothreitol. The concentrations of dithiothreitol were 0 (lane **C** and **J**), 0.01 (lane **D**), 0.05 (lane **E**), 0.2 (lane **F** and **L**), 1 (lane **G** and **L**), 2 (lane **H** and **M**), and 10 (lane **I** and **N**) mM. Control pDNA in the absence (lane **B**) or in the presence of 10 mM dithiothreitol (lane **O**) and 1 kbp molecular weight ladder (lane **A**) were also loaded as references.

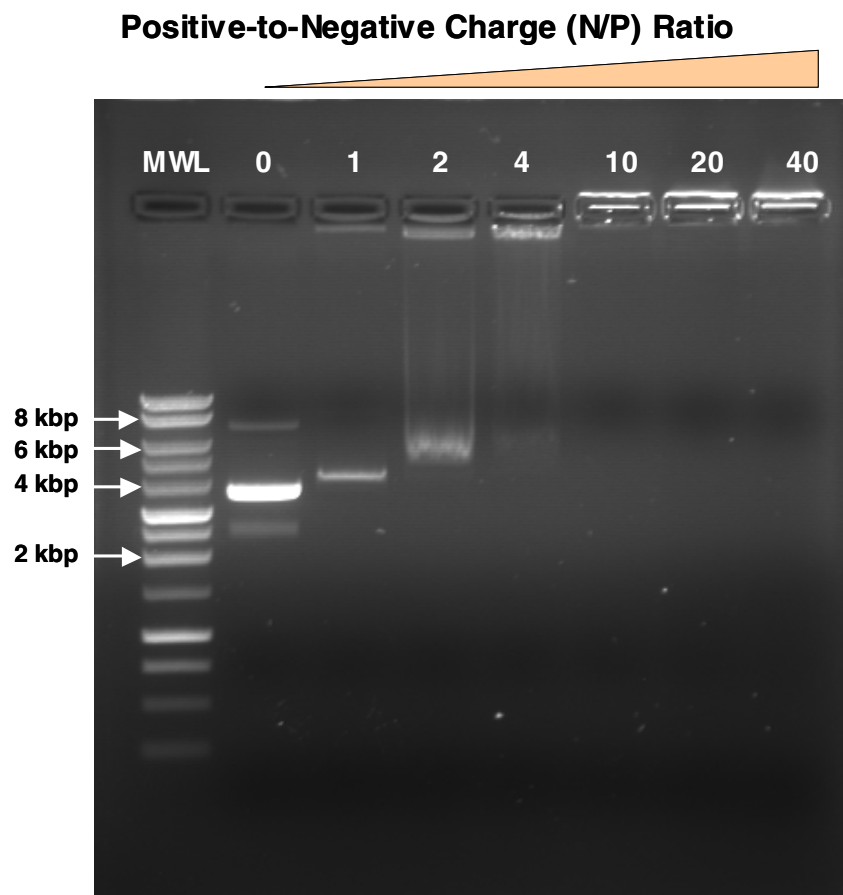


Figure 4-8: Gel retardation study with nanogel-pDNA complex at various N/P ratios. Cationic nanogel was complexed with pDNA at different N/P ratios (i.e., positive to negative charge ratio: 0 to 40) and the complex was loaded on 0.8% agarose gel. Electrophoresis was conducted at 90 volts for 45 min at room temperature.

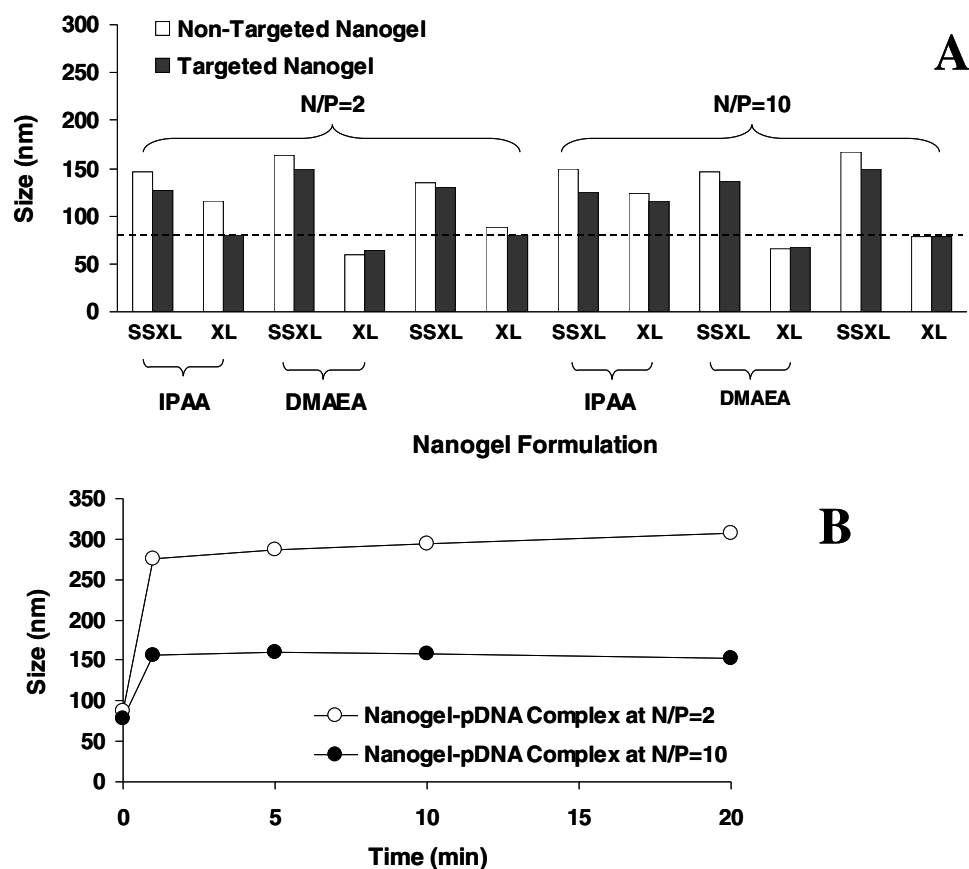


Figure 4-9: Size of nanogels in various compositions (**A**) and nanogel-pDNA complexes at different N/P ratios (**B**). [**A**] Size of nanogel at 2-4 mg/mL in water was measured in NICOMP for 15 min at room temperature. Nanogel contained disulfide crosslinker (SSXL) or regular non-cleavable crosslinker (XL) along with imidazole (IPAA) or dimethylamine (DMAEA) moiety. The dotted line represents typical size of polymerized nanogel, 80 nm. [**B**] Into 0.5 mg nanogel in 0.5 mL water, 5 μ g of pDNA water solution (5 μ L) was added to form the complex. Following a brief vortex, the complex was loaded on the NICOMP for size measurement with channel width of 15 μ sec.

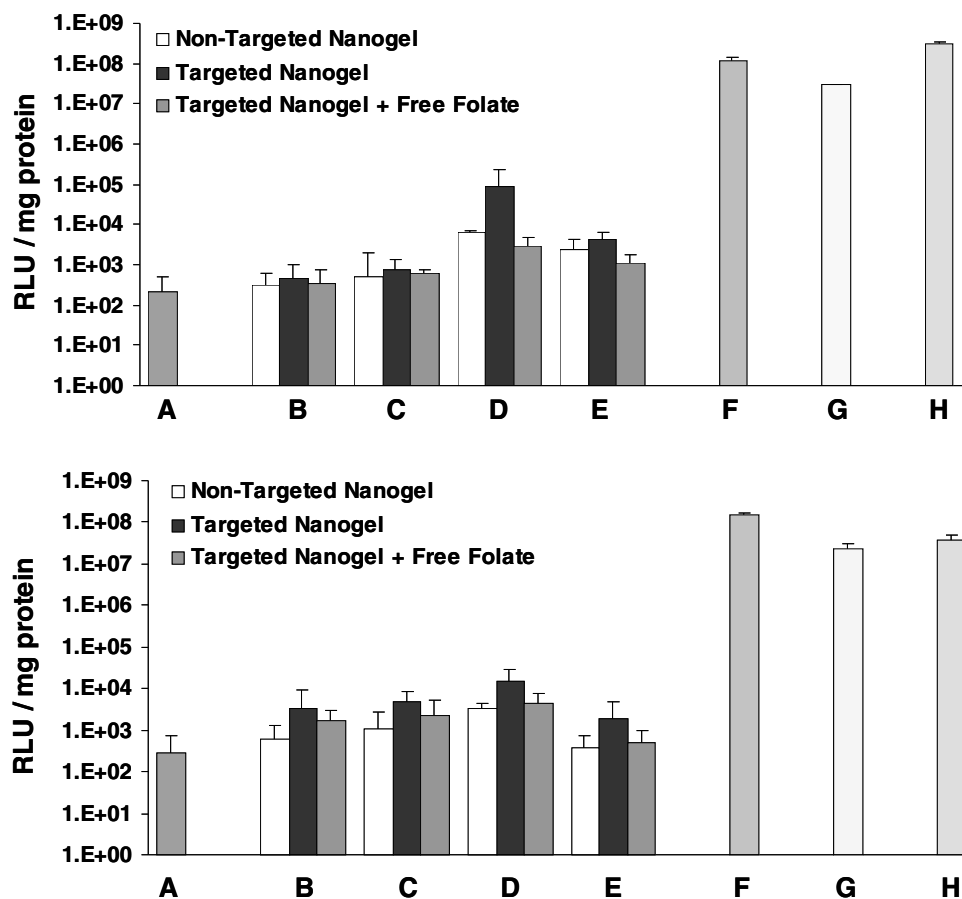


Figure 4-10: Transfection of KB cells with nanogel-pDNA complex in Opti-MEM (**upper panel**) or in the presence of serum (**lower panel**). Cationic nanogel (0.1 mg) was complexed with 3 μ g of pDNA at N/P ratio 4 and the complex was fed to 5×10^4 KB cells per well in 24-well plate. Transfection was continued for 4 hrs. Formulation-containing medium was then replaced with fresh media and cells were further incubated for additional 44 hrs before luciferase assay. Data were represented as gene expression (relative light unit, RLU) normalized by protein amount in Y-axis versus test formulations in X-axis. Test groups in graphs **A** and **B** are represented as follows: **A**, pDNA alone; **B** and **D**, disulfide crosslinked nanogel; **C** and **E**, non-cleavable crosslinker containing nanogel; **B** and **C**, dimethylamine-containing nanogel; **D** and **E**, nanogels without weak base; **F**, Lipofectamine[®] 2000; and **G** and **H**, PEI of 25 kDa at N/P ratio 4 and 10, respectively.

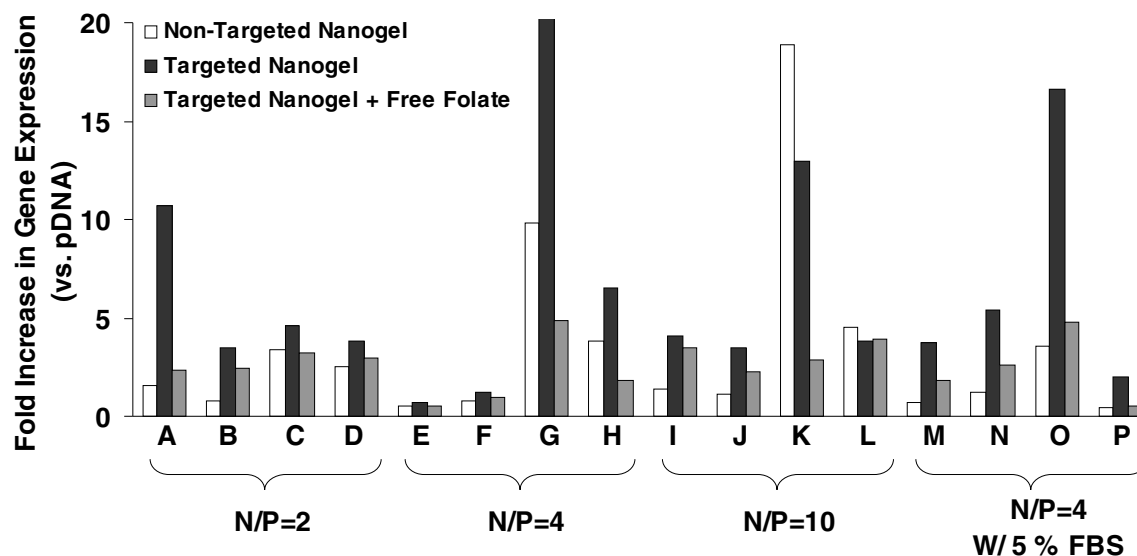


Figure 4-11: Summary of transfection studies with various nanogel-pDNA complexes in KB cells. Cationic nanogel was complexed with pDNA at different N/P ratios and the complex was treated to 5×10^4 KB cells per well in 24-well plate. Transfection scheme for the respective experiment was described in **Figures 4-6** and **4-10**. Gene expression was measured using luciferase assay and normalized by the amount of pDNA (i.e., 1 μ g). Data was represented as fold increase in gene expression compared to pDNA alone in Y-axis versus test formulations with various N/P ratios in X-axis. Test groups are represented as follows: A, C, E, G, I, K, M, and O, disulfide crosslinked nanogel; B, D, F, H, J, L, N, and P, non-cleavable crosslinker containing nanogel; A, B, E, F, I, J, M, and N, dimethylamine-containing nanogel; and C, D, G, H, K, L, O, and P, nanogel without weak base. In M-P, transfection was performed in the presence of 5 % serum containing media.

4.5 References

- Anderson R.G., Brown M.S., Beisiegel U. and Goldstein J.L. (1982). "Surface distribution and recycling of the low density lipoprotein receptor as visualized with antireceptor antibodies." *J Cell Biol* 93 (3): 523-31.
- Anderson R.G. and Jacobson K. (2002). "A role for lipid shells in targeting proteins to caveolae, rafts, and other lipid domains." *Science* 296 (5574): 1821-5.
- Anderson R.G., Kamen B.A., Rothberg K.G. and Lacey S.W. (1992). "Potocytosis: sequestration and transport of small molecules by caveolae." *Science* 255 (5043): 410-1.
- Antony A.C. (1996). "Folate receptors." *Annu Rev Nutr* 16: 501-21.
- Arap W., Pasqualini R. and Ruoslahti E. (1998). "Cancer treatment by targeted drug delivery to tumor vasculature in a mouse model." *Science* 279 (5349): 377-80.
- Atkinson S.F., Bettinger T., Seymour L.W., Behr J.P. and Ward C.M. (2001). "Conjugation of folate via gelonin carbohydrate residues retains ribosomal-inactivating properties of the toxin and permits targeting to folate receptor positive cells." *J Biol Chem* 276 (30): 27930-5.
- Belloq N.C., Pun S.H., Jensen G.S. and Davis M.E. (2003). "Transferrin-containing, cyclodextrin polymer-based particles for tumor-targeted gene delivery." *Bioconjug Chem* 14 (6): 1122-32.
- Benns J.M., Choi J.S., Mahato R.I., Park J.S. and Kim S.W. (2000). "pH-sensitive cationic polymer gene delivery vehicle: N-Ac-poly(L-histidine)-graft-poly(L-lysine) comb shaped polymer." *Bioconjug Chem* 11 (5): 637-45.
- Benns J.M. and Kim S.W. (2000). "Tailoring new gene delivery designs for specific targets." *J Drug Target* 8 (1): 1-12.
- Berg T., Blomhoff R., Naess L., Tolleshaug H. and Drevon C.A. (1983). "Monensin inhibits receptor-mediated endocytosis of asialoglycoproteins in rat hepatocytes." *Exp Cell Res* 148 (2): 319-30.
- Boussif O., Lezoualc'h F., Zanta M.A., Mergny M.D., Scherman D., Demeneix B. and Behr J.P. (1995). "A versatile vector for gene and oligonucleotide transfer into cells in culture and in vivo: polyethylenimine." *Proc Natl Acad Sci U S A* 92 (16): 7297-301.
- Branden L.J., Mohamed A.J. and Smith C.I. (1999). "A peptide nucleic acid-nuclear localization signal fusion that mediates nuclear transport of DNA." *Nat Biotechnol* 17 (8): 784-7.

- Bretscher M.S. and Pearse B.M. (1984). "Coated pits in action." *Cell* 38 (1): 3-4.
- Bruckheimer E., Harvie P., Orthel J., Dutzar B., Furstoss K., Mebel E., Anklesaria P. and Paul R. (2004). "In vivo efficacy of folate-targeted lipid-protamine-DNA (LPD-PEG-Folate) complexes in an immunocompetent syngeneic model for breast adenocarcinoma." *Cancer Gene Ther* 11 (2): 128-34.
- Carpenter G. and Cohen S. (1979). "Epidermal growth factor." *Annu Rev Biochem* 48: 193-216.
- Fahrenkrog B. and Aeby U. (2003). "The nuclear pore complex: nucleocytoplasmic transport and beyond." *Nat Rev Mol Cell Biol* 4 (10): 757-66.
- Faraasen S., Voros J., Csucs G., Textor M., Merkle H.P. and Walter E. (2003). "Ligand-specific targeting of microspheres to phagocytes by surface modification with poly(L-lysine)-grafted poly(ethylene glycol) conjugate." *Pharm Res* 20 (2): 237-46.
- Gao X., Cui Y., Levenson R.M., Chung L.W. and Nie S. (2004). "In vivo cancer targeting and imaging with semiconductor quantum dots." *Nat Biotechnol* 22 (8): 969-76.
- Garin-Chesa P., Campbell I., Saigo P.E., Lewis J.L., Jr., Old L.J. and Rettig W.J. (1993). "Trophoblast and ovarian cancer antigen LK26. Sensitivity and specificity in immunopathology and molecular identification as a folate-binding protein." *Am J Pathol* 142 (2): 557-67.
- Goldstein J.L. and Brown M.S. (1974). "Binding and degradation of low density lipoproteins by cultured human fibroblasts. Comparison of cells from a normal subject and from a patient with homozygous familial hypercholesterolemia." *J Biol Chem* 249 (16): 5153-62.
- Guo W. and Lee R.L. (1999). "Receptor-targeted gene delivery via folate-conjugated polyethylenimine." *AAPS PharmSci* 1 (4): E19.
- Hattori Y. and Maitani Y. (2005). "Folate-linked lipid-based nanoparticle for targeted gene delivery." *Curr Drug Deliv* 2 (3): 243-52.
- Hilgenbrink A.R. and Low P.S. (2005). "Folate receptor-mediated drug targeting: from therapeutics to diagnostics." *J Pharm Sci* 94 (10): 2135-46.
- Hofland H.E., Masson C., Iginla S., Osetinsky I., Reddy J.A., Leamon C.P., Scherman D., Bessodes M. and Wils P. (2002). "Folate-targeted gene transfer in vivo." *Mol Ther* 5 (6): 739-44.
- Hood J.D., Bednarski M., Frausto R., Guccione S., Reisfeld R.A., Xiang R. and Cheresch D.A. (2002). "Tumor regression by targeted gene delivery to the neovasculature." *Science* 296 (5577): 2404-7.

- Hopkins C.R. (1985). "The appearance and internalization of transferrin receptors at the margins of spreading human tumor cells." *Cell* 40 (1): 199-208.
- Juillerat-Jeanneret L. and Schmitt F. (2006). "Chemical modification of therapeutic drugs or drug vector systems to achieve targeted therapy: Looking for the grail." *Med Res Rev* ??? (???): ???
- Kamen B.A. and Capdevila A. (1986). "Receptor-mediated folate accumulation is regulated by the cellular folate content." *Proc Natl Acad Sci U S A* 83 (16): 5983-7.
- Kelemen L.E. (2006). "The role of folate receptor alpha in cancer development, progression and treatment: cause, consequence or innocent bystander?" *Int J Cancer* 119 (2): 243-50.
- Kosower N.S. and Kosower E.M. (1978). "The glutathione status of cells." *Int Rev Cytol* 54: 109-60.
- Kukowska-Latallo J.F., Candido K.A., Cao Z., Nigavekar S.S., Majoros I.J., Thomas T.P., Balogh L.P., Khan M.K. and Baker J.R., Jr. (2005). "Nanoparticle targeting of anticancer drug improves therapeutic response in animal model of human epithelial cancer." *Cancer Res* 65 (12): 5317-24.
- Kulkarni R.P., Mishra S., Fraser S.E. and Davis M.E. (2005). "Single cell kinetics of intracellular, nonviral, nucleic acid delivery vehicle acidification and trafficking." *Bioconjug Chem* 16 (4): 986-94.
- Leamon C.P., Cooper S.R. and Hardee G.E. (2003). "Folate-liposome-mediated antisense oligodeoxynucleotide targeting to cancer cells: evaluation in vitro and in vivo." *Bioconjug Chem* 14 (4): 738-47.
- Leamon C.P. and Low P.S. (1991). "Delivery of macromolecules into living cells: a method that exploits folate receptor endocytosis." *Proc Natl Acad Sci U S A* 88 (13): 5572-6.
- Leamon C.P., Weigl D. and Hendren R.W. (1999). "Folate copolymer-mediated transfection of cultured cells." *Bioconjug Chem* 10 (6): 947-57.
- Lee R.J. and Huang L. (1996). "Folate-targeted, anionic liposome-entrapped polylysine-condensed DNA for tumor cell-specific gene transfer." *J Biol Chem* 271 (14): 8481-7.
- Lee R.J. and Low P.S. (1994). "Delivery of liposomes into cultured KB cells via folate receptor-mediated endocytosis." *J Biol Chem* 269 (5): 3198-204.
- Lee R.J., Wang S. and Low P.S. (1996). "Measurement of endosome pH following folate receptor-mediated endocytosis." *Biochim Biophys Acta* 1312 (3): 237-42.
- Leong K.W., Mao H.Q., Truong-Le V.L., Roy K., Walsh S.M. and August J.T. (1998). "DNA-polycation nanospheres as non-viral gene delivery vehicles." *J Control Release* 53 (1-3): 183-93.

- Li S., Deshmukh H.M. and Huang L. (1998). "Folate-mediated targeting of antisense oligodeoxynucleotides to ovarian cancer cells." *Pharm Res* 15 (10): 1540-5.
- Lu Z.R., Shiah J.G., Sakuma S., Kopeckova P. and Kopecek J. (2002). "Design of novel bioconjugates for targeted drug delivery." *J Control Release* 78 (1-3): 165-73.
- Mayor S., Rothberg K.G. and Maxfield F.R. (1994). "Sequestration of GPI-anchored proteins in caveolae triggered by cross-linking." *Science* 264 (5167): 1948-51.
- McKenzie D.L., Kwok K.Y. and Rice K.G. (2000). "A potent new class of reductively activated peptide gene delivery agents." *J Biol Chem* 275 (14): 9970-7.
- Midoux P. and Monsigny M. (1999). "Efficient gene transfer by histidylated polylysine/pDNA complexes." *Bioconj Chem* 10 (3): 406-11.
- Mineo C. and Anderson R.G. (2001). "Potocytosis. Robert Feulgen Lecture." *Histochem Cell Biol* 116 (2): 109-18.
- Nakashima-Matsushita N., Homma T., Yu S., Matsuda T., Sunahara N., Nakamura T., Tsukano M., Ratnam M. and Matsuyama T. (1999). "Selective expression of folate receptor beta and its possible role in methotrexate transport in synovial macrophages from patients with rheumatoid arthritis." *Arthritis Rheum* 42 (8): 1609-16.
- Nimjee S.M., Rusconi C.P. and Sullenger B.A. (2005). "Aptamers: an emerging class of therapeutics." *Annu Rev Med* 56: 555-83.
- Pack D.W., Putnam D. and Langer R. (2000). "Design of imidazole-containing endosomolytic biopolymers for gene delivery." *Biotechnol Bioeng* 67 (2): 217-23.
- Pastan I.H. and Willingham M.C. (1981). "Journey to the center of the cell: role of the receptosome." *Science* 214 (4520): 504-9.
- Pollard H., Remy J.S., Loussouarn G., Demolombe S., Behr J.P. and Escande D. (1998). "Polyethylenimine but not cationic lipids promotes transgene delivery to the nucleus in mammalian cells." *J Biol Chem* 273 (13): 7507-11.
- Prasad P.D., Ramamoorthy S., Moe A.J., Smith C.H., Leibach F.H. and Ganapathy V. (1994). "Selective expression of the high-affinity isoform of the folate receptor (FR-alpha) in the human placental syncytiotrophoblast and choriocarcinoma cells." *Biochim Biophys Acta* 1223 (1): 71-5.
- Putnam D., Gentry C.A., Pack D.W. and Langer R. (2001). "Polymer-based gene delivery with low cytotoxicity by a unique balance of side-chain termini." *Proc Natl Acad Sci U S A* 98 (3): 1200-5.
- Raden D. and Gilmore R. (1998). "Signal recognition particle-dependent targeting of ribosomes to the rough endoplasmic reticulum in the absence and presence of the nascent polypeptide-associated complex." *Mol Biol Cell* 9 (1): 117-30.

- Reddy J.A., Abburi C., Hofland H., Howard S.J., Vlahov I., Wils P. and Leamon C.P. (2002). "Folate-targeted, cationic liposome-mediated gene transfer into disseminated peritoneal tumors." *Gene Ther* 9 (22): 1542-50.
- Reddy J.A., Dean D., Kennedy M.D. and Low P.S. (1999). "Optimization of folate-conjugated liposomal vectors for folate receptor-mediated gene therapy." *J Pharm Sci* 88 (11): 1112-8.
- Reddy J.A. and Low P.S. (1998). "Folate-mediated targeting of therapeutic and imaging agents to cancers." *Crit Rev Ther Drug Carrier Syst* 15 (6): 587-627.
- Reddy J.A. and Low P.S. (2000). "Enhanced folate receptor mediated gene therapy using a novel pH-sensitive lipid formulation." *J Control Release* 64 (1-3): 27-37.
- Ross J.F., Chaudhuri P.K. and Ratnam M. (1994). "Differential regulation of folate receptor isoforms in normal and malignant tissues in vivo and in established cell lines. Physiologic and clinical implications." *Cancer* 73 (9): 2432-43.
- Rothberg K.G., Ying Y.S., Kolhouse J.F., Kamen B.A. and Anderson R.G. (1990). "The glycopospholipid-linked folate receptor internalizes folate without entering the clathrin-coated pit endocytic pathway." *J Cell Biol* 110 (3): 637-49.
- Sabharanjak S. and Mayor S. (2004). "Folate receptor endocytosis and trafficking." *Adv Drug Deliv Rev* 56 (8): 1099-109.
- Salazar M.D. and Ratnam M. (2007). "The folate receptor: what does it promise in tissue-targeted therapeutics?" *Cancer Metastasis Rev* 26 (1): 141-52.
- Sapra P. and Allen T.M. (2003). "Ligand-targeted liposomal anticancer drugs." *Prog Lipid Res* 42 (5): 439-62.
- Saul J.M., Annapragada A., Natarajan J.V. and Bellamkonda R.V. (2003). "Controlled targeting of liposomal doxorubicin via the folate receptor in vitro." *J Control Release* 92 (1-2): 49-67.
- Schachtschabel U., Pavlinkova G., Lou D. and Kohler H. (1996). "Antibody-mediated gene delivery for B-cell lymphoma in vitro." *Cancer Gene Ther* 3 (6): 365-72.
- Shen F., Ross J.F., Wang X. and Ratnam M. (1994). "Identification of a novel folate receptor, a truncated receptor, and receptor type beta in hematopoietic cells: cDNA cloning, expression, immunoreactivity, and tissue specificity." *Biochemistry* 33 (5): 1209-15.
- Shimizu N., Chen J., Gamou S. and Takayanagi A. (1996). "Immunogene approach toward cancer therapy using erythrocyte growth factor receptor-mediated gene delivery." *Cancer Gene Ther* 3 (2): 113-20.

- Subramanian A., Ranganathan P. and Diamond S.L. (1999). "Nuclear targeting peptide scaffolds for lipofection of nondividing mammalian cells." *Nat Biotechnol* 17 (9): 873-7.
- Sudimack J. and Lee R.J. (2000). "Targeted drug delivery via the folate receptor." *Adv Drug Deliv Rev* 41 (2): 147-62.
- Toffoli G., Cernigoi C., Russo A., Gallo A., Bagnoli M. and Boiocchi M. (1997). "Overexpression of folate binding protein in ovarian cancers." *Int J Cancer* 74 (2): 193-8.
- Turek J.J., Leamon C.P. and Low P.S. (1993). "Endocytosis of folate-protein conjugates: ultrastructural localization in KB cells." *J Cell Sci* 106 (Pt 1): 423-30.
- Ullrich A., Bell J.R., Chen E.Y., Herrera R., Petruzzelli L.M., Dull T.J., Gray A., Coussens L., Liao Y.C., Tsubokawa M. and et al. (1985). "Human insulin receptor and its relationship to the tyrosine kinase family of oncogenes." *Nature* 313 (6005): 756-61.
- Wang S., Lee R.J., Cauchon G., Gorenstein D.G. and Low P.S. (1995). "Delivery of antisense oligodeoxyribonucleotides against the human epidermal growth factor receptor into cultured KB cells with liposomes conjugated to folate via polyethylene glycol." *Proc Natl Acad Sci U S A* 92 (8): 3318-22.
- Wang S., Lee R.J., Mathias C.J., Green M.A. and Low P.S. (1996). "Synthesis, purification, and tumor cell uptake of ⁶⁷Ga-deferoxamine--folate, a potential radiopharmaceutical for tumor imaging." *Bioconjug Chem* 7 (1): 56-62.
- Wang S. and Low P.S. (1998). "Folate-mediated targeting of antineoplastic drugs, imaging agents, and nucleic acids to cancer cells." *J Control Release* 53 (1-3): 39-48.
- Weitman S.D., Frazier K.M. and Kamen B.A. (1994). "The folate receptor in central nervous system malignancies of childhood." *J Neurooncol* 21 (2): 107-12.
- Wu M., Gunning W. and Ratnam M. (1999). "Expression of folate receptor type alpha in relation to cell type, malignancy, and differentiation in ovary, uterus, and cervix." *Cancer Epidemiol Biomarkers Prev* 8 (9): 775-82.
- Yang J., Chen H., Vlahov I.R., Cheng J.X. and Low P.S. (2007). "Characterization of the pH of folate receptor-containing endosomes and the rate of hydrolysis of internalized acid-labile folate-drug conjugates." *J Pharmacol Exp Ther* 321 (2): 462-8.

CHAPTER V

CONCLUSIONS AND FUTURE PROSPECTS

5.1 Summary of Conclusions

The present dissertation work describes a series of successive efforts to develop a potent gene delivery system using the polymeric nanogel that was developed earlier by our colleagues on this UNC campus (McAllister *et al.* 2002). The current study deals with the modification of the nanogel with three specific goals. First, the addition of weak bases to the nanogel imparts an acid buffering capacity for endosomal escape. Secondly, disulfide bonds incorporated in the nanogel matrix should trigger site-specific degradation of the nanogel and facilitate the release of pDNA from the nanogel polyplex. Lastly, the conjugation of folate as a targeting ligand promotes the cell-specific binding of the nanogel polyplex to result in enhanced transfection efficiency. All of these modifications were achieved by synthesizing weak base-, disulfide-, and folate-containing monomers and preparing nanogels from those monomers. The successful syntheses of the first two monomers were represented in **Chapter II**. The weak base-containing nanogel showed buffering capacity around the pK_a of the incorporated base monomer. Interestingly, morpholine- and imidazole-containing nanogels represented almost 2-fold higher buffer capacities at endosomal pH (~6) than PEI.

A series of attempts were made to entrap pDNA inside the neutral nanogel. It is the polarity of pDNA that makes this scenario feasible since pDNA expects to stay in aqueous phase during the microemulsion formation and the subsequent polymerization. The final nanogel formulation was intended to entrap pDNA inside the matrix without any electrostatic interaction. **Chapter III** addresses two important issues in preparing pDNA-entrapped nanogel formulation; 1) how stable pDNA would be under free-radical-initiated polymerization, and 2) how much pDNA could be entrapped in the nanogel. It was established that pDNA remained intact during polymerization when added at a relatively high concentration. Pre-condensation of pDNA using protamine improved the entrapment efficiency up to 56% of initially loaded pDNA. However, transfection efficiency of this formulation was only modest. We attribute this to the minimal amount of pDNA entrapped in the nanogel. We speculate that this was in turn caused by compromised microemulsion system in the presence of methanol that was added to dissolve crosslinkers. It is also possible that the energetic involved in pDNA association with the aqueous phase of a microemulsion was not sufficient enough to bend and compact pDNA.

Chapter IV is concerned with complexing pDNA with pre-made cationic nanogel. In this approach, the nanogel also expressed folic acid as a targeting ligand. It was synthesized as a monomer and incorporated into the nanogel during polymerization. The overall transfection efficiency using this formulation was inferior to those with commercial transfecting reagents by 3-4 orders of magnitude. Nevertheless, this part of study led to the following conclusions. First, targeting strategy will be needed for the cell-specific binding of gene vectors. Second, the incorporation of a cleavable linker will be necessary even with the

presence of targeting ligands. Most importantly, the present finding strongly implies that the electrostatically neutral gene vector will be favored for the success of targeting strategy.

5.2 Future Prospects

Although only a minimal level of transfection was achieved by pDNA-entrapping nanogel (**Chapter III**), entrapment of pDNA inside nanogel is still an attractive formulation. Very low or almost no positive charges will be required in this formulation, which could reduce vector-mediated cytotoxicity. By retaining pDNA inside, it could provide enhanced protection from a premature degradation by nucleases when used *in vivo*. The hypothesis behind this formulation was that the energetics involved in pDNA bendability could be overcome by simply forming microemulsion as implied in Budker *et al.* (2002). However, the aqueous phase in the present microemulsion system did not appear to provide energy enough to condense pDNA. Accordingly, condensing reagents such as protamine had to be added to ensure pDNA packing prior to the entrapment. Since a regular emulsion system usually contains much larger amount of aqueous layer than does a microemulsion (i.e., 30% vs. 3%), it could afford more energy to compact pDNA more efficiently.

Microemulsion is in essence a ternary phase system consisting of aqueous phase, continuous phase, and interface. Equilibrium via a balanced weight ratio among these phases is elemental to form a microemulsion, which could be disturbed by any additional components. Although addition of a small amount of methanol and an increased amount of

monomers did not affect the eventual nanogel formation significantly, reduced entrapment efficiency and the subsequent instability of pDNA were observed. Better understanding of the stability of the pDNA tertiary structure under this system will be required to achieve an advanced pDNA-entrapping formulation.

One of the key findings in **Chapter IV** was that a high N/P ratio in pDNA-containing complexes can diminish specific binding of the targeted formulation to the cell. The importance of neutral charge of the vector formulation can be found in several other investigations. Lee and Huang (1996) showed that transfection efficiency of folate-containing liposome-polylysine (PLL)-DNA, so-called LPD, particle in KB cells is significantly higher when the net charge of LPD particle was slightly positive or negative. Too much cations or anions on the particles reduced gene expression. Interestingly, more profound targeting effect was observed in the negatively charged particles. Dendrimer-containing, targeted lipoplex system developed by Reddy and colleagues (1999) also showed an effective transfection efficiency only when the lipoplex system was slightly cationic. Anionic or additional positive charge containing systems represented significantly reduced gene expression. Another noticeable observation from these studies is that zero charge on the vector system will cause aggregation and reduce transfection efficiency. However, there is no agreement on which charge in excess (i.e., slightly positive or slightly negative) will provide better gene transfection. It appears to be dependent on the individual vector system.

Preparing virus-sized DNA particles without using any pre-made particulate system has drawn a great deal of attention among many investigators (Blessing *et al.* 1998; Ouyang *et al.* 2000). These approaches exploited the electrostatic interaction of cationic surfactants toward pDNA and consequential pDNA collapse. Alternatively, Leamon and colleagues

(1999) used PLL of 331 kDa modified with folate-PEG conjugate to form a condensed pDNA particle and demonstrated a promising transfection capacity of the complex.

Integrating all of these previous findings and the knowledge learned from this dissertation research, one can develop a following approach. First, use protamine as a condensing reagent. Protamine has already been demonstrated to possess a superior capability in condensing pDNA through multiple previous investigations including the present dissertation work (see **Chapter III** and the references therein). Protamine can be modified with pre-made folate-PEG conjugate (e.g., compound **8** in **Figure 4-1**) before forming a complex with pDNA. Since protamine is exceptionally efficient in condensing pDNA even with low N/P ratio (i.e., positive-to-negative charge ratio of less than one) and a relatively small molecule (5.1 kDa), further modification such as disulfide incorporation may be superfluous. An example of PEG modification of protamine can be found in Chang *et al.* (2005). However, the effect of PEG modification on the DNA condensing capability of protamine has not yet been determined. The success of this approach thus will be dependent on the integrity of the condensing ability of the modified protamine. Also, the overall charge of the final complex will need to be systemically monitored as an independent variable. This part of the proposed study is an ongoing project conducted by Dr. David Gaul.

The size of gene vectors appears to play an important role in many aspects. Extracellularly, it affects the blood circulation time, extravasation, and entry into target cells (Stolnik *et al.* 1995; Ishida *et al.* 1999). Many investigators including Nakanishi and Noguchi (2001) implied that there must be an optimal size range of particles for transfection efficiency. However, the results reported by different authors are still somewhat contradictory. As

shown in **Figure 4-9A**, the sizes of nanogels were different depending on the composition, ranging from 60 to 180 nm. The changes in size are inevitable in preparing the nanogels of different compositions. For this reason, any further investigation on the effect of nanogel size on the transfection efficiency should not continue as an extension of the present dissertation work. The discrepancy or the lack of agreement in the effect of size of gene vectors might well be due to the heterogeneity within a conventional vector system and a variety of compositions represented by different systems.

In this context, the PRINT (see **Appendix I**) technology could offer a valuable opportunity to draw more conclusive results on the size effect of gene vectors. With a relatively little amount of efforts on the optimization, PRINT particles can have a potential to provide virtually homogeneous gene vector mimics especially in size. It is also possible to have a series of particles in different sizes of broad spectrum while other independent variables (e.g., compositions, charges, surface properties, and surface modification) remain exactly the same. However, the difficult task would be how to accommodate all the components into the PRINT particles that are required in overcoming the cellular barriers in gene transfection discussed in **Chapter I**.

Unlike virus that has a full package of strategies to unravel various hurdles in transporting its genetic information into the nucleus, current non-viral vectors do not or cannot have such a multifunctional ability. From this realistic viewpoint alone, it would be imperative to determine the rate-limiting steps in the overall transfection process. The task would entail determining the actual amount of pDNA present in the endosome, the efficiency of pDNA escaping into the cytosol, the cytosolic stability, the number of copies that reach to

and translocate into the nucleus and the eventual transcription efficiency. There have been several efforts to decipher the inside of the cellular trafficking. The methodology involves confocal-image-assisted three dimensionally integrated quantification (Hama *et al.* 2006), and cytoplasmic/nuclear microinjection of gene vectors (Pollard *et al.* 1998; Cornelis *et al.* 2002). Although elaborate experimental design is required, such strategically designed experiments will provide an exact understanding of the actual relevance of each of the intracellular barriers.

5.3 Concluding Remarks

One of the ideal structures of a gene vector would be an environment-reacting device, simply as smart as the virus. Although numerous investigations in the past have accumulated significant amounts of knowledge to improve gene vectors, the science of non-viral vectors is still in its infancy. The present dissertation work started with several theories previously addressed on the way of developing a novel gene vector. Efforts on the physically entrapping of pDNA inside the nanogel matrix encountered multiple obstacles in the preparation. This approach might have been too ambitious at this stage but the unsuccessful results left behind many lessons. On the other hand pDNA-nanogel complex was also not able to surpass the current ‘holy grail’ transfecting reagents such as PEI. Nevertheless, all the findings and every piece of the information obtained from this dissertation work may broaden our knowledge on this field and should be a part of the elaborate efforts to develop a new generation of vectors for more efficient gene therapy.

5.4 References

- Blessing T., Remy J.S. and Behr J.P. (1998). "Monomolecular collapse of plasmid DNA into stable virus-like particles." *Proc Natl Acad Sci U S A* 95 (4): 1427-31.
- Budker V.G., Slattum P.M., Monahan S.D. and Wolff J.A. (2002). "Entrapment and condensation of DNA in neutral reverse micelles." *Biophys J* 82 (3): 1570-9.
- Chang L.C., Lee H.F., Chung M.J. and Yang V.C. (2005). "PEG-modified protamine with improved pharmacological/pharmaceutical properties as a potential protamine substitute: synthesis and in vitro evaluation." *Bioconjug Chem* 16 (1): 147-55.
- Cornelis S., Vandenbranden M., Ruyschaert J.M. and Elouahabi A. (2002). "Role of intracellular cationic liposome-DNA complex dissociation in transfection mediated by cationic lipids." *DNA Cell Biol* 21 (2): 91-7.
- Hama S., Akita H., Ito R., Mizuguchi H., Hayakawa T. and Harashima H. (2006). "Quantitative comparison of intracellular trafficking and nuclear transcription between adenoviral and lipoplex systems." *Mol Ther* 13 (4): 786-94.
- Ishida O., Maruyama K., Sasaki K. and Iwatsuru M. (1999). "Size-dependent extravasation and interstitial localization of polyethyleneglycol liposomes in solid tumor-bearing mice." *Int J Pharm* 190 (1): 49-56.
- Leamon C.P., Weigl D. and Hendren R.W. (1999). "Folate copolymer-mediated transfection of cultured cells." *Bioconjug Chem* 10 (6): 947-57.
- Lee R.J. and Huang L. (1996). "Folate-targeted, anionic liposome-entrapped polylysine-condensed DNA for tumor cell-specific gene transfer." *J Biol Chem* 271 (14): 8481-7.
- McAllister K., Sazani P., Adam M., Cho M.J., Rubinstein M., Samulski R.J. and DeSimone J.M. (2002). "Polymeric nanogels produced via inverse microemulsion polymerization as potential gene and antisense delivery agents." *J Am Chem Soc* 124 (51): 15198-207.
- Nakanishi M. and Noguchi A. (2001). "Confocal and probe microscopy to study gene transfection mediated by cationic liposomes with a cationic cholesterol derivative." *Adv Drug Deliv Rev* 52 (3): 197-207.
- Ouyang M., Remy J.S. and Szoka F.C., Jr. (2000). "Controlled template-assisted assembly of plasmid DNA into nanometric particles with high DNA concentration." *Bioconjug Chem* 11 (1): 104-12.
- Pollard H., Remy J.S., Loussouarn G., Demolombe S., Behr J.P. and Escande D. (1998). "Polyethylenimine but not cationic lipids promotes transgene delivery to the nucleus in mammalian cells." *J Biol Chem* 273 (13): 7507-11.

- Reddy J.A., Dean D., Kennedy M.D. and Low P.S. (1999). "Optimization of folate-conjugated liposomal vectors for folate receptor-mediated gene therapy." *J Pharm Sci* 88 (11): 1112-8.
- Stolnik S., Illum L. and Davis S.S. (1995). "Long Circulating Microparticulate Drug Carriers." *Adv Drug Deliv Rev* 16 (2-3): 195-214.

APPENDIX I

PHARMACOKINETICS AND BIODISTRIBUTION OF PRINT PARTICLES IN MICE

A.1 Introduction

Biomedical applications of synthetic particles of submicron to micron size were pioneered by the investigators in diagnostic field as exemplified by use of particulates in gamma scintigraphy for lymphatics (Trubetskoy *et al.* 1996). Since the burst of developmental activities with particulate drug carriers including emulsions in early 1980s, intense research in drug delivery over the past few decades has witnessed the design and construction of valuable nanocarriers such as liposomes, micelles, dendrimers, polymer particles, and colloidal precipitates (Barenholz 2001; Torchilin 2004; Lee *et al.* 2005; Moghimi *et al.* 2005; Vicent and Duncan 2006). However, the biomedical applications of the fabricated particles are on hold mainly due to lack of basic understanding of the particle-host interaction at both organ/tissue and (sub)cellular level as dictated by physicochemical properties of the particles. As expected, these particles are considered as foreign by the host when systemically administered. The clearance of colloidal particles from the blood circulation has been reported to occur by phagocytes and/or endothelial cells, mainly in the liver, the spleen, and the bone marrow as well as lung endothelia (e.g., Senior 1987; McLean *et al.* 1997). The pharmacokinetic fate and relative distribution of the injected particles in these organs are known to depend on various factors such as the size, surface properties of

the particles, compositions and the type of serum proteins adsorbed onto the surface of particles. Particle size has been reported to play a key role in blood clearance. For example, microspheres with hydrodynamic radii of over 200 nm exhibited a more rapid rate of clearance than particles with radii under 200 nm (Moghimi *et al.* 1993). The final biodistribution is also affected by particle size. Particles having a diameter of below 150 nm produced an increased uptake in the bone marrow of rabbits, whereas particles of 250 nm in diameter were mostly sequestered in the spleen and liver with a reduced uptake by the bone marrow (Porter *et al.* 1992). The difference in the uptake and biodistribution of particles having different compositions may well imply the presence of opsonins that are specific to a certain type of phagocyte. For instance, cholesterol-rich liposomes were found to be more accumulated in spleen than liver probably due to the adsorption of opsonins specific to splenic phagocytes instead of Kupffer cell-specific opsonins (Moghimi and Patel 1988). When introduced directly to systemic circulation, these particles are rapidly cleared by reticuloendothelial system (RES) (Breton *et al.* 1998) and significant reduction of RES uptake of particles has been reported when particle surface is modified (e.g., PEGylation) (Harper *et al.* 1991; Stolnik *et al.* 1994; Lacasse *et al.* 1998).

Poly(ethylene glycol) derivatives are known to impart biocompatibility, solubility, stability, and increased circulation times to proteins, liposomes, and other synthetic particles (Allen *et al.* 1995; Gregoriadis 1995; Papisov 1998; Torchilin 1998; Woodle 1998). PEG chains larger than 2 kDa are required in order to expect a significant coating effect (Kenworthy *et al.* 1995) by imposing a major steric pressure between particles and opsonins (Jeon *et al.* 1991). This may well be due to the conformational flexibility of PEG chains and

resulting polarity increase. The density of PEG chains on the surface of particles also determines the success of steric stabilization since low surface chain density can lead to gaps in the PEG protective layer where opsonins can freely bind to the particle surface while too high surface coverage can restrict the motion of PEG chains and decrease the steric hindrance properties of PEG layer (Storm *et al.* 1995). Closely related to this issue, a minimum effective hydrodynamic layer thickness has been suggested to be around 5% of the particle's diameter (Stolnik *et al.* 1995). While use of larger molecular weight PEG was found to lead to longer blood circulation for the particles in vivo, another general trend was that PEGylation shifted the final biodistribution of particles toward the spleen over the liver (Peracchia *et al.* 1999). Lastly, the effect of surface charges on in vivo pharmacokinetics and biodistribution of particulates [e.g., poly (D, L-lactic-co-glycolic acid)] has also been intensively explored by many investigators (e.g., Vinogradov *et al.* 2002; Torchilin and Lukyanov 2003).

Synthetic particles as a drug carrier attract more attention from investigators in various fields especially in delivering biochemically labile substances such as siRNA and oligonucleotides since these sensitive cargos need to remain intact during the transition to the target site. In many instances, the site of action is cytoplasm or nucleus in a specific cell type in a given tissue or organ. Although the pharmacokinetic behaviors of particulate drug carriers have been intensively investigated as exemplified with liposomes (Senior 1987), most of these studies are dealing with relatively heterogeneous particulates in terms of size, composition and shape. These particulates are also unstable in the blood. The incomplete assessment of the pharmacokinetic profile and biodistribution of particulate drug carriers

might lead to premature rejection of a viable new formulation entering the drug development (Duncan 2003). Thus, a model particle system that possesses real homogeneity in size, charge, surface property and stability could provide more reliable information on the pharmacokinetic behavior and biodistribution of the respective systems.

New particle fabrication procedure, called PRINT (Particle Replication In Non-wetting Templates), has been recently developed exploiting the low surface energy of novel fluoropolymeric molds (Rolland *et al.* 2005). The molds are derived from liquid perfluoropolyether precursors, which can be photochemically crosslinked at room temperature. The resulting elastomeric solids enable high-resolution imprint lithography, a technique found in the microelectronics field, to fabricate a variety of organic particles of precisely defined size and shape. The preparation of particles using this technique requires very mild processing conditions, which allow for labile cargos such as nucleic acids to be loaded more readily. Since PRINT features precise control over size, shape, composition, porosity, texture, and modulus of the particles through the judicious choice of a master template, it provides a unique opportunity to investigate the pharmacokinetic fate and biodistribution of a population of truly homogeneous particles with a variety of independent variables that can be varied with ease. In this chapter, the first *in vivo* study of PRINT particles is documented following *i.v.* bolus tail vein injection of fluorescently- or radio-labeled PRINT particles into healthy mice.

A.2 Materials and Methods

A.2.1 Materials

FluorocurTM, the perfluoropolyether used as the molding material in the PRINT process, was purchased from Liquidia Technologies (Product # 2M-140). Silicon templates used for PRINT processing were obtained from Benchmark Technologies. Trimethylolpropane ethoxylate triacrylate ($M_n = 428$ g/mol) was purchased from Aldrich and was passed through a short plug of alumina prior to use to remove inhibitor. Poly(ethylene glycol) dimethyl ether ($M_n = 550$ g/mol) and 2,2-diethoxyacetophenone were purchased from Aldrich and used as received. Poly(ethylene glycol) monomethyl ether monomethacrylate ($M_n = 1,000$ g/mol) was purchased from Polysciences (Warrington, PA) and used as received. *Para*-hydroxystyrene [10% (w/w) in propylene glycol] was purchased from Alfa Aesar (Ward Hill, MA) and used as received without further purification. Fluorescein *O*-acrylate, 5-(iodoacetamido) fluorescein, and PBS were purchased from Sigma. Dialysis cassettes (3.5 kDa MWCO) and Iodogen[®] pre-coated tubes were purchased from Pierce Biotechnology (Rockford, IL). Radioactive iodide (Na^{125}I) was purchased from Perkin Elmer Life and Analytical Sciences, Inc (Waltham, MA) as 100 mCi/mL in 10^{-5} M NaOH. C57BL/6J mice were purchased from The Jackson Laboratory (Bar Harbor, Maine). Ketamine HCl (100 mg/mL) was purchased from Abbott Laboratories (Abbott Park, IL) and diluted with equivalent volume of 1 X PBS before injection. All animal experiments were conducted in accordance with guidelines set forth by The University of North Carolina at Chapel Hill, and approval was obtained for the completion of these experiments.

A.2.2 Preparation of PRINT Particles

A.2.2.1 Fluorescently-Labeled PRINT Particles

The fabrication of patterned FluorocurTM molds, a low surface energy perfluoropolyether molds, has been described elsewhere (Rolland *et al.* 2005). Briefly, 20 mL of FluorocurTM resin containing 0.1% (w/w) of 2,2-diethoxyacetophenone was pooled in the center of an 8 inch patterned master (with feature sizes of 200 nm) that was set up inside an enclosed UV chamber. Ten minutes was allowed to pass so that the FluorocurTM resin was spread out over the entire 8-inch wafer. The entire system was then purged with nitrogen for 3 minutes. Following this, the coated wafer was exposed to UV irradiation ($\lambda = 365$ nm, power > 20 mW/cm²) for 2 min to cure the FluorocurTM resin. The elastomeric mold was then removed from the master template by gently peeling it away from the silicon surface.

From the mold obtained above, PRINT particles were prepared by Dr. DeSimone's lab in UNC Chemistry Department. The preparative procedure described elsewhere (Gratton *et al.* 2007) was slightly modified to incorporate fluorescent monomers. The composition of PRINT particles were; 77% (w/w) PEG triacrylate ($M_n = 428$ g/mol), 20% PEG monomethyl ether monomethacrylate ($M_n = 1000$ g/mol), 1% 2,2-diethoxyacetophenone, and 2% fluorescein *O*-acrylate. A 10% (w/v) solution of this mixture in 2-propanol (filtered through a 0.22 μ m PTFE filter) was prepared. This solution (1 mL) was then sprayed onto a FluorocurTM patterned mold using an air brush and residual 2-propanol was allowed to evaporate over 10 min. A poly(ethylene) sheet (American Plastics Company, Beltsville, MD)

was then placed over the 8-inch (diameter) mold ensuring that the entire active area was covered. This poly(ethylene) sheet was then peeled back at a rate of approximately 2.5 cm/min. Following this, the mold was placed in a UV curing chamber. The chamber was purged with nitrogen for 3 min and UV irradiation was applied ($\lambda = 365$ nm, power > 20 mW/cm²) for 2 min. To facilitate removal of the particles from the mold, a physical means for harvesting the particles was utilized. Specifically, a 2 mL aliquot of acetone (filtered through a 0.22 μ m PTFE filter) was placed on the particle-filled mold and this drop of acetone was gently moved along the surface of the mold using a slide glass. The movement of the slide glass facilitated release of the particles from the mold.

The suspended particles were collected in a 50-mL Falcon tube and diluted to the 50-mL mark with filtered acetone. The suspension was vortexed for 10 min and was centrifuged at 2,500 x g for 30 min using IEC CENTRA CL2 Centrifuge (Thermo Electron Corporation, Waltham, MA). The supernatant was removed via aspiration and the particle pellet was re-dispersed in 50 mL of fresh acetone by vortexing for 10 min followed by centrifugation for an additional 30 min. This process was repeated once again. After aspiration, the particles were re-dispersed in 5 mL of distilled water by sonicating the dispersion for 15 min. The particle dispersion was filtered through a 20- μ m filter into a fresh 50-mL Falcon tube, and diluted to the 50 mL mark with acetone. This particle suspension was then centrifuged for one hour. The supernatant was removed via aspiration and the particle pellet was re-dispersed in 50 mL of fresh acetone by vortexing for 10 min followed by centrifugation for an additional 30 min. This process was repeated once again (with acetone) and after aspiration the particles were re-dispersed in a minimal amount of acetone, transferred to a tarred

Eppendorf tube, and centrifuged for 20 min. The supernatant was removed and the pellet was dried in a vacuum oven overnight, massed, and dispersed in the appropriate amount of sterile water to make a 10 mg/mL dispersion of particles.

For the study described below, four different sizes of cylinders with a diameter 0.2, 0.5, 1, or 7 μm were fabricated and one of the test groups (7 μm) was prepared to mimic erythrocytes. Different porosities of 7 μm -particles were also manipulated by adding 50% PEG dimethyl ether ($M_n = 550$ g/mol) as porogen during harvesting. Aspect ratio (i.e., ratio of height to diameter) was 1.0 in all the particle groups except for 7 μm , in which it was 0.2.

A.2.2.2 Radiolabeled PRINT Particles

The generation, purification and harvesting of radiolabeled particles was conducted similarly to the procedures used for fluorescently labeled particles mentioned above. But, the composition was modified to incorporate phenol moieties on the particles. The PRINT particles were derived from a mixture composed of 78% (w/w) PEG triacrylate, 20% PEG monomethyl ether monomethacrylate, 1% 2,2-diethoxyacetophenone, and 1% *p*-hydroxystyrene (PHS).

A.2.3 Characterization of Fluorescently-Labeled PRINT Particles

A.2.3.1 Stability of Fluorescein-Conjugated Particles in Liver Homogenate

PRINT particles (0.2 mg) of 0.2 or 2 μm were diluted in 0.3 mL PBS or liver homogenate derived from a virgin mouse. The 2- μm particles used here were prepared in the same manner as described above but not used for animal study. These samples were introduced to a dialysis cassette of 3.5 kDa MWCO, which were then placed in a 100-mL beaker containing 70 mL of PBS. Dialysis was performed at 37°C for 24 hrs. At specified time points, 1 mL of diffusate was collected from outside of the cassette and replaced with 1 mL of fresh PBS. Fluorescence intensity was measured, after 1- to 5-fold dilution, on a Perkin Elmer LS50B spectrofluorometer (Perkin Elmer Life and Analytical Sciences, Inc., Waltham, MA) using 495/520 nm for excitation/emission wavelength and a slit width of 15/20. As a positive control for dialysis setting, 5-(iodoacetamido) fluorescein of MW 515.3 was added to a separate dialysis cassette and monitored along with other test groups. Liver homogenate alone was also incubated under the same condition and used for obtaining a background value.

A.2.3.2 Kinetics of Fluorescence Intensity from Particles in NaOH

Into 0.4 mL of 1 N NaOH or distilled water, 100 μL of a particle stock solution in water (0.1 mg/mL) was added and incubated at 37°C for a designated time (i.e., 0, 20, 40 min, 1.5, 6, 16, and 24 hrs). At each time point, 2 μL of reaction mixture was removed and subject to fluorescence measurement using Nanodrop Model 3300 (NanoDrop Technologies, Wilmington, DE) at 520 nm for emission.

A.2.4 Pharmacokinetic and Biodistribution Studies of Fluorescently-Labeled PRINT Particles

Female C57BL/6J mice were housed under specific pathogen-free conditions for one week and were used at 8 weeks of age (~18 g). Animals were injected intravenously via bolus tail vein administration with 0.32 mg of fluorescently-labeled PRINT particles in 100 μ L of PBS. At 10, 30 min, 1, 3, and 8 h after dosing, groups of four mice were anesthetized by intraperitoneal injection of 100 μ L of ketamine-HCl solution in PBS (50 mg/mL). Blood was collected via cardiac puncture and serum was separated by centrifugation (Eppendorf Centrifuge 5415D) at 12,000 x g for 10 min at 4°C. Organs and tissues harvested (liver, kidneys, spleen, lungs, and heart) were weighed, homogenized (Power Gen 700, Fisher Scientific) and centrifuged (Beckman GS-6R, Fullerton, CA) at 250 x g for 5 min. Serum and supernatant from organs/tissues were collected into a 2-mL polypropylene microcentrifuge tube (Fisher Scientific) and 0.1 mL of each sample was added into the mixture of 0.39 mL of 1 N NaOH and 0.01 mL of 5% deoxycholic acid. The mixture was then incubated at 37°C water bath (Fisher Scientific) for 24 hrs before analysis. Fluorescence intensity was measured by loading 2 μ L of hydrolyzed sample on Nanodrop Model 3300 (NanoDrop Technologies, Wilmington, DE) at 520 nm.

To convert relative fluorescence intensity into actual amount of particles, a calibration curve was prepared in each organ/tissue for all the particle test groups with different sizes by adding a series of known amounts of fluorescently-labeled particles into constant weight of organs or tissues. After thorough homogenization, supernatant was separated, hydrolyzed as

mentioned above, and subject to fluorescence measurement. In case of blood samples, standard particles were added to constant volume of blood aliquots followed by serum separation. After hydrolyzed in the same manner as in organ samples, serum was subject to fluorescence measurement to obtain a calibration curve.

A.2.5 Iodination of PRINT Particles

PRINT particles were prepared similarly to fluorescently labeled particles. The monomer composition was 78% PEG₄₂₈ triacrylate, 20% PEG₁₀₀₀ monomethoxymethacrylate, 1% *p*-hydroxystyrene, and 1% 2,2-diethoxyacetophenone (w/w). Into an Iodogen® pre-coated tube, 10 mg of particles suspended in 1 mL of water was added. Each tube contained 50 µg of Iodogen as an oxidizing agent. PBS (10 X) was added to the tube in such a way the final concentration of PBS in the reaction was 0.5 X. It was then followed by the addition of 10 µL (1 mCi) of Na¹²⁵I at 100 mCi/mL in 10⁻⁵ M NaOH (pH 8-11). Iodogen oxidizes iodine to iodous ion that is a good electrophile and chemically attached to the *ortho* position of phenyl moiety on the particles. The reaction was allowed to proceed for 15 min at room temperature while swirling the tube gently every 1 min for 30 sec. After 15 min, the reaction mixture was transferred to a clean pre-weighed 2-mL microcentrifuge tube to stop the reaction. For safety, KI was added to the microcentrifuge tube to a final concentration of 1 mM. The original reaction tube was rinsed with 100 µL of water twice and both washes were combined into the microcentrifuge tube containing the reaction mixture. As a reducing agent, 1 µmol of NaHSO₃ was added and vortex-mixed.

The reaction mixture was centrifuged for 10 min at 15,000 x g using a microcentrifuge (Eppendorf, Westbury, NY) at room temperature. Supernatant was removed and 500 µL of fresh distilled water was added to the particles for wash. Washing step was repeated until CPM measured by a hand-held radioactivity counter Model Monitor 4/4EC (S. E. International, Inc., Summertown, TN) in the supernatant reached baseline value or plateau (~ 200 CPM). Supernatant was removed and the pellet was dried using a Speed-Vac (Savant SC 110, Global Medical Instrumentation, Inc, Ramsey, MN) for 20 min. The tube containing dried particles was weighed to get the net weight of labeled particles. Particles were re-dispersed in 500 µL of freshly distilled water. This served as a stock solution for specific activity measurement and animal injection. Specific activity was determined by putting 3 µL of purified particles suspended in water to a 12 x 75 mm glass tube (Fisher Scientific) and reading radioactivity in a gamma counter (Beckman Gamma 5500B, Beckman, Fullerton, CA). The specific activity, calculated from the CPM measured and the mass of particles remained as pellet, was 1.23×10^7 CPM/mg of particles.

A.2.6 Pharmacokinetic and Biodistribution Studies of Radiolabeled PRINT Particles

Female C57BL/6J mice were housed under specific pathogen-free conditions for one week and were used at 8 weeks of age (~18 g). Animals were injected intravenously via tail vein at a dose of 0.32 mg of [¹²⁵I]-labeled PRINT particles with a specific activity of 1.4 µCi/mg in 100 µL of PBS. At 10, 30 min, 1, 3, and 8 h after dosing, groups of four mice were anesthetized by intraperitoneal injection of 100 µL of ketamine HCl solution in PBS (50 mg/mL). Blood was collected via cardiac puncture and subject to for radioactivity

measurement as whole blood. Samples of blood and tissues harvested (liver, kidneys, spleen, lung, heart, femur bone marrow, thyroid and whole tail) were weighed and analyzed for the total radioactivity in a Beckman Gamma 5500B gamma counter (Beckman, Fullerton, CA). Additional four animals were kept in a metabolic cage after injection of the [125 I]-labeled PRINT nanoparticles. At 24 h post-injection, urine and feces accumulated were collected for radioactivity measurements without any further treatment.

After animals were sacrificed the blood as well as the organs were removed, weighed, and analyzed for radioactivity. Fat (perirenal site), muscle (right or left leg thigh), head, legs, intestines, and the remainder of the body were also analyzed for additional radioactivity. For data presentation, % ID (injected dose) was calculated and presented for each organs or tissues collected. Elemental pharmacokinetic parameters in blood were attained by fitting data to two-compartment model using WinNonlin 5.0.1 (Pharsight Corporation, Mountain View, CA).

A.3 Results and Discussion

A.3.1 Characterization of Fluorescently-Labeled PRINT Particles

As shown in **Figure A-1**, particles prepared from FluorocurTM mold were all cylindrical with an aspect ratio of 1 or 0.2 (only for 7 μm particles). Scanning electron microscopy performed in dried particles and dynamic light scattering of particles dispersed in PBS showed that the actual sizes were smaller, especially in the height than anticipated (**Table A-1**). Scanning electron microscopy measurement was closer to the size of master template than that of DLS. The diameter of mice erythrocytes (6.6-6.7 μm) is known to be a bit smaller than that ($> 7 \mu\text{m}$) of rats or monkeys (Gregory 2000). The size of erythrocyte mimics (i.e., 7 μm non-porogen) tested in this study turned out to be very close to that of mouse cells. PEG dimethyl ether ($M_n = 550 \text{ g/mol}$) was added to another set of 7 μm particles to see how the addition of porosity affects on the bioenvironmental behavior of erythrocyte mimics. Unfortunately, the diameter of porogen-containing particles ($\sim 5 \mu\text{m}$) was significantly smaller than that ($\sim 6.3 \mu\text{m}$) of non-porogen counterpart. The difference in size as well as in porosity of erythrocyte mimics might change the response of the body that encountered those particles following systemic administration.

Prior to the main PK study of fluorescently labeled PRINT particles, the stability of fluorescent label was established in PBS as well as liver homogenate. This is important since the label is to serve as a probe of particles in vivo. Liver was selected for this test because it is abundant in enzymes (Imai 2006) and is an organ where foreign particulates are expected

to accumulate. **Figure A-2A** shows that no fluorescence was detected outside the dialysis bag (3.5 kDa MWCO) that contained fluorescein-PRINT particles of 2 μm in PBS up to 22 hrs at 37°C. Fluorescence intensity measured outside the dialysis bag gradually increased when particles (200 nm or 2 μm) were incubated with liver homogenate. This is attributed to leakage of liver component as the background value from liver homogenate alone was also increased in similar manner. A small MW (515 g/mol) fluorescent molecule, 5-(iodoacetamido) fluorescein, was incubated with liver homogenate and served as positive control group. As expected, rapid increase of fluorescence intensity was observed. When fluorescence intensities were measured inside of dialysis bags containing fluorescein-particles in PBS or liver homogenate at 22 hrs of incubation at 37°C, no significant loss of intensity was observed while only 5% of initial fluorescence intensity remained in the bag containing 5-(iodoacetamido) fluorescein (**Figure A-2B**). Taken together, these data clearly support that the linkage between fluorescein molecule and PRINT particle remains intact in the presence of liver enzymes at least during the tested period of time.

Self-quenching of fluorescein and other xanthene-type dyes is due to homo resonance energy transfer (HRET) between fluorescein molecules and has been studied by many investigators (e.g., Lakowicz *et al.* 2003). The so-called Forster distance for HRET is about 4.2 nm (Kawski 1983). Thus HRET is expected to occur when a particle contains more than a single fluorescein molecule and the distance between the fluorophores is smaller than 4.2 nm. The overall net result will be decreased intensities with increasing labeling density. If each molecule of fluorescein can be released (i.e., by hydrolysis of ester bonds) from the particle in the tissue samples after collection, the intensity would increase and the analytical

sensitivity gets higher. As shown in **Figure A-3**, when serum and organ homogenate containing PRINT particles are incubated with NaOH in the presence of deoxycholic acid, the particle could be degraded, releasing fluorescein molecules. To optimize the incubation time of hydrolysis, PRINT particles of various sizes were incubated at 37°C with 1 N NaOH until the fluorescence intensity leveled off (**Figure A-4**). In all cases, fluorescence intensity in the NaOH-treated particles significantly increased compared to their counterparts in water and reached a plateau by 24 hrs of incubation (**Figure A-4**).

However, the maximum intensity observed was not identical among particles of different sizes; highest in 7 µm porogen particles and lowest in 7 µm non-porogen. It is likely due to the fact that porogen particle is associated with high porosity that would facilitate more extensive hydrolysis. This interpretation is consistent with the finding that 200-nm particle featuring a high surface area-to-volume ratio also showed a high intensity (i.e., the ratio is 6.25- and 25-fold larger than that of 500-nm and 1-µm particles, respectively). There was, however, a discrepancy between the actual rank order of maximum intensity and the theoretical expectation in 500-nm and 1-µm particles. No explanation is offered for this finding at present.

A.3.2 Pharmacokinetic and Biodistribution Studies of Fluorescently-Labeled PRINT Particles

Upon IV injection, 200-nm and 500-nm particles stayed in the circulation fairly well up to 8 hrs in contrast to 500-nm particles (**Figure A-5** and **A-6A**). No measurable amount

of 1- μ m particles was found in the blood throughout the study period while rapid accumulation was observed in organs such as liver and spleen. In some instances a significant amount of injected dose could have been retained in the injection site (i.e., tail), verified in a subsequent experiment (see more later). The total recovery of 1- μ m particles at 10 and 30 min was quite low (\sim 15-20%) while it was respectably 40 to 90% at later time points (**Figure A-7**), supporting the speculation. As shown in **Figure A-7**, the total recovery (\sim 15-60%) with 7- μ m particles fluctuated with time but was rarely close to 100%. These recoveries may also reflect those retained in the injection site on the tail. Indeed there has been some concern about injected compounds remaining in the tail with high probability (Groman and Reinhardt 2004). Unfortunately, evaluation of particle retention in the tail was not determined in particular series of study. However, it was measured with radiolabeled particles. It is discussed in section **A.3.3**.

The life span of red blood cells was reported to be approximately 40 days in mice (Van Putten and Croon 1958), which is shorter than in rats (\sim 60 days) or in human (\sim 120 days, Shemin and Rittenberg 1946). The rapid disappearance of 7- μ m, erythrocyte-mimicking particles observed here clearly indicate an ample room for improvement. Nonetheless it is most interesting to note that as much as 10-20% of 7- μ m porogen particles (**Figure A-5E**) remained in the blood up to 3 hrs while 7- μ m regular particles (**Figure A-5D**) disappeared rapidly within 30 min. Effect of particle density and elasticity implied with the observation warrants further investigation.

For 200-nm, 500-nm and 1- μ m particles (**Figure A-5A-C** and **Figure A-6B** and **D**), the main organs of accumulation were liver and spleen. An earlier indication that blood vessel capillaries have organ-related differences has been verified with transmission electron microscopy in the 1950s (e.g., Bennett *et al.* 1959). These studies identified three general types of capillaries; continuous, fenestrated, and discontinuous. Unlike the capillaries containing fenestrated (e.g., renal glomeruli and intestinal villi) or continuous (e.g., heart, lung and brain) endothelium, sinusoidal capillaries in liver, spleen and bone marrow are lined with discontinuous endothelium. They have transcellular openings not covered by a diaphragm and permit the extravasation of macromolecules (Majno and Joris 1978; Pasqualini *et al.* 2002). Thus, the observation made in the present study is consistent with this notion and earlier reports with other foreign particulates (Wisse and De Leeus 1984; Senior 1987). For instance, the predominant uptake of liposomes by reticuloendothelial system (e.g., macrophages in liver, spleen and lymph nodes) has been well established in earlier studies (Schwendener *et al.* 1984; Senior 1987; Moghimi *et al.* 1991).

In the case of 500-nm particles, a significant amount was also found in the lungs (**Figure A-5B**), the first organ that particles would encounter upon tail vein injection. Again it was also the main organ of accumulation in both cases of 7- μ m particles (**Figure A-5D** and **E**, see **Figure A-6F** also). Fidler and colleagues (1980) investigated the retention of liposomes of different sizes and compositions in the lung following systemic administration in mice. They found that large liposomes such as multilamellar vesicle (> 1 μ m in diameter) were retained in the lung more efficiently (by 3-5 fold) than were small unilamellar vesicles (< 100 nm). Interestingly, reducing the size of multilamellar vesicle by extruding them

through membrane filters (1- μ m pore size) reduced lung retention by 2-fold. The effect of size on the lung accumulation was also reported by other groups (e.g., Finkelstein and Weissmann 1978). Liposomal composition was also found to be a significant factor in determining retention within the lungs with negatively charged liposomes more efficiently retained than neutral or positively charged ones (Kimelberg 1976; Fidler *et al.* 1980). Noticeably, lung becomes more important organ to investigate under disease states since it represents a major site of metastatic diseases such as cancer (Fidler 1980). Although it is not known the cause of the present finding, physical trapping of transiently aggregated particles could explain the relatively high accumulation in the lung.

A.3.3 Pharmacokinetic and Biodistribution Studies of Radiolabeled PRINT Particles

Several different monomers were added to introduce specific functionality into the PRINT nanoparticles. Poly(ethylene glycol) monomethyl ether monomethacrylate ($M_n=1000$ g/mol) was used to increase steric pressure between particles and opsonins and reduce RES uptake. The phenol-containing monomer, *p*-hydroxystyrene (**A** in **Figure A-8**), provided a chemical handle for a gentle radioiodination of the particles. In this study, 200-nm [125 I]-labeled PRINT particles were administered into healthy C57BL/6J mice via tail vein bolus injection. The particles were radiolabeled using Iodogen[®] (**C** in **Figure A-8**) following the procedure recommended by the supplier (Pierce Biotechnology). Iodogen oxidizes iodide (I^-) to electrophilic iodous ion (I^+) that conjugates to the *ortho* position of phenol moiety on the particle. Small amount of radiolabeled (hot) particles (**D** in **Figure A-8**) was mixed with cold particles (**B** in **Figure A-8**) to achieve the dose of 1.4 μ Ci (3×10^6 dpm) / 0.32 mg / mouse.

The tissue distribution was monitored using a gamma counter, and the percent recovery of injected dose was calculated from the measured radioactivity.

Figure A-9 shows the tissue distribution of 200-nm PRINT nanoparticles at 10 min, 30 min, 1 h, 3 h, 8 h, and 24 h post-injection. Throughout the time-course of the study, the 200-nm PRINT particles were distributed mainly in the liver and spleen. The total recovery from these two organs amounts to as much as 30% over the 24-hr study period. This is in agreement with the observation in the previous study using fluorescein-labeled particles and consistent with fact that the sinusoidal walls of these organs are lined with discontinuous endothelium, allowing passive entrapment of foreign particulates (see section **A.3.2**). Although the present study does not provide any direct evidence for or against it, it is likely that these particles are eventually taken up by the resident macrophages possibly subsequent to opsonization with serum proteins (Chonn *et al.* 1995).

The particle accumulation was not significant in other organs harvested, often ~ 1% of the injected dose was found in the kidneys, heart, and lungs. Incomplete removal of residual blood in these organs could lead to a slight overestimation on the extent of particle accumulation reported. Tails were collected in an effort to monitor the amount of nanoparticles that were retained at the injection site. A significant amount of injected particles were found in the tail, especially for the initial 3-hr period. Upon injection of a large number of fine particles in relatively short period (~ 100 billion particles in 5 seconds), blood vessels could rupture and create endothelial gaps for particle retention. Finally, a trace but significant amount of radioactivity was observed in thyroid gland, possibly indicating the

biodegradation of particles, yielding radioactive iodine (I_2). The thyroid gland accounts for 80% of the body's iodine pool and converts iodine into the thyroid hormones thyroxine (T_4) and triiodothyronine (T_3). These hormones are released into the bloodstream, controlling the body's metabolism (Cavalieri 1997). Production of iodine from biochemical degradation of iodinated proteins or peptides is not uncommon (Wolf *et al.* 1993) and may explain at least in part the observation that total recovery decreased steadily over the 24 h period studied.

Total recovery of the radioiodinated particles was found to decrease with time, beginning with an 82% at 10 min post-injection and ending with a 25% recovery after 24 hrs (**Figure A-10**). Here, the total recovery was calculated from radioactivity measured only from the blood, liver, kidneys, spleen, lungs, heart, tail, bone marrow, and thyroid. In an effort to achieve a full mass balance, additional four mice were kept in a metabolic cage for 24 hrs to collect urine and feces for analysis. For these mice, additional tissues and body parts such as fat, muscle, head, legs, intestines, and the remainder of the body were also analyzed for additional radioactivity. It was found that with these additional measurements, the total recovery at 24 hr post-injection improved from 25% to 59%. The appearance of radioactivity in the thyroid gland throughout the study period (approximately 1% of injected dose) and in urine 24 hr after dosing (as much as 8.6%) may suggest particle degradation (Takakura and Hashida 1996). Another hypothesis for the time-dependent decrease in total recovery of radioactivity is that volatile radioactive iodine could be formed and expelled continuously out of the body via the lungs. This hypothesis has yet to be tested using a closed circuit type of metabolic cages.

As shown in **Figure A-11**, the disappearance of PRINT particles from circulation was bi-exponential. The data set was fitted to a two-compartmental pharmacokinetic model with reversible distribution between central and peripheral compartments and with elimination from the central compartment (see **Figure A-12** for the model used). The pharmacokinetic parameters (**Table A-2**) obtained using WinNonlin 5.0.1 show the initial phase of rapid distribution with an apparent $t_{1/2}$ of 17 min. Close examination of the individual parameters shows that the movement of particles from central to peripheral compartment (k_{12} , 1.26 hr^{-1}) is approximately 1.5-fold faster than the reverse directional input to the central compartment from peripheries (k_{21} , 0.82 hr^{-1}) and 2-fold faster than the disappearance from the central compartment (k_{10} , 0.54 hr^{-1}). The rapid distribution is not surprising considering that the PRINT particles were grafted with a low molecular weight PEG chain (9 mol %, 20% w/w of 1-kDa PEG monomethyl ether). It has been suggested that the optimal coating for the developing long-circulating liposomes is 3-7 mol % of 2-5 kDa PEG (Moghimi *et al.* 2001). The shorter PEG chains used in the current particle formulation may not offer a sufficient thickness of PEG cloud to effectively block the adsorption of opsonic proteins and or interaction with phagocytes. The subtle combination of the degree of PEG incorporation and the molecular weight of PEG in prolonging the circulatory $t_{1/2}$ is well documented for other types of nanocarriers (Drummond *et al.* 1999; Moghimi *et al.* 2001; Owens and Peppas 2006).

Volumes of distribution in central and peripheral compartments were found to be 3 and 5 mL, respectively. Considering the blood volume of approximately 1.7 mL/20 g mouse, liver of 0.8 g, and spleen of < 0.1 g, these values appear to be somewhat exaggerated, however, they certainly rule out any significant extravasation. Since the stability of the

radiolabel is not well established in the present study and since it is the radioactivity that is monitored, it is difficult to unambiguously interpret the slow phase of radioactivity decay in the later time-points with an apparent $t_{1/2}$ of 3.8 hrs. The appearance of radioactivity in urine strongly suggests that these PRINT particles and/or their degradation products must be cleared readily from the blood. Thus, the slow elimination phase may well represent slow re-distribution of particles or particle remnants between the blood and organs/tissues.

The AUC, a measure of total availability of particles in the circulation for organ distribution extrapolated to infinite time, was determined to be 189 $\mu\text{g}\cdot\text{hr}/\text{mL}$. Unmodified, conventional liposomes show dose-dependent pharmacokinetic parameters, including AUC upon intravenous administration. A liposome dose equivalent to the dose studied in the present study, 18 mg/kg, shows AUC values of approximately 70 to 700 $\mu\text{g}\cdot\text{hr}/\text{mL}$, and the present data are certainly in agreement with that reported for liposomes (Allen and Hansen 1991).

A.4 Conclusions

This chapter is concerned with the *in vivo* characterization of nanofabricated particles that are monodisperse in size and shape. Herein reported is the first pharmacokinetic evaluation of PRINT-derived cylinders of various sizes, ranged from 200 nm to 7 μm .

For 200-nm particles, 5-20% of injected dose stayed in the blood up to 8 hrs while particles of 500 nm showed relatively rapid disappearance from the blood. No measurable amount of 1- μm particles was found in the blood throughout the study period. Most interestingly, as much as 10-20% of 7- μm porogen particles remained in the blood up to 3 hrs while 7- μm regular particles disappeared rapidly within 30 min. For 200-, 500-nm and 1- μm particles, the main organs of accumulation were livers and spleen, organs of which sinusoids are with discontinuous endothelium. Increased amount of 500-nm particle was found in the lungs, the first organ that particles would encounter upon tail vein injection. Again it was the main organ of accumulation in both cases of 7- μm particles. During the 24-hr period studied, close to 100% of injected dose was recovered from the harvested organs and blood except the 7- μm particles. The low recovery of these may well represent those retained in the injection site on the tail.

The biodistribution of radiolabeled particles was performed to verify the previous investigation using fluorescently labeled particles. 200-nm PRINT particles showed similar tissue distribution to that of fluorescently-labeled particles (i.e., liver and spleen were the main organs of accumulation upon *i.v.* injection). The findings that trace but significant

amount of particles were accumulated in thyroid glands and urine appears to support possible degradation of particles. Radiolabeled particles were cleared from the blood rapidly with elimination half-life of 3.8 hrs.

PRINT particles are associated with unprecedented monodispersity as well as the ability to address several different design criteria comprehensively, simultaneously, and independently. Thus they offer an excellent opportunity to test the effects of size, shape, composition, surface properties, and the addition of biological targeting ligands on the biological fate of particles as drug carriers. The basic understanding of their pharmacokinetic behavior will ultimately leads to optimizing pharmacodynamics of drug-carrying PRINT particles.

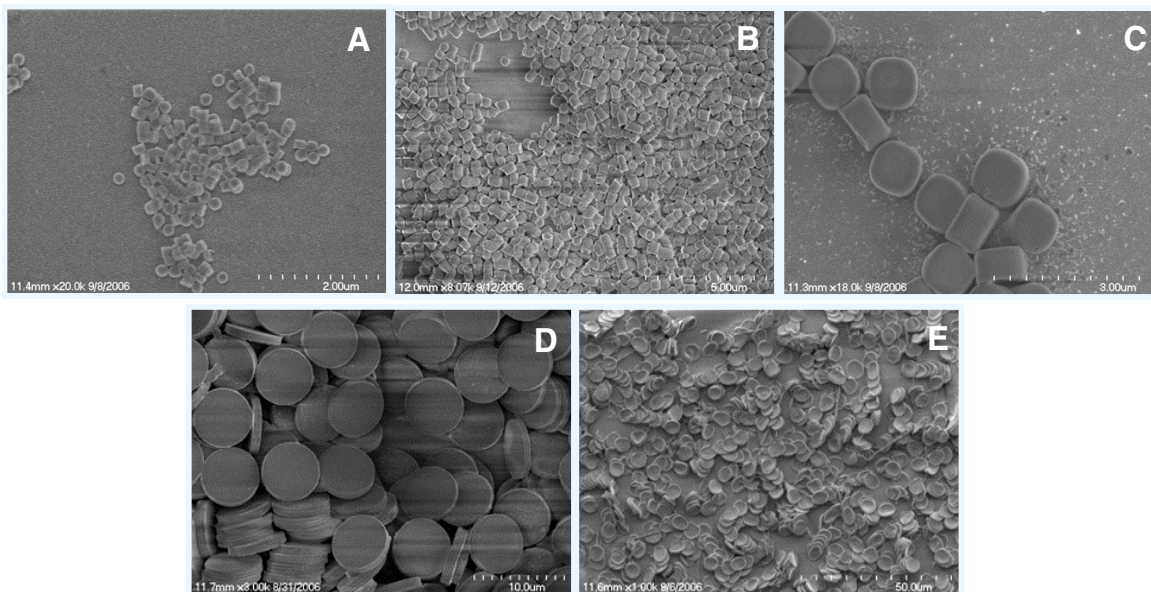


Figure A-1: Scanning electron micrographs of PRINT particles (data from S. Gratton and P. Pohlhaus in DeSimone Lab of UNC chemistry Department): **A**, 200 nm; **B**, 500 nm; **C**, 1 μm ; **D**, 7 μm ; and **E**, 7 μm containing 50% PEG₅₅₀ dimethyl ether (porogen). Hitachi Model S-4700 was used with samples prepared by placing a drop of particle dispersions (0.5 mg/mL) on a slide glass followed by Pd/Au alloy (1.5 nm) coating. Sample was in dry condition during observation conducted under low vacuum (10^{-3} Torr).

Table A-1^a: Particle Sizes Measured by SEM and DLS

Test Group	Master Template ^b	Size by SEM ^c (μm)		Size by DLS ^d (μm)
		Width (Diameter)	Height	
200 nm	0.2 x 0.2 μm	0.20 ± 0.01	0.16 ± 0.01	0.27 ± 0.02
500 nm	0.5 x 0.5 μm	0.41 ± 0.03	0.43 ± 0.02	0.39 ± 0.05
1 μm	1 x 1 μm	0.97 ± 0.04	0.68 ± 0.05	0.62 ± 0.02
7 μm	7 x 1.4 μm	6.30 ± 0.20	0.90 ± 0.20	N/A
7 μm w/ 50% porogen	7 x 1.4 μm	5.00 ± 0.20	0.80 ± 0.10	N/A

^a; Data were from S. Gratton and P. Pohlhaus of DeSimone Lab of UNC Chemistry Department.

^b; Size of mold could represent intended sizes of particles.

^c; Scanning electron microscopy (SEM) was performed on Hitachi Model S-4700 by placing a drop of particle dispersions (0.5 mg/mL) on a slide glass followed by Pd/Au alloy (1.5 nm) coating. Sample was in dry condition during observation conducted under low vacuum (10^{-3} Torr).

^d; Dynamic light scattering (DLS) was carried out to measure the sizes of particles dispersed in PBS solution (0.5 mg/mL) using a 90Plus Particle Size Analyzer at 25 °C.

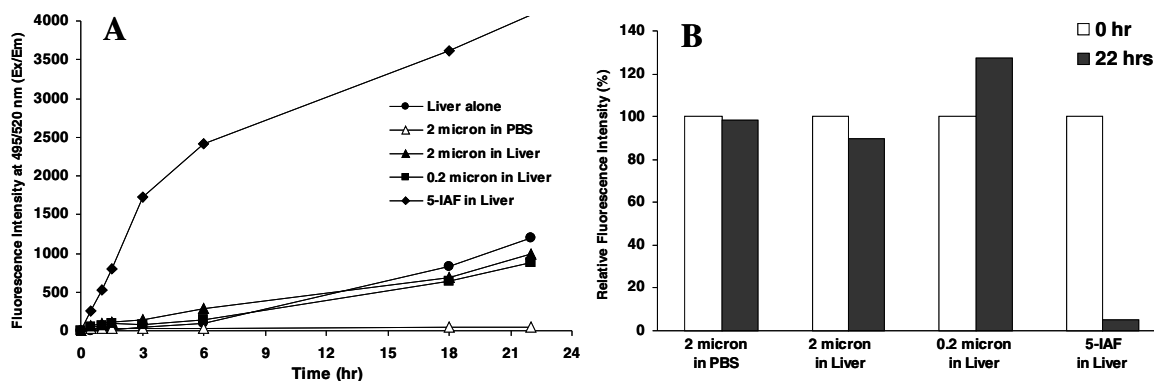


Figure A-2: Stability of PRINT particles in liver homogenates as studied in a dialysis set-up. Dialysis cassette (3.5 kDa MWCO) containing 0.2 mg of PRINT particles (200 nm or 2 μ m) in 300 μ L liver homogenate from mouse or PBS was incubated in a 100-mL beaker containing 70 mL of PBS. The cassette was placed in 37°C water bath and incubated for 22 hrs. At a given specified time point, aliquot of diffusate was removed and subject to fluorescence measurement (A). Relative fluorescence intensity (B) was calculated by subtracting initial fluorescence (T = 0 hr) from the fluorescence measured at each time point (i.e. 0 and 22 hrs). As a positive control, 5-(iodoacetamido) fluorescein (IAF) was incubated in liver homogenate and dialysis was performed in the same manner as the other test groups.

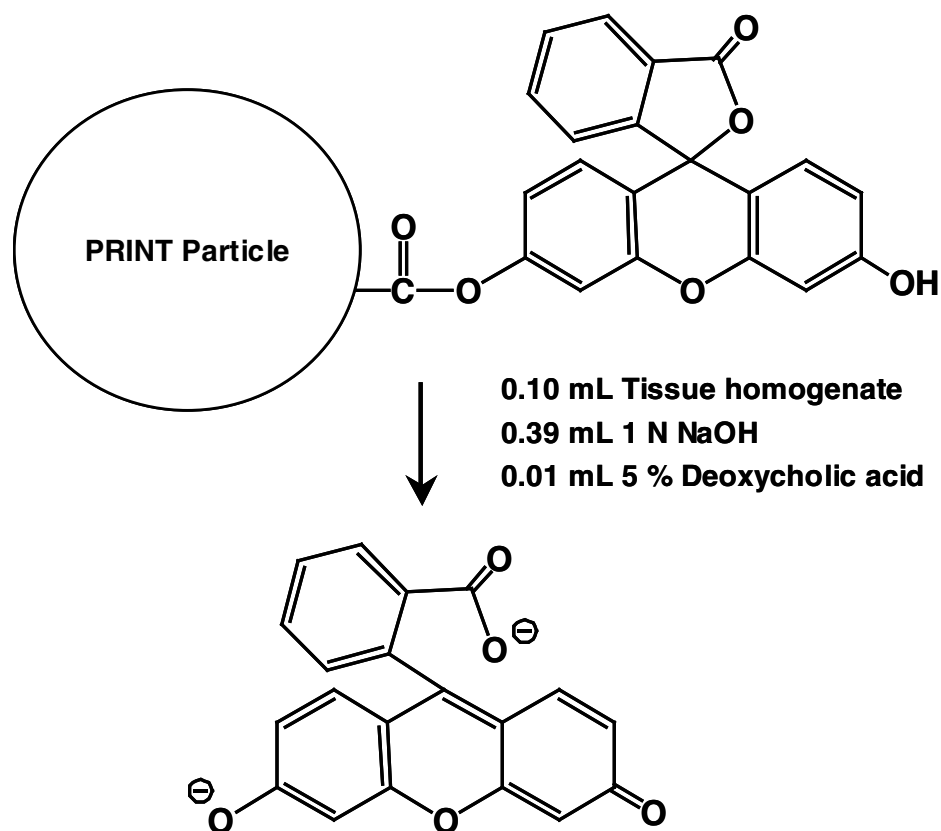


Figure A-3: Hydroxide ion-catalyzed hydrolysis of fluorescein-labeled PRINT particles. Fluorescein molecules are released from the surface and the matrix of particles by base treatment. The hydrolyzed product was expected to have same excitation and emission wavelengths as those of parent molecule. Tissue homogenate hydrolyzed was then subject to fluorescence measurement without any further purification.

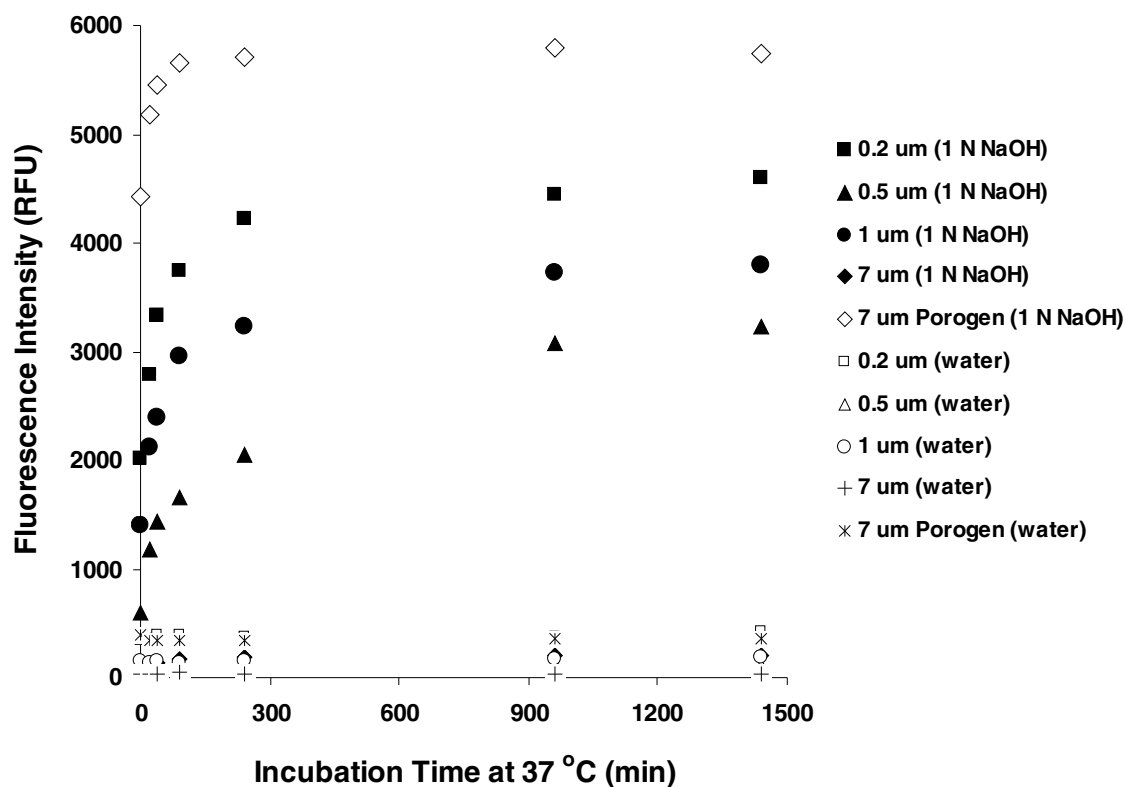


Figure A-4: Kinetics of fluorescence intensity from PRINT particles that were incubated with NaOH. Particles (10 μg) of various sizes in water (100 μL) were added into 0.4 mL of 1 N NaOH or distilled water and the mixture was incubated at 37°C up to 24 hrs. At a given time interval (i.e., 0, 20, 40 min, 1.5, 6, 16, and 24 hrs), 2 μL of reaction mixture was removed and subject to fluorescence measurement. A Nanodrop Model 3300 was used using 520 nm for emission.

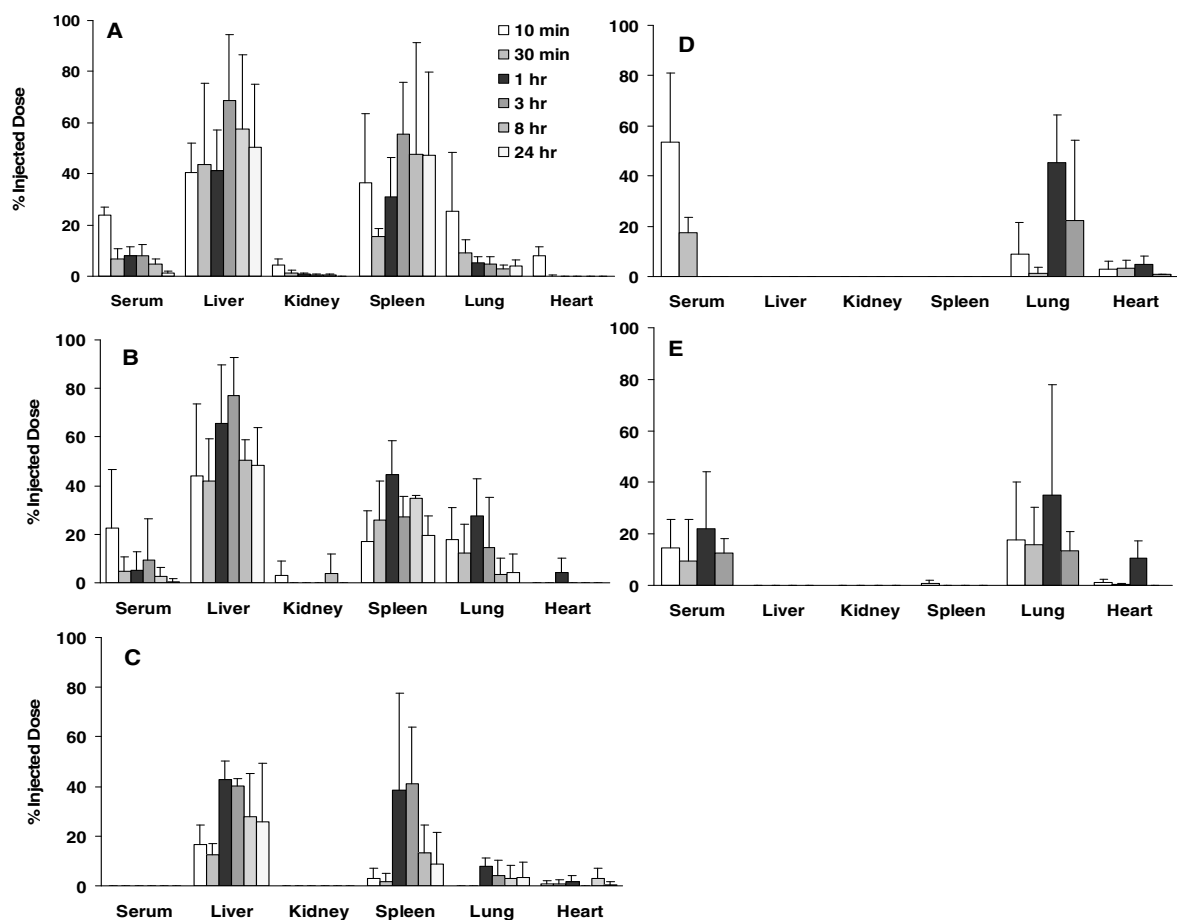


Figure A-5: Biodistribution of fluorescently-labeled PRINT particles of various sizes (A, 200 nm; B, 500 nm; C, 1 μ m; D, 7 μ m; and E, 7 μ m with 50% porogen) following IV bolus tail vein injection of 0.32 mg particles per mouse (n=3 or 4). Animals in D and E were monitored only up to 3 hrs post-injection. Serum was separated from blood collected through heart puncture. Other organs were harvested at a specified time point, homogenized and supernatant was separated using low speed centrifugation (250 x g, 5 min). Fluorescence measurement in serum and organ homogenates was performed after NaOH-hydrolysis at 37°C for 24 hrs. The fluorescence was then converted into the amount of particles using a pre-established calibration curve. The percent injected dose was calculated from the amount of particles in samples and initially administered dose.

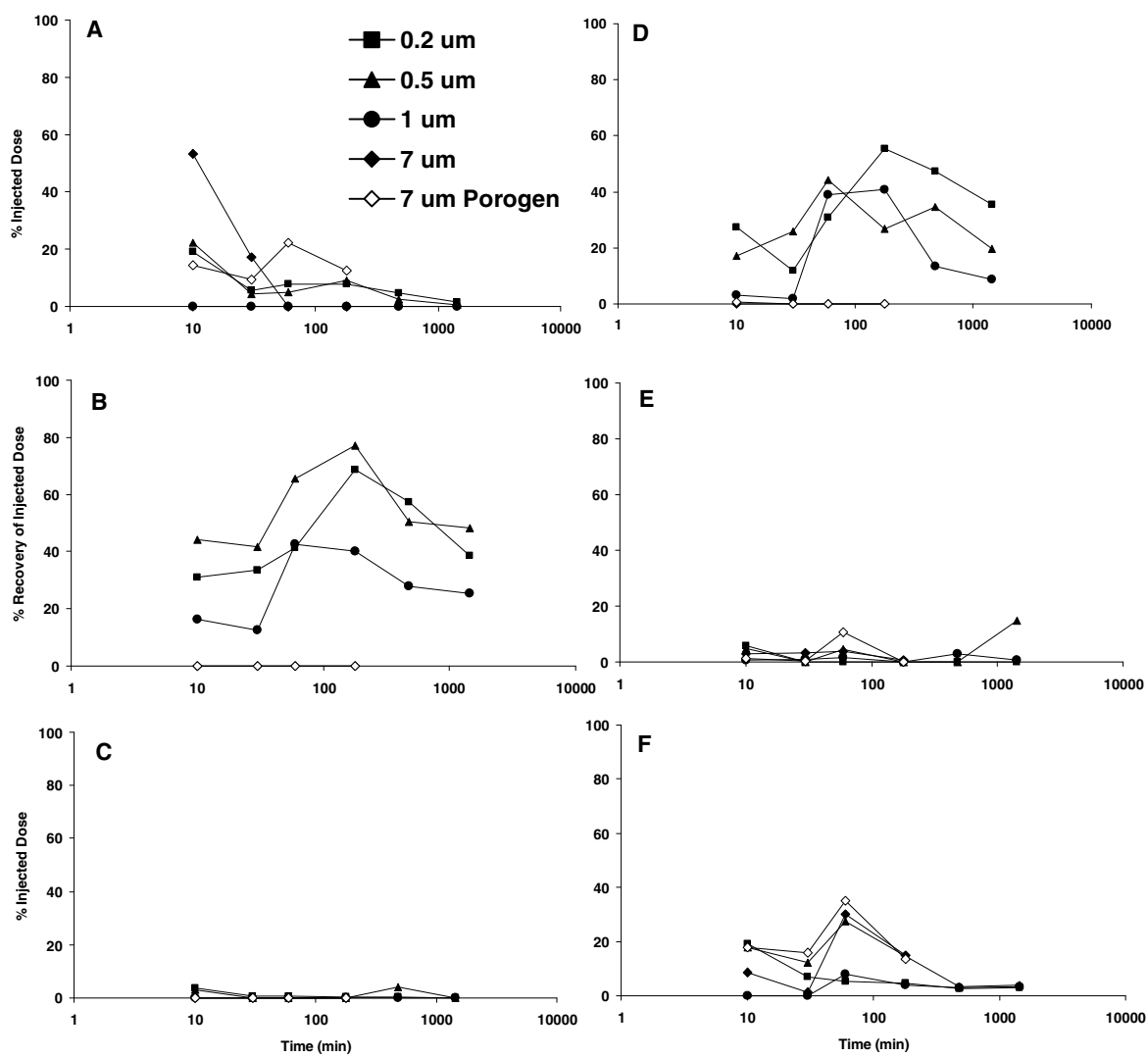


Figure A-6: Biodistribution of fluorescently-labeled PRINT particles represented by organ or tissue (**A**, Serum; **B**, Liver; **C**, Kidney; **D**, Spleen; **E**, Heart; and **F**, Lung). Serum and organ samples were collected and processed for fluorescence measurement as described in **Figure 5-5**. The fluorescence was then converted into the amount of particles using a pre-established calibration curve. The percent injected dose was calculated from the amount of particles in samples and initially administered dose, 0.32 mg/mouse.

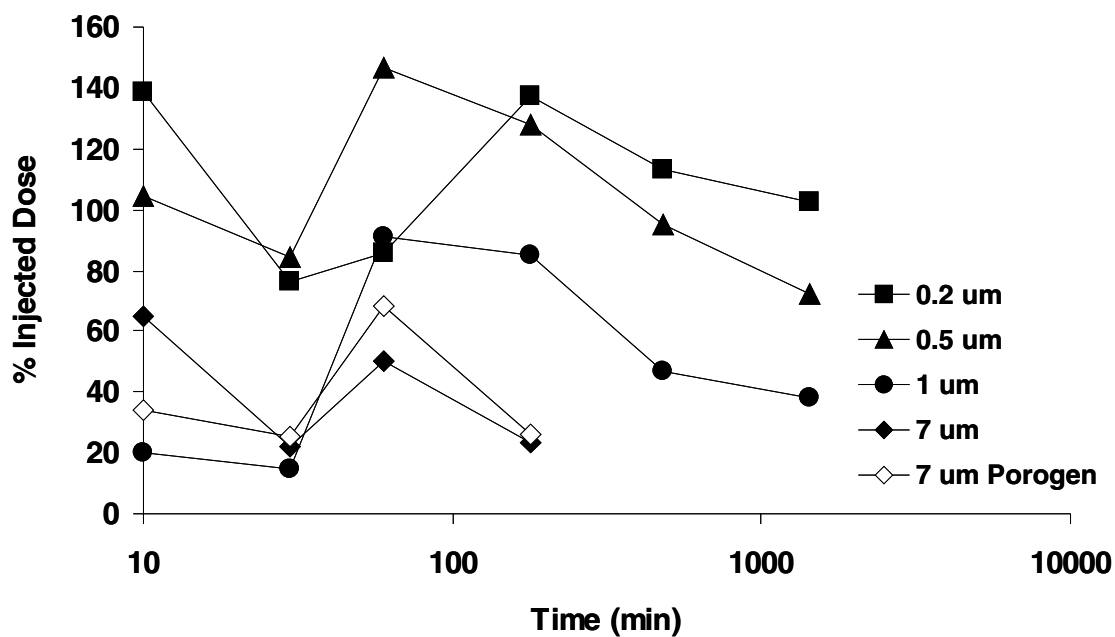


Figure A-7: Total recovery of fluorescein-labeled PRINT particles. Percent recovery of injected dose in all the organs including serum were combined and the sum was represented as a function of time. Erythrocyte mimic (i.e., 7 μm) and its porogen-containing derivative (7 μm Porogen) were tested only up to 3 hrs post-injection.

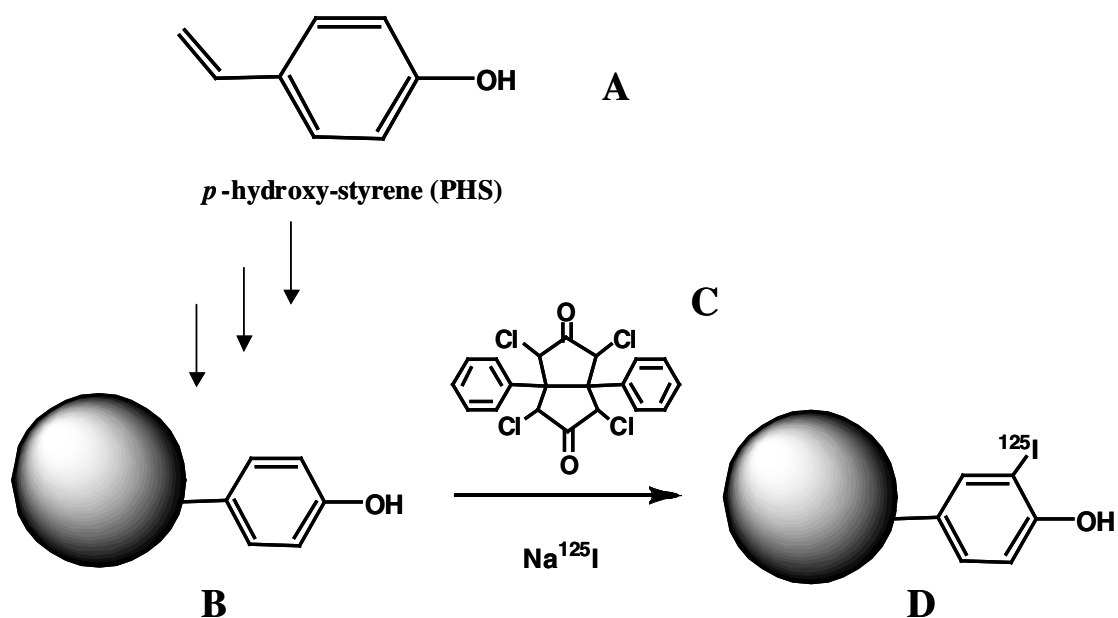


Figure A-8: Iodination of PRINT particle using Iodogen[®] pre-coated tube. *Para*-hydroxystyrene (**A**) was incorporated into particle and served as chemical handle for iodination. PRINT particle containing phenol moiety (**B**) was incubated for 15 min in an Iodogen[®] (**C**) pre-coated tube in the presence of Na^{125}I . Iodinated particle (**D**) was rinsed with distilled water several times and mixed with cold particle (**B**) in such a way each mouse was dosed with 1.4 μCi / 0.32 mg particle.

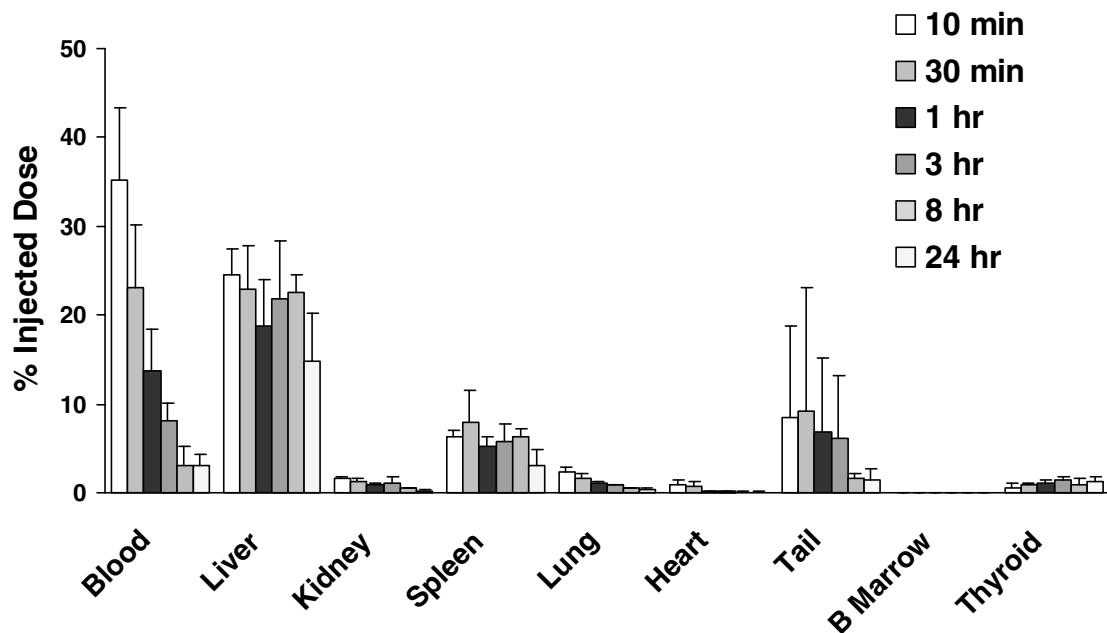


Figure A-9: Biodistribution of [^{125}I]-PRINT particles of 200 nm following IV bolus tail vein injection of 1.4 μCi (0.32 mg particles) per mouse. Radioactivity of whole blood and organs were measured using a gamma counter without any additional treatment or homogenization after harvesting at designated time points. The percent injected dose was calculated from the direct reading of CPM in samples and initial dose.

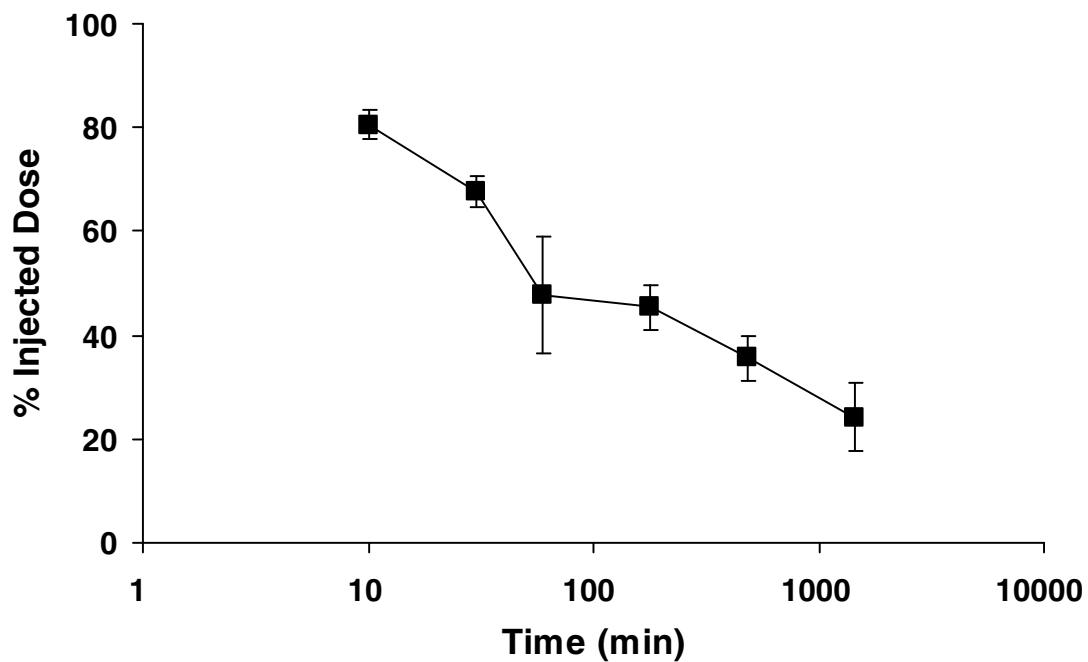


Figure A-10: Total recovery of 200 nm [^{125}I]-PRINT particles. Percent recovery of injected dose in all the organs and tissues including blood were combined and the sum is presented as a function of time. This data do not contain the amount found in excreta (urine and feces) or in other tissues collected at 24-hr time point such as fat, muscle, leg, head, intestine, and rest of the body.

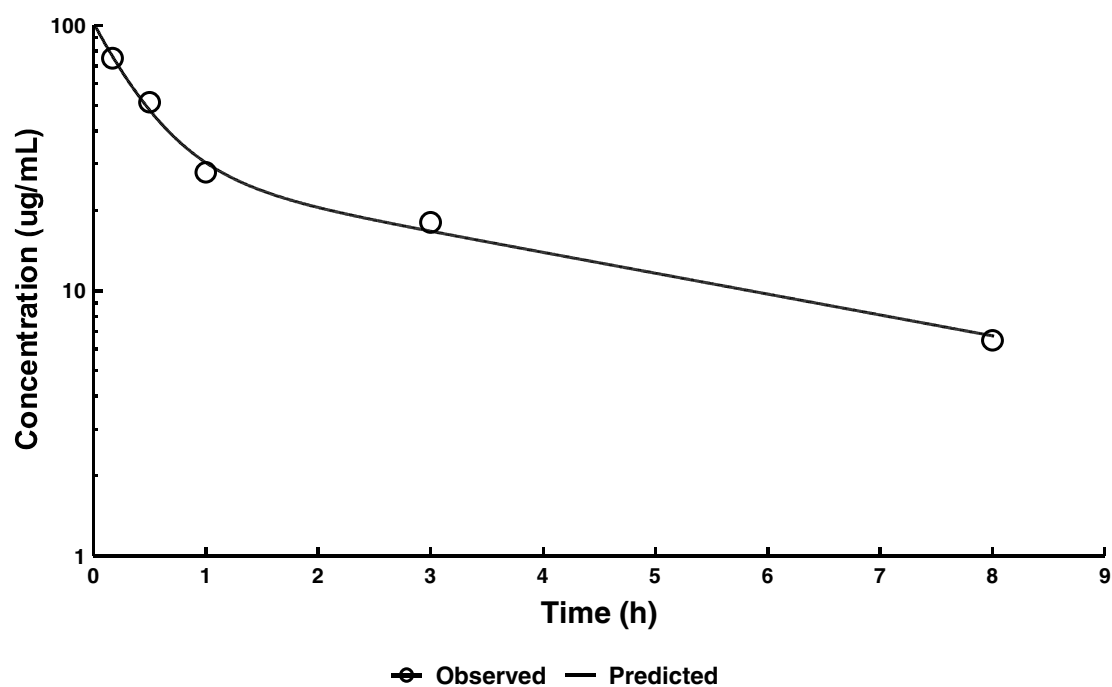


Figure A-11: Blood concentration as a function of time following IV bolus tail vein injection of 1.4 μCi (0.32 mg particles per mouse) [^{125}I]-PRINT particles of 200 nm in mice (n=3 or 4). The data was fitted to two-compartment model shown in **Figure A-12**. The line was obtained from WinNonlin 5.0.1 with the parameters presented in **Table A-2**.

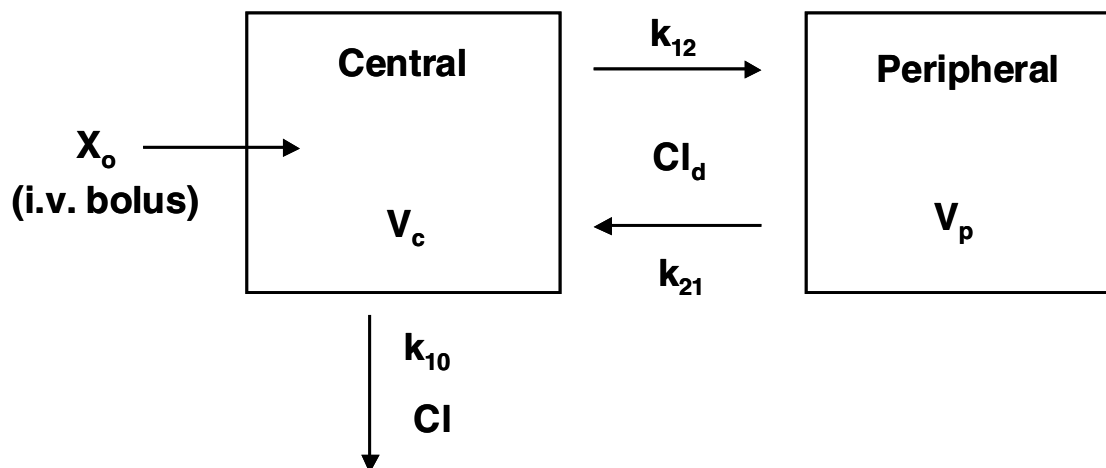


Figure A-12: Two-compartment model used in the calculation of PK parameters in blood. Represented in the scheme are initial dose (X_o , intravenous bolus injection), volume of distribution of central compartment (V_c), volume of distribution of peripheral compartment (V_p), total clearance of the central compartment (Cl), distribution clearance (Cl_d), elimination constants from central compartment (k_{10}), central to peripheral compartment (k_{12}), and peripheral to central compartment (k_{21}).

Table A-2: Blood PK Parameters Estimated from Two-Compartment Model

Parameters	Equation applied	
A^a	WinNonlin value	73 $\mu\text{g/mL}$
B^a	WinNonlin value	29 $\mu\text{g/mL}$
α^a	WinNonlin value	2.44 hr^{-1}
β^a	WinNonlin value	0.18 hr^{-1}
V_c^b	$\text{Dose}/(A+B)$	3.1 mL
Cl^b	$\text{Dose}/[(A/\alpha)+(B/\beta)]$	1.7 mL/hr
k_{21}^b	$(A*\beta+B*\alpha)/(A+B)$	0.82 hr^{-1}
k_{10}^b	$(\alpha*\beta)/k_{21}$	0.54 hr^{-1}
k_{12}^b	$\alpha+\beta-k_{21}-k_{10}$	1.26 hr^{-1}
Cl_d^b	$k_{12}*V_c$	4.0 mL/hr
V_p^b	$(k_{12}*V_c)/k_{21}$	4.9 mL
AUC	$(A/\alpha)+(B/\beta)$	189 $\mu\text{g}\cdot\text{hr/mL}$
$t_{1/2\alpha}^c$	$0.693/\alpha$	17 min
$t_{1/2\beta}^d$	$0.693/\beta$	3.8 hr

^a; Parameters shown in the following equation for two-compartment model, $C=A*e^{-(\alpha*t)}+B*e^{-(\beta*t)}$, wherein C, comprehensive concentration; A, initial concentration of distribution phase; B, initial concentration of terminal phase; α , elimination constant of distribution phase; β , elimination constant of terminal phase; and t, time.

^b; Parameters described in **Figure A-12**.

^c; Half-life of distribution phase

^d; Half-life of terminal phase

A.5 References

- Allen T.M. and Hansen C. (1991). "Pharmacokinetics of stealth versus conventional liposomes: effect of dose." *Biochim Biophys Acta* 1068 (2): 133-41.
- Allen T.M., Hansen C.B. and Demenezes D.E.L. (1995). "Pharmacokinetics of Long-Circulating Liposomes." *Adv Drug Deliv Rev* 16 (2-3): 267-284.
- Barenholz Y. (2001). "Liposome application: problems and prospects." *Current Opinion in Colloid & Interface Science* 6 (1): 66-77.
- Bennett H.S., Luft J.H. and Hampton J.C. (1959). "Morphological Classifications of Vertebrate Blood Capillaries." *Am J Physiol* 196 (2): 381-390.
- Breton P., Guillon X., Roy D., Lescure F., Riess G., Bru N. and Roques-Carnes C. (1998). "Physico-chemical characterization, preparation and performance of poly (methylidene malonate 2.1.2) nanoparticles." *Biomaterials* 19 (1-3): 271-81.
- Cavalieri R.R. (1997). "Iodine metabolism and thyroid physiology: current concepts." *Thyroid* 7 (2): 177-81.
- Chonn A., Semple S.C. and Cullis P.R. (1995). "Beta 2 glycoprotein I is a major protein associated with very rapidly cleared liposomes in vivo, suggesting a significant role in the immune clearance of "non-self" particles." *J Biol Chem* 270 (43): 25845-9.
- Drummond D.C., Meyer O., Hong K., Kirpotin D.B. and Papahadjopoulos D. (1999). "Optimizing liposomes for delivery of chemotherapeutic agents to solid tumors." *Pharmacol Rev* 51 (4): 691-743.
- Duncan R. (2003). "The dawning era of polymer therapeutics." *Nat Rev Drug Discov* 2 (5): 347-60.
- Fidler I.J. (1980). "Therapy of spontaneous metastases by intravenous injection of liposomes containing lymphokines." *Science* 208 (4451): 1469-71.
- Fidler I.J., Raz A., Fogler W.E., Kirsh R., Bugelski P. and Poste G. (1980). "Design of liposomes to improve delivery of macrophage-augmenting agents to alveolar macrophages." *Cancer Res* 40 (12): 4460-6.
- Finkelstein M. and Weissmann G. (1978). "The introduction of enzymes into cells by means of liposomes." *J Lipid Res* 19 (3): 289-303.
- Gratton S.E.A., Pohlhaus P.D., Lee J., Guo J., Cho M.J. and DeSimone J.M. (2007). "Nanofabricated particles for engineered drug therapies: A preliminary biodistribution study of PRINT™ nanoparticles." *J Control Release* (accepted for publication).

- Gregoriadis G. (1995). "Engineering liposomes for drug delivery: progress and problems." *Trends Biotechnol* 13 (12): 527-37.
- Gregory T.R. (2000). "Nucleotypic effects without nuclei: genome size and erythrocyte size in mammals." *Genome* 43 (5): 895-901.
- Groman E.V. and Reinhardt C.P. (2004). "Method to quantify tail vein injection technique in small animals." *Contemp Top Lab Anim Sci* 43 (1): 35-8.
- Harper G.R., Davies M.C., Davis S.S., Tadros T.F., Taylor D.C., Irving M.P. and Waters J.A. (1991). "Steric stabilization of microspheres with grafted polyethylene oxide reduces phagocytosis by rat Kupffer cells in vitro." *Biomaterials* 12 (7): 695-700.
- Imai T. (2006). "Human carboxylesterase isozymes: catalytic properties and rational drug design." *Drug Metab Pharmacokinet* 21 (3): 173-85.
- Jeon S.I., Lee J.H., Andrade J.D. and Degennes P.G. (1991). "Protein Surface Interactions in the Presence of Polyethylene Oxide .1. Simplified Theory." *Journal of Colloid and Interface Science* 142 (1): 149-158.
- Kawski A. (1983). "Excitation-Energy Transfer and Its Manifestation in Isotropic Media." *Photochemistry and Photobiology* 38 (4): 487-508.
- Kenworthy A.K., Hristova K., Needham D. and McIntosh T.J. (1995). "Range and magnitude of the steric pressure between bilayers containing phospholipids with covalently attached poly(ethylene glycol)." *Biophys J* 68 (5): 1921-36.
- Kimelberg H.K. (1976). "Differential distribution of liposome-entrapped [3H]methotrexate and labelled lipids after intravenous injection in a primate." *Biochim Biophys Acta* 448 (4): 531-50.
- Lacasse F.X., Filion M.C., Phillips N.C., Escher E., McMullen J.N. and Hildgen P. (1998). "Influence of surface properties at biodegradable microsphere surfaces: effects on plasma protein adsorption and phagocytosis." *Pharm Res* 15 (2): 312-7.
- Lakowicz J.R., Malicka J., D'Auria S. and Gryczynski I. (2003). "Release of the self-quenching of fluorescence near silver metallic surfaces." *Anal Biochem* 320 (1): 13-20.
- Lee C.C., MacKay J.A., Frechet J.M. and Szoka F.C. (2005). "Designing dendrimers for biological applications." *Nat Biotechnol* 23 (12): 1517-26.
- Majno G. and Joris I. (1978). "Endothelium 1977: a review." *Adv Exp Med Biol* 104: 169-225, 481-526.
- McLean J.W., Fox E.A., Baluk P., Bolton P.B., Haskell A., Pearlman R., Thurston G., Umemoto E.Y. and McDonald D.M. (1997). "Organ-specific endothelial cell uptake of cationic liposome-DNA complexes in mice." *Am J Physiol* 273 (1 Pt 2): H387-404.

- Moghimi S.M., Hedeman H., Muir I.S., Illum L. and Davis S.S. (1993). "An investigation of the filtration capacity and the fate of large filtered sterically-stabilized microspheres in rat spleen." *Biochim Biophys Acta* 1157 (3): 233-40.
- Moghimi S.M., Hunter A.C. and Murray J.C. (2001). "Long-circulating and target-specific nanoparticles: Theory to practice." *Pharmacological Reviews* 53 (2): 283-318.
- Moghimi S.M., Hunter A.C. and Murray J.C. (2005). "Nanomedicine: current status and future prospects." *FASEB J* 19 (3): 311-30.
- Moghimi S.M. and Patel H.M. (1988). "Tissue specific opsonins for phagocytic cells and their different affinity for cholesterol-rich liposomes." *FEBS Lett* 233 (1): 143-7.
- Moghimi S.M., Porter C.J., Muir I.S., Illum L. and Davis S.S. (1991). "Non-phagocytic uptake of intravenously injected microspheres in rat spleen: influence of particle size and hydrophilic coating." *Biochem Biophys Res Commun* 177 (2): 861-6.
- Owens D.E. and Peppas N.A. (2006). "Opsonization, biodistribution, and pharmacokinetics of polymeric nanoparticles." *International Journal of Pharmaceutics* 307 (1): 93-102.
- Papisov M.I. (1998). "Theoretical considerations of RES-avoiding liposomes: Molecular mechanics and chemistry of liposome interactions." *Adv Drug Deliv Rev* 32 (1-2): 119-138.
- Pasqualini R., Arap W. and McDonald D.M. (2002). "Probing the structural and molecular diversity of tumor vasculature." *Trends Mol Med* 8 (12): 563-71.
- Peracchia M.T., Fattal E., Desmaele D., Besnard M., Noel J.P., Gomis J.M., Appel M., d'Angelo J. and Couvreur P. (1999). "Stealth PEGylated polycyanoacrylate nanoparticles for intravenous administration and splenic targeting." *J Control Release* 60 (1): 121-8.
- Porter C.J., Moghimi S.M., Illum L. and Davis S.S. (1992). "The polyoxyethylene/polyoxypropylene block co-polymer poloxamer-407 selectively redirects intravenously injected microspheres to sinusoidal endothelial cells of rabbit bone marrow." *FEBS Lett* 305 (1): 62-6.
- Rolland J.P., Maynor B.W., Euliss L.E., Exner A.E., Denison G.M. and DeSimone J.M. (2005). "Direct fabrication and harvesting of monodisperse, shape-specific nanobiomaterials." *J Am Chem Soc* 127 (28): 10096-100.
- Schwendener R.A., Lagocki P.A. and Rahman Y.E. (1984). "The effects of charge and size on the interaction of unilamellar liposomes with macrophages." *Biochim Biophys Acta* 772 (1): 93-101.
- Senior J.H. (1987). "Fate and behavior of liposomes in vivo: a review of controlling factors." *Crit Rev Ther Drug Carrier Syst* 3 (2): 123-93.

- Shemin D. and Rittenberg D. (1946). THE LIFE SPAN OF THE HUMAN RED BLOOD CELL, *J Biol Chem.* **166**: 627-636.
- Stolnik S., Dunn S.E., Garnett M.C., Davies M.C., Coombes A.G., Taylor D.C., Irving M.P., Purkiss S.C., Tadros T.F., Davis S.S. and et al. (1994). "Surface modification of poly(lactide-co-glycolide) nanospheres by biodegradable poly(lactide)-poly(ethylene glycol) copolymers." *Pharm Res* 11 (12): 1800-8.
- Stolnik S., Illum L. and Davis S.S. (1995). "Long Circulating Microparticulate Drug Carriers." *Adv Drug Deliv Rev* 16 (2-3): 195-214.
- Storm G., Belliot S.O., Daemen T. and Lasic D.D. (1995). "Surface Modification of Nanoparticles to Oppose Uptake by the Mononuclear Phagocyte System." *Adv Drug Deliv Rev* 17 (1): 31-48.
- Takakura Y. and Hashida M. (1996). "Macromolecular carrier systems for targeted drug delivery: pharmacokinetic considerations on biodistribution." *Pharmaceutical Research* 13 (6): 820-831.
- Torchilin V.P. (1998). "Polymer-coated long-circulating microparticulate pharmaceuticals." *J Microencapsul* 15 (1): 1-19.
- Torchilin V.P. (2004). "Targeted polymeric micelles for delivery of poorly soluble drugs." *Cell Mol Life Sci* 61 (19-20): 2549-59.
- Torchilin V.P. and Lukyanov A.N. (2003). "Peptide and protein drug delivery to and into tumors: challenges and solutions." *Drug Discov Today* 8 (6): 259-66.
- Trubetskoy V.S., Frank-Kamenetsky M.D., Whiteman K.R., Wolf G.L. and Torchilin V.P. (1996). "Stable polymeric micelles: lymphangiographic contrast media for gamma scintigraphy and magnetic resonance imaging." *Acad Radiol* 3 (3): 232-8.
- Van Putten L.M. and Croon F. (1958). The Life Span of Red Cells in the Rat and the Mouse as Determined by Labeling with DFP32 in Vivo, *Blood.* **13**: 789-794.
- Vicent M.J. and Duncan R. (2006). "Polymer conjugates: nanosized medicines for treating cancer." *Trends Biotechnol* 24 (1): 39-47.
- Vinogradov S.V., Bronich T.K. and Kabanov A.V. (2002). "Nanosized cationic hydrogels for drug delivery: preparation, properties and interactions with cells." *Adv Drug Deliv Rev* 54 (1): 135-47.
- Wisse E. and De Leeus A.M. (1984). Structural Elements Determining Transport and Exchange Processes in the Liver. Davis S. S., Illum L., McVie J. G. and Tomlinson E., Elsevier Scientific, Amsterdam: 1-23.

- Wolf H., Marschall F., Scheffold N., Clausen M., Schramm M. and Henze E. (1993).
"Iodine-123 labelling of atrial natriuretic peptide and its analogs: initial results."
European Journal of Nuclear Medicine 20 (4): 297-301.
- Woodle M.C. (1998). "Controlling liposome blood clearance by surface-grafted polymers."
Adv Drug Deliv Rev 32 (1-2): 139-152.

APPENDIX II

MANUSCRIPT ACCEPTED FOR PUBLICATION

This manuscript was accepted for publication in *Journal of Controlled Release* (2007)

Nanofabricated particles for engineered drug therapies: A preliminary biodistribution study of PRINTTM nanoparticles

Stephanie E. A. Gratton ^a, Patrick D. Pohlhaus ^a, Jin Lee ^b, Ji Guo ^a,
Moo J. Cho ^b, Joseph M. DeSimone ^{a,c,d,e,*}

^a *Department of Chemistry, University of North Carolina at Chapel Hill, Chapel Hill, NC 27599, USA*

^b *School of Pharmacy, University of North Carolina at Chapel Hill, Chapel Hill, NC 27599, USA*

^c *Department of Chemical Engineering, North Carolina State University, Raleigh, NC 27695, USA*

^d *Lineberger Comprehensive Cancer Center, University of North Carolina at Chapel Hill, Chapel Hill, NC 27599, USA*

^e *Department of Pharmacology, University of North Carolina at Chapel Hill, Chapel Hill, NC 27599, USA*

* Corresponding author. Tel.: +1 919 962 2166; fax: +1 919 962 5467.
E-mail address: desimone@unc.edu

Abstract

A novel method for the fabrication of polymeric particles on the order of tens of nanometers to several microns is described. This imprint lithographic technique called **PRINT**TM (Particle Replication In Non-wetting Templates), takes advantage of the unique properties of elastomeric molds comprised of a low surface energy perfluoropolyether network, allowing the production of monodisperse, shape-specific nanoparticles from an extensive array of organic precursors. This engineered nature of particle production has a number of advantages over the construction of traditional nanoparticles such as liposomes, dendrimers, and colloidal precipitates. The gentle “top down” approach of PRINT enables the simultaneous and independent control over particle size and shape, composition, and surface functionality, and permits the loading of delicate cargos such as small organic therapeutics and biological macromolecules. Thus, this single tool serves as a comprehensive platform for the rational design and investigation of new nanocarriers in medicine, having applications ranging from therapeutics to advanced diagnostics. Preliminary *in vitro* and *in vivo* studies were conducted, demonstrating the future utility of PRINT particles as delivery vectors in nanomedicine. Monodisperse neutral 200 nm poly(ethylene glycol)-based (PEG) particles were fabricated using PRINT methodology and characterized via scanning electron microscopy and dynamic light scattering. Incubation with HeLa cells showed very little cytotoxicity, even at high concentrations. The biodistribution and pharmacokinetics of [¹²⁵I]-labeled particles were studied in healthy mice following tail vein bolus intravenous administration. The particles were distributed mainly to the liver and the spleen with an apparent distribution $t_{1/2}$ of approximately 17 min followed by slow redistribution with a $t_{1/2}$

of 3.3 h. The volume of distribution for the central and peripheral compartments was found to be approximately 3 and 5 mL, respectively.

Key words: PRINT, biodistribution, nanoparticles, pharmacokinetics, nanomedicine

1. Introduction

Despite continued progress in the identification, characterization, and synthesis of advanced therapeutics, the full potential of such innovations can only be achieved with the concomitant realization of *in vivo* profiles ideal for pharmacological intervention. In the realm of drug discovery, the hindrance to obtaining such a profile may be as simple as poor solubility in biological media. For instance, it has been reported that ten percent of marketed drugs suffer from solubility problems, over a third of pipeline drugs are poorly soluble, and almost two-thirds of drugs coming from early pre-clinical development have low solubility [1]. As such, almost forty percent of all possible drug targets fail early due to poor solubility characteristics. More complex problems with drug candidates may include unfavorable pharmacokinetics, and high systemic toxicity. Particular attention must also be given when considering the delivery of biochemically labile substances such as siRNA and other oligonucleotides for gene therapy, as these sensitive cargos need to be protected during circulation. In addition, they need to be delivered to the appropriate tissue or organ, and released intracellularly into the cytosol or nucleus to be effectively used as therapeutics. Finally, the efficient delivery of detection and imaging agents is an extremely important step in the early diagnosis and treatment of disease.

The development and utilization of nanocarriers in response to many of the aforementioned problems encountered *in vivo* has led to dramatic improvements in the

biological profile of important therapies. Intense research in drug delivery over the past few decades has seen the design and construction of valuable nanocarriers such as liposomes, micelles, dendrimers, polymer particles, and colloidal precipitates [2-9]. However, only a handful of drugs and imaging agents delivered using these classical approaches have made it into the clinic [1,8]. One underlying reason for the delayed development is that none of these approaches offers the ability to comprehensively, simultaneously, and independently address several different design criteria. The ability to meet such demanding parameters is quintessential to the design of effective delivery vectors and has been the focus of intense research in our laboratory. Herein, we report the utilization of recent breakthroughs in the nanofabrication of polymeric particles to develop an effective platform delivery system for use in nanomedicine.

Our technique, called **PRINT** (**P**article **R**eplication **I**n **N**on-wetting **T**emplates), is based on the exploitation of the low surface energy of novel fluoropolymeric molds (Fig. 1) [10-12]. The molds are derived from liquid perfluoropolyether (PFPE) precursors, which can be photochemically crosslinked at room temperature. The resulting elastomeric solids enable high-resolution imprint lithography, an emerging technique from the microelectronics industry, to fabricate a variety of organic particles. PRINT is therefore an adaptation of the highly precise mass production technologies used today for the fabrication of nanoscale, silicon-based devices found in the microelectronics field. By developing lithographic technologies that are able to fabricate transistors that are smaller and smaller, companies have been able to increase the number of transistors on a microprocessor to over one billion: this represents an increase of over six orders of magnitude since the early 1970's [13,14]. The minimum feature size currently found on each individual transistor is under 100 nm

(approximately the size of an individual virus particle) [15,16]. The state-of-the-art in the microelectronics industry has finally reached the size scale appropriate for the ideal drug delivery vector. It is now timely to envision and propose the use of lithographic techniques found in the microelectronics industry to fabricate carriers of precise size for use in nanomedicine. Indeed, transistors in today's microelectronic devices are even smaller than traditional drug delivery carriers that have been studied over the last 25 years: micelles, liposomes, and polymer particles.

In hindsight it may be easy to envision the connection between emerging technologies in the microelectronics industry and unfulfilled needs in the field of nanomedicine, however several key challenges are standing in the way of implementing such techniques to fabricate organic carriers. Electronic devices are made from silicon, other inorganic materials, and metals; and the highly developed and proven techniques used to fabricate microprocessors are harsh, often involving the use of oxygen and chlorine etching plasmas, high temperatures, corrosive solvents, acids, bases, and extremely intense deep UV radiation (today 193 nm excimer laser). Moreover, the transistors are permanently adhered to, or are made a part of a two-dimensional surface, with no interest paid to delamination from the surface or bulk collection. Therefore, in order to be successful for nanomedicine, significant re-engineering and innovation is needed. For example, there is no known method or strategy in the suite of available microelectronics fabrication technologies that allows one to make nanoscale structures on a surface and then to harvest those structures to yield isolatable nano-objects or particles. Indeed, particles are the antithesis of the microelectronics industry and are avoided at all costs in the fabrication facilities where class 10 clean rooms are the norm (no more than 10 particles exceeding 0.5 microns per cubic feet of air) to avoid defects in the finished

products. In addition, ideal carriers for therapeutics would require the use of very mild processing conditions since the carriers, cargos, and targeting ligands would be composed of delicate organic molecules (e.g. bioabsorbable materials, siRNA, therapeutics, antibodies, etc.). PRINT technology addresses these issues and allows gentle imprint lithography to be employed in the high-resolution fabrication of organic nanocarriers.

The nature of PRINT technology takes drug delivery for the first time into the uncharted realm of engineered drug therapies given its *à la carte* approach and versatility. This innovative tool allows for the simultaneous control over all of the parameters that are essential in the rational design of conventional delivery vectors in nanomedicine. PRINT allows for the precise control over particle size (20 nm to >100 µm) through use of an appropriately designed master template. The advanced imprint lithography of PRINT ensures replication of the identical master features to afford particles that are truly monodisperse. Particle shape is also controlled through the judicious choice of a master, and geometries such as spheres, cylinders, discs, and toroids with defined aspect ratios can be accommodated. The composition of particles made using PRINT is also readily tunable and amendable to the inclusion of a variety of organic matrices including albumin, hydrogels, PLLA, PLGA, etc. (Fig. 2). Moreover, the porosity, texture, and modulus of the particles can be altered in a logical fashion through careful alteration of the matrix formulation. In view of the fact that PRINT is compatible with a wide range of chemistries and the gentle nature in which particles are fabricated, this technology enjoys the straightforward incorporation of a variety of cargos. The inclusion of hydrophilic or hydrophobic therapeutic molecules, biologicals, peptides, proteins, oligonucleotides, siRNA, contrast agents, radiotracers, and fluorophores can be accommodated through inclusion in the particle matrix. The

concentration of such cargos in the particles can be exactly chosen to meet specific needs and standards since PRINT does not rely on the kinetic trapping of external molecules during particle fabrication as is the case with liposomes and micelles. Finally, particle surface properties are readily modified through either the matrix composition or post-functionalization with surface moieties. Thus, particle surfaces are amenable to decoration with targeting peptides, antibodies, aptamers, avidin/biotin complexes, cationic/anionic charges, and “stealth” poly(ethylene glycol) (PEG) chains for steric stabilization. We believe that PRINT is the only technology that can independently design in these attributes to create truly engineered nanovectors for drug therapies. For the first time, key therapeutic parameters such as bioavailability, biodistribution, and target-specific cell penetration can be simultaneously designed into a therapy. In this report we document the first *in vivo* study of PRINT particles administered intravenously into healthy mice. The promising biodistribution profile and blood pharmacokinetics of 200 nm non-targeted radiolabeled PEG-based nanogels fabricated using PRINT methodology are discussed.

2. Materials and Methods

2.1 Materials

FluorocurTM, the perfluoropolyether used as the molding material in the PRINT process, was purchased from Liquidia Technologies (Product # 2M-140). Trimethylolpropane ethoxylate triacrylate ($M_n = 428$ g/mol) (Aldrich), was passed through a short plug of alumina prior to use to remove inhibitor. Poly(ethylene glycol) monomethyl ether monomethacrylate ($M_n = 1,000$ g/mol) (Polysciences), *para*-hydroxystyrene (Alfa Aesar, 10% (w/w) in propylene glycol) and 2,2-diethoxyacetophenone (Aldrich) were used

as received without further purification. Iodogen® pre-coated tubes were purchased from Pierce Biotechnology, Inc., and radioactive iodine (Na^{125}I) was purchased from Perkin Elmer Life and Analytical Sciences, Inc. as 100 mCi/mL in 10^{-5} M NaOH. HeLa cells and all cell culture media (MEM, OptiMEM) were purchased from the tissue culture facility at The University of North Carolina at Chapel Hill. CellTiter 96* AQueous One Solution Cell Proliferation Assay (MTS) was purchased from Promega Corporation. The lysis agent used for negative controls in *in vitro* viability studies with HeLa cells was the lysis solution contained in the CytoTox-ONE™ Homogeneous Membrane Integrity Assay kit (Promega). Silicon templates used as masters were obtained from Benchmark Technologies. C57BL/6J mice were purchased from The Jackson Laboratory. Ketamine HCl (100 mg/mL) was purchased from Abbott Laboratories. Cholesterol and 1,2-Distearoyl-*sn*-Glycero-3-Phosphocholine (DSPC) were purchased from Avanti Polar Lipids, Incorporated. Abraxane™ (for Injectable Suspension) was purchased from The University of North Carolina at Chapel Hill pharmacy and reconstituted with water immediately prior to use. All animal experiments were conducted in accordance with guidelines set forth by The University of North Carolina at Chapel Hill, and approval was obtained for the completion of these experiments.

2.2 Preparation of PRINT nanoparticles

The fabrication of patterned Fluorocur™ molds has been described elsewhere [10]. Briefly, 20 mL of Fluorocur™ resin containing 0.1% (w/w) of 2,2-diethoxyacetophenone was pooled in the center of an 8 inch patterned master (with feature sizes of 200 nm) which was set up inside an enclosed UV chamber. Ten minutes was allowed to pass so that the

FluorocurTM resin was spread out over the entire 8 inch wafer. The entire system was then purged with nitrogen for 3 minutes. Following this, the coated wafer was exposed to UV irradiation ($\lambda = 365$ nm, power > 20 mW/cm²) for 2 minutes to cure the FluorocurTM resin. The elastomeric mold was then removed from the master template by gently peeling it away from the silicon surface.

In these experiments, the PRINT particles were derived from a mixture composed of 78% (w/w) PEG triacrylate, 20% (w/w) PEG monomethyl ether monomethacrylate, 1% (w/w) 2,2-diethoxyacetophenone, and 1% (w/w) *para*-hydroxystyrene. A 10% (w/v) solution of this mixture in 2-propanol (filtered through a 0.22 μ m PTFE filter) was prepared. This solution (1 mL) was then sprayed onto a FluorocurTM patterned mold using an air brush and residual 2-propanol was allowed to evaporate over 10 minutes. A poly(ethylene) sheet (American Plastics Co.) was then placed over the 8 inch (diameter) mold ensuring that the entire active area was covered. This poly(ethylene) sheet was then peeled back at a rate of approximately 2.5 cm/min. Following this, the mold was placed in a UV curing chamber. The chamber was purged with nitrogen for 3 minutes and UV irradiation was applied ($\lambda = 365$ nm, power > 20 mW/cm²) for 2 minutes.

To facilitate removal of the particles from the mold, a physical means for harvesting the particles was utilized. Specifically, a 2 mL aliquot of acetone (filtered through a 0.22 μ m PTFE filter) was placed on the particle-filled mold and this drop of acetone was gently moved along the surface of the mold using a glass slide. The movement of the glass slide facilitated release of the particles from the mold. The suspended particles were collected in a 50 mL Falcon tube and diluted to the 50 mL mark with filtered acetone after particle collection was complete. The suspension was vortexed for 10 minutes and was centrifuged at

3200 rpm for 30 minutes using a IEC CENTRA CL2 Centrifuge (Thermo Electron Corporation). The supernatant was removed via aspiration and the particle pellet was redispersed in 50 mL of fresh acetone by vortexing for 10 minutes followed by centrifugation for an additional 30 minutes. This process was repeated once more and after aspiration the particles were redispersed in 5 mL of distilled water by sonicating the dispersion for 15 minutes. The particle dispersion was filtered through a 20 μ m filter into a fresh 50 mL Falcon tube, and diluted to the 50 mL mark with acetone. This particle suspension was then centrifuged for one hour. The supernatant was removed via aspiration and the particle pellet was redispersed in 50 mL of fresh acetone by vortexing for 10 minutes followed by centrifugation for an additional 30 minutes. This process was repeated once more (with acetone) and after aspiration the particles were redispersed in a minimal amount of acetone, transferred to a tarred Eppendorf tube, and centrifuged in a microfuge (Fisher Scientific) for 20 minutes. The supernatant was removed and the pellet was dried in a vacuum oven overnight, massed, and dispersed in the appropriate amount of sterile water to make a 10 mg/mL dispersion of particles.

2.3 Preparation of liposomes

Lipids (DSPC:Cholesterol, 55:45 mol) were dissolved in chloroform and evaporated to dryness in a rotary evaporation under reduced pressure at 50°C. After leaving the lipid film overnight under reduced pressure, the film was hydrated with PBS at pH 7.0. Unilamellar liposomes were formed by extrusion with 20 passes through a double-stacked polycarbonate membrane (Whatman Nucleopore) with a pore size of 200 nm, resulting in a liposome

diameter of 177 nm with a polydispersity of 0.026 as determined by dynamic light scattering [17,18].

2.4 Particle size analysis of PRINT nanoparticles using scanning electron microscopy (in the dry state)

The size of PRINT nanoparticles was analyzed via scanning electron microscopy (Hitachi model S-4700). Particle dispersions were prepared at concentrations of 0.5 mg/mL, and a drop of this solution was placed on a glass slide. The drop was then allowed to dry, and the glass slide was coated with 1.5 nm of Pd/Au alloy using a Cressington 108 auto sputter coater (Cressington Scientific Instruments Ltd.). The Pd/Au coated glass slide was then adhered to the sample holder using double-sided adhesive tape, and placed inside the vacuum chamber of the SEM and observed under low vacuum (10^{-3} Torr).

2.5 Particle size analysis of PRINT nanoparticles, liposomes, and AbraxaneTM using dynamic light scattering (in suspension)

The size and polydispersity of PRINT nanoparticles was analyzed via dynamic light scattering (DLS) using a 90Plus Particle Size Analyzer (Brookhaven Instruments Corporation). The particles were dispersed in PBS at a concentration of 0.5 mg/mL and measured without filtration at 25 °C and 37 °C. AbraxaneTM (for Injectable Suspension) was reconstituted with 0.9% (w/v) NaCl to a concentration of 0.5 mg/mL, and the DSPC:CHOL liposomes were diluted using PBS to a concentration of 0.5 mg/mL, and both were measured under the same conditions as PRINT particles.

2.6 Zeta potential measurements

The zeta potential of PRINT nanoparticles was measured using a ZetaPlus Zeta Potential Analyzer (Brookhaven Instruments Corporation). The nanoparticles were dispersed in water at a concentration of 0.3 mg/mL and the zeta potential was measured.

2.7 Radiolabeling of PRINT nanoparticles with ^{125}I

PRINT nanoparticles were radiolabeled using IodogenTM solid phase oxidant in the presence of Na^{125}I . Briefly, 10 mg of PRINT particles in 1 mL of H_2O , 53 μL of phosphate buffered saline, and 1 mCi of Na^{125}I in 10 μL of 10^{-5} M NaOH were added to an IodogenTM pre-coated tube (50 μg of IodogenTM reagent) and the tube was swirled every other minute for 15 minutes. The radiolabeled particle solution was then transferred to a pre-weighed 1.5 mL Eppendorf tube. The original reaction tube was rinsed with one 20 μL portion of 1 mM KI and with two 100 μL portions of water and the rinsing solutions were added to the tube containing radiolabeled particles followed by the addition of NaHSO_3 (1 $\mu\text{mol}/10$ μL). The particle dispersion was then centrifuged for 10 minutes at 15,000 x g using an Eppendorf centrifuge 5415 D (Eppendorf). The supernatant was removed and the particles were washed with four 500 μL portions of water and evaporated to dryness in a SpeedVac SC100 (Savant Instruments). The total mass recovered was 9.45 mg. The specific activity was measured with a Beckman Gamma 5500B gamma counter (Laboratory Technologies) and found to be 5.5 $\mu\text{Ci}/\text{mg}$ PRINT particles.

2.8 *In vitro* cytotoxicity

HeLa cells were seeded in 100 μL of media [Minimum Essential Medium (MEM) containing Earle's salts and supplemented with 1 mM sodium pyruvate and non-essential amino acids] at a density of 5×10^3 cells per cm^2 into a 96-well microtitre plate. Cells were allowed to adhere for 24 h before MEM was replaced with Opti-MEM (90 μL per well) and the particle preparation (10 μL per well in PBS). Positive controls contained PBS alone. HeLa cells were incubated with the PRINT particles for 4 h at 37 °C in a humidified 5% CO_2 atmosphere. After the 4 h incubation period, negative controls were prepared by the addition of 2 μL of lysis solution to a few wells containing cells only. After 2 minutes, the MTS assay solution was added (20 μL per well) into each well. The cells were then incubated for an additional 1 h at 37 °C in a humidified 5% CO_2 atmosphere. The optical density at 450 nm was measured using a BioRad Model 3550 microplate reader (BioRad Laboratories). The viability of the cells exposed to neutral PRINT particles was expressed as a percentage of the viability of cells grown in the absence of particles.

2.9 Biodistribution of [^{125}I]-labeled PRINT particles

Mice were housed under specific pathogen-free conditions for one week and were used at 8 weeks of age (~18 g). Animals were injected intravenously via bolus tail vein administration with 0.32 mg of [^{125}I]-labeled PRINT particles with a specific activity of 4.3 $\mu\text{Ci}/\text{mg}$ in 100 μL of PBS (phosphate buffered saline, Sigma-Aldrich). At 10 min, 30 min, 1, 3, and 8 h after dosing, groups of four mice were anesthetized by intraperitoneal injection of 100 μL of ketamine HCl solution in PBS (50 mg/mL). Blood was collected via cardiac puncture. Samples of blood and organs harvested (liver, kidneys, spleen, lungs, and heart)

were weighed and counted to determine the total radioactivity in a Beckman Gamma 5500B gamma counter (Laboratory Technologies). An additional four animals were kept in a metabolic cage after injection of the [125 I]-labeled PRINT nanoparticles. At 24 h post-injection, urine and feces were accumulated for radioactivity measurements. After these animals were sacrificed (as described above) the blood as well as the organs were removed, weighed, and assayed for radioactivity.

3. Results and Discussion

3.1 The Print Process

In the PRINT process (Fig. 1), the permanent silicon master template is fabricated using advanced lithographic techniques. The liquid PFPE fluoropolymer is then added to the surface of the master template. A positive spreading coefficient allows the perfluoropolyether to wet the nanoscale features of the master template with extremely high fidelity. After the fluoropolymer has wet the master template it is photochemically cross-linked and peeled away to generate a precise mold having nanoscale cavities. The low surface energy and high gas permeability of the PRINT mold enables the organic liquid precursor to the drug carrier particles to fill the cavities through capillary action, but it does not form an inter-connecting “flash” layer of liquid wetting the land area between the cavities. Such specific wetting and filling enables the fabrication of freestanding and harvestable particles that have the same precise shape of the silicon master template from which they were derived. Once the liquid in the mold cavities is converted to a solid using a wide range of gentle chemistries, the array of organic particles can be removed from the mold either by physical methods or by bringing the mold in contact with an adhesive layer (e.g. surgical adhesive/water soluble excipient

layer). Physical methods were used herein to harvest the PRINT particles which were then purified, characterized, and radiolabeled for biodistribution studies.

3.2 Characterization of PRINT Nanoparticles

The particle composition was engineered to produce biologically relevant delivery vectors. Several monomers were added to introduce specific functionality into the hydrogel nanoparticles: poly(ethylene glycol) triacrylate, poly(ethylene glycol) monomethyl ether monomethacrylate, and *p*-hydroxystyrene (PHS) (Fig. 3). Poly(ethylene glycol) derivatives have long been known to impart biocompatibility, solubility, stability, and increased circulation times to proteins, liposomes, and particles [19-23]. The phenol-containing monomer, PHS, was selected as a chemical handle so that gentle radioiodination of the particles was possible. The uniformity of size and shape of the hydrogels was confirmed using scanning electron microscopy (SEM, Fig. 4). The micrographs show the isolation of thousands of virtually identical cylindrical particles, thus verifying PRINT's ability to copy the nanoscale features of a patterned wafer with high precision. The diameter of the particles in the dry state was determined from the scanning electron micrographs to be 201 ± 10 nm and the height was determined to be 155 ± 10 nm. A dry sample is required for SEM and thus the micrographs obtained do not represent the dispersion the particles have once in solution.

The nanocarriers used most frequently today for the delivery of therapeutics in the clinic can best be classified under the general heading of self-assembled structures. Nanovectors fitting this description include micelles, liposomes, and protein aggregates. As a result of their inherent dynamic nature, these nanoparticles derived from the self-assembly of small molecules would be expected to undergo structural changes once *in vivo*. As such, it is

difficult to make a direct connection between the particle formulation prior to administration and the therapeutic outcome. As an example of this behavior, the size and polydispersity of liposomes, AbraxaneTM (albumin-bound paclitaxel), and PRINT particles in water were investigated via dynamic light scattering at room temperature (25 °C) and then at physiological temperature (37 °C) over the course of several hours (Fig. 5). At 25 °C all three particles have a low polydispersity immediately upon formation or dispersion. Upon heating to 37 °C, the mean diameter and polydispersity of liposomes changes dramatically as a function of time. After 3 h at 37 °C, the Abraxane particles decompose as expected. Over the time course of 6 h at physiological temperature, the PRINT particles remain stable as observed by a steady size and polydispersity. This could be an important attribute in the design of nanocarriers, since it is expected that the size and polydispersity of dynamic structures may change even more rapidly once in the serum.

3.3 Cytotoxicity studies in vitro

The cytotoxicity of the PRINT nanoparticles was assessed in a cursory manner using a MTS cell viability assay [24]. This particular assay is a colorimetric evaluation that determines the number of living cells by quantifying the amount of formazan product present, which is directly proportional to the number of viable cells. The MTS assay solution (a modified version of the MTT assay) contains a tetrazolium compound [3-(4,5-dimethylthiazol-2-yl)-5-(3-carboxymethoxyphenyl)-2-(4-sulfophenyl)-2H-tetrazolium, MTS] and an electron-coupling reagent, phenazine ethosulfate, which forms a stable compound that is soluble in cell culture media. MTS is reduced into formazan by living cells only, which can be quantified by its absorbance. Figure 6 shows high absorbance of the formazan relative to

the negative control, supporting the non-toxic nature of the nanoparticles, even at high concentrations (100 µg/mL is equivalent to 800,000 particles/cell). Based on the toxicity data obtained, the PRINT nanoparticles appear biocompatible and suitable for future *in vivo* studies.

3.4 In vivo biodistribution studies of PRINT particles in healthy mice

In this study, 200 nm [¹²⁵I]-labelled PRINT particles were administered into healthy C57BL/6J mice via tail vein bolus injection at a dose of 20 mg/kg. The particles were radiolabeled using Iodogen® following the procedure recommended by the supplier (Pierce). The tissue distribution was monitored using a gamma counter, and the percent recovery of injected dose was calculated from the measured radioactivity. Figure 7 shows the tissue distribution of 200 nm PRINT nanoparticles at 10 min, 30 min, 1 h, 3 h, 8 h, and 24 h post-injection. Throughout the time-course of the study, the 200 nm PRINT particles were distributed mainly in the liver and spleen. The total recovery from these two organs amount to as much as 30% over the 24 h study period. This observation is consistent with the fact that the sinusoidal walls of these organs are lined with discontinuous endothelium that allows for passive entrapment of foreign particulates [25,26]. Although the present study does not provide any direct evidence for or against it, it is likely that these particles are eventually taken up by the resident macrophages possibly subsequent to opsonization with serum proteins [27].

The particle accumulation was not significant in other organs harvested, often ~ 1% of the injected dose was found in the kidneys, heart, and lungs. The extent of particle accumulation reported in these organs may slightly over-represent the actual accumulation

since the organs were not thoroughly rinsed to remove residual blood. Tails were collected in an effort to monitor the amount of nanoparticles that were retained at the injection site. A significant amount of injected particles were found in the tail, especially for the initial 3 h period. This may be due to the rupture of blood vessels upon rapid injection of a large number of fine particles in a short period of time (< 5 seconds), creating endothelial gaps for particle retention. Finally, a trace but significant amount of radioactivity was observed in thyroid gland, possibly indicating the biodegradation of particles, yielding radioactive I_2 . Production of iodine from biochemical degradation of iodinated proteins or peptides is not uncommon and is also consistent with the observation that total recovery decreased steadily over the 24 h period studied (*vide infra*) [28].

Total recovery of the radioiodinated particles was found to decrease with time, beginning with an $81 \pm 6 \%$ recovery at 10 minutes post-injection and ending with a $24 \pm 7 \%$ recovery after 24 h (data not shown). Here, the total recovery was calculated from radioactivity measured only from the blood, liver, kidneys, spleen, lungs, heart, tail, bone marrow, and thyroid. In an effort to achieve a full mass balance, four mice were kept in metabolic cages for 24 h so that urine and feces could be collected and analyzed. For these mice, additional tissues and body parts such as fat, muscle, head, legs, intestines, and the remainder of the body were also analyzed for additional radioactivity. It was found that with these additional measurements, the total recovery at 24 h post-injection improved from $24 \pm 7 \%$, with the main organs only, to $58 \pm 4 \%$. The appearance of radioactivity in the thyroid gland throughout the study period (approximately 1% of injected dose) and in urine 24 h after dosing (as much as 8.6%) may suggest particle degradation [29]. This is also

consistent with a hypothesis that loss of volatile radioactive iodine via the lungs could have contributed to the time-dependent decrease in total recovery of radioactivity observed.

As shown in Figure 8, the disappearance of PRINT particles from circulation was bi-exponential. The data set was fitted to a two-compartmental pharmacokinetic model with reversible distribution between central and peripheral compartments and with elimination from the central compartment. The pharmacokinetic parameters obtained using WinNonLin 5.0.1 (Pharsight Corporation) show the initial phase of rapid distribution with an apparent $t_{1/2}$ of 17 min. The rapid distribution is not surprising considering that the steric coat on the PRINT particles is only a low molecular weight PEG chain (9 mol %, 20% w/w of 1-kDa PEG monomethyl ether). It has been suggested that the optimal coating for the creation of long-circulating liposomes is 3-7 mol % of 2-5 kDa PEG [30]. The shorter PEG chains used in the current particle formulation may not offer a radius of protection that is sufficient to effectively block the adsorption of opsonic proteins. The subtle nuances that both the degree of PEG incorporation and the molecular weight of PEG play in prolonging the circulatory $t_{1/2}$ are well documented for other types of nanocarriers [30-32].

Volumes of distribution of central and peripheral compartments were found to be 3 and 5 mL, respectively. Considering the blood volume of approximately 1.7 mL/20 g mouse, liver of 0.8 g, and spleen < 0.1 g, these values appear to be somewhat exaggerated, however, they certainly rule out any significant extravasation. Since the stability of the radiolabel is not well established in the present study and since it is the radioactivity that is monitored, it is difficult to unambiguously interpret the slow phase of radioactivity decay in the later time-points with an apparent $t_{1/2}$ of 3.3 h. The appearance of radioactivity in urine strongly suggests that these PRINT particles and/or their degradation products must be cleared rapidly

from the blood. Thus, the slow elimination phase may well represent slow re-distribution of particles or particle remnants between the blood and organs/tissues.

The AUC, a measure of total availability of particles in the circulation for organ distribution extrapolated to infinite time, was determined to be 191 $\mu\text{g}\cdot\text{h}/\text{mL}$. Unmodified, conventional liposomes show dose-dependent pharmacokinetic parameters, including AUC upon i.v. administration. A liposome dose equivalent to the dose studied in the present study, 20 mg/kg, shows AUC values of approximately 70 to 700 $\mu\text{g}\cdot\text{h}/\text{mL}$, and the present data are certainly in agreement with that reported for liposomes [33].

4. Conclusions

This paper is concerned with the characterization of nanofabricated particles that are monodisperse in size and shape. It includes the first pharmacokinetic evaluation of PRINT-derived cylinders of 200 nm. PRINT allows for powerful realizations regarding pharmacokinetics of nanoparticles since intersubject variation can be ascribed fully to the subject and not to variations of the nanocarrier. This is a significant step in pharmacokinetic analysis since it eliminates the effect that polydisperse samples can have on biodistribution. This in turn allows us to be able to precisely demonstrate the effect of size, composition, the addition of cargo, modulus, and functionalization on biodistribution, which has never been possible until now. Current efforts are focused on the creation of long-circulating PRINT particles for the eventual use in engineered drug therapies. Results will be reported in due course.

PRINT is the first general, singular method capable of forming organic nanoparticles in which critical design parameters can be precisely and independently tailored bringing a

greater understanding of cause-and-effect to the field of nanomedicine. With the unprecedented ability of PRINT technology to control particle size, shape, composition, modulus, cargo, and surface properties, questions such as “what interrelated role does shape, size and mechano-chemico functionality play on the biodistribution of carriers *in vivo*?” and, “how can this understanding translate into more efficacious detection, diagnosis, therapeutic and prevention strategies?” can finally begin to be answered. As such, PRINT is a significant scientific and technological breakthrough, which will allow the fabrication of heretofore inaccessible populations of nanobiomaterials which are poised to revolutionize and accelerate our translational understanding, detection, and treatment of disease.

5. Acknowledgements

The authors would like to thank Michael J. Barrett for his gracious help with light scattering, Kevin P. Herlihy for his artistic rendition of the PRINT process, CHANL (especially Carrie Donley), Ginger Denison-Rothrock (Liquidia Technologies) and Mary Napier for useful discussions, and John An for his help with cell work. This work was supported in part by the STC Program of the NSF (CHE-9876674), NIH P01-GM59299, NIH U54-CA119343 (the Carolina Center of Cancer Nanotechnology Excellence), the William R. Kenan Professorship of the University of North Carolina at Chapel Hill, and Liquidia Technologies.

Fig. 1. Illustration of **PRINT**. Fabrication of the silicon master template (**box, upper left**); Wetting of the silicon master with (green) liquid fluoropolymer, followed by curing (**top row**); PFPE elastomeric mold produced with nanoscale features from the master (**upper right**); Confining (red) organic liquid to cavities by applying pressure between mold and a PFPE surface (**middle row**); Removal of organic particles from mold with adhesive layer (**bottom left**); Dissolution of adhesive layer producing free particles (**bottom right**)

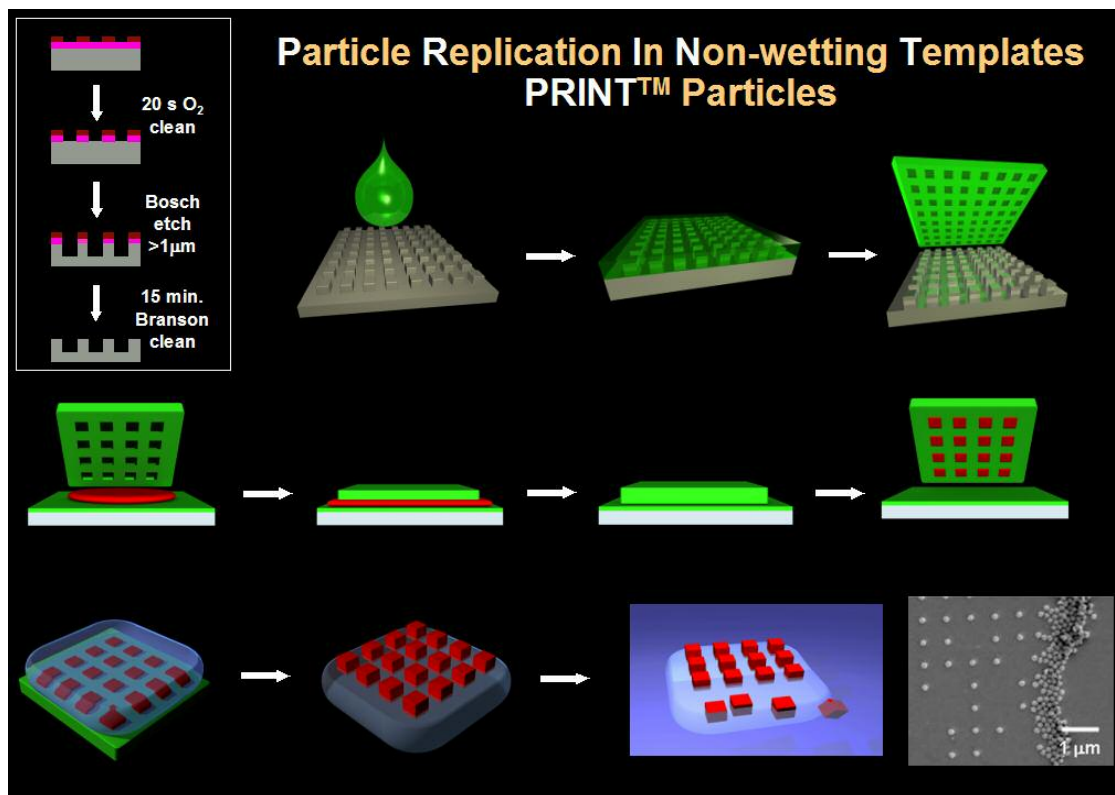


Fig. 2. Results of the **PRINT** Process. **Top row, left to right:** **A)** SEM of an etched silicon wafer master template of 3 μm posts having a height of 1.7 μm ; **B)** Cured PFPE mold of the master template shown in A; **C)** PFPE mold containing PEG particles prior to harvesting; **D)** Harvested and dispersed PEG **PRINT** particles. **Bottom row, left to right:** **E)** SEM of an etched silicon wafer patterned with approximately 400 billion posts that are 100 nm in diameter and 400 nm tall; **F)** A cured PFPE mold of the silicon master template shown in E; **G)** 100 nm PEG particles made using **PRINT** and transferred to a medical adhesive layer for surface functionalization and subsequent harvesting

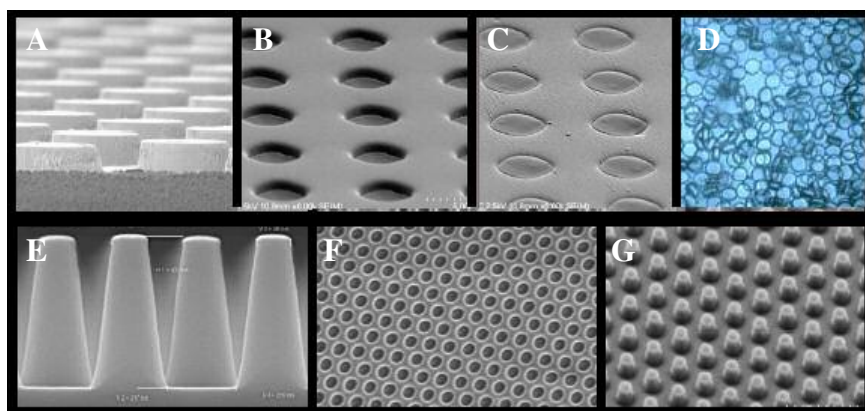


Fig. 3. Chemical structures of monomers and a partial structure of the PRINT nanogel. *p*-Hydroxystyrene was introduced for radioiodination at 1% (w/w). Throughout the present study, it is assumed that iodinated PRINT nanogels behave the same as unmodified particles.

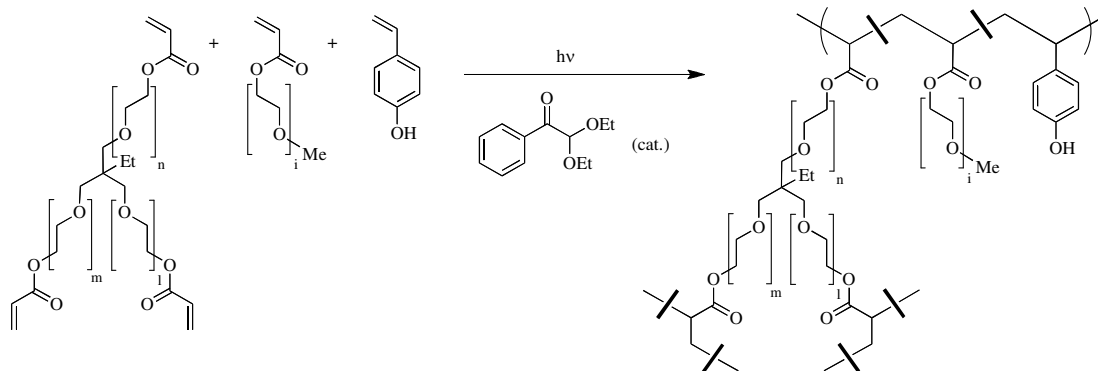


Fig. 4. Scanning electron micrographs of 200 nm PRINT particles used in the present study

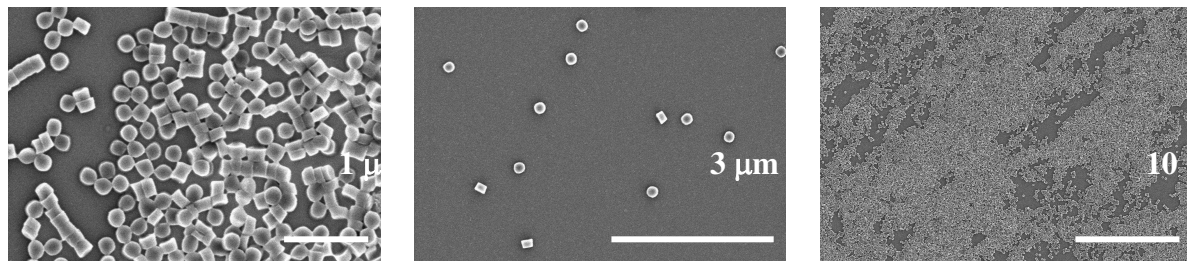


Fig. 5. A time-dependent study of the mean diameter, polydispersity and stability of PRINT particles (left), liposomes (middle), and AbraxaneTM (right) using dynamic light scattering

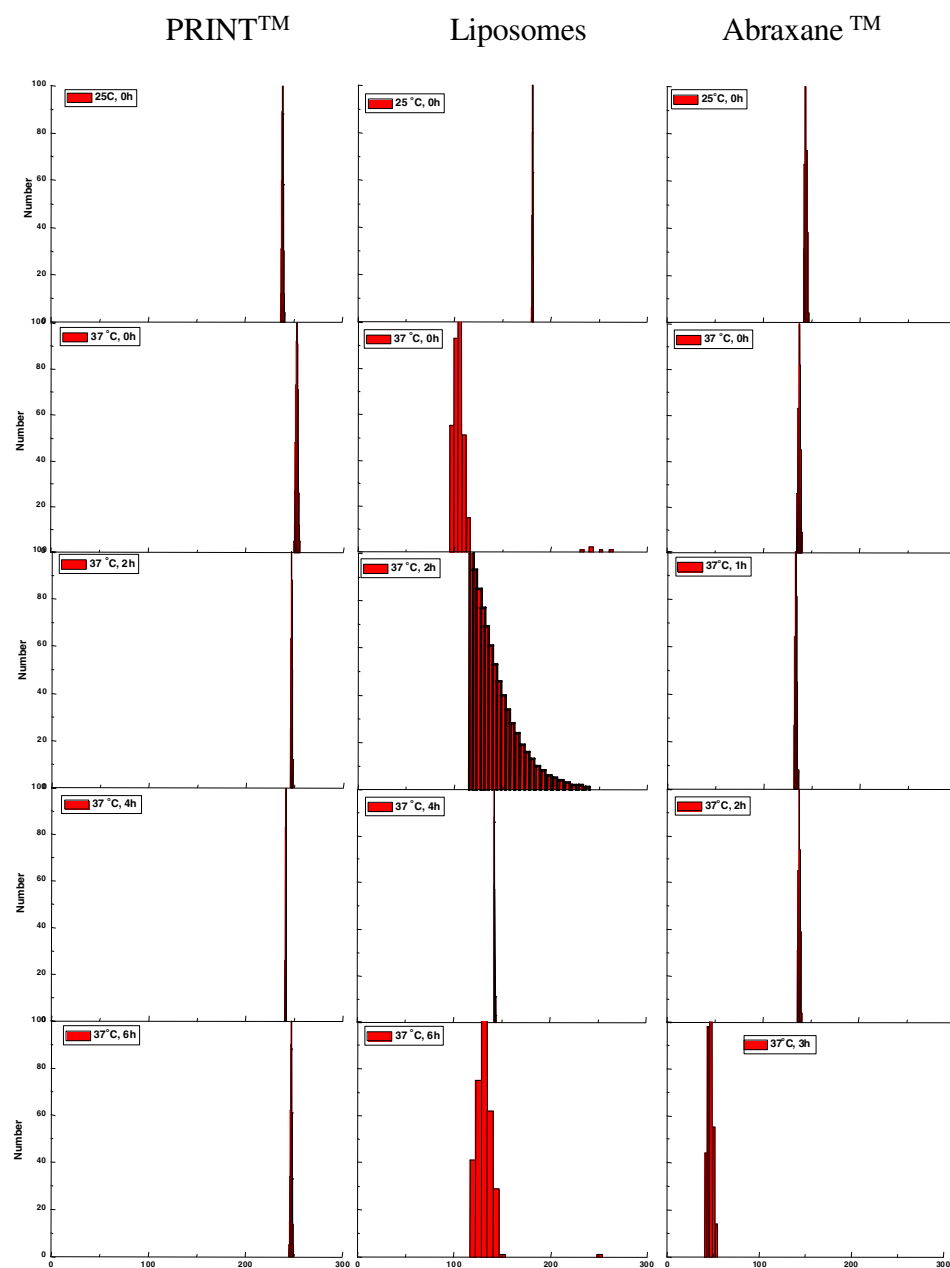


Fig. 6. MTS assay depicting the non-toxic nature of 200 nm PRINT particles incubated with HeLa cells. Approximately 10^3 cells were plated per 1 cm^2 . Cells were exposed to varying concentrations of PRINT particles in 0.1 mL media for 4 h at 37 °C before the MTS assay was performed. Control wells, where the cells were exposed to only PBS serve as 100% in normalization. Vertical bars stand for one SD with $n = 5$.

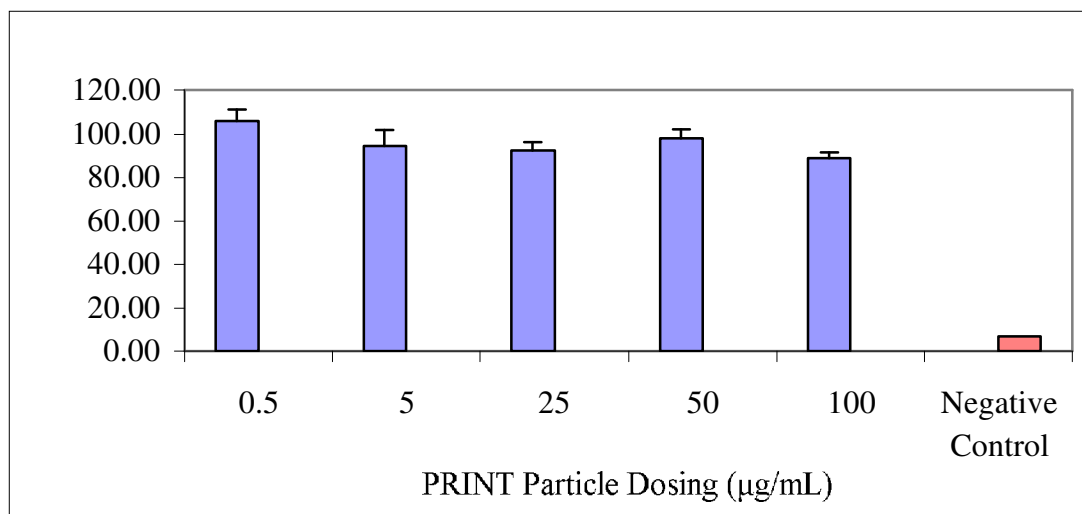


Fig. 7. Biodistribution of 200 nm [125 I]-labeled PRINT particles in healthy mice subsequent to bolus tail vein injection at a dose of 20 mg/kg. The organ accumulation is expressed as a percent of injected dose after animals were sacrificed at 10 min, 30 min, 1, 3, 8, and 24 h post-intravenous injection. The organ data is presented as the mean \pm SD with n = 4. The recovery found in the blood assumes a blood volume of 2.18 mL/25 g mouse [34].

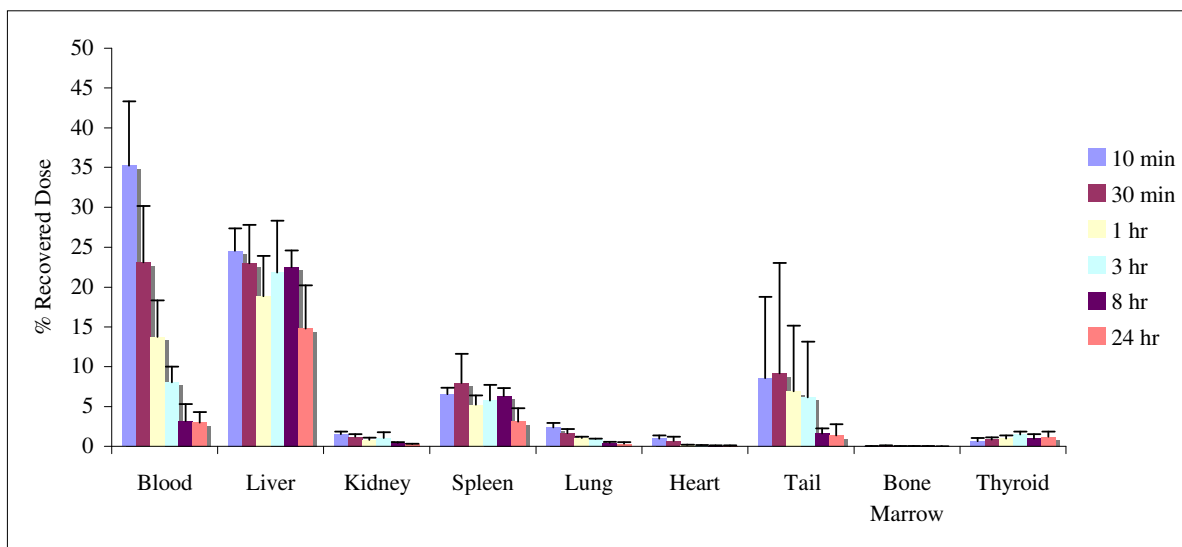
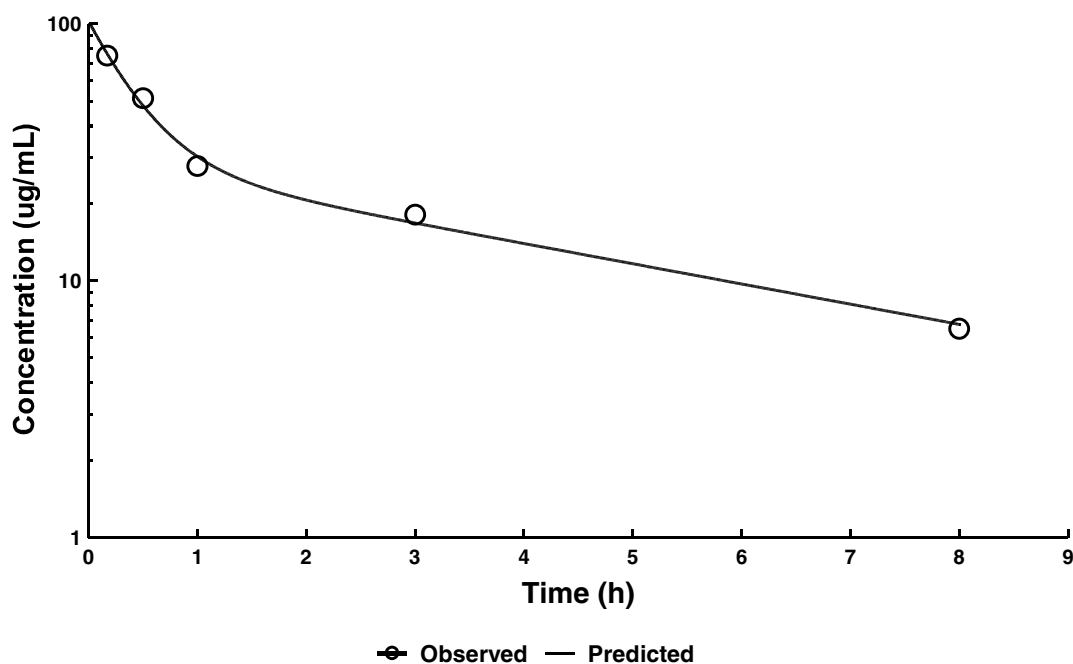


Fig. 8. Blood pharmacokinetic profile of PRINT particles in healthy C57BL/6J mice. At given time intervals, four animals were sacrificed and blood was collected via cardiac puncture. Radioactivity observed was converted to particle concentration using the specific radioactivity measured and assuming a total blood volume of 2.18 mL/25 g mouse [34]. The data was subject to two-compartmental analysis (WinNonlin) resulting in pharmacokinetic parameters discussed in the text. For simplicity, data obtained 24 h post-injection are not shown in the figure or used for PK parameter determination.



6. References

- [1] S. Riley, Innovation in Drug Delivery: The future of nanotechnology and non-invasive protein delivery, Business Insights Ltd. (2006) 25-26.
- [2] S. M. Moghimi, A. C. Hunter, J. C. Murray, Nanomedicine: current status and future prospects, *FASEB J.* 19 (3) (2005) 311-330.
- [3] Y. Barenholz, Liposome application: problems and prospects, *Curr. Opin. Colloid Interface Sci.* 6 (1) (2001) 66-77.
- [4] G. S. Kwon, K. Kataoka, Block copolymer micelles as long-circulating drug vehicles, *Adv. Drug Delivery Rev.* 16 (1995) 295-309.
- [5] C. C. Lee, J. A. MacKay, J. M. J. Frechet, F. C. Szoka, Designing dendrimers for biological applications, *Nat. Biotechnol.* 23 (12) (2005) 1517-1526.
- [6] V. P. Torchilin, Targeted polymeric micelles for delivery of poorly soluble drugs, *Cell. Mol. Life Sci.* 61 (2004) 2549-2559.
- [7] M. J. Vicent, R. Duncan, Polymer conjugates: nanosized medicines for treating cancer, *Trends Biotechnol.* 24 (1) (2006) 39-47.
- [8] R. Duncan, The dawning era of polymer therapeutics, *Nat. Rev. Drug Discovery* 2 (5) (2003) 347-360.
- [9] K. McAllister, P. Sazani, M. Adam, M. J. Cho, M. Rubinstein, R. J. Samulski, J. M. DeSimone, Polymeric Nanogels Produced via Inverse Microemulsion Polymerization as Potential Gene and Antisense Delivery Agents, *J. Am. Chem. Soc.* 124 (51) (2002) 15198-15207.
- [10] J. P. Rolland, B. W. Maynor, L. E. Euliss, A. E. Exner, G. M. Denison, J. M. DeSimone, Direct fabrication and harvesting of monodisperse, shape-specific nanobiomaterials, *J. Am. Chem. Soc.* 127 (28) (2005) 10096-10100.
- [11] J. P. Rolland, E. C. Hagberg, G. M. Denison, K. R. Carter, J. M. DeSimone, High-resolution soft lithography: enabling materials for nanotechnologies, *Angew. Chem., Int. Ed. Engl.* 43 (43) (2004) 5796-5799.
- [12] L. E. Euliss, J. A. DuPont, S. Gratton, J. DeSimone, Imparting size, shape, and composition control of materials for nanomedicine, *Chem. Soc. Rev.* 35 (11) (2006) 1095-1104.
- [13] Y. N. Patt, S. J. Patel, M. Evers, D. H. Friendly, J. Stark, One Billion Transistors, One Uniprocessor, One Chip, *Computer* 30 (9) (1997) 51-57.

- [14] R. Hiremane, From Moore's Law to Intel Innovation-Prediction to Reality, Technology@Intel Magazine (2005) 2-9.
- [15] T. S. Baker, N. H. Olson, S. D. Fuller, Adding the third dimension to virus life cycles: three-dimensional reconstruction of icosahedral viruses from cryo-electron micrographs, *Microbiol. Mol. Biol. Rev.* 63 (4) (1999) 862-922.
- [16] www.intel.com, 1/22/07.
- [17] Z. Huang, X. Guo, W. Li, J. A. MacKay, F. C. Szoka, Jr., Acid-triggered transformation of diortho ester phosphocholine liposome, *J. Am. Chem. Soc.* 128 (1) (2006) 60-61.
- [18] M. Grit, D. J. A. Crommelin, The effect of aging on the physical stability of liposome dispersions, *Chemistry and Physics of Lipids* 62 (2) (1992) 113-22.
- [19] M. C. Woodle, Controlling liposome blood clearance by surface-grafted polymers, *Adv. Drug Delivery Rev.* 32 (1998) 139-152.
- [20] M. I. Papisov, Theoretical considerations of RES-avoiding liposomes: Molecular mechanics and chemistry of liposome interactions, *Adv. Drug Delivery Rev.* 32 (1998) 119-138.
- [21] T. M. Allen, C. B. Hansen, D. E. L. de Menezes, Pharmacokinetics of long-circulating liposomes, *Adv. Drug Delivery Rev.* 16 (1995) 267-284.
- [22] G. Gregoriadis, Engineering liposomes for drug delivery: progress and problems, *Trends Biotechnol.* 13 (12) (1995) 527-37.
- [23] V. P. Torchilin, Polymer-coated long-circulating microparticulate pharmaceuticals, *J. Microencapsulation* 15 (1) (1998) 1-19.
- [24] J. A. Barltrop, T. C. Owen, A. H. Cory, J. G. Cory, 5-(3-Carboxymethoxyphenyl)-2-(4,5-dimethylthiazolyl)-3-(4-sulfophenyl)tetrazolium, inner salt (MTS) and related analogs of 3-(4,5-dimethylthiazolyl)-2,5-diphenyltetrazolium bromide (MTT) reducing to purple water-soluble formazans as cell-viability indicators, *Bioorg. Med. Chem. Lett.* 1 (11) (1991) 611-614.
- [25] E. Wisse, A. M. De Leeus, in: S. S. Davis, L. Illum, J. G. McVie, E. Tomlinson (Eds.), *Structural Elements Determining Transport and Exchange Processes in the Liver*, Elsevier Scientific, Amsterdam, 1984, pp. 1-23.
- [26] J. H. Senior, Fate and behavior of liposomes in vivo: a review of controlling factors, *Crit. Rev. Ther. Drug Carrier Syst.* 3 (2) (1987) 123-193.
- [27] A. Chonn, S. C. Semple, P. R. Cullis, β 2-glycoprotein I is a major protein associated with very rapidly cleared liposomes in vivo, suggesting a significant role in the

- immune clearance of "non-self" particles, *J. Biol. Chem.* 270 (43) (1995) 25845-25849.
- [28] H. Wolf, F. Marschall, N. Scheffold, M. Clausen, M. Schramm, E. Henze, Iodine-123 labelling of atrial natriuretic peptide and its analogs: initial results, *Eur. J. Nucl. Med. Mol. Imag.* 20 (4) (1993) 297-301.
- [29] Y. Takakura, M. Hashida, Macromolecular carrier systems for targeted drug delivery: pharmacokinetic considerations on biodistribution, *Pharm. Res.* 13 (6) (1996) 820-831.
- [30] S. M. Moghimi, A. C. Hunter, J. C. Murray, Long-circulating and target-specific nanoparticles: Theory to practice, *Pharmacol. Rev.* 53 (2) (2001) 283-318.
- [31] D. E. Owens, N. A. Peppas, Opsonization, biodistribution, and pharmacokinetics of polymeric nanoparticles, *Int. J. Pharm.* 307 (1) (2006) 93-102.
- [32] D. C. Drummond, O. Meyer, K. Hong, D. B. Kirpotin, D. Papahadjopoulos, Optimizing liposomes for delivery of chemotherapeutic agents to solid tumors, *Pharmacol. Rev.* 51 (4) (1999) 691-743.
- [33] T. M. Allen, C. Hansen, Pharmacokinetics of stealth versus conventional liposomes: effect of dose, *Biochim. Biophys. Acta* 1068 (2) (1991) 133-141.
- [34] K. Kataoka, T. Matsumoto, M. Yokoyama, T. Okano, Y. Sakurai, S. Fukushima, K. Okamoto, G. S. Kwon, Doxorubicin-loaded poly(ethylene glycol)-poly(b-benzyl-L-aspartate) copolymer micelles: their pharmaceutical characteristics and biological significance, *J. Controlled Release* 64 (2000) 143-153.